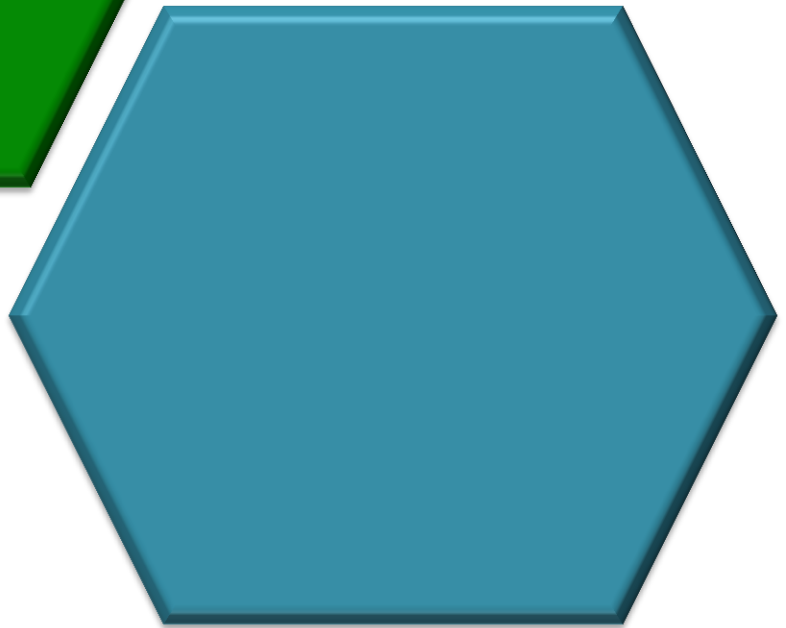
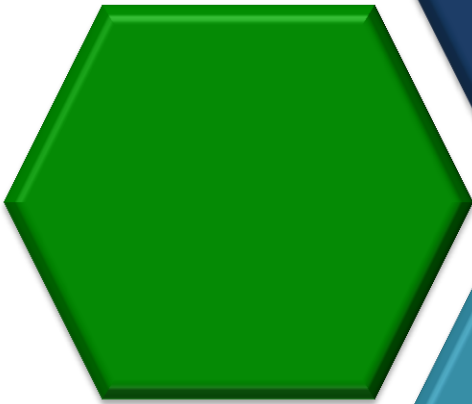


Mass spectrometric characterization of flavonoids and *in vitro* intestinal transport and bioactivity



Gerard Bryan L. Gonzales

Promotors:

Prof. dr. ir. John Van Camp

NutriFOODChem Unit, Department of Food Safety and Food Quality,
Faculty of Bioscience Engineering, Ghent University, Ghent, Belgium

Prof. dr. ir. Katleen Raes

Laboratory of Food Microbiology and Biotechnology, Department of
Industrial Biological Sciences, Faculty of Bioscience Engineering, Ghent
University, Kortrijk, Belgium

Prof. dr. ir. Guy Smagghe

Laboratory of Agrozoology, Department of Crop Protection, Faculty of
Bioscience Engineering, Ghent University, Ghent, Belgium

Examination Committee:

Chairman:

Prof. dr. Colin Janssen

Laboratory for Environmental Toxicology and Aquatic Ecology, Faculty
of Bioscience Engineering, Ghent University, Ghent, Belgium

Secretary:

Prof. dr. ir. Tom Van de Wiele

Center for Microbial Ecology and Technology, Department of
Biochemical and Microbial Technology, Faculty of Bioscience
Engineering, Ghent University, Ghent, Belgium

Prof. dr. ir. Bruno De Meulenaer

NutriFOODChem Unit, Department of Food Safety and Food Quality,
Faculty of Bioscience Engineering, Ghent University, Ghent, Belgium

Prof. dr. ir. Yvan Larondelle

Institute of Life Sciences, Faculty of Bioscience Engineering, Université
Catholique de Louvain, Louvain-la-Neuve, Belgium

dr. Francisco Tomás Barberán

Quality, safety and bioactivity of plant foods, CEBAS-CSIC, Murcia,
Spain

dr. Kris Morreel

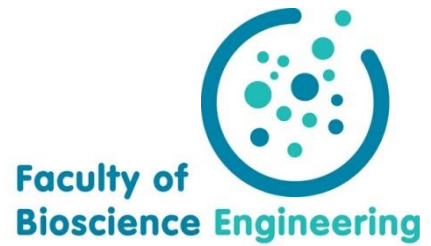
Department of Plant Systems Biology, Flemish Institute for
Biotechnology (VIB), Ghent, Belgium

Dean:

Prof. dr. ir. Marc Van Meirvenne

Rector:

Prof. dr. Anne De Paepe



**MASS SPECTROMETRIC CHARACTERIZATION OF
FLAVONOIDS AND *IN VITRO* INTESTINAL TRANSPORT
AND BIOACTIVITY**

GERARD BRYAN GONZALES

Thesis submitted in fulfillment of the requirements for the degree of
Doctor (PhD) in Applied Biological Sciences: Chemistry and Bioprocess Technology

Dutch translation of the title:

Massaspectrometrische karakterisatie van flavonoïden en in vitro intestinaal transport en bioactiviteit

Cover design by: Marc Van Lerberge

To refer to this thesis:

Gonzales, GB (2016). Mass spectrometric characterization of flavonoids and in vitro intestinal transport and bioactivity. PhD dissertation, Faculty of Bioscience Engineering, Ghent University, Belgium

ISBN: 978-90-5989-880-6

The author and promotors gave the authorization to consult and copy parts of this work for personal use only. Every other use is subject to copyright laws. Permission to reproduce any material contained in this work should be obtained from the author.

Financial support and Grants

Ghent University Special Research Fund (BOF), Ghent University, Belgium

Hercules Foundation (AUGE028, AUGE014, AUGE013)

COST Action Infogest Short-term scientific mission 2014

Acknowledgements

Special thanks also go to Sofie Coelus, Geert Geominne, and Geert Meesen for their technical support. The hospitality and guidance of the Institute of Food Research, especially of Dr. Alan Mackie, Dr. Balazs Bajka and Neil Rigby, during my short-term scientific mission is also highly appreciated. Further, I would like to express my most heart-felt gratitude to my promoters, Prof John Van Camp, Prof Guy Smagghe and Prof Katleen Raes, members of my PhD examination committee, all scientific collaborators, especially Dr. Charlotte Grootaert, colleagues at UGent, my former students, my family, and all the friends and loved-ones who accompanied me along the way.

Lastly, I dedicate this PhD to my biggest inspiration – the person who taught me science, *nanay* Dr. Dulce M. Flores (deceased).

Daghang salamat sa inyong tanan!

Bryan

TABLE OF CONTENTS

LIST OF ABBREVIATIONS	XII
RESEARCH FRAMEWORK AND OBJECTIVES	1
SUMMARY	5
SAMENVATTING	9
CHAPTER 1. LITERATURE REVIEW	15
1.1. FLAVONOIDS	15
1.2. FLAVONOID ANALYSIS USING LIQUID CHROMATOGRAPHY-MASS SPECTROMETRY (LC-MS)	16
1.2.1. <i>Separation of flavonoids in reversed-phase liquid chromatography</i>	16
1.2.2. <i>Mass spectrometric analysis of flavonoids</i>	18
1.2.3. <i>Tandem MS and collision induced dissociation (CID) for structural characterization</i>	20
1.2.3.1. Flavonoid-O-glycosides.....	20
1.2.3.2. Flavonoid-C-glycosides	22
1.2.3.3. Acylated flavonoid glycosides.....	23
1.2.3.4. Flavonoid metabolic conjugates	23
1.3. STRUCTURE-ACTIVITY RELATIONSHIP (SAR) ANALYSES	25
1.4. FLAVONOID INTERACTIONS AND THEIR EFFECT ON BIOAVAILABILITY AND BIOACTIVITY.....	26
1.4.1 <i>Binding of flavonoids to α-amylase and α-glucosidase and their interaction with food carbohydrates</i>	26
1.4.2. <i>Flavonoid interaction to lipase and effect of fat consumption on bioavailability</i>	28
1.4.3. <i>Interaction of flavonoids with food proteins and proteolytic enzymes</i>	30
1.5. OVERALL INTESTINAL PERMEABILITY.....	31
1.6. USE OF CELL CULTURES IN THE STUDY OF FLAVONOIDS	33
1.6.1. <i>In vitro cellular models of the intestines</i>	33
1.6.2. <i>Co-culture models in the study of flavonoids</i>	35
1.7. CELLULAR UPTAKE AND TRANSPORT OF FLAVONOIDS	36
1.7.1. <i>Solute carrier transporters</i>	37
1.7.2. <i>Sodium-glucose linked transporters</i>	37
1.7.3. <i>Bilitranslocase</i>	38
1.8. CELLULAR METABOLISM OF FLAVONOIDS.....	38
1.8.1. <i>Deglycosylation</i>	38
1.8.2. <i>Glucuronidation</i>	39
1.8.3. <i>Sulfation</i>	40
1.8.4. <i>ATP-binding cassette (ABC) transporters</i>	41
1.8.4.1. P-glycoprotein	42
1.8.4.2. Multidrug resistance proteins (MRP).....	44
1.8.4.3. Breast cancer resistance proteins (BCRP)	45
1.9. FLAVONOIDS IN SYSTEMIC CIRCULATION AND THEIR DISTRIBUTION TO TARGET TISSUES	45
1.9.1. <i>Deglucuronidation</i>	47
1.10. SPECIFIC CELLULAR BIOACTIVITY OF FLAVONOIDS.....	48
1.10.1. <i>Prevention of cellular reactive oxygen species (ROS) damage</i>	48
1.10.1.1. Suppression of ROS production.....	49
1.10.1.2. Scavenge of ROS.....	49
1.10.1.3. Upregulation of anti-oxidant defenses	50

1.10.2. DNA damage repair.....	50
--------------------------------	----

**CHAPTER 2: ULTRA(HIGH)-PRESSURE LIQUID CHROMATOGRAPHY-
ELECTROSPRAY IONIZATION- TIME-OF-FLIGHT-ION MOBILITY-HIGH
DEFINITION MASS SPECTROMETRY FOR THE RAPID IDENTIFICATION AND
STRUCTURAL CHARACTERIZATION OF FLAVONOID GLYCOSIDES FROM
CAULIFLOWER WASTE 53**

2.1. ABSTRACT	53
2.2. INTRODUCTION	54
2.3. MATERIALS AND METHODS.....	55
2.3.1. Reagents.....	55
2.3.2. Fragmentation behavior of flavonoid standards.....	56
2.3.3. T-wave ion mobility separation (IMS).....	56
2.3.4. Extraction of phenolic content.....	56
2.3.5. Acid and alkaline hydrolysis.....	57
2.3.6. Sample preparation and clean-up.....	57
2.3.7. U(H)PLC-DAD-ESI-IMS-HDMS/MS ^E analysis.....	57
2.4. RESULTS AND DISCUSSION.....	58
2.4.1. Fragmentation behavior of flavonoid standards.....	58
2.4.2. Glycosilation of 3- and 7-mono-O-glycosides	59
2.4.3. Glycosilation of 3,7-diO-glycosides	59
2.4.4. Analysis of phenolics from cauliflower waste methanolic extract.....	62
2.4.4.1. Chromatographic behavior and acid, alkaline hydrolysis.....	62
2.4.4.2. Identification of flavonoid glycosides from <i>Brassica</i> waste methanolic extract.....	63
2.5. CONCLUSION.....	72

**CHAPTER 3: COMBINED ALKALINE HYDROLYSIS AND ULTRASOUND-ASSISTED
EXTRACTION FOR THE RELEASE OF NONEXTRACTABLE PHENOLICS FROM
CAULIFLOWER (*BRASSICA OLERACEA* VAR *BOTRYTIS*) WASTE 75**

3.1. ABSTRACT	75
3.2. INTRODUCTION	76
3.3. MATERIALS AND METHODS.....	77
3.3.1. Reagents.....	77
3.3.2. Conventional extraction of EP and collection of residues containing NEP	77
3.3.3. Measurement of total phenolic content (TPC).....	78
3.3.4. Alkaline hydrolysis and choice of solvent on the total phenolic content (TPC) of residues	78
3.3.5. Effect of sonication and combination with alkaline hydrolysis (sonicated alkaline hydrolysis)	78
3.3.6. Optimization of the sonicated alkaline treatment of the residue.....	79
3.3.7. Solid phase extraction (SPE)	79
3.3.8. Identification of compounds using U(H)PLC-ESI-MS and quantification by U(H)PLC-DAD	80
3.3.9. Statistical Analysis	80
3.4. RESULTS AND DISCUSSION.....	81
3.5. CONCLUSIONS	87

**CHAPTER 4: LIQUID CHROMATOGRAPHY – MASS SPECTROMETRY COUPLED
WITH MULTIVARIATE ANALYSIS FOR THE CHARACTERIZATION AND**

DISCRIMINATION OF EXTRACTABLE AND NONEXTRACTABLE POLYPHENOLS AND GLUCOSINOLATES FROM RED CABBAGE AND BRUSSELS SPROUTS WASTE

STREAMS.....	91
4.1. ABSTRACT	91
4.2. INTRODUCTION	92
4.3. MATERIALS AND METHODS.....	92
4.3.1. <i>Reagents and plant material</i>	92
4.3.2. <i>Solvent extraction of EP and collection of residues containing NEP</i>	93
4.3.3. <i>Measurement of total phenolic content (TPC)</i>	93
4.3.4. <i>Sonicated alkaline hydrolysis of the residue left after solvent extraction</i>	93
4.3.5. <i>Solid phase extraction (SPE)</i>	94
4.3.6. <i>Identification of compounds using U(H)PLC-ESI-MS</i>	94
4.3.7. <i>Data analysis</i>	94
4.4. RESULTS AND DISCUSSION	94
4.4.1. <i>Optimization of the release of NEP from the residue of solvent extraction</i> ...	94
4.4.2. <i>Characterization of phenolic compounds</i>	96
4.4.2.1. <i>Flavonoid glycosides</i>	101
4.4.2.2. <i>Phenolic acid glycosides</i>	102
4.4.2.3. <i>Anthocyanins</i>	102
4.4.2.4. <i>Glucosinolates</i>	103
4.4.3. MULTIVARIATE ANALYSIS OF THE POLYPHENOLIC PROFILE OF THE DIFFERENT PLANT MATERIALS.....	103
4.4.3.1. <i>Brussels sprouts</i>	103
4.4.3.2. <i>Red cabbage</i>	106
4.5. CONCLUSION.....	109

CHAPTER 5: USE OF METABOLOMICS AND FLUORESCENCE RECOVERY AFTER PHOTBLEACHING TO STUDY THE *IN VITRO* INTESTINAL TRANSPORT AND INTESTINAL MUCUS DIFFUSION OF POLYPHENOLS FROM CAULIFLOWER WASTE

.....	113
5.1. ABSTRACT	113
5.2. INTRODUCTION	114
5.3. MATERIALS AND METHODS	115
5.3.1. <i>Materials</i>	115
5.3.2. <i>Extraction of Brassica oleracea polyphenols</i>	116
5.3.3. <i>Simulated in vitro digestion</i>	116
5.3.4. <i>Measurement of total phenolic content (TPC)</i>	116
5.3.5. <i>Cell culture</i>	117
5.3.6. <i>Transepithelial transport experiment</i>	117
5.3.7. <i>UPLC-MS analysis</i>	118
5.3.8. <i>Porcine small intestinal mucus collection and preparation</i>	118
5.3.9. <i>Polyphenol diffusion and recovery through intestinal mucus using fluorescence recovery after photobleaching (FRAP)</i>	118
5.3.10. <i>Effect of cauliflower waste polyphenols on the biophysical properties of intestinal mucus</i>	119
5.3.10.1. <i>Particle tracking microrheology</i>	119
5.3.10.1. <i>Bulk rheology</i>	120
5.3.11. <i>Data analysis</i>	120

5.4.	RESULTS AND DISCUSSION.....	121
5.4.1.	<i>Total phenolic content during in vitro digestion</i>	121
5.4.2.	<i>Changes in the phenolic profile during in vitro digestion</i>	122
5.4.3.	<i>Mucosal diffusion of polyphenols using FRAP</i>	127
5.4.4.	<i>Effect of polyphenols on the biophysical properties of ex vivo porcine mucus</i> 128	
5.4.5.	<i>Caco-2 transport experiments</i>	129
5.5.	CONCLUSIONS.....	132

CHAPTER 6: 2 AND 3D QUANTITATIVE STRUCTURE-PERMEABILITY RELATIONSHIP OF FLAVONOIDS IN CACO-2 CELLS USING STEPWISE MULTIPLE LINEAR REGRESSION (SMLR), PARTIAL LEAST SQUARES REGRESSION (PLSR), AND PHARMACOPHORE (GALAHAD)-BASED COMPARATIVE MOLECULAR SIMILARITY INDEX ANALYSIS (COMSIA)..... 135

6.1.	ABSTRACT.....	135
6.2.	INTRODUCTION.....	136
6.3.	MATERIALS AND METHODS.....	137
6.3.1.	<i>Data collection</i>	137
6.3.2.	<i>2D Quantitative-structure activity relationship (QSPR)</i>	139
6.3.3.	<i>3D Quantitative-structure activity relationship</i>	139
6.3.3.1.	Pharmacophore alignment.....	139
6.3.3.2.	COMSIA studies.....	140
6.3.3.3.	ADMET prediction using commercial application.....	140
6.4.	RESULTS AND DISCUSSION.....	140
6.4.1.	<i>2D QSPR using stepwise multiple linear regression</i>	140
6.4.2.	<i>2D QSPR using partial least squares regression</i>	142
6.4.3.	<i>Pharmacophore (GALAHAD)-based 3D QSPR (COMSIA)</i>	143
6.4.3.1.	Pharmacophore alignment.....	143
6.4.3.2.	COMSIA analysis.....	144
6.4.4.	<i>ADMET prediction</i>	148
6.5.	CONCLUSION.....	149

CHAPTER 7: QUERCETIN MITIGATES VALINOMYCIN-INDUCED CELLULAR STRESS VIA STRESS-INDUCED METABOLISM AND CELL UPTAKE 153

7.1.	ABSTRACT.....	153
7.2.	INTRODUCTION.....	154
7.3.	<i>Materials and methods</i>	155
7.3.1.	Materials.....	155
7.3.2.	Cell culture.....	155
7.3.3.	Effect of quercetin and valinomycin treatments on cellular stress.....	155
7.3.4.	Flow cytometric analysis.....	156
7.3.5.	LC-MS analysis.....	157
7.3.6.	Cellular flavonoid localization.....	157
7.4.	RESULTS AND DISCUSSION.....	158
7.4.1.	<i>Effect of quercetin and valinomycin treatments on cellular viability</i>	158
7.4.2.	<i>Quercetin metabolism and intracellular accumulation</i>	160
7.4.3.	<i>Flavonoid intracellular location</i>	163
7.5.	CONCLUSIONS.....	166

CHAPTER 8. COLLISION CROSS SECTION PREDICTION OF DEPROTONATED PHENOLICS IN A TRAVELLING-WAVE ION MOBILITY SPECTROMETER USING MOLECULAR DESCRIPTORS AND CHEMOMETRICS.....	171
8.1. ABSTRACT	171
8.2. INTRODUCTION	172
8.3. MATERIALS AND METHODS.....	174
8.3.1. <i>Chemical reagents</i>	174
8.3.2. <i>Collision cross section (CCS) measurement in TWIMS</i>	174
8.3.3. <i>Collision cross section prediction</i>	175
8.4. RESULTS AND DISCUSSION.....	176
8.4.1. <i>Measurement of the CCS in negative mode</i>	176
8.4.2. <i>Molecular descriptors and fscaret feature selection</i>	179
8.4.3. <i>Collision cross section prediction using chemometric tools</i>	180
8.4.3.1. SMLR.....	182
8.4.3.2. PCR and PLS.....	183
8.4.4. <i>Comparison of the different models with mobcal (N₂)</i>	187
8.5. CONCLUSIONS	189
CHAPTER 9: GENERAL DISCUSSION, CONCLUSIONS AND FUTURE PERSPECTIVES	195
9.1. STRUCTURAL CHARACTERIZATION OF FLAVONOIDS.....	196
9.2. GETTING MORE OUT OF AGRO-INDUSTRIAL BY-PRODUCTS: THERE'S MORE IN WASTE THAN INITIALLY THOUGHT	197
9.3. INTESTINAL TRANSPORT OF FLAVONOID GLYCOSIDES.....	198
9.4. DISADVANTAGES OF CURRENT <i>IN VITRO</i> MODELS FOR INTESTINAL ABSORPTION	201
9.4.1. <i>Lack of β-glucosidases in current in vitro intestinal models</i>	201
9.4.2. <i>Intestinal mucus layer: a missing link in the study of flavonoid bioavailability</i> 201	
9.5. CELLULAR BIOACTIVITY AND THE ROLE OF LOCAL CONCENTRATION	205
9.6. TOWARDS BETTER METABOLITE IDENTIFICATION USING ION MOBILITY SPECTROMETRY.....	207
9.7. GENERALIZATION	209
REFERENCES	213
CURRICULUM VITAE.....	235

List of abbreviations

MS	Mass spectrometry
HPLC	High performance liquid chromatography
U(H)PLC	Ultra-high performance liquid chromatography
ESI	Electrospray ionization
HDMS	High definition mass spectrometry
IMS	Ion mobility separation/spectrometry
MS ⁿ	Multistage fragmentation
TOF	Time-of-flight
CID	Collision-induced dissociation
SAR	Structure-activity relationship
QSAR	Quantitative structure activity relationship
ABC	ATP-binding cassette
P-gP	P-glycoprotein
BCRP	Breast cancer resistance protein
MRP	Multidrug resistance protein
GAE	Gallic acid equivalents
LOD	Limit of detection
LOQ	Limit of quantification
PCA	Principal components analysis
OPLS-DA	Orthogonal partial least squares – discriminant analysis
SPE	Solid phase extraction
TPC	Total phenolic content
EP	Extractable phenolics
NEP	Nonextractable phenolics
FRAP	Fluorescence recovery after photobleaching
SMLR	Stepwise multiple linear regression
MTT	3-(4,5-dimethylthiazol-2-yl)-2,5-diphenyltetrazolium bromide
SRB	Sulforhodamine B
ROS	Reactive oxygen species
ppm	Parts per million
CCS	Collision cross section
PCR	Principal components regression

RESEARCH FRAMEWORK AND OBJECTIVES

Flavonoids are plant metabolites that belong to a diverse group of polyphenols. Interest towards flavonoid studies has been fueled by the increasing evidence of their health-promoting benefits over recent years. However, understanding their bioactivity entails detailed analysis on their structure, metabolism, bioavailability, and mechanism of action. The initial step in this undertaking is the full characterization of the flavonoids found in the plant material being studied. Recently, the surge in the improvement of instrumentation, especially with high resolution mass spectrometry, has elevated our current analytical capabilities enabling us to perform more accurate, robust, and even multi-targeted analyses contrary to conventional techniques with low analytical specificity. This capacity is even more improved with the use of computational techniques that provide additional information on molecular structure and changes in the polyphenolic profile of different matrices. High resolution mass spectrometry and its associated computational techniques have therefore been major analytical tools in the analysis of flavonoids from plant matrices. Also, these techniques have contributed much in the field of bioanalysis. More importantly, these techniques allowed us to investigate the survival of flavonoids after digestion and intestinal absorption. Recently, computational techniques are also used as a tool for confident metabolite identification.

Although the use of human and/or animal subjects provide the best picture on the role of flavonoids on health, this approach is mired with ethical issues, high costs, and very high variability in the obtained results. Recently, various *in vitro* and *in silico* approaches have been developed to simulate the *in vivo* situation, which also provide substantial and significant information that corroborates with the results of *in vivo* studies. Thus, use of high performance analytical techniques together with *in vitro* and *in silico* models in the study of flavonoids may provide novel insights into their bioavailability and bioactivity.

Vegetables belonging to the *Brassica* family have long been reported to contain a wide array of bioactive polyphenols, especially flavonoids. Numerous researches have been devoted on the quantification and characterization of the flavonoid content of the edible fraction of these vegetables. However, much of plant material is actually thrown away as waste during harvest, which also contains large amounts of flavonoids. Thus, this rich source of valuable polyphenols remains underutilized. Valorization of *Brassica* waste may therefore provide a new source of potential bioactive ingredients which could be used in the development of functional food products.

Consequently, this PhD has been undertaken to determine the potential of *Brassica*, more specifically cauliflower waste, as a new source of bioactive flavonoids. To attain this objective, the use of high definition mass spectrometry in combination with *in vitro*, *ex vivo* and *in silico* models to study flavonoid composition, bioavailability and bioactivity was investigated. Also, the use of an emerging technology, ion mobility spectrometry, for the improvement of metabolite identification was explored.

Therefore, the objectives of this PhD are the following:

1. Develop a method for the structural characterization of flavonoids using ultraperformance liquid chromatography-electrospray ionization – ion mobility spectrometry – high definition mass spectrometry (MS^E) **(Chapter 2)**
2. Analyze and distinguish the extractable and nonextractable polyphenolic fractions of *Brassica* waste samples using an improved extraction method and multivariate analysis **(Chapters 3 & 4)**
3. Investigate the bioavailability and intestinal mucus diffusion of flavonoid glycosides isolated from cauliflower waste using metabolomics and microscopy techniques **(Chapter 5)**
4. Determine the structural requirements of flavonoids necessary to allow intestinal transport **(Chapter 6)**
5. Investigate the bioactivity of flavonoids against valinomycin-induced toxicity in Caco-2 cells **(Chapter 7)**
6. Investigate the use of ion mobility for improved metabolite identification using computational techniques **(Chapter 8)**

The schematic outline of this PhD thesis is presented in Figure 1.

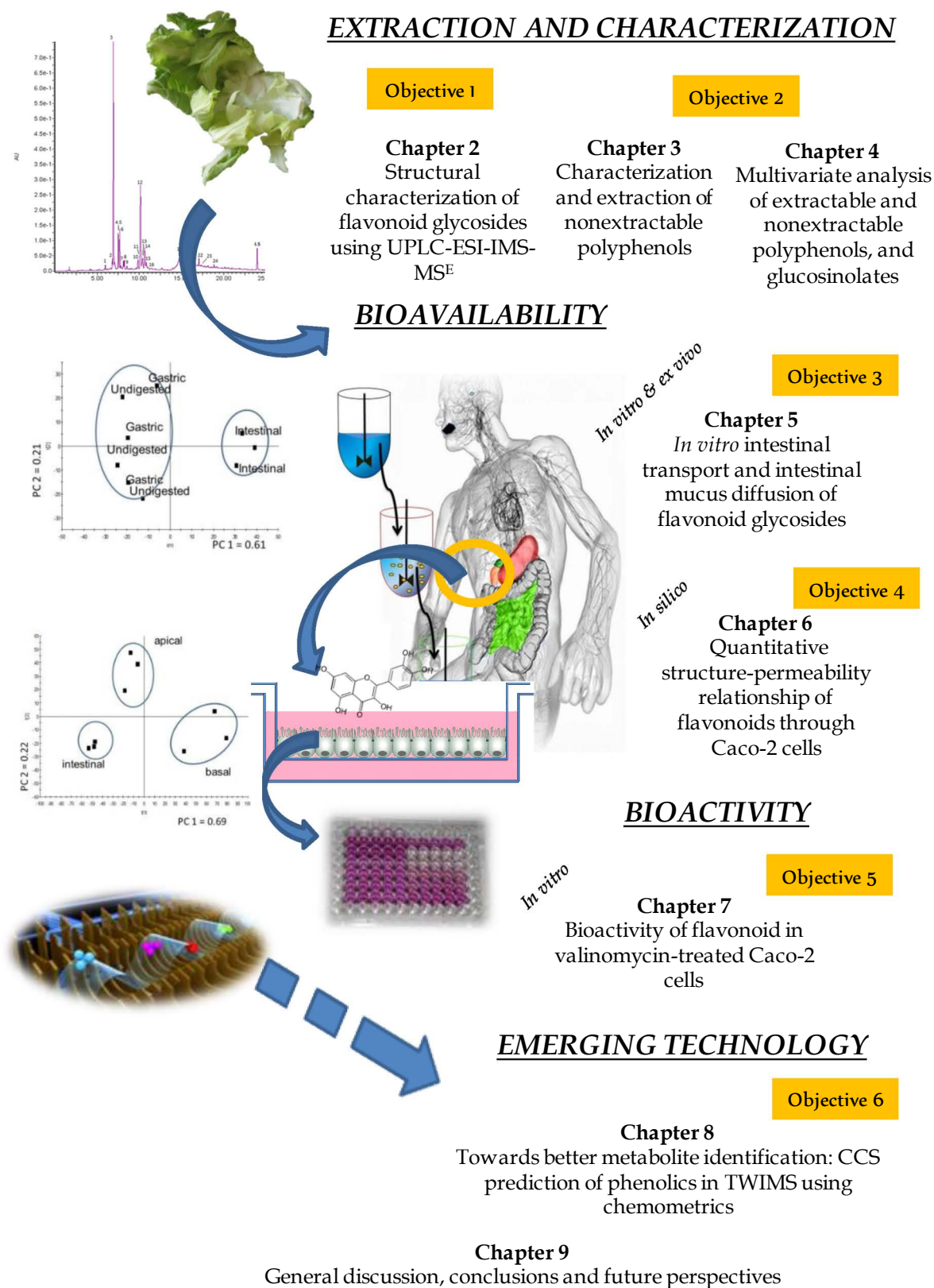


Figure 1. Schematic outline of this PhD research

SUMMARY

This PhD thesis aimed to develop mass spectrometric techniques to study the characterization, *in vitro* bioavailability and bioactivity of flavonoids. The investigated flavonoids were obtained from an underutilized source, the agro-industrial waste stream of *Brassica*, which was previously reported to be a source of flavonoids. Thus, this PhD also indirectly aimed to add value and valorize these waste products as potential sources of bioactive molecules.

To achieve these goals, seven (7) different experiments (**chapters 2-8**) were conducted to (1) characterize the flavonoid composition of the *Brassica* waste stream, (2) optimize the methods to increase flavonoid extraction yield, (3) investigate the *in vitro* bioavailability of the extracted flavonoids, (4) predict the intestinal absorption potential of the flavonoids, (5) study the mechanism of its bioactivity, and (6) explore emerging technologies to develop better metabolite identification strategies.

In **Chapter 1**, an exhaustive review on the literature regarding flavonoids is given. The structures of the different kinds of flavonoids are initially described. Then, various mass spectrometric techniques to quantify and structurally characterize flavonoids are presented. To better understand the bioavailability and bioanalytical challenges of flavonoids, a review about the interactions of flavonoids with various enzymes, food constituents, and transporters during digestion, absorption, distribution and metabolism is presented. Here, such interactions are presented in a structure-property relationship perspective to better understand the role of flavonoid structure on their bioavailability and bioactivity. Lastly, the use of cell cultures to simulate intestinal absorption is described as well as the metabolic fates of flavonoids during cellular metabolism.

Chapter 2 describes a rapid and reliable method for structural characterization of flavonoid glycosides from cauliflower waste. Conventionally, flavonoid glycosides are analyzed using multi-stage mass spectrometric techniques, which are time consuming and normally require inputs from the operator. In this chapter, we show the advantage of using MS^E, a data-independent strategy that operates in simultaneous alternating low and high collision energies to provide both precursor and product ions in a single chromatographic run. Further, ion mobility spectrometry (IMS) was enabled to increase peak capacity and ensure the correct structural identification of the flavonoid glycosides. Using this technique, 19 flavonoid glycosides were annotated in a single injection without the need of manual intervention. The MS^E technique developed herein was then used for the structural characterization of flavonoids for all the succeeding chapters.

Polyphenol analysis is usually conducted on plant extracts obtained from conventional solvent extraction methods. **Chapter 3** reports that more than half of the total polyphenols in the cauliflower waste are unreported since conventional solvent extraction methods miss out a large pool of nonextractable polyphenols. Nonextractable polyphenols are bound to the plant matrix by physical entrapment or by ester linkages. In this chapter, we report the use of ultrasound-assisted extraction combined with alkaline hydrolysis to release the nonextractable polyphenols from the residue left after conventional solvent extraction. After optimization, the highest polyphenol yield was obtained after treating the residues with 2M NaOH at 60°C for 30 minutes of sonication. The nonextractable fraction contained more than double the amount of polyphenols than in the extractable fraction. The polyphenols in the nonextractable fraction were identified as flavonoid glycosides and phenolic acids using UPLC-ESI-MS^E. **Chapter 4** on the other hand describes the use of multivariate analysis to distinguish the polyphenolic and glucosinolate profiles of the extractable fraction versus the nonextractable fraction of Brussels sprouts and red cabbage. It was found that different polyphenols reside in either fraction and the profiles in various parts of the plant may also be different. Like in the previous chapter, the polyphenolic content of the nonextractable fractions of these plants exceeds that of the extractable fraction, which therefore highlights the need to analyze both fractions when reporting the total phenolic content of plant matrices. This study also shows that different extraction methods may influence the type of polyphenols extracted.

After a detailed characterization of the flavonoid composition of the cauliflower waste extract, it is then essential to know whether these flavonoids survive gastric and intestinal digestion. **Chapter 5** details the use of metabolomics to study the *in vitro* intestinal transport of flavonoid glycosides from cauliflower waste using simulated gastrointestinal digestion and Caco-2 cell transport models. Also, the ability of these compounds to diffuse through the intestinal mucus layer was investigated using fluorescence recovery after photobleaching microscopic technique in *ex vivo* porcine intestinal mucus. Flavonoid glycosides are stable under gastrointestinal digestion conditions and diffuse efficiently through the mucus layer to reach the epithelial surface. However, almost no absorption of intact flavonoid glycosides was detected. The inability of the Caco-2 cells to release β -glucosidases to release the flavonoid aglycone is a major drawback of this *in vitro* model. *In vivo*, the epithelium cleaves the glycoside moiety and releases the aglycone, which may be metabolized, effluxed or transported.

Chapter 6 provides a computational analysis on the structural requirements needed for flavonoid Caco-2 transport. A structure-Caco-2 permeability model was developed using

stepwise multiple linear regression (SMLR), partial least squares regression (PLSR) and a pharmacophore (GALAHAD)-based comparative molecular field analysis (COMFA). A robust 3D model with high predictive ability ($R^2_{\text{training}} = 0.96$, $R^2_{\text{test}} = 0.95$, $q^2 = 0.625$) was developed and used to describe the structural features necessary for Caco-2 cell transport. According to the model, flavonoid structure, especially hydrophobicity and the location of hydrogen bond acceptors and donors, greatly influences their transportability. The hydrophilic nature of flavonoid glycosides is the key reason for their inability to be transported intact by the Caco-2 cells, as observed in the previous chapter.

Flavonoids undergo extensive phase I and II metabolism as well as efflux by intestinal cells, as detailed in chapter 1. In **Chapter 7**, the bioactivity of flavonoids against valinomycin-induced stress in Caco-2 cells was investigated. Here, we used quercetin, a flavonoid found in *Brassica* waste, as a representative/model of flavonoids. Quercetin was metabolized into methyl, sulfate and glucuronide derivatives, which were mostly effluxed out of the cells. However, quercetin and one of the three methyl-quercetin isomers were found to remain in/on the cell. Without valinomycin, quercetin and methyl-quercetin are localized on the cell membrane but were found to have penetrated throughout the cytoplasm upon co-administration with valinomycin. Also, the amount of methyl-quercetin accumulated in the cells significantly increased upon co-administration with valinomycin. This change in localization and increase in methyl-quercetin accumulation reduced the levels of intracellular reactive oxygen species caused by valinomycin. This provides a novel mechanism on the mode of action of quercetin metabolites upon cellular stress caused by valinomycin.

The success of unraveling the metabolic fates of flavonoids rests on the confident identification of these metabolites. Although the MS^E technique developed in Chapter 2 could be used for the rapid characterization of flavonoid-*O*-glycosides, especially if the glycosylation occurs at the C3 and C7 positions, this method is unable to elucidate the exact glycosylation point of *C*-glycosides and *O*-glycosylation at the B-ring. Also, certain isomers, such as catechin and epicatechin are difficult to distinguish since they produce similar MS/MS spectra. Recently, IMS has received immense amount of attention in the literature due to its ability to distinguish isomers, and thus its ability to predict glycosylation or metabolic conjugation site. This is because different molecules with the same mass but differing in 3D conformation could be separated by their collision cross sections (CCS) in the IMS. Thus, the ability to predict the CCS of a molecule could aid in the correct identification of metabolites. Currently, the most popular method to predict CCS uses an atomistic approach which is highly computationally expensive and inefficient. In **Chapter 8**, a highly predictive yet highly efficient method for predicting

CCS has been developed using molecular descriptors and chemometrics. The CCS of phenolics, including flavonoids, was predicted without the need for a hypercomputing facility but still at the same level of predictive ability. This method is therefore more suited for routine analysis and is easier to integrate to metabolite identification platforms.

Finally, **Chapter 9** presents the general discussions and conclusion, as well as the future perspectives in the use of mass spectrometry for flavonoid research and the gaps in our current knowledge in understanding flavonoid bioavailability and bioactivity.

SAMENVATTING

In dit doctoraatsonderzoek werden massaspectrometrische methoden geoptimaliseerd voor de karakterisatie van flavonoïden, alsook voor het meten en evalueren van hun *in vitro* biobeschikbaarheid en bioactiviteit. De onderzochte flavonoïden werden verkregen uit een onvoldoende gevaloriseerde agro-industriële nevenstroom van *Brassica*, die reeds eerder bekend stond als belangrijke bron van flavonoïden. Op indirecte wijze tracht dit doctoraatsonderzoek dus ook een toegevoegde waarde te creëren voor deze nevenstromen alsook hun valorisatie te stimuleren als potentiële bronnen van bioactieve moleculen.

Om deze doelstellingen te bereiken werden zeven (7) verschillende experimenten (**hoofdstukken 2-8**) uitgevoerd met name (1) de karakterisatie van de flavonoïden samenstelling van de *Brassica* nevenstroom, (2) optimalisatie van methoden ter verhoging van het extractierendement van flavonoïden, (3) onderzoek naar de *in vitro* biobeschikbaarheid van de geëxtraheerde flavonoïden, (4) voorspellen van het potentieel voor intestinale absorptie van flavonoïden, (5) onderzoek naar het mechanisme van hun bioactiviteit, en (6) exploreren van verbeterde identificatiestrategieën voor metabolieten.

In **Hoofdstuk 1** wordt een literatuuroverzicht rond flavonoïden gegeven. De structuren van de verschillende soorten flavonoïden worden initieel beschreven. Vervolgens worden verschillende massaspectrometrische technieken voorgesteld voor de kwantificatie en structurele karakterisatie van flavonoïden. Om de biobeschikbaarheid en bioanalytische uitdagingen van flavonoïden beter te begrijpen, wordt in het literatuuroverzicht aandacht besteed aan interacties van flavonoïden met verschillende enzymen, voedingscomponenten, en transportmechanismen tijdens vertering, absorptie, distributie en metabolisme. Deze interacties worden besproken in relatie tot hun structuur-eigenschap relatie om zo de invloed van de structuur van flavonoïden op hun biobeschikbaarheid en bioactiviteit beter te begrijpen. Tot slot werd ook het gebruik van celculturen voor simulatie van intestinale absorptie alsook de conversie van flavonoïden tijdens het cellulair metabolisme beschreven.

Hoofdstuk 2 bespreekt een snelle en betrouwbare methode voor de structurele karakterisatie van flavonoïdeglycosiden aanwezig in *Brassica* nevenstromen. Conventioneel worden flavonoïdeglycosiden geanalyseerd met multi-trap massa spectrometrische methoden. Deze zijn tamelijk tijdsintensief en vragen input van de operator. In dit hoofdstuk tonen we het voordeel van het gebruik van MS^E, een data-onafhankelijke strategie die gebruik maakt van simultaan alterneren van lage en hoge

botsingsenergie om zowel precursor en productionen te genereren in één enkele chromatografische analyse. Door gebruik te maken van ionen mobiliteitschromatografie (IMS) werd de piekcapaciteit verhoogd en kon hierdoor het correct structureel identificeren van flavonoïdeglycosiden worden verzekerd. Met deze techniek werden 19 flavonoïde glycosiden geïdentificeerd in één enkele injectie zonder manuele interventie. De MS^E techniek die hier werd ontwikkeld kon dan worden gebruikt voor het ophelderen van de flavonoïdestructuur in alle verdere hoofdstukken.

Analyse van polyfenolen wordt gewoonlijk uitgevoerd op plantenextracten bekomen met conventionele solvent extractiemethoden. **Hoofdstuk 3** toont aan dat meer dan de helft van de totale hoeveelheid polyfenolen in een nevenstroom van bloemkool (*Brassica*) niet gerapporteerd worden gezien conventionele solvent extractiemethoden ongeschikt zijn voor extractie van een groot deel van de niet-extraheerbare polyfenolen. Deze laatste zijn gebonden aan de plantmatrix door fysische insluiting of door esterbindingen. In dit hoofdstuk rapporteren we het gebruik van ultrasoon extractive gelinkt met alkalische hydrolyse voor het vrijstellen van niet-extraheerbare polyphenolen uit het residu bekomen na conventionele solvent extractie. Na optimalisatie werd de hoogste opbrengst aan polyfenolen bekomen na behandeling van de residu's met 2M NaOH bij 60°C voor 30 minutes sonicatie. De niet-extraheerbare fractie bevatte meer dan het dubbele van de hoeveelheid aan polyfenolen gevonden in de extraheerbare fractie. De polyfenolen in de niet-extraheerbare fractie werden geïdentificeerd als flavonoïdeglycosiden en fenolische zuren op basis van UPLC-ESI-MS^E analyse. **Hoofdstuk 4** beschrijft het gebruik van multivariate data-analyse om het profiel van polyfenolen en glucosinolaten in de extraheerbare fractie te vergelijken met deze van de niet-extraheerbare fractie in spruiten en rode kool. Verschillende types polyfenolen werden weergevonden in beide fracties en bovendien waren er ook verschillen alnaarlang het plantendeel (bladeren tov stengels). Net zoals in hoofdstuk 3 blijkt het gehalte polyfenolen in de niet-extraheerbare fractie van deze planten groter te zijn dan deze in de extraheerbare fractie, wat aantoonst dat beide fracties belangrijk zijn om een volledig beeld te vormen van het total polyfenolgehalte in de plant. Deze studie toont ook aan dat verschillende extractiemethoden het type geëxtraheerde polyfenolen kunnen beïnvloeden.

Na een gedetailleerde karakterisatie van de samenstelling aan flavonoïden in de extracten van *Brassica* nevenstromen, is het belangrijk inzicht te krijgen of deze flavonoïden stabiel zijn tijdens gastro-intestinale vertering. **Hoofdstuk 5** maakt gebruik van metabolomics om de *in vitro* intestinaal transport van flavonoïdeglycosiden uit bloemkool nevenstromen te bestuderen, gebruik makende van gesimuleerde *in vitro* gastro-intestinale vertering en Caco-2 cel transport modellen. Daarnaast wordt, gebruik

makende van FRAP (fluorescence recovery after photobleaching) microscopie in *ex vivo* intestinale mucus van het varken, nagegaan of deze flavonoïde componenten doorheen een intestinale mucuslaag kunnen diffunderen. Flavonoïdeglycosiden zijn stabiel tijdens gastro-intestinale vertering en diffunderen efficiënt doorheen de mucuslaag om uiteindelijk het epithelium te bereiken. Er werd echter zo goed als geen absorptie van intacte flavonoïdeglycosiden gedetecteerd. Caco-2 cellen hebben geen mogelijkheid om β -glucosidasen te produceren wat essentieel is om flavonoïde aglyconen vrij te stellen. Dit is een belangrijk nadeel van het gebruikte *in vitro* model. Tijdens *in vivo* omstandigheden, zal het epithelium de glycosidegroep afsplitsen en het aglycon vrijstellen, wat op zijn beurt kan worden gemetaboliseerd, geëfluxed of getransporteerd.

Hoofdstuk 6 geeft een computationele analyse van de structurele noden voor Caco-2 transport van flavonoïden. Een structuur-Caco-2 permeabiliteitsmodel werd ontwikkeld op basis van stapsgewijze multiple lineaire regressie (SMLR), partial least squares regressie (PLSR) en een pharmacophore (GALAHAD)-based comparative molecular field analyse (COMFA). Een robuust 3D model met hoge voorspellende waarde ($R^2_{\text{training}} = 0.96$, $R^2_{\text{test}} = 0.95$, $q^2 = 0.625$) werd ontwikkeld en gebruikt om de structurele kenmerken nodig om Caco-2 cel transport te voorspellen. Volgens dit model beïnvloeden de flavonoïdestructuur, vooral de hydrophobiciteit en de locatie van de H-brug acceptoren en donoren, de transporteerbaarheid van de flavonoïden. Het hydrofiel karakter van de flavonoïdeglycosiden is de voornaamste reden waarom zij niet intact door Caco-2 cellen kunnen getransporteerd worden, zoals werd bevestigd in hoofdstuk 5.

Flavonoïden ondergaan uitvoerig fase I en II metabolisme net als efflux door intestinale cellen, zoals beschreven in hoofdstuk 1. In **hoofdstuk 7** wordt de bioactiviteit van flavonoïden onder invloed van valinomycine-geïnduceerde stress in Caco-2 cells onderzocht. Er werd gewerkt met quercetine, een flavonoïde aanwezig in *Brassica* nevenstromen, als representatief model voor flavonoïden. Quercetine werd gemetaboliseerd tot methyl, sulfaat en glucuronide derivaten, die grotendeels verwijderd worden uit de cel. Echter, quercetine en één van de drie methyl-quercetine isomeren bleven in de cel of verbonden met de cel. Zonder aanwezigheid van valinomycine, zijn quercetine en methyl-quercetine gelocaliseerd op de celmembraan maar na co-administratie van valinomycine penetreren deze tot in het cytoplasma. De hoeveelheid methyl-quercetine geaccumuleerd in de cellen blijkt tevens significant verhoogd te zijn na co-administratie van valinomycine. Door verandering van lokalisatie en toename van methyl-quercetine accumulatie daalde het gehalte aan intracellulaire reactieve zuurstof moleculen geïnduceerd door valinomycine. Dit geeft een nieuw mechanisme waarmee quercetine metabolieten cellulaire stress veroorzaakt door valinomycine kunnen verlagen.

Het al of niet succesvol ontrafelen van het metabolisme van flavonoïden, hangt in belangrijke mate af van een voldoende betrouwbare identificatie van de gevormde metabolieten tijdens het metabolisme. Ondanks dat de MS^E techniek ontwikkeld in hoofdstuk 2 gebruikt kan worden voor de snelle karakterisatie van flavonoïde-*O*-glycosiden, vooral als de glycosylatie gebeurt aan de C3 en C7 posities, is deze methode niet geschikt om de exacte glycosylatieplaats van *C*-glycosiden en *O*-glycosylatie aan de B-ring te achterhalen. Daarnaast blijken sommige isomeren, zoals catechine en epicatechine, moeilijk te onderscheiden omwille van hun gelijkaardige MS/MS spectra. Vrij recent kreeg IMS veel aandacht in de literatuur gezien hier wel de mogelijkheid bestaat om isomeren van elkaar te onderscheiden, en dus ook de kans om de glycosylatie en metabolische conjugatieplaats beter te voorspellen. Dit omwille van het feit dat verschillende moleculen met dezelfde massa maar met verschillen in 3D structuur gescheiden kunnen worden via collision cross sections (CCS) in de IMS. Bijgevolg kan de mogelijkheid om de CCS van een molecule te voorspellen helpen in de correcte identificatie van de metabolieten. De meest populaire methode op dit moment om CCS te voorspellen maakt gebruik van een atomische benadering die tegelijkertijd dure investering vraagt in apparatuur (computers) vraagt alsook inefficiënt werkt. In **hoofdstuk 8** werd een zeer predictieve en tegelijkertijd efficiënte methode voor het voorspellen van CCS ontwikkeld gebruik makende van molculaire descriptors en chemometrics. De CCS van polyfenolen, inclusief flavonoïden, werd voorspeld zonder gebruik te maken van complexe computerinfrastructuur maar nog steeds met dezelfde voorspellingsgraad. Deze method is daarom geschikt voor een meer routinematige analyse en is ook eenvoudiger om te integreren in metabolite identificatie platformen.

Tot slot wordt in **hoofdstuk 9** een algemene discussie en conclusie gepresenteerd, alsook enkele toekomstperspectieven in het gebruik van massaspectrometrie voor flavonoïde onderzoek om zo onze ontbrekende kennis omtrent het begrijpen van de biobeschikbaarheid en bioactiviteit van flavonoïden verder aan te vullen.

Chapter 1

Literature Review

Chapter 1. Literature Review

1.1. Flavonoids

Flavonoids are a large group of secondary plant metabolites, which typically consist of a 15-carbon skeleton consisting of 2 benzene rings attached via a heterocyclic pyrane ring, labeled as rings A, B and C, in a C₆-C₃-C₆ arrangement. Flavonoids occur either as glycosides, methylated derivatives, bio-conjugates after phase I/II metabolism or aglycones (the basic structure). The position of the B ring may be at the C₂-position in the case of most flavonoids or in the C₃-position in the case of isoflavones. Common hydroxylation points are at positions 5, 7 (A ring), 3', 4', 5' (B ring), 3 and 2 (C ring). Differences also depend on the presence of the C₂=C₃ double bond, and C₄-ketone moiety. Figure 1.1 shows the basic structures and common classes of flavonoids [1,2]. They are widely available in plant foods, such as *Brassica* vegetables, onions, fruits and its derivatives like wines and juices.

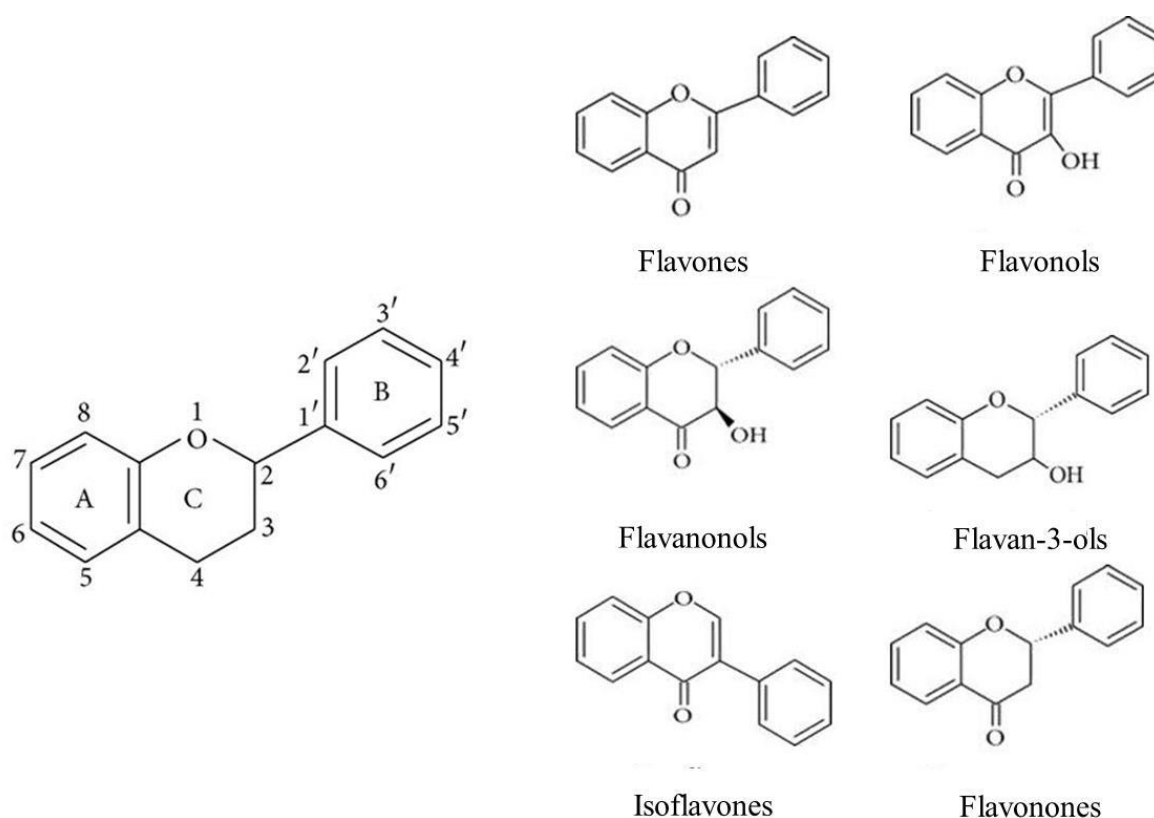


Figure 1.1. Basic structure of the common classes of flavonoids

Interest on flavonoids exists after they have been shown to exert a variety of biological activities, including anti-oxidative [3,4], anti-hypertensive [5,6], anti-obesity [7], anti-viral, hepatoprotective, and immune-regulatory activities [8]. Albeit their health-promoting benefits, their poor oral bioavailability has been regarded as a major hurdle in

using these compounds as health-promoting ingredients [9]. Generally, factors such as food matrix interactions, food processing, and host (human)-related factors (e.g. age, occurrence of certain diseases, lifestyle), and the flavonoids' chemical structure cause their poor oral bioavailability [10].

Over the past years, several techniques to characterize flavonoids from dietary sources and to elucidate their bioactive potential have been developed. The most promising tool for flavonoid characterization has been mass spectrometry coupled to chromatography, most especially liquid chromatography. Liquid chromatography-mass spectrometry (LC-MS) is commonly used for the identification and quantification of flavonoids from dietary sources as well as their metabolites after cellular metabolic transformations.

Metabolism of flavonoids on the other hand has been widely investigated using both *in vivo* and *in vitro* approaches. Various cells lines have been used to study the bioavailability and bioactivity of flavonoids, as well as their metabolic fates. In the following sections, recent developments in the use of mass spectrometry and cell-based techniques to study flavonoids and their *in vitro* bioavailability and bioactivity will be discussed in further detail.

1.2. Flavonoid analysis using liquid chromatography-mass spectrometry (LC-MS)

1.2.1. Separation of flavonoids in reversed-phase liquid chromatography

High Performance/Pressure Liquid chromatography (HPLC) has been extensively used for the separation of flavonoids prior to MS analysis. Of the various HPLC methods available, reversed-phase (RP) HPLC has been the most popular [11]. The name "reversed-phase" explains that the stationary phase is hydrophobic and the mobile phase is hydrophilic, which is reverse of the normal LC conditions, wherein the stationary phase is hydrophilic and the mobile phase is composed of (hydrophobic) organic solvents, such as hexane and ethyl acetate [12]. Flavonoid analysis is almost exclusively performed using RP-LC due to its suitability for the separation of flavonoids based on the nature of the aglycone (including the oxidation state, substitution patterns and stereochemistry), the nature and degree of glycosylation as well as the nature and degree of acylation [11].

Retention time in RP-HPLC is typically based on hydrophobicity, specifically the hydrophobic interaction of the flavonoid to the immobilized hydrophobic ligands attached to the stationary phase, i.e., C18 sorbent. The hydrogen bonding capacity of the flavonoid to the changing mobile phase composition (initially a highly aqueous solution

into a solution of high organic solvent concentration in a gradient elution) allows its partitioning from the sorbent to the mobile phase [11,13]. Thus, as the concentration of organic solvent in the elution gradient increases, different flavonoids exit from the LC column and are detected by detectors, usually a UV/Vis detector and/or a mass spectrometer. The flavonoids therefore elute in increasing order of hydrophobicity [11-13] and their hydrogen bonding capacity to the mobile phase [13]. Given this, the structure of the flavonoid and its conjugation conditions affect its separation within the RP-HPLC system.

Generally, flavonoids elute from RP-HPLC columns in the following sequence: flavanols<flavanones<flavonols<flavones (anthocyanins elute close to flavanols using mobile phases with neutral pH) [11]. The presence of a hydroxyl moiety (-OH) in the aglycone structure introduces a hydrogen bond donor/acceptor [13] and increases its polarity [14], which therefore decreases its hydrophobicity. Whereas, methylation (-CH₃) of these OH groups prevents their ability to form hydrogen bonds, and thus once again increases its hydrophobicity. Glycosylation on the other hand, not only reduced the hydrophobicity by adding a hydrophilic moiety, but also due to the addition of multiple hydrogen bonding donors/acceptors to the structure, which interacts better with the polar mobile phase [13]. Acylation of the glycosyl groups increase retention in the apolar sorbent relative to its corresponding glycosylated derivative [11]. Prenylation, which is the addition of a lipophilic moiety to the aglycone increases overall hydrophobicity of the flavonoid [14]. The combination of these modifications (glycosylation, methylation and prenylation) and differences in the aglycone structure result in a wide range of retention times for flavonoids in RP-HPLC analysis.

Recently, a quantitative structure-retention time relationship was developed to explain the effect of molecular structure on the retention of flavonoids in RP-HPLC using artificial neural networks. Akbar et al. [15] found a good relationship between the flavonoids' van der Waals volume, electronegativity, mass and polarizability and their retention times. On the other hand, using a similar approach, Lei et al. [14] found that the presence of a prenyl group at the C-3 position, the number of prenyl groups, log *P* values, the number of glycosyl groups and the glycosylation at the C-7 position are the main determinants of flavonoid retention times in a C18 column in an RP-HPLC analysis. Although it has been suggested that retention time prediction could be used to validate the identities of flavonoids not included in their database, it must be considered that retention time in HPLC analysis does not only depend on the analyte and the column but also on instrumental conditions, such as temperature, dead volume, condition (degradation) of the column, length of the column and connectors, and many others. Also, the predictive

errors of the developed models reached up to 1 minute, which in HPLC parlance is impractical. Therefore, the direct application of retention time prediction for metabolite identification may not be effective and/or useful strategy. Nonetheless, these models have enabled us to understand the effect of flavonoid structure on their separation in an RP-HPLC set-up.

A major advancement in HPLC technology came with the discovery that reducing the particle size of the packing material (sorbent) in an HPLC column highly improves its performance. The main principle of this improvement is governed by the van Deemter equation which confirms the relationship between linear velocity (flow rate) and plate height (column efficiency). In the equation, particle size of the columns plays a major role such that, as particle size decreases to less than 2 μm , a significant increase in efficiency, analysis time and peak capacity is attained [16]. With the introduction of columns packed with sub-2 μm particles, compared to the 3-5 μm particle size for conventional HPLC, great improvement in the analytical performance of LC systems was achieved [17]. However, using small particle sizes for packing HPLC columns results in higher back pressures of up to 1,200 bars compared to 600 bars in conventional HPLC systems. This technology has therefore been named (Ultra)High Pressure Chromatography or UPLC (a Waters trademark). As a consequence of the higher peak efficiency, the peaks are narrower/sharper and the limits of detection are lower, which makes UPLC more sensitive than conventional HPLC [18]. Therefore the coupling of UPLC to mass spectrometry provides a powerful tool for the analysis of flavonoids in complex matrices, such as food, biofluids, and cellular extracts.

1.2.2. Mass spectrometric analysis of flavonoids

After a successful separation of the flavonoids using liquid chromatography (LC), flavonoid quantification and structural elucidation could be done using mass spectrometry (MS). This coupling is often called LC-MS. LC-MS is rarely used for full structural characterization as NMR spectrometry is still the preferred method for this purpose. However, although NMR spectrometry has been proven to provide full structural characterization, even the stereochemistry of the analyte, LC-MS remains to be a more popular analytical technique due to its ease of operation, analytical speed and higher sensitivity. Also, NMR analysis requires more sample (compared to the sub-ppb levels reached by LC-MS) and only a few labs in the world have access to such high-end and expensive instrumentation [19,20].

The basic principle of MS is to generate ions in the gas phase, separate the ions based on their *mass-to-charge ratio* (m/z) and to detect them qualitatively and quantitatively by

their respective m/z and abundance [21]. Thus, the initial step in LC-MS analysis is to convert the solvent phase eluent of the LC into gas-phase ions to be introduced to the MS. This is achieved by ionization techniques. In its infancy, flavonoid ionization for MS analysis was achieved using fast atom bombardment technique. This ionization procedure involved the bombardment of flavonoids in solution with high energy atoms (argon or xenon) or cesium ions at energies of 8-30 keV at high temperature [22]. This caused the flavonoid analyte to fragment into gas phase ions while the solvent evaporates due to the high temperature. Yet, the application of MS in the analysis of flavonoids (and many other molecules) has tremendously increased with the introduction of "soft ionization" techniques. Of the various techniques, electrospray ionization (ESI) in negative mode has been the most popular ionization technique for most flavonoids since ionization efficiency is better than in the positive mode. Positive mode is especially important for naturally positively charged molecules such as anthocyanins [18]. This soft ionization technique also allowed the analyst to detect the intact flavonoid pseudomolecular ion in contrast to the earlier "hard" ionization techniques.

ESI ionization typically involves three steps, (1) dispersal of a fine spray of charged droplets, (2) solvent evaporation due to the high desolvation temperature, and (3) the ejection of charge molecules from the highly charged droplet, as depicted in Figure 1.2. Briefly, charged droplets are produced after passing a stream of analytes in solution (from LC) into the electrospray. Due to the high temperature in the source, these droplets reduce in size, and thus increase the charge density of the droplet. Finally, the electric field strength within the densely charged droplet reaches a critical point at which it is kinetically and energetically possible for ions at the surface of the droplet to be ejected into the gas phase [23]. Typical nomenclature for pseudomolecular ions in negative mode is $[M-H]^-$.

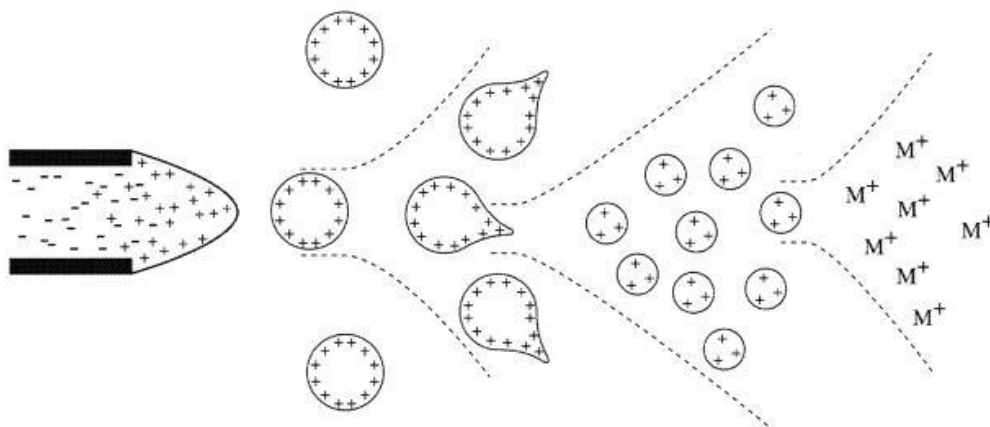


Figure 1.2. Mechanism of electrospray ionization (positive mode) [23]. For negative mode ionization, a negative charge is induced

In ESI-MS, the ion signal is proportional to the analyte concentration [23]. Therefore, for quantification of flavonoids, the ion signal is used to draw a calibration curve and to determine the concentration of the flavonoid in the solution. However, a critical issue in ESI is ion suppression, which results from the presence of less volatile compounds that can change the efficiency of droplet formation or droplet evaporation, which in turn affects the amount of charged ion in the gas phase that ultimately reaches the detector. It is caused by interfering compounds, such as salts, which could be present in the plant or biological matrix being analyzed [24]. To address this issue, good sample preparation techniques are a prerequisite, such as solid-phase extraction.

1.2.3. Tandem MS and collision induced dissociation (CID) for structural characterization

The use of high resolution MS has enabled us to measure the exact mass of flavonoids up to <1ppm from its true value. Therefore, mass information can be used to determine the identity of flavonoids. However, structural information is further enhanced by using tandem MS, of which collision induced dissociation (CID) has been proven to be the most important tool for the structural elucidation of flavonoid structure [18,22]. Tandem MS is the integration of 2 or more mass analyzers, and the ability to induce fragmentation of the ions to reveal structural clues. Mass analyzers such as triple-quadrupoles have been extensively used for this purpose. Also, analysis can be made using ion trap analyzers, which can perform multiple tandem MS experiments (MS^n) for enhanced structural characterization. With respect to flavonoid glycosides and other conjugates (such as phase I/II metabolites), tandem MS is able to obtain the following information: (1) molecular mass, (2) structure of the aglycone, (3) information about acylation of sugar hydroxyl groups and possible methylation and metabolic transformation of aglycone hydroxyls, (4) number of sugar attachments and their point of attachment to the aglycone structure.

1.2.3.1. Flavonoid-O-glycosides

Theoretically, glycosylation of flavonoids can occur at any of the hydroxyl groups of the aglycone structure, but certain positions are favored, such as the C-7 position for flavones, flavonols, flavanones, and isoflavones and C-3 position for flavonols. The differentiation of these positional glycosides can be achieved by analyzing their distinct fragmentation behavior in negative mode [19,25]. Cleavage at the glycosidic O-linkages leads to the elimination of monosaccharide residues for mono-O-glycosides, i.e., 162u (hexose), 146u (deoxyhexose), 132u (pentose) or 176u (uronic acid) [20]. Thus, monitoring the loss of monosaccharide masses from the precursor ion provides a clue on

the type of monosaccharide attached to the aglycone (Figure 1.3) However, it has been earlier reported that cleavage of a polysaccharide into sugar units does not occur in negative mode [26]. Therefore, a loss of a polysaccharide, which is a combination of masses of their individual sugar units, is possible. In positive ionization, where an inner sugar cleavage is possible [27], the loss of individual monosaccharides indicates the sequence of the monosaccharides that comprise the glycoside polymer.

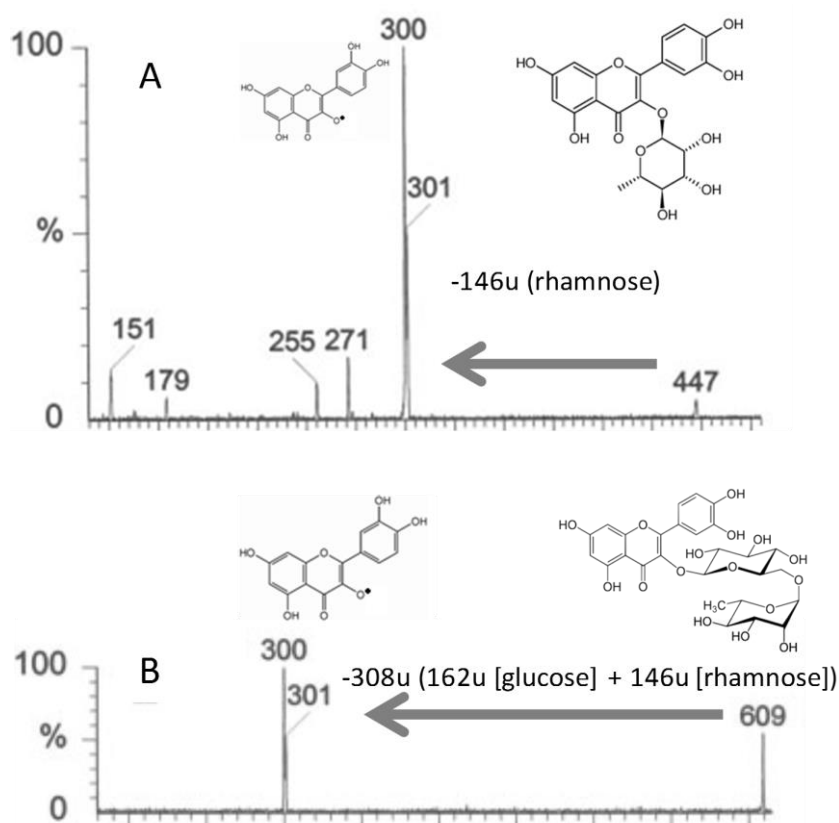


Figure 1.3. (A) Fragmentation of quercetin-3-O-rhamnoside during 40V CID. The loss of 146u signified that the quercetin aglycone had a deoxyhexose conjugate (rhamnose). (B) Fragmentation of rutin (quercetin-3-O-rhamnoglucoside) at 40V CID. The loss of a single disaccharide (rhamno-glucoside) is due to the absence of internal sugar cleavage.

Adapted from Hvattum and Ekeberg [28].

The attachment of the glycoside moiety can be deduced based on the spectra by observing the presence of a radical ion. Glycosides at the C-7 position typically produce $[M-H]^-$ ions, whereas C-3 glycosides produce a radical ion $[M-H]^{\bullet}$ due to the hemolytic cleavage of the O-glycosidic bond between the aglycone and the sugar moiety [19,20,28]. For di-O-glycosides, a higher abundance of the $[M-H]^-$, which corresponds to the C-7 glycoside fragment, is observed compared to the $[M-H]^{\bullet}$ ion, which is typically the C-3 glycoside fragment [25,28]. Figure 1.4 presents the fragmentation behavior of a

C-3 glycoside, C-7 glycoside and a di-O-glycoside, which is the basis for the identification of these flavonoids structures.

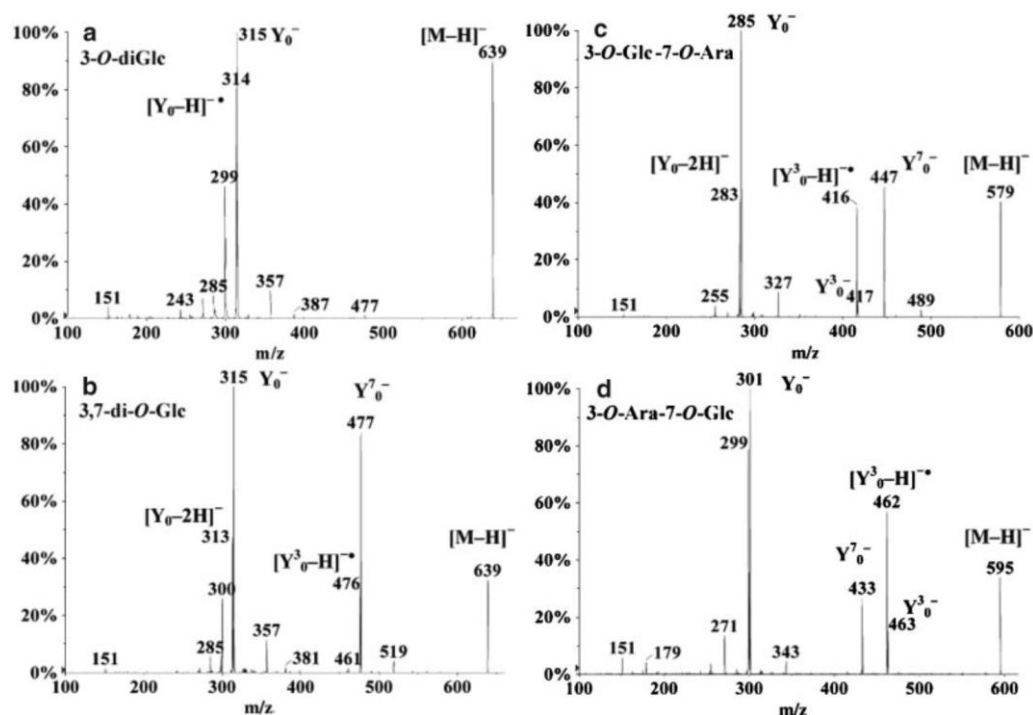


Figure 1.4. Differentiation of di-O-glycosides and O-diglycosides, as well as sugar distribution determination in case of 3,7-di-O-glycosides. Product ion spectra of deprotonated (a) isorhamnetin-3-O-glucoside, (b) isorhamnetin-3,7-di-O-glucoside, (c) kaempferol-3-O-glucoside-7-O-arabinoside, and (d) quercetin-3-O-arabinoside-7-O-glucoside [19,25].

Glycosylation at the B ring has also been reported, especially for onion quercetin glycosides. This method therefore cannot elucidate this structure and higher order fragmentation is required for the analysis of these structures.

1.2.3.2. Flavonoid-C-glycosides

In flavonoid-C-glycosides, the sugar moiety is directly attached to the aglycone backbone via an acid-resistant C-C bond. C-glycosylation has been exclusively found in the C6 or C8 positions. For negative mode analysis, C-glycosides can be detected by monitoring the glycosyl cross-ring cleavage leading to the loss of -120, -90 and -60 Da during CID. Structural characterization of C-glycosides remains difficult and requires higher order fragmentation ($MS^{n>3}$). Nonetheless, it has been found that C-6 glycosides show more extensive fragmentation than C-8 glycosides [19,20].

1.2.3.3. Acylated flavonoid glycosides

Several flavonoids in nature contain acyl moieties, which alter their physical and biological characteristics. Same as for glycosides, the characterization of acyl conjugates could be elucidated by monitoring the neutral losses of the acyl or acylglycoside moieties during CID. The most common acyl groups (Figure 1.5) include acetyl, malonyl, benzoyl, galloyl, coumaroyl, feruloyl and sinapoyl groups with observed neutral losses of -42 Da, -86 Da, -104 Da, -146 Da, -176 Da, and -206 Da, respectively. The exact location of the acylation site is often difficult to elucidate. However, it is predominantly located at the C6-position of a hexose moiety, although other locations are likely [20].

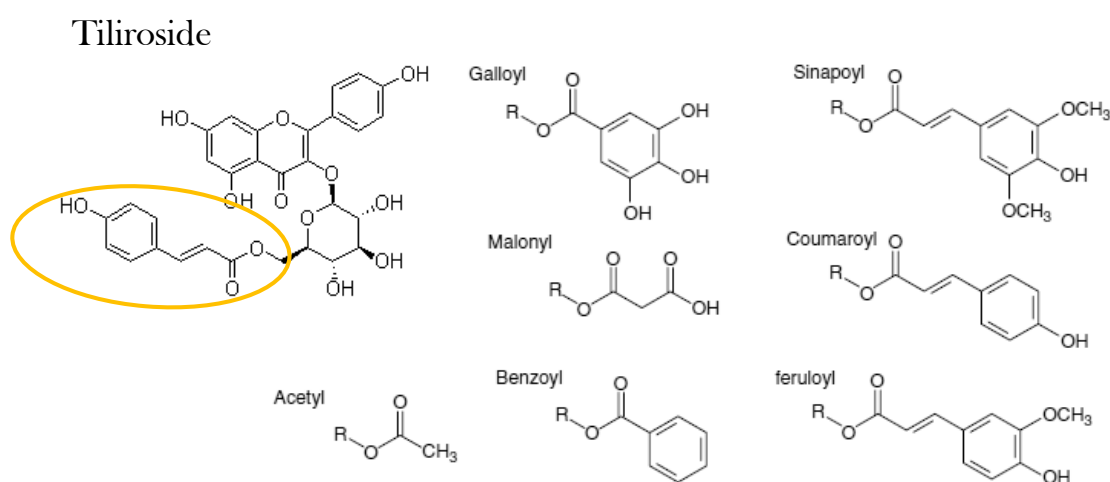


Figure 1.5. Tiliroside (Kaempferol 3-*O*- β -D-(6''-*O*-(*E*)-*p*-coumaroyl)glucopyranoside) with its acyl moiety highlighted. Other possible acyl moieties are presented. Adapted from Cuyckens and Claeys [20].

1.2.3.4. Flavonoid metabolic conjugates

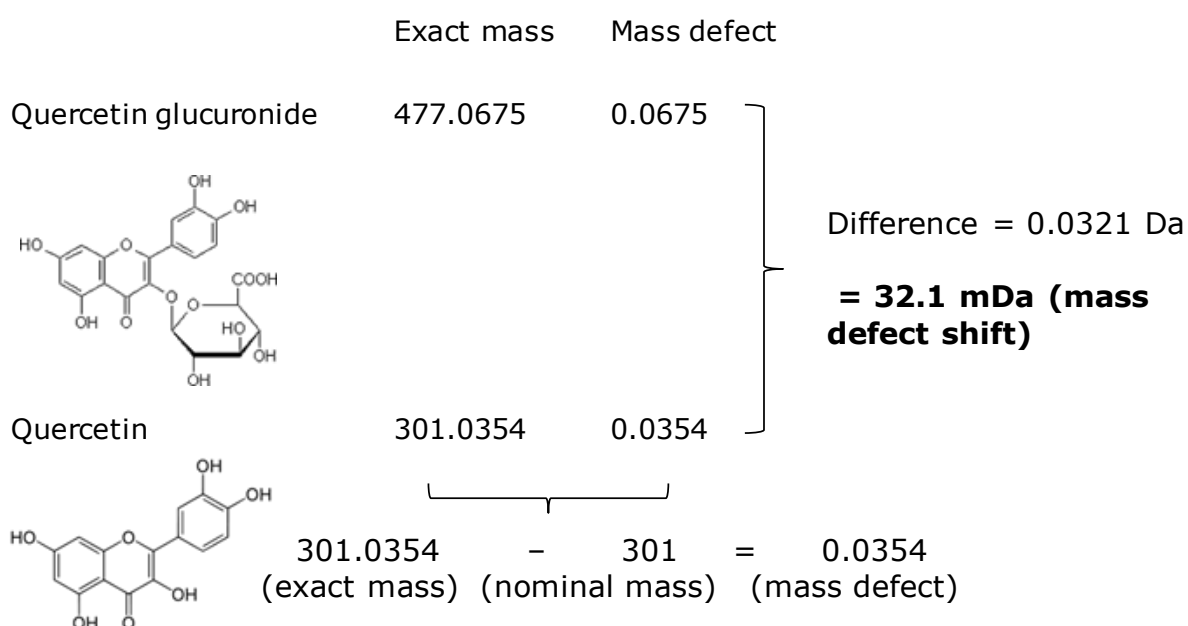
As discussed in the later sections, flavonoids undergo extensive phase I and II metabolism following oral administration. The most common metabolic conjugates are glucuronides, sulfates, and methylates. Identification of these metabolites is typically based on their neutral losses after MS/MS CID fragmentation. With the increase in analytical capacity, modern high-resolution accurate mass LC-MS have evolved to resolve metabolite ions and isobaric interferences when they were separated by greater than 50mDa in a mass range of 200-1000 Da. Because of this, a technique called *mass defect filtering* has been developed, which is able to remove interfering isobars and thus reduce the chances for having false-positive identifications. Mass defect is the difference between the molecule's exact monoisotopic mass (301.0354 for quercetin) and nominal mass (301 for quercetin). The concept of mass defect filter started when it was realized that mass defect of metabolites incurs certain predictable shifts compared to the mass

defect of the parent compound [29]. The expected mass shifts and mass defects of the common flavonoid metabolites are shown in Table 1.1.

Table 1.1. Expected mass shifts and mass defect shifts of flavonoid metabolites (Taken from Zhang et al. [29])

Biotransformation	Mass shift / Neutral loss (Da)	Mass defect shift (mDa)	Molecular formula change
Glucuronidation	176.0321	32.1	+C ₆ H ₈ O ₇
Sulfate conjugation	80.0432	43.2	+SO ₃
Methylation	14.0157	15.7	+CH ₂

Mass defect filter is currently integrated in metabolite identification/search softwares as a tool for the efficient prediction and annotation of expected and unexpected metabolites. The following scheme explains the principle of mass defect filter.



Unlike in plants where conjugation of the glycosides often occurs at the C-3 and C-7 of the A and C rings, metabolic conjugation has been shown to also commonly occur at the C-4' position of the B ring [30]. Thus, the rules previously laid for the structural annotation of flavonoid glycosides do not necessarily cover flavonoid phase I/II metabolites. For this purpose, more precise methods are needed.

Post-column metal complexation has been previously shown to differentiate positional isomers based on their product ion spectra. This method involves the infusion of metal ions to the flow stream of the LC before it reaches the MS. In this way, flavonoid-metal adducts are formed and detected by the MS. The fragmentation of these adducts depends on where the conjugation site is in the aglycone structure. Therefore, using this method, the conjugation site of the metabolic transformation could be elucidated [31]. However, carefully choosing the metal complex is necessary since some metals neutralize the flavonoid, making it invisible to the mass spectrometer. Infusing metals into the ESI source also introduces dirt into the system, which therefore requires constant cleaning. Currently, more advanced methods such as ion mobility spectrometry are being used for metabolite identification but no data on flavonoids have been reported in the literature.

1.3. Structure-activity relationship (SAR) analyses

SAR analysis is a technique to discern the structural or chemical features that lead to a desired activity or property [32]. The fundamental premise of SAR is that chemical and physical properties of molecules determine its biological/toxicological/physical behavior [33]. SAR is useful in ascertaining the relative importance of certain functional groups in relation to a given biological or physical activity. Therefore, investigators are able to examine which constitutes a class of molecules that are active, what determines their activity, and what distinguishes them from non-active compounds [33]. When used to explain the presence or absence of certain functional groups, it will be hereto referred as qualitative SAR, whereas when predictive mathematical models are made, the term quantitative SAR (QSAR) will be used. The majority of the biological activities presented in the following sections covers only qualitative SAR, which is partly due to the lack of data regarding screening large amounts of flavonoids. Nonetheless, such qualitative SARs, although not mathematically predictive, are highly comprehensible even to those not familiar with SAR techniques.

The goal of QSAR modeling is to construct a mathematical relationship between the molecular structural descriptors and activity or property [32]. This typically involves four steps: extracting descriptors from the molecular structure, choosing the appropriate descriptors that are relevant to the property in question, using the values of the descriptors as independent variables to explain the property observed through the use of computational techniques, and validation of the model [34]. By far the most common computational methods used in 2D QSAR analysis are multiple linear regression (MLR) and partial least squares regression (PLSR). MLR and PLSR are both modeling methods that predict the activity or property as a linear function of molecular descriptors [34].

MLR models the activity to be predicted as a linear function of all descriptors. The problem with this technique arises in the case of large descriptors-to-compounds ratios, where multi-collinearity occurs. This makes the model rather unstable, especially when predicting external datasets or when compounds not included in the dataset are used to develop the model [34]. Nonetheless, stepwise MLR (SMLR) is a very popular technique, perhaps due to its ease of operation and interpretability.

PLSR on the other hand is a developed generalization of MLR. Unlike MLR, PLSR can analyze data with strongly collinear, noisy, and numerous independent variables [35]. PLSR assumes that a large number of descriptors can actually be explained by a small amount of latent variables by decomposing the input matrix of descriptors into orthogonal score vectors. These score vectors then serve as new predictors [34,35]. For this reason, PLS has been successfully used for analyzing even more complex molecular descriptors such as in 3D QSAR analysis. Techniques for 3D QSAR have been increasingly popular over the recent years because the descriptors used in these analyses usually comprise of location-dependent structural characteristics [36], which makes it easier for non-experts to interpret QSAR results. Comparative Molecular Field Analysis (COMFA) is by far the most studied and applied 3D-QSAR technique [33]. Generally, this technique involves a crucial alignment step of molecular 3D structures. Then steric (Lennard-Jones) and electrostatic (Coulombic) interactions of a probe atom within the molecule are calculated at uniform grid points and placing these values in a matrix. PLSR is then used to generate a model that associates these interactions to the observed activity/property, to verify the predictive ability of the generated model, and to use the model for predicting the activity of new compounds not in the model. The beauty of this technique lies in its ability to plot the interactions to their corresponding region within the molecular structure, which also corresponds to a particular molecular moiety [33]. Somehow considered as a development of COMFA, Comparative Molecular Similarity Index Analysis (COMSIA) extends to more spatial descriptors, such as hydrophobicity, hydrogen bond acceptors and donors. It also does not involve cut-off values, which makes the calculations outside the molecular surface possible, thus making COMSIA a more reliable technique [37].

1.4. Flavonoid interactions and their effect on bioavailability and bioactivity

1.4.1 Binding of flavonoids to α -amylase and α -glucosidase and their interaction with food carbohydrates

The increased prevalence of diabetes mellitus has attracted attention to carbohydrate digestion in general and has prompted the search for post-prandial hyperglycemia

reducing strategies. In this context, the effect of flavonoids on the delay in glucose absorption by inhibiting carbohydrate-hydrolyzing enzymes in the digestive tract has been investigated [38,39]. Both α -glucosidase and α -amylase are key enzymes involved in the digestion of carbohydrates in humans [40]. Human α -amylase is produced in the salivary glands and the pancreas and is responsible for rapidly converting digestible starch into sugar monomers [41,42]. Human α -glucosidase is an enzyme found in the small intestinal epithelium, which catalyzes the hydrolysis of disaccharides, mainly sucrose and maltose, and other oligosaccharides into simple sugars [43].

Several polyphenols, especially flavonoids, have been reported to inhibit these enzymes. This has been extensively reviewed [42,44,45], and based on the results, a qualitative SAR can be summarized as follows:

1. Hydroxyl groups, especially at the C5 and C7-positions of the A-C ring and C3' and C4'-positions of the B ring, increase the inhibitory activity of flavonoids towards α -glucosidase and α -amylase.
2. Methylation and methoxylation, which "blocks" the free hydroxyl groups decrease inhibitory activity.
3. Although glycosylation obviously increases the number of free hydroxyl groups, the inhibitory activity of flavonoid glycosides is much lower than that of their aglycone counterparts.
4. Planarity of the flavonoids, which is due to the unsaturation of the C2-C3 bonds increases α -glucosidase and α -amylase inhibitory activity.
5. Galloylcatechins have a higher inhibition than non-galloylated catechins and catechins are influenced by the presence of hydroxyl moieties in the C3 and C5-positions of the A-C ring, number of hydroxyl groups in the B-ring or C-ring and the 2,3-cis/trans isomerism [46].
6. Increased inhibitory activity has been observed for flavonoids having the B-ring attached to the C-2 position rather than to the C3-position (in the case of isoflavones) [40,41].

It has also been previously reported that an increased number of hydrogen bond donors and acceptors is related with a higher human α -amylase inhibition *in vitro* (correlation values $R^2 = 0.69$ and 0.54 , respectively). Also, XlogP3, a measure of compounds' partitioning coefficient and thus lipophilicity, negatively correlates with percent inhibition. This suggests that the interaction of the flavonoids towards the α -amylase is not governed by hydrophobic interaction, but rather by hydrogen bonding [42].

A predictive 2D-QSAR model was built for the inhibitory activity of flavonoids against a model α -glucosidase from yeast using MLR of molecular descriptors calculated using DRAGON, wherein topological charge index (JGI2), information index (CIC2) and the number of exo-conjugated C atoms (nCconjR) were found to correlate with inhibitory activity ($R^2_{\text{training}}=0.771$, $R^2_{\text{test}}=0.851$, $Q^2=0.832$) [47]. Although the authors interpreted the model as being related to the number of hydroxyl groups and the presence of the C2=C3 bond, it is hard to generate a direct link between the molecular parameters of the model to the actual structural properties that govern the inhibitory effect, which is typical for QSAR models employing indices as descriptors. In the end, it seems that both α -amylase and α -glucosidase share the same properties in terms of structural requirements for inhibition.

On the other hand, *in vivo* studies indicate that flavonoid-carbohydrate interactions affect flavonoid bioavailability. Human feeding studies have demonstrated that co-administration of flavonoids with a carbohydrate-rich food enhanced flavonoid absorption, which was explained by their protective effect against microbial deterioration in the intestines, the release of bound flavonoids through fermentation, and the activity of a carbohydrate-flavonol transporter (GLUT) [48-50]. The latter however remains questionable since it has been previously argued that flavonoids are not transported by glucose transporters [51]. This issue therefore needs further investigation.

1.4.2. Flavonoid interaction to lipase and effect of fat consumption on bioavailability

Pancreatic lipase plays an important role in the digestion and absorption of triacylglycerols in the intestines after a fat-rich diet. Dietary fat is not directly absorbed by the body unless the fat has been subjected to hydrolysis by the lipase, more specifically converting triacylglycerols into sn2-monoglycerol and sn1,3-fatty acids. Pancreatic lipase constitutes 50-70% of the lipolytic activity whereas gastric lipase contributes to 10-30%. Lingual lipase has a minimal contribution [52]. Among many treatment approaches for obesity, retarding lipase activity may therefore offer an effective alternative [53]. With the development and success of tetrahydrolipstatin (Orlistat®), a potent clinically approved lipase inhibitor, this enzyme has been targeted as a valid approach in the treatment of obesity by reducing the amount of absorbed fat from food [54]. Consequently, lipase inhibition has been the most widely studied mechanism for the determination of anti-obesity potential of natural products [52].

Several papers reported the anti-obesity potential of polyphenols through several mechanisms, which include pancreatic lipase inhibition. In fact, several polyphenol-rich

plant extracts have been shown to inhibit pancreatic lipase activity [52,53]. Yet, lipase inhibition of a wide range of isolated flavonoids or flavonoid standards has not been found in literature (except for catechin derivatives). Therefore, it is difficult to generate a qualitative, even more quantitative, structure-activity relationship.

According to few available studies, it appears that increasing the hydroxyl moieties in the C3-position of flavonoids contributes to their lipase inhibitory potential. In addition to the effect of galloylation in flavan-3-ols at the C3 position, there is also a dramatic increase in the lipase inhibitory activity when a hydroxyl moiety in the C3 position is present like in the case of quercetin and luteolin, wherein quercetin contains a hydroxyl moiety at the C3 position while luteolin does not. Further, replacing the C3 hydroxyl moiety with a benzene ring in the case of genistein, an isoflavone, also dramatically decreases its inhibitory potency. In a study of quercetin esterified with various acyl chains of different length at the C3-position, it was found that there is a direct relationship between lipase inhibitory activity and the length of the acyl chain attached to the C3-position ($R^2 = 0.91$) [55], which indicates that changes in this position in the flavonoid skeleton may indeed affect lipase inhibitory activity.

The direct interaction of flavonoids with fats has not been well studied [50,56]. In a review by Bordenave et al. [56], a list of calculated octanol-water partition coefficients for different flavonoids was reported, which could be used to explain the ability of flavonoids to stabilize emulsions and partition to the fat region. Therefore, it can be said that flavonoids interact with fats by means of hydrophobic interactions, which are rather weak. Using a Caco-2/HT29-MTX co-culture model, Jailani and Williamson [57] found that co-administration of flavonoids with commonly used dietary oils altered the absorption behavior of flavonoids depending on their hydrophobicity. For instance, addition of oil significantly increased the production of quercetin and kaempferol conjugates (especially sulfates) at the basolateral compartment by up to 3 and 4 times, respectively. The transport of galangin through the cells was however inhibited by the presence of oils on the apical side, which is surprising since galangin is more hydrophobic and should partition with the fat more than quercetin and kaempferol. It is however unclear from the paper if the fat was emulsified in the cell culture medium. Emulsification is necessary to ensure that the compounds of interest do not partition to the fat phase and float away from the cells, and also to allow penetration to the mucus layer.

In parallel, an *in vivo* test using pig models revealed that higher levels of dietary fat content increased flavonoid absorption, which was attributed to the increased secretion of bile salts forming micellar structures during administration of a high fat diet [58]. This

in vivo study confirms the importance of micellar incorporation of flavonoids for intestinal absorption. The increased absorption of flavonoids upon fat ingestion also implies that the interaction of flavonoids with pancreatic lipases is indeed minimal.

1.4.3. Interaction of flavonoids with food proteins and proteolytic enzymes

Perhaps the most popular interaction in the study of flavonoid bioavailability is the interaction of the flavonoids with food proteins. This effect does not only reduce the bioavailability of the flavonoid but also of the food protein itself. Unfortunately, studies on the structure-affinity relationship of flavonoids to food proteins have been limited to mainly milk proteins.

In a study on bovine milk proteins (BMP) [59,60], the affinity of flavonoids towards such proteins was highly affected by their molecular properties and structure, which may be summarized as follows:

1. Hydroxylation of the A and B rings significantly improves binding to BMP.
2. Methylation and methoxylation of such rings therefore diminishes their affinity.
3. Glycosylation of the flavonoids strongly reduces the affinity of flavonoids towards BMP by 1-2 orders of magnitude.
4. Hydrogenation of the C₂=C₃ double bond of the C ring strongly reduces binding affinity by up to 75-fold. Planarity is therefore a key structural requirement for affinity.
5. Galloylation of catechins significantly improved binding affinity by at least 100-fold.

On a quantitative perspective, Xu and Chen [60] argued that the binding affinity of flavonoids to BMP is increasing with increasing partition coefficient (XlogP₃) and has a negative correlation with the number of hydrogen bond acceptors and donors. This suggests that hydrophobicity of the flavonoids plays a crucial role in the binding of flavonoids with food proteins. The same conclusion was made when analyzing the potential of food proteins as carriers for flavonoids [61]. Also, it was suggested that the topological polar surface area (TPSA) of flavonoids decreases with increasing binding affinity, which explains the low affinity of flavonoid glycosides to BMP compared to their aglycone counterparts [60]. However, the data presented in the paper did not give a reliable quantitative relationship because of the low correlation values ($R^2 = 0.42$ for XlogP₃ vs. binding affinity; $R^2 = 0.27$ for TPSA vs. binding affinity). However, a higher correlation between the Mulliken electronegativity and the binding affinity was found ($R^2 = 0.65$). Despite a higher correlation, this molecular property may not fulfill the requirements for a predictive QSAR model. Nonetheless, this structural information provides a qualitative view on the important molecular features that affect binding of flavonoids with food proteins.

According to Xiao et al. [59], flavonoids lose their anti-oxidative properties when bound to food proteins. Also, it is apparent that the molecular features important for food protein binding are the same features that enhance α -amylase and α -glucosidase inhibitory activities. This is not surprising since the enzymes are after all proteins themselves. However, one must therefore be careful in the use of flavonoids as anti-obesity and/or anti-diabetic agents as co-administration of a high protein diet may reduce their functionality. Further, when the dietary intervention is aimed at increasing the oral bioavailability of flavonoids, high protein diets may not be co-administered as these diminish the bioavailability of the flavonoid in question.

Proteolytic enzymes have also been investigated for their interaction with flavonoids. However, these studies have focused on the inhibitory activity of flavonoids with relevance to intracellular proteases and not the gastric and intestinal ones.

1.5. Overall intestinal permeability

Flavonoids, upon reaching the small intestines, undergo hydrolysis of their glycosidic moieties and severe phase 1 and 2 metabolism, which include glucuronidation, sulfation and methylation [62-65]. Therefore, the bioavailability of the parent flavonoid structures remains a big determinant for its bioactivity [66]. The structure of flavonoids has long been regarded as a critical determining criterion for bioavailability [62,64]. Figure 1.6 summarizes the findings of a much quoted review involving 97 bioavailability studies [63] with regards to bioavailability of flavonoids.

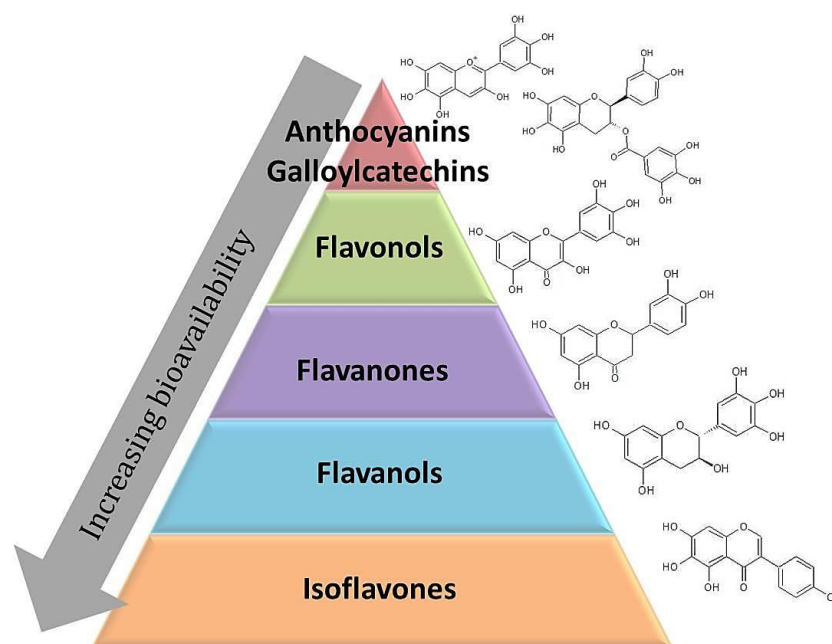


Figure 1.6. Bioavailability of flavonoids

Figure 1.6 provides a qualitative view on the absorbability of flavonoids in the intestines. However, due to the extremely wide range and variability in terms of structure within each group, it is difficult to generalize the absorbability of flavonoids only based on which group they belong to. For instance, methylation of the hydroxyl groups of the flavonols has been found to significantly increase their passage through intestinal cell models [67,68]. Also, the degree of glycosylation and the type of sugar have been shown to affect the bioavailability of the flavonoids compared to their aglycone counterpart [65,69,70]. For instance, administration of quercetin-3-O-glucoside to rats and pigs resulted in higher levels of quercetin metabolites in plasma compared to rutin (quercetin-3-O-glucorhamnoside), which was almost undetected in plasma until 3 hours after intake. This delayed peak in plasma concentration was attributed to the microbial deglycosilation of rutin in the duodenum and the lack of rhamnosidases in the epithelium [69,71]. Since the study of a wider range of flavonoids in human trials presents financial, technical and ethical hurdles, researchers have focused on the use of intestinal cell models to further study the intestinal uptake of flavonoids.

Predictive models have also been increasingly important in drug design and discovery over the past decade [72,73]. Several predictive models for intestinal absorption have been proposed, however not focusing on flavonoids as such. An influential example is the "Lipinski rule-of-5", which resulted from the analysis of the World Drug Index (WDI) [74]. In this rule-of-5, compounds that are likely absorbable through the intestines contain at most 5 H-bond donors, 10 H-bond acceptors, have a molecular weight of <500 Da and the Log P (lipophilicity index) > 5. Applying this rule to flavonoids, it can be said that structures containing many hydroxyl, glycosidic and galloyl moieties are less likely to be absorbed through the intestines. In contrast, methylated compounds lose their H-bond acceptor/donor properties and have higher logP values, which make them highly absorbable.

Another approach used for the prediction of intestinal absorption of potential drugs was proposed by Egan et al. [75] who analyzed the drug-likeness of thousands of known orally delivered drugs, which have been assayed for Caco-2 cell permeability. Using pattern recognition, it was found that 2 molecular descriptors, polar surface area (PSA) and AlogP98 (lipophilicity index) play a crucial role in determining intestinal absorption.

Using the model proposed by Egan et al. [75], it was shown that glycosylated flavonoids fall outside the intestinal absorption region (99% confidence) along with flavonoids with more than 6 hydroxylation points within the aglycone structure. All the other compounds,

such as those with <6 hydroxyl groups, isoflavones and methylated flavonoids are projected to have over 90% absorbability. Increasing the polar surface area seems to have a negative effect on absorbability, while hydrophobicity of the flavonoids favor intestinal absorption. This principle, in fact, has been the foundation of many other intestinal permeability models. However, these rules must be viewed as mere guidelines and not absolute cut-offs [72].

Quantitative SAR devoted to flavonoids remains scarce in literature. This is due to the limited amount of *in vitro* studies comprising a wide range of flavonoids, and the maximum number of flavonoids analyzed in a single study so far is 36, albeit from different chemical classes [76]. The development of such models however are useful in high-throughput screening of bioavailable flavonoids or when synthesizing flavonoid-based drugs. In the study of Tian et al [76], it was found that the octanol/water partition coefficient correlated well with the apparent permeability of isoflavones, flavones and dehydroflavones. However, there was a poor correlation with flavonols, which they considered as due to high cell accumulation, with some exceptions due to efflux mechanisms and compounds instability. This therefore means that lipophilicity is a good indicator for many other types of flavonoids, but this alone cannot explain intestinal permeability characteristics of flavonoids.

1.6. Use of cell cultures in the study of flavonoids

1.6.1. In vitro cellular models of the intestines

Human colorectal adenocarcinoma Caco-2 cells have been used in *in vitro* studies as an intestinal model for more than 30 years. The cell line was developed by the Sloan-Kettering Institute for Cancer Research [77]. The use of Caco-2 cells to simulate human intestinal absorption grew as more and more evidence suggested that drug transport in humans *in vivo* is highly correlated to the apparent permeability values measured using Caco-2 cells for certain drugs, such as ranitidine HCl, metoprolol tartrate, piroxicam [78], minoxidil [79], naproxen, antipyrine and metoprolol [80]. These drugs however are known to diffuse passively both in Caco-2 cells and human intestinal tissue, thus implying that Caco-2 permeability data is rather correlated to passive diffusion and not for actively transported drugs. Caco-2 cell permeability however was found to be 79- and 27-fold lower for the hydrophilic slowly-passively transported drugs terbutaline and atenolol, respectively. The carrier-mediated transport rates of L-dopa, L-leucine and D-glucose were also much slower in Caco-2 cells than in human jejunum. These data indicates that Caco-2 cells are useful to predict passive intestinal transport of molecules in human intestines, but is not a good model for the transport of hydrophilic and actively-

transported molecules. This has been attributed to the lack of transporter expression in Caco-2 cell lines compared to the real human intestinal epithelium [80]. Nonetheless, the use of cell culture models in the study of intestinal transport has provided novel insights into the intestinal uptake of flavonoids.

The Caco-2 cell line (Figure 1.7) is a heterogeneous population due to different transport rates, brush border assembly, and other differentiation characteristics of the population. During the rapid growth phase, the Caco-2 cells form semi-spheroid clusters, which are clearly separated due to tight junction formation at the cell borders. Upon confluency and differentiation, the apical membrane is covered by brush border microvilli perpendicular to the surface, which contributes to the morphological polarization of the monolayer [81]. Although the parental cell line is derived from a human colon carcinoma, the Caco-2 cells spontaneously differentiate resulting in a monolayer of cells that have morphological and functional characteristics of mature enterocytes. This spontaneous process occurs according to a mosaic pattern with areas containing undifferentiated (sub-confluent) cells proceeding to heterogeneously polarized and differentiated cells, and finally to homogeneously polarized and differentiated cells [82]. However, several reports still suggest that this parental cell line is not homogeneous, which results in variations and lack of reproducibility. To address this, clones such as TC-7 were isolated from the late passage of parental Caco-2 cells to obtain a more homogeneous population, thus improved reproducibility and more developed intercellular junctions [82,83]. The TC7 clone is characterized for having a higher expression of glucose transporters (SGLT and GLUT) [82]. It was also reported to show minimal differences in terms of paracellular transport and passive diffusion properties compared to the parental Caco-2 cell line. However, P-glycoprotein-mediated active efflux of cyclosporin was found to be higher in TC7 cells compared to the Caco-2 parental line. Thus, Turco et al. [83] remarked that TC7 cell lines may not be a suitable model for intestinal absorption of highly lipophilic and poorly absorbed compounds, and compounds where transporter-mediated routes and/or first pass metabolism are involved. The validity of using TC7 cell lines in the study of flavonoid intestinal transport should therefore be revisited.

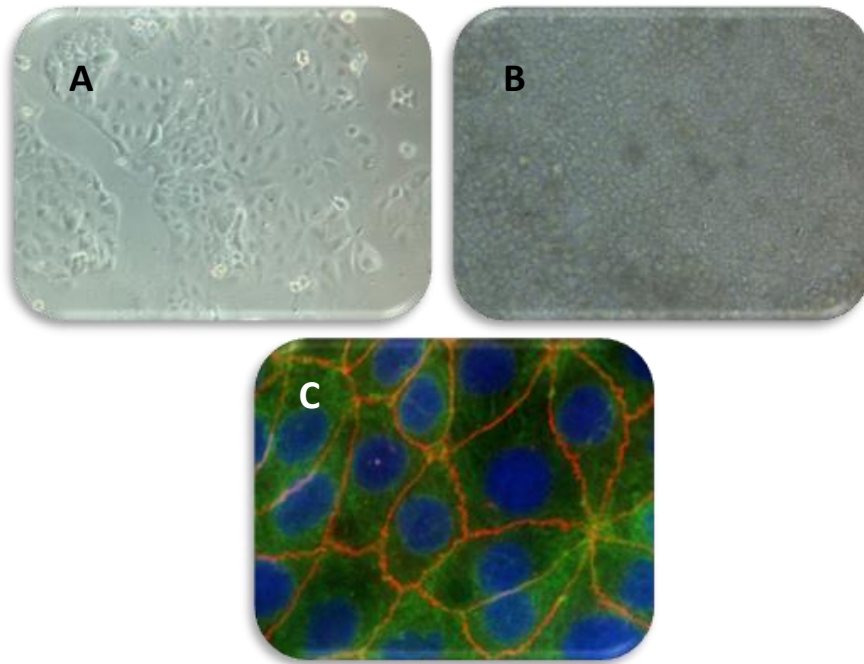


Figure 1.7. Undifferentiated (A) and differentiated (B) Caco-2 cells imaged with phase-contrast microscopy; differentiated Caco-2 cells visualized via confocal microscopy (C) showing the nucleus (blue), ZO-1 tight junction protein (red), and actin (green) taken from [84]

HT29 cells are also human carcinoma cells that retained certain characteristics of the normal tissue. When grown under standard conditions, they form a multilayer of nonpolarized undifferentiated cells [85]. In fact, in the postconfluent state, they comprise a heterogeneous mix of >95% undifferentiated cells with a small portion of differentiated mucin-producing (goblet) and absorptive cells [86]. The morphology of HT29 cells can be modulated to express certain pathways of enterocyte differentiation via treatment with various inducers or modifying the growth conditions. For instance, when grown in glucose-free medium, these cells differentiate and acquire the morphological features of absorptive epithelial cells or goblet cells [87] which secrete mucin. Mucins are O-glycosylated high-molecular-weight glycoproteins that constitute the mucus secreted by these cells [88]. A stable homogeneous differentiated mucin-secreting clone, HT29-MTX, was developed by stepwise adaptation to methotrexate [89].

1.6.2. Co-culture models in the study of flavonoids

Current trends in the study of flavonoids involve the use of multicellular or co-culture systems to further simulate physiological conditions. Co-cultures in flavonoid research have been done by either culturing 2 cell lines together in a single plate (contact system) or by using a transwell setup, which could either have contact and/or noncontact cultures, although other set-ups exist for other purposes.

Transwell systems are multi-well plate assemblies with porous membrane inserts wherein multiple cells can be cultured simultaneously with or without direct contact. Contact transwell systems have recently been used as a model for flavonoid intestinal absorption and the most popular approach is co-culturing Caco-2 cells with TC7 or HT-29 clones. By co-culturing Caco-2 and TC7 cells Barrington et al. [90] reported the mechanisms in the efflux of kaempferol and galangin conjugates wherein sulfated conjugates were preferentially effluxed back to the apical side, whereas glucuronides were transported to the basolateral side of the cells. Although the use of TC7 monocultures for studying flavonoid intestinal transport may not be a very accurate approach as earlier mentioned, optimizing the ratio of Caco-2:TC7 populations in the co-culture set-up could yield a more representative and homogeneous model.

The inability of Caco-2 cells to produce a mucosal layer is one of the biggest disadvantages of this cellular model. To simulate the presence of the intestinal mucosa, Caco-2 cells are co-cultured with mucus-secreting clones of HT29 cells, most popularly HT29-MTX. HT29-MTX cells when co-cultured with Caco-2 cells confer considerable changes in the absorption of various macromolecules and metabolites compared to a Caco-2 monoculture. A higher ratio of HT29-MTX/Caco-2 imparts a decrease in transelectrical epithelial resistance since HT29-MTX cells lack tight junctions, which leads to a favorable paracellular transport [91,92]. Recently, a Caco-2/HT29-MTX co-culture system was used to investigate the effect of edible oils on quercetin, kaempferol, and galangin transport. Results suggested that aglycones and conjugates were transported to the basolateral compartment of the co-culture and that metabolism was enhanced with the addition of oils, except for galangin [57]. It must be noted, however, that HT29-MTX cells mainly produce gastric-type mucins, MUC5AC, which are different from those that are produced in the intestines, MUC2 and MUC3 [88,93]. Therefore, the use of the Caco-2/HT29-MTX co-culture model to simulate intestinal absorption of flavonoids is not entirely representative of the *in vivo* situation and should be improved. HT29 clones, HT29-FU, which is produced after exposure to 5-fluorouracil (5-FU), and HT29-B6, which is isolated from HT29 cultures grown in glucose-free medium and induced via cholinergic stimulation, produces colonic-type mucin, MUC2, which could provide a better representation of the intestinal mucus [86,94-96]. However, while Caco-2/HT29-B6 co-culture has already been used to study flavonoid intestinal absorption, the use of HT29-FU or Caco-2/HT29-FU co-culture has not yet been reported in the literature.

1.7. Cellular uptake and transport of flavonoids

Flavonoids and their metabolites are taken up differently by different cell types. The 'classical' absorption pathway of flavonoids is passive diffusion through the cell membrane. However, membrane transport proteins also play a crucial role in cellular flavonoid absorption [97].

1.7.1. Solute carrier transporters

Solute carriers (SLCs) are membrane-associated transporters that mediate the passage of solutes such as peptides, bile acids, and drugs across cell membranes [97-101]. They include organic anion-transporting polypeptide (OATP), organic anion transporters (OAT), and monocarboxylic acid transporters (MCT) [102]. It has been generally accepted that SLCs play a significant role in cellular trafficking of various drugs [97] and that their activity increases with decreasing extracellular pH [97,99,100]. OATPs are located on the apical side of intestinal cells and have been recognized for the uptake of quercetin in Caco-2 cells at low pH, while passive diffusion is responsible for transport at higher pH [103]. MCTs are also present at the apical side of intestinal cells and are responsible for the absorption of epigallocatechin-3-gallate (EGCG) [97]. This finding indicated that the galloyl moiety is crucial for recognition by this transporter [99].

1.7.2. Sodium-glucose linked transporters

Flavonoid conjugates, just like glucose, have polar characters and can only cross lipid-rich cell membranes with the help of membrane-associated carrier protein active transporters. Sodium-glucose linked transporters (SGLTs) are a family of glucose transporters that transport glucose against the concentration gradient into the cells by coupling this transport with the transport of sodium 'downhill'. There are 2 reported SGLT clones [104], SGLT1 and SGLT2, which are expressed in intestinal, endothelial and kidney cells. In the latter, the transporters are located in the proximal tubules and are responsible for the renal glucose reabsorption, but a direct link with flavonoid uptake is inconclusive [105,106]. The expression of SGLT1 in intestinal cells has been linked to a higher uptake of flavonoid conjugates. It has been previously shown that flavonoid glycosides can be transported across intestinal cells by the SGLT1 when there is no efficient uptake by passive diffusion [107]. But the cellular uptake of glycosides via this pathway is limited even when glucose is absent [98]. It has been demonstrated that quercetin-4'- β -glucoside is transported across the apical membrane of intestinal cells and SGLT1-transfected CHO cells [108]. It was later reported that quercetin-3-glucoside is taken up across the intestinal cells by SGLT1 in rat small intestines [109]. However, this conclusion was later disputed by using SGLT1-expressing *Xenopus laevis* oocytes. In this study, the direct analysis of transport currents of SGLT1 indicated that neither quercetin, luteolin, apigenin, naringenin, pelarginidin, daidzein, or genistein, nor any of their

glycosylated derivatives are substrates of this transporter [51]. Contradictory results regarding the involvement of SGLT in flavonoid intestinal transport exist and thus require further elucidation.

1.7.3. Bilitranslocase

Bilitranslocase is a membrane protein with a transport function and was originally isolated from rat liver. It has been suggested that this protein has a high affinity for various flavonoids to mediate their uptake into the human liver (HepG2), endothelial (HUVEC), and intestinal (Caco 2) cells [110]. Bilitranslocase is found at the apical side of intestinal tissue, where it is only expressed in areas where the enterocytes are fully differentiated: on the villi and in the upper part of the Lieberkühn's crypts. Although quercetin is taken up by Caco-2 cells via bilitranslocase, conjugates of quercetin are however not substrates of this transporter [111-114].

1.8. Cellular metabolism of flavonoids

Dietary flavonoids are usually administered orally as glycosides. These compounds are deglycosylated and subsequently undergo extensive first-pass metabolism in the small intestine and subsequently also in the liver [115]. Glucuronidation and sulfation are the most common first-pass metabolic pathways [65,116]. Because of this extensive metabolism, flavonoid conjugates are more present in the plasma than as an aglycone [100]. The circulating conjugates can be excreted via urine or they serve as 'aglycone carrier' in the bloodstream. Deglucuronidation also plays a crucial role in the cellular metabolism of flavonoids since it releases the active aglycone in the target organs [101,117].

1.8.1. Deglycosylation

The permeability of aglycones in intestinal cells (Caco-2) is at least 5 times higher than their glucosides [118]. The poor cellular uptake of glycosides can be caused by: (i) slow passive diffusion because of poor lipid solubility and multiple hydroxyl groups, (ii) poor uptake by glucose transporters or (iii) fast efflux by MRPs [98]. Thus, it is crucial to hydrolyze the glycosides to obtain a better cellular uptake [119]. This metabolic process is also important since it is likely that the aglycone is more bioactive than its glycoside counterpart [120]. Deglycosylation of flavonoid glycosides is done by the action of: (i) lactase phloridzin hydrolase, (ii) cytosolic β -glucosidase, and (iii) microbial hydrolase.

Lactase phloridzin hydrolase (LPH) is a brush-border enzyme in small intestinal cells [121]. It has been observed that LPH has substrate specificity for flavonoid-O- β -

glucosides. The released aglycone can then enter the epithelial cells via passive diffusion due to its lipophilicity and its proximity to the cellular membrane [65,98]. Dietary flavonoids and isoflavone glycosides are typically hydrolyzed by LPH [117].

Alternatively, cytosolic- β -glucosidase (CBG) hydrolyzes glycosides intracellularly when these are transported in the intestinal cells by SGLT1 [122]. This enzyme is complementary to LPH since it is incapable of hydrolyzing 3-O-linked glucosides such as quercetin-3-glucoside [117,123]. Both LPH and CBG are expressed by the Caco-2 cell line and *ex vivo* human small intestinal samples [124]. However, β -glucosidase activity in Caco-2 cells is much lower compared to actual intestinal tissue samples [121,125]. On the other hand, the flavonoids that reach the colon can be hydrolyzed by the colon microbiota, but it is thus important to notice that the hydrolysis is not limited to the colon as scientists initially thought [126].

1.8.2. Glucuronidation

Glucuronides are one of the predominant forms of flavonoids circulating in the blood [127]. It has been generally accepted that the glucuronidation process is crucial to detoxify xenobiotics by decreasing their pharmacological activity [30]. Although, recent reports suggest that glucuronides also perform biological functions *in vivo*. Epicatechin-5-O-glucuronide, for example, elicits anti-oxidative activities like its aglycone counterpart [128]. Glucuronidation occurs at the hydroxyl moiety attached to the aromatic ring. When the flavonoid possesses more hydroxyl groups, multiple glucuronide isomers can exist [129], and the position at which the glucuronidation occurs affects its biological activity [130]. For instance, glucuronidation at the C3 position reduces the xanthine oxidase and lipoxygenase inhibition potency of flavonoids [131].

Glucuronidation is mediated by UDP-glucuronosyltransferases (UGTs) [132]. Human UGTs can be classified into 4 families on the basis of their amino acid sequence: UGT1, UGT2, UGT3, and UGT4, and they are distributed in the intestinal tract and in the liver [30,130].

Glucuronidation has been the most studied metabolic fate of flavonoids, wherein it was demonstrated that glucuronidation is regiospecific and is strongly affected by the structure of the flavonoid [130,133-135]. In this section, both intestinal and hepatic glucuronidation are discussed since they share the same mechanism although with different kinetics.

In general, SAR of flavonoids to *in vitro* glucuronidation activity of UGT isoforms can be summarized as follows:

1. Flavonols are the least glucuronidated flavonoids.
2. When the C3-OH group is removed (in the case of flavones), glucuronidation activity increases.
3. Glucuronidation is even more intensified when the C2=C3 bond is removed (in the case of flavanones), which relates to the importance of structural planarity.
4. Addition of hydroxyl groups in the A-ring was also found to increase glucuronidation while glycosylation decreases it.
5. In a study of monohydroxyflavones exposed to human jejunum S9 fraction, it was found that glucuronidation is favored in the following order: C3' and C6 >> C4', C3, C2', C7 >> C5 hydroxyflavone. However, using mouse liver S9 fraction, it seemed that the C7 position is more preferred than C3, C3' or C6.
6. In dihydroxyflavones (dHF), 3',7-dHF had the highest intrinsic clearance compared to a 2',7dHF and 4',7dHF. This, together with the result from monohydroxyflavones, indicates the importance of the C3'-hydroxyl moiety for the effective glucuronidation of flavonoids in general (Wong et al., 2009). However, it was observed that glucuronidation was limited to the C7 and C3-hydroxyl groups using mouse liver S9 fraction.
7. Increasing the number of hydroxyl groups on both A- and B- rings (except for 4'-OH moiety) enhances the glucuronidation activity of flavones, while adding a 3-OH hydroxyl group does not seem to have an effect.

1.8.3. Sulfation

Besides glucuronidation, another first-pass metabolism pathway is sulfation. Sulfation is done for the same reason as glucuronidation, to detoxify the xenobiotics and potential toxins [136]. It is done by members of the sulfotransferase (SULT) superfamily that are active in the tissues where first-pass metabolism occurs, such as the liver and the intestines [101]. This pathway is important in the understanding of flavonoid bioavailability since sulfated flavonoids have been reported to be effluxed back into the intestinal lumen and thus are not well absorbed [90]. Among its many isoforms, the mammalian SULT1A3 has been reported to be the most important isoform for the metabolism of phenolic compounds, such as flavonoids [133,137]. Literature regarding the structure-sulfation relationship on a wide range of flavonoids remains scarce. However, according to several studies, it was found that there is a preference for sulfation at the C7-OH moiety [133,137,138]. In a study of 16 different flavonoids from different flavonoid classes, it was clearly shown that sulfation occurred mostly at the C7-OH position and removing this hydroxyl moiety reduces or inhibits sulfation. Also, any

attachment to the C3-position (whether a hydroxyl group or the B ring) reduces the sulfation activity [137].

To explain the sulfation behavior of the SULT1A3 isoform, docking studies using the crystal structure of SULT1A3 have been done. It was found that the C7-OH group can easily be docked to the active site of SULT1A3 and yields the highest fit and docking score. Also, the 7-OH group is able to form hydrogen bonds with the basic residue Lys106 and the deprotonated N-3 atom on His108. It was also found that the phenyl ring at the C2-position (C-ring except for isoflavones) interacts with the hydrophobic residues Tyr76, Phe142, Tyr240, Val241, and Leu 247, such that hydroxylation of this ring (for instance C4'-OH) drastically reduces its binding affinity. Similarly, hydroxylation at the C3-position introduces unwanted bulk or steric hindrance which affects the flexibility of the C2-phenyl group, thus again reducing binding affinity [137].

1.8.4. ATP-binding cassette (ABC) transporters

ABC transporters are energy-dependent efflux pumps that are involved in drug efflux. This superfamily includes P-glycoprotein (P-gp), multidrug resistant proteins (MRP), and breast cancer resistance protein (BCRP) [139]. P-gp, MRP2, and BCRP are located in the apical membrane of the intestinal cell [65,97-99,140,141] whereas MRP1 is observed in the basolateral membrane [142-144] (Figure 1.8). These transporters in the intestinal cells limit the availability of their substrates, such as (polar) flavonoids, by direct intestinal excretion [145-148]. Aside from being substrates, some flavonoids are also inhibitors of ABC transporters [149]. When the flavonoids inhibit ABC transporter, poorly absorbed drugs can accumulate more than usual. This can also lead to drug intoxication, especially for drugs with a narrow therapeutic window [101]. On the other hand, the inhibition of ABC transporters has also been used as a strategy to increase absorption of drugs.

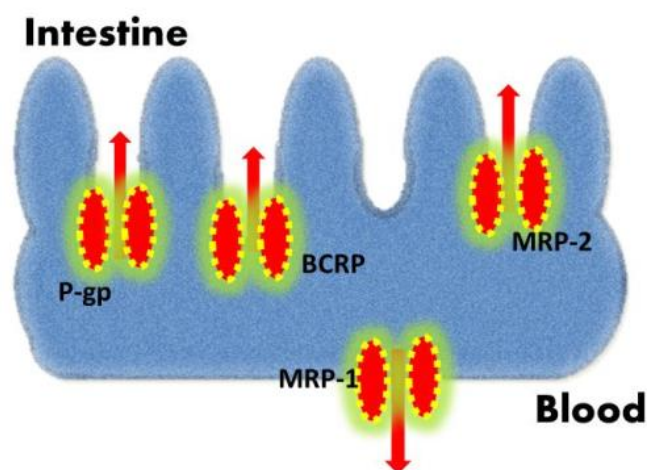


Figure 1.8. ABC transporters on the apical and basal compartments of Caco-2 cells. P-glycoprotein (P-gp), breast cancer resistance protein (BCRP), multidrug resistant protein (MRP). Adapted from Alvarez et al. [150]

The interaction of flavonoids with these ABC transporters is highly affected by their structure. In the following section, the structural characteristics necessary for ABC transporter interaction are described, which ultimately dictates whether a flavonoid is absorbed or effluxed out of the cells.

1.8.4.1. P-glycoprotein

P-glycoprotein is a 170 kDa transmembrane protein, which is known for actively transporting drugs out of the cells in an ATP-dependent manner [151,152]. Structural analysis of the protein sequence showed 1,276 amino acids in mice, comprising of 2 homologous halves containing a transmembrane domain (TMD) composed of six membrane-spanning α -helices involved in efflux and drug binding, and a cytosolic nucleotide binding domain (NBD) with characteristic Walker motifs A and B and an ABC transport S signature, which have been shown to possess ATPase activity [151,152]. This transporter has a rather broad spectrum of substrates including many therapeutic drugs. Such substrates have been observed to share similar properties, such as being hydrophobic, positively charged or neutral and having a planar structure [153].

It is known that flavonoids exert P-glycoprotein competitive inhibition, based on the physical properties earlier described. In general, the following observations regarding flavonoid-P-glycoprotein interaction have been reported in literature [153-156]:

1. Flavonols, chalcones and flavones are generally active, while flavanones and isoflavones have lower P-glycoprotein inhibitory activities;
2. The hydroxyl groups at the 5- and 3-positions are required for inhibitory activity against P-glycoproteins;

3. Highly hydrophilic compounds, such as rutin and other flavonoid glycosides, do not interact with P-glycoproteins;
4. Increasing the number of hydroxyl groups in the A and C rings increases the affinity of flavonoids to P-glycoprotein;
5. Ring B attached to the C2-position entails higher affinity than when it is attached to the C3-position, in the case of isoflavones;
6. The presence of the C2=C3 double bond increases the affinity of flavonoids to P-glycoprotein;
7. Hydroxylation at the C4' and C3' position reduces flavonoid-P-glycoprotein affinity while methoxylation at the C4' position increases it.

A stepwise multiple linear regression was used to create a QSAR model from an *in vitro* analysis of 22 flavonoids using human colorectal carcinoma (HCT15) cells. The model with the highest adjusted R² was reported as [157]:

$$\begin{aligned} \log \text{ activity (at } 50\mu\text{M flavonoid)} &= 81.34(7\text{-OH}) - 50.37(3'\text{-OH}) - 65.93(4'\text{-OH}) + \\ &58.81(5'\text{-OH}) + 40.83(\text{flavanol}) - 101.9(\text{isoflavones}) + 12.13(\text{clogP}) + 115.81 \\ &(\text{Adjusted } R^2 = 0.7126, F = 4.53, p < 0.02) \end{aligned}$$

In this model, it was observed that hydroxylations at positions C3' and C4' and the position of the B-ring (isoflavones) negatively affect the modulation activity of flavonoids to P-glycoproteins. Conversely, hydroxylations at C7, C5' and ClogP positively influence the activity of flavonoids against P-glycoproteins. Although the adjusted R² value is relatively high, validation steps were not performed in this study, which is extremely important when making QSAR models. Therefore, the robustness and actual predictability of this model cannot be assured. Nonetheless, the results of the model complemented well with the generally observed structural trends, as enumerated above.

Kothandan et al. [152] on the other hand used docking and 3D QSAR approaches (COMFA and COMSIA) to explain the structural features of flavonoids relevant for P-glycoprotein inhibition. For both COMFA and COMSIA analysis, both ligand-based alignment (atom-atom alignment) and receptor-guided alignment (based on docking pose) were employed. Based on their docking results, it seems that the potential sites for conjugation include Asn1043, Asp1049, Pro1051 and Asn1248. The success of the COMFA and COMSIA methods to produce a highly predictive model also indicates that the location of certain functional groups indeed plays a role in the interaction of the flavonoids with P-glycoprotein. According to their COMFA and COMSIA receptor-guided

model, hydrophobic and bulky, and possibly methylated moieties around the A-ring increase the affinity of the flavonoid towards the P-glycoprotein binding site.

1.8.4.2. Multidrug resistance proteins (MRP)

MRP is another type of ABC transporter consisting of nine members, which vary in terms of substrate specificity, tissue distribution and intracellular location. The most commonly studied are MRP1 and MRP2. Although both transporters share many substrates and approximately 49% sequence similarity [158], MRP1 is usually found on the basal membrane while MRP2 is found on the apical membrane of intestinal cells (previously shown in Figure 1.8). MRP1 is also less substrate specific than MRP2. Overexpression of both MRP1 and MRP2 has been found to confer multidrug resistance to a variety of anti-cancer drugs [158]. Being on the apical region, MRP2 is however more physiologically relevant than MRP1 and is thus expected to limit oral bioavailability and facilitate the biliary and renal secretion of its metabolites [150,153]. However, considering the stricter substrate specificity of MRP2, only a few flavonoids have been found to inhibit MRP2, which implies that a QSAR is difficult to establish.

Using stepwise linear regression, with MRP1 competitive inhibition as the dependent variable and 5 structural descriptors (number of OCH₃ groups, number of OH groups, log dihedral angle of the C3-C2-C1'-C2' bonds, lipophilicity, and number of pyrogallol and catechol moieties), van Zanden et al. [158] reported that MRP1 inhibition by flavonoids may be explained by the following equation:

$$\%inhibition = 45.46 + 18.94(\#OCH_3) + 12.47(\#OH) - 48.25(\log \text{ dihedral angle})$$
$$(R^2 = 0.77, p < 0.001)$$

The results of this model suggest that the dihedral angle of the B and C rings negatively affects inhibition, which implies that a rather planar structure should be a prime requirement for MRP1 inhibition. Also, increasing the number of methoxyl groups and increasing the number of hydroxyl groups both increase the flavonoid-induced inhibition of MRP1 to a relatively similar degree. This result is however somewhat odd since increasing the number of OCH₃ moieties in the flavonoid structure should cause a decrease in the amount of hydroxyl groups in the structure. Also, the lack of essential validation steps in the modeling procedure makes this model a rough estimation rather than an absolute reliable model.

1.8.4.3. Breast cancer resistance proteins (BCRP)

A recent addition to the ABC transporter family is the breast cancer resistant protein (BCRP), which is a 655-amino acid protein with a molecular weight of 72.1 kDa. Unlike other ABC transporters that contain 12 transmembrane domains and 2 ATP binding sites, BCRP only consists of 6 transmembrane domains and 1 ATP binding domain; hence, it is called a half ABC transporter and may require the formation of a homodimer to function [153,159]. BCRP is ubiquitously located in the body with high mRNA expression in the placenta and lower level in the brain, prostate, intestines, testis, ovary, and liver. Substrate specificity is somewhat similar yet much more restrictive than P-glycoproteins [32,154]. However, it has been previously reported that BCRP expression in the intestines is higher than P-glycoproteins, and thus may restrict more the oral bioavailability of its substrates. BCRP is located at the luminal side of the intestines and thus at the apical side of polarized cells [32,153,154].

A number of researchers have extensively studied the SAR of flavonoids with BCRP and their findings can be summarized as follows [32,159-161]:

1. The presence of the C2=C3 double bond increases BCRP inhibition, thus implying the necessity for structure planarity;
2. Hydroxylation at positions C5 and C7 (moderate effect) increases BCRP inhibition, while methylation at such positions reduce activity;
3. Placing the B ring to position C3 (in the case of isoflavones) eliminated BCRP inhibitory activity;
4. Hydroxylation at positions C3, C6 and C8 reduces its activity, while methoxylation of these hydroxyl moieties reverses the effect. In the case of the C4' position, $\text{OCH}_3 > \text{OH} > \text{H}$;
5. Addition of a prenyl moiety to positions C6 and C8 increases the BCRP inhibitory activity;
6. Glycosylation reduces the inhibitory activity.

1.9. Flavonoids in systemic circulation and their distribution to target tissues

Once compounds or their conjugated metabolites manage to pass through the intestinal barrier, they must then be transported through the circulatory system to their target tissues. However, the bioactivity of these compounds may be influenced by their affinity to proteins inherent in the blood. As with food proteins earlier discussed, flavonoids have also been shown to interact with some blood proteins.

Human serum albumin (HSA) is the most abundant protein in plasma and serves as a depot and carrier for many different types of compounds in blood, which then affects their pharmacokinetics and metabolic fates [162]. In fact, it was found that the distribution and metabolism of many bioactive compounds are correlated with their affinities towards HSA [163]. As the “free drug” hypothesis suggests, only compounds unbound to plasma protein exert biological activity, which therefore suggests that flavonoids with high binding affinity towards HSA may lose their biological activity once they reach the blood. As summarized by Xiao and Kai [164] in their review, the structure-affinity relationship of flavonoids to plasma proteins is as follows:

1. Increase in the hydroxyl groups of the A and B ring increases the affinity of flavonoids to plasma protein while addition of a hydroxyl group at the C ring will weaken it.
2. Methylation of these hydroxyl groups further enhances their binding to plasma proteins.
3. The presence of the unsaturated bond at C2=C3, typical for flavonols, strengthens protein binding.
4. Glycosylation greatly reduces plasma protein binding affinity.
5. Galloylation increases the binding of catechins to plasma proteins.

Given these characteristics, it can be implied that hydrophobicity plays a crucial role in protein binding; methylation, C2=C3 bond makes the flavonoid more lipophilic whereas glycosylation makes it hydrophilic. Indeed, it has been previously reported that compounds with reduced lipophilicity also exhibit reduced protein binding [165]. It is interesting to note that characteristics of flavonoids with higher overall intestinal permeability are similar to the structural requirements for protein binding. For instance, while it has been reported that methylated flavonoids pass through the intestinal cells intact, such compounds have high plasma protein binding affinities, as discussed above [164].

However, Smith et al. [165] argued that the “free drug” hypothesis may have been misunderstood and that most *in vitro* studies dealing with aglycones and purified plasma proteins may not represent the *in vivo* situation. Further, as discussed in the earlier chapters, flavonoids experience extensive first-pass metabolism, especially glucuronidation, which therefore restricts the passage of aglycones through the intestinal cells intact, although there have been very few exemptions reported (Williamson, 2002).

Unfortunately, to the best of my knowledge, there are no studies regarding the comparative protein binding of flavonoid metabolites, especially glucuronides. However,

the results of the *in vitro* assays mentioned above clearly show that flavonoid glucuronides may have low plasma protein binding affinity because glucuronidation increases the aqueous solubility of flavonoids. This implies that glucuronides may freely diffuse to the target tissues, where they are deglucuronidated. Therefore, while glucuronidation has been perceived as something that limits the oral bioavailability of the flavonoid aglycone, it may well be that this mechanism is the perfect carrier of flavonoids to target tissues because of their potentially high free drug concentration in the blood. In case any aglycone would be able to pass through the intestines intact, they would face extensive binding to plasma proteins anyway, which ultimately reduces their biological activity. In this regard, current strategies to improve bioavailability by by-passing the glucuronidation stage may need to be re-evaluated.

1.9.1. Deglucuronidation

One may argue that flavonoid glucuronides lose much of their biological activity compared to their aglycone counterparts, which has been demonstrated by many *in vitro* studies. However, flavonoid aglycones are not found in the blood after oral administration and yet, flavonoid-rich diets still resulted in profound physiological changes in the body [166,167]. Hence flavonoid metabolites must be converted back to the active aglycone form upon reaching target tissues, which has been confirmed by a few studies.

The deglucuronidation process is essential to convert the pharmacologically inactive conjugate into the active aglycone [167]. This crucial metabolic pathway is executed by the lysosomal enzyme β -glucuronidase. Further, β -glucuronidase activity has been demonstrated in the liver, specifically the hydrolyzation of quercetin glucuronides in HepG2 cells [168]. The released aglycones are then taken up and can be metabolized further in the target tissues [169]. O'Leary et al. [169] showed that the hepatic β -glucuronidase activity in Fisher 334 rats increased when the rats were treated with N-diethylnitrosamine (carcinogenic compound) and phenobarbital (tranquilizer). Thus, during the hepatic carcinogenesis, there is an increase in the conversion of quercetin glucuronides into quercetin aglycones, which could render biological activity.

Kidney cells of castrated male pigs also express β -glucuronidase activity. The aglycone concentration in this tissue is, however, rather low, which can be explained by a subsequent sulfation or a re-glucuronidation [170]. It has been published that β -glucuronidase activity in liver and kidney cells increases with age. This is most likely due to the increased fragility of the lysosomal membrane that allows leakage of the enzyme [171].

HUVEC cells have been reported not to take up or metabolize epicatechin conjugates. Upon treatment of a mix of epicatechin metabolites, no epicatechin aglycone has been detected intracellularly or in the cell culture medium of HUVEC cells, thus suggesting the absence of glucuronidases. This observation suggests that the bioactivity of flavonoid conjugates is restricted to the endothelial cell membrane [172]. However, glucuronidase activity has been observed in RBE4 cells since the media of the cell culture contains high levels of native hesperitin and naringenin after incubating the cells with the glucuronides [172].

The conversion of luteolin monoglucuronide into its free aglycone during inflammation in human neutrophils was first observed by Shimoi et al. [136]. Perez-Vizcaino et al. [118] also confirmed an increase in β -glucuronidase activity of neutrophils during inflammation to alleviate the inflammation. Also, livers of hepatocarcinogenic rats have higher β -glucuronidase activity than healthy rats. This signified that β -glucuronidases are specifically activated in inflammatory tissues, such as cancerous tissues [173]. On the other hand, Ishisaka et al. [174] reported that the increased β -glucuronidase activity of injured cells is associated with mitochondrial dysfunction. Deglucuronidation has been recently regarded as the reason for the bioactivity of flavonoids, albeit only present in low concentrations in plasma – a major dilemma in the “flavonoid paradox” [175]. However, the complete conjugation-deconjugation cycle of flavonoids in health and stressed states has not been fully elucidated. This information could provide a definitive proof on the bioactivity of flavonoids despite having low bioavailability in humans.

Given these, it can be said that keeping a constant supply of flavonoid glucuronides in the blood stream may be beneficial as tissues can secrete β -glucuronidases to release the bioactive aglycone when they are needed. Due to a high clearance rate, it is therefore advised to have a constant dose of flavonoids in the diet in order to keep a high level of glucuronides in the blood.

1.10. Specific cellular bioactivity of flavonoids

1.10.1. Prevention of cellular reactive oxygen species (ROS) damage

Antioxidant activity is perhaps the most well-known and important bioactive property of flavonoids [176-179]. This activity can be performed by three mechanisms: (i) suppression of ROS production, (ii) scavenge of ROS and (iii) up-regulation of antioxidant defenses.

1.10.1.1. Suppression of ROS production

Flavonoids suppress ROS production by either inhibiting certain enzymes and/or by chelating trace elements that cause the radical production [178,180-182]. Flavonoids have also been reported to inhibit xanthine oxidase and protein kinase C, which are crucial for superoxide anion production [183,184]. Further, inhibition of cyclooxygenase, lipoxygenase, glutathione-S-transferase, NADH oxidase and succin-oxidase, which are enzymes involved in ROS generation, is also an important mechanism for flavonoid antioxidant activity [185].

Free iron can leach from iron storage proteins, such as ferritin, or from enzymatic [4Fe-4S] clusters [186]. The concentration of free copper in vivo increases when copper-sequestering proteins are inhibited or when the cells are exposed to elevated copper concentrations [187]. Free iron and copper then react with oxygen to produce ROS. Flavonoids act by chelating the free metals, thus preventing ROS production. Based on SAR studies, it was found that flavonoids chelate metals via: (i) the catechol moiety in ring B, (ii) the 3-hydroxyl, 4-oxo groups in the heterocyclic ring (iii) and the 4-oxo, 5-hydroxyl groups between the heterocyclic and the A ring (Figure 1.9). The catechol ring appears to be the most involved in metal chelation according to the reported higher chelation of quercetin (with catechol ring) than kaempferol (without catechol ring) [178]. Figure 1.9 shows the potent chelating sites of the flavonoid aglycone.

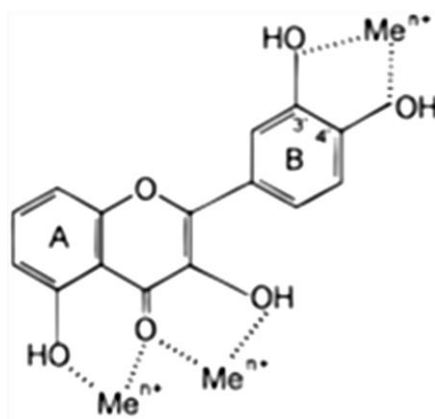


Figure 1.9. Binding sites for trace metals at flavonoid structure. Taken from Pietta [3]

1.10.1.2. Scavenge of ROS

The scavenging pathway of ROS by flavonoids has been described several times [180,188-193]. Due to their low redox potentials ($0.23 < E_7 < 0.75$ V) [178], flavonoids are capable of reducing superoxide, peroxy, alkoxy, hydroxyl radicals and other highly oxidizing radicals with potentials between 2.13 and 1.0 V [194].

Flavonoids donate a proton (H atom) to radicals (R•), resulting in an aroxyl radical (FI-O•) and RH. This aroxyl radical either interacts with another radical resulting in the termination or either with oxygen, generating a superoxide anion and quinone. The latter reaction is responsible for the pro-oxidative activity of flavonoids; generally this reaction occurs when a high concentration of trace metals is present. Besides scavenging, flavonoids can stabilize free radicals by forming a complex with them [178].

1.10.1.3. Upregulation of anti-oxidant defenses

The upregulation of anti-oxidant defenses by flavonoids has been observed as a mechanism to prevent cellular ROS damage [195]. Flavonoids, in particular procyanidin B2, increase the activity of various protective enzymes such as glutathione peroxidase (GPx), glutathione reductase (GR) and glutathione-S-transferase (GST). GPx catalyses the reduction of peroxide and GR recycles oxidized glutathione back to reduced glutathione to restore its anti-oxidative properties [196]. GST catalyzes the reaction of endogenous glutathione with electrophiles, the formed conjugates can be easily removed [195].

1.10.2. DNA damage repair

ROS causes oxidative damage to biologic macromolecules including nucleic acids [197]. One of the main forms of DNA oxidation is 8-oxo-7,8-dihydroguanine. This oxidized compound has important mutagenic properties and leads to G:C → T:A transversion through mispairing in replication [181,198]. The base excision repair (BER) is a crucial pathway for the repair of oxidatively damaged DNA bases. It has been reported that human 8-oxoguanine-DNA glycosylase (hOGG1) and apurinic/apyrimidinic endonuclease remove the damaged base [181,199] and DNA polymerase β subsequently fills the gap [181,200-202]. Abalea et al. [203] concluded from their experiment with primary rat hepatocytes that myricetin increases the DNA polymerase β mRNA levels at concentration of 100 $\mu\text{mol/L}$. The increase in mRNA expression of DNA polymerase β , hOGG1 and apurinic/apyrimidinic endonuclease by naringenin in prostate cancer cells has also been earlier reported [204]. In addition, luteolin has been found to increase the mRNA expression of hOGG1 in cells [181,198].

Chapter 2

UPLC-ESI- TOF-IMS-HDMS for the rapid structural
characterization of flavonoid glycosides from cauliflower
waste

Chapter 2: Ultra(high)-pressure liquid chromatography-electrospray ionization- time-of-flight-ion mobility-high definition mass spectrometry for the rapid identification and structural characterization of flavonoid glycosides from cauliflower waste

2.1. Abstract

In this paper, a strategy for the detection and structural elucidation of flavonoid glycosides from a complex matrix in a single chromatographic run using U(H)PLC-ESI-IMS-HDMS/MS^E is presented. This system operates using alternative low and high energy voltages that is able to perform the task of conventional MS/MS in a data-independent way without re-injection of the sample, which saves analytical time. Also, ion mobility separation (IMS) was employed as an additional separation technique for compounds that are co-eluting after U(H)PLC separation. First, the fragmentation of flavonoid standards was analyzed and criteria were set for structural elucidation of flavonoids in a plant extract. Based on retention times, UV spectra, exact mass, and MS fragment characteristics, such as abundances of daughter ions and the presence of radical ions ($[Y_0-H]^*$), a total 19 flavonoid glycosides, of which 8 non-acylated and 11 acylated, were detected and structurally characterized in a cauliflower waste extract. Kaempferol and quercetin were the main aglycones detected while sinapic and ferulic acid were the main phenolic acids. Other flavonoid with higher order of glycosylation were also found although their structure could not be elucidated. The proposed method can be used as a rapid screening test for flavonoid identification and for routine analysis of plant extracts, such as these derived from cauliflower waste. The study also confirms that agroindustrial wastes, such as cauliflower leaves, could be seen as a valuable source of different bioactive phenolic compounds.

Keywords: flavonoids, ion mobility, mass spectrometry

Redrafted from:

Gonzales GB, Raes K, Coelus S, Struijs K, Smagghe G, Van Camp J. 2014. Ultra (high)-pressure liquid chromatography–electrospray ionization-time-of-flight-ion mobility-high definition mass spectrometry for the rapid identification and structural characterization of flavonoid glycosides from cauliflower waste. *Journal of Chromatography A* 1323, 39-48

2.2. Introduction

Flavonoids are the most widely spread and diverse group of polyphenols, which belong to a large family of secondary plant metabolites [205]. To date, more than 8000 different flavonoids have been identified, where the most abundant aglycones are quercetin and kaempferol [206]. These often occur as complex conjugates with glycosides and acyl groups [4,206]. Recently, much attention has been given to these metabolites due to their biological activity, which include, among others, anti-oxidant activity [3,4], angiotensin-converting enzyme inhibitory activity [6,207], anti-obesity activity [7], among others. The biological effects of flavonoids on mammalian cells has already been extensively reviewed elsewhere [8].

LC coupled to MS/MS has been the method of choice for many chemists for the detection and structural identification of flavonoid glycosides since producing isolated components in sufficient quantities for NMR analysis is difficult [20]. These techniques (especially those using ion traps and orbitraps), although sensitive, are limited to certain transitions that are monitored, require multiple injections and involve manual identification of parent compounds, which are then subjected to succeeding MS experiments (MS^n) [208]. This process is therefore time-consuming, which makes it unsuitable for routine analysis and screening of a wide array of samples. Recently, the use of U(H)PLC- MS^E has been used as a rapid, data-independent strategy that collects both precursor and product ion information in one chromatographic run. This method uses parallel alternative scans of low and high energy which provides precursor ion, accurate mass fragments, and neutral loss information "all-in-one" [209-212]. This therefore eliminates the need for manual parent ion selection in MS^n experiments that require multiple injections, thus cutting analysis time. However, as complex samples, such as plant extracts, contain a wide array of metabolites and other components, U(H)PLC analysis is sometimes not enough to separate all these to obtain a single component that is passed onto the MS in an LC-MS system. Once compounds are convoluted, they enter into the MS at the same time, which makes structural analysis using MS^E rather difficult and ambiguous [213]. To address this, a further separation step is essential.

Ions generated after ionization (ESI, MALDI, etc) may be further separated by exploiting their different behaviors across a tube filled with an inert gas. Ion mobility refers to the velocity of an ion across a drift tube filled with a neutral gas, often nitrogen, under the influence of a weak electric field. In a drift tube, smaller molecules experience lesser collisions with the gas and thus travel faster than larger molecules [214-216]. This therefore provides an additional separation of compounds found in complex matrices.

This added orthogonal separation technique can therefore make structural elucidation of molecules from plant extracts more efficient [214]. By combining ion mobility to LC-MS^E, a system composed of LC separation-ionization-ion mobility separation (IMS)-ion detection and mass analysis is created, which can serve as an alternative to traditional tandem MS.

Vegetables belonging to the *Brassica* group have been found to be an excellent source of polyphenols, especially flavonoid glycosides mainly composed of quercetin and kaempferol [4,206,217-219]. Considering that vegetables belonging to this group are one of the most consumed [220], a wide variety of *Brassica* species and cultivars have been analyzed for their phenolic contents [219,221,222]. However, most studies have mainly focused on the edible parts of the vegetables. To the best of our knowledge, very limited researches have been done on the waste stream of *Brassica*. Selected *Brassica* waste streams have been previously analyzed for their anti-oxidative effects, which were attributed to the content of phenolic compounds [221,223]. Llorach et al [224] studied the flavonoid composition of cauliflower agroindustrial products (mainly leaves). They used LC-MSⁿ after isolation of individual compounds, where 23 flavonoid glycosides, mainly kaempferol and quercetin conjugates with 1-4 glucose units and hydroxycinnamic acids, free kaempferol and 4 hydroxycinnamic acid derivatives were detected [224]. Studying the flavonoid content of these waste products is an initial step into the valorization of agricultural waste into high value added products.

In this paper, we describe a strategy for the detection and structural elucidation of flavonoids and flavonoid glycosides in a single chromatographic run using U(H)PLC-DAD-ESI-IMS-HDMS/MS^E. Initially, fragmentation behavior of flavonoid standards under MS^E conditions was studied and separation by IMS was optimized. Information on their fragmentation behavior was then used as basis for the structural characterization of phenolics from a sample matrix. With this, a method for the simultaneous detection, identification, and structural characterization of polyphenols in a single chromatographic run was developed, which could be used for routine analysis of complex samples, such as cauliflower waste.

2.3. Materials and Methods

2.3.1. Reagents

Rutin, baicalin, hesperidin, quercetin-3-*O*-glucoside, kaempferol, quercetin, hesperitin, myricetin, isorhamnetin, *p*-coumaric, sinapic, and ferulic acids were purchased from Sigma (St. Louis, MO) while robinin was from Phytolab (Vestenbergsgreuth, Germany).

U(H)PLC-MS grade methanol and formic acid were bought from Biosolve (Valkenswaard, the Netherlands). Analytical grade methanol used for extraction, HCl and NaOH were purchased from VWR International (Leuven, Belgium). LEU-ENK was purchased from Waters (Milford, MA, USA).

2.3.2. Fragmentation behavior of flavonoid standards

Solutions (ca. 10ppm) of 9 flavonoid standards, robinin, quercetin-3-*O*-glucoside, quercetin-3-*O*-rutinoside (rutin), hesperetin-7-*O*-rutinoside (hesperidin), baicalein 7-*O*-glucuronide (baicalin), kaempferol, quercetin, isorhamnetin, and myricetin, were prepared in 50% (v/v) methanol + 0.1% (v/v) formic acid and directly injected to the Waters Synapt G1 HDMS (Waters Corp., Milford, MA, USA) equipped with an ESI source via direct injection at a flow rate of 5 μ L/min. Solutions of (ca. 10ppm) of ferulic, sinapic, coumaric, benzoic, gallic acids were also prepared and analyzed in the same way. Data were acquired in continuum negative ionization V-mode for 2 minutes. Source parameters for the MS were set as follows: capillary voltage, 2kV; sampling cone voltage, 40V; extraction cone voltage, 4V; source temperature 150°C; desolvation temperature, 350°C; cone gas flow rate, 50L/h; desolvation gas flow rate, 550 L/h. Trap and transfer collision energies were set at 6 volts for the low energy and 45 volts for high energy. Mass range was set at 100-1500Da with a scan speed of 0.2s per scan using the MassLynx software 4.1 (Waters Corp., Milford, MA, USA).

2.3.3. T-wave ion mobility separation (IMS)

IMS was optimized by injecting a sample extract spiked with various flavonoid aglycones and glycosides directly into the MS in IMS mode using a 250 μ L analyte syringe at a flow of 5 μ L/min. IMS parameters were then optimized to ensure that the components are separated over the entire drift time range. Nitrogen gas was used with a flow rate of 30 ml/min. Bias voltage was set to 40V. IMS T-wave velocity and height were 850 m/s and 8V, respectively. Transfer T-wave velocity and height were adjusted to 60 m/s and 30V, respectively. Mobility trapping was set at maximum value of 30V. In this approach, intact ions are allowed to pass through the trap cell and separated in the drift tube. Then high energy CID (45V) was applied after the ions have been separated, which makes it possible to associate the product ions to their respective precursor ions (time aligned). Time aligned parallel (TAP) chromatograms were obtained using Waters MS^E data viewer software.

2.3.4. Extraction of phenolic content

Cauliflower (*Brassica oleracea* L. var. *botrytis*) byproducts (outer leaves) were obtained in a field in Ieper (Belgium) during harvest (July 2012) and stored at -20°C until

processing. Frozen leaves were ground using liquid nitrogen and homogenized using a stirrer. Extraction was based on the method of Olsen et al. [225]. Briefly, approximately 5 grams of leaves were placed in 50 mL tubes and homogenized with 15mL methanol at 10.000 rpm using an ultraturrax for 45 seconds. The tubes were then placed on ice for 15 seconds. The mixture was centrifuged at 13.000xg for 10 minutes at 4°C. Supernatant was collected. The residue was re-extracted with 80% MeOH using the same procedure. All supernatants were pooled and the volume was adjusted to 50mL using methanol. The extract was stored in a -20°C freezer until further use. Extractions and analyses were done in triplicate.

2.3.5. Acid and alkaline hydrolysis

Acid hydrolysis was performed by adding equal amounts of 4M HCl to the methanolic extract (1mL:1mL) for 1 hour at 100°C. Alkaline hydrolysis on the other hand was done by adding 4M NaOH to the methanolic extract (1mL:1mL) at room temperature overnight. The pH of the alkaline hydrolysate was then adjusted to 2 using 4M HCl. Vials were flushed with nitrogen for 15 seconds before covering to minimize possible oxidation. The samples were then subjected to solid phase extraction (SPE) clean-up to remove the salts.

2.3.6. Sample preparation and clean-up

A 1mL-aliquot of the extract was diluted in 20mL of 0.1% (v/v) formic acid (in ultrapure water) and loaded into a preconditioned C18 solid phase extraction (SPE) cartridge (500mg/4mL) (Davison Discover Science, Deerfield, IL, USA). Preconditioning was done by loading the column with 2x3mL methanol and 2x3mL water, allowed to stand for at least 2 minutes for every solvent, prior to use. After loading the sample, the cartridge was washed with 5mL of 0.1% (v/v) formic acid and the phenolic compounds were recovered using 3mL of methanol containing 0.1% (v/v) formic acid. The samples were then dried using nitrogen and redissolved in 1mL of 10% methanol (0.1% v/v formic acid) prior to LC-MS analysis.

2.3.7. U(H)PLC-DAD-ESI-IMS-HDMS/MS^E analysis

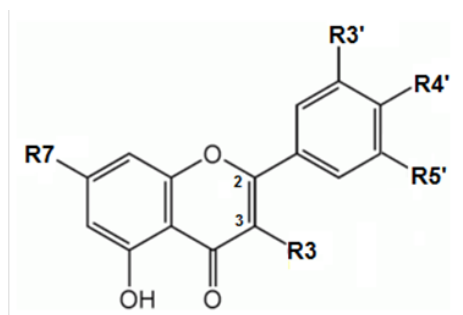
LC-MS analysis was performed with a Waters Acquity UPLC system (Waters Corp., Milford, MA, USA) connected to a Synapt HDMS TOF mass spectrometer (Waters Corp., Milford, MA, USA). Chromatographic separation was done on a Waters Acquity BEH C18 column (2.1 mm ×150 mm, 1.7 µm particle size) attached to a Waters VanGuard Pre-column (2.1mm x 5mm) using gradient elution. The mobile phase was composed of (A) water containing 0.1% (v/v) formic acid and (B) methanol containing 0.1% (v/v) formic acid. The column temperature was maintained at 40 °C, while the temperature of the

autosampler was held at 10°C. 5 µL of sample was injected and a flow rate of 250 µL/min was applied during the gradient elution. The elution program was as follows: 0 min, 10% B; 0–6 min, 0–20% B linear; 6–12 min, 20% B isocratic; 12–13 min, 20–30% B linear; 13–23 min, 30–50% B linear; 23–30 min, 50–90% B linear; 30–35 min, 90% isocratic; 35–40 min, 90–10% B linear; and 40–45 min 10% B isocratic. DAD spectra were recorded between 200–500nm. The eluent was then directed to the mass spectrometer equipped with an electrospray ionization source and lockspray interface for accurate mass measurement. Leucine-enkephalin, 2ng/mL was used as a reference and was introduced by a Waters 515 pump at a flow rate of 0.03 ml/min. MS parameters were as described above (see section 2.3.2).

2.4. Results and Discussion

2.4.1. Fragmentation behavior of flavonoid standards

The fragmentation pattern of 5 flavonoid glycosides with different sites of glycosylation (3-*O*; 7-*O*; 3,7-*O*) was studied. Figure 2.1 shows the structures of the flavonoid standards used. The results are shown in Fig 2 and 3. Parent ions were detected when using a low voltage of 6V. Fragmentation was observed at higher voltages, while at 45V, all relevant product ions were observed. 3-*O*-glycosides remained intact below 23V while further increase in the voltage led to fragmentation. Also at 23V, 3,7-*O*-glycosides only lose the glucose unit attached to the 7- position, while all of the 7- *O*-glycosides were fragmented into their corresponding aglycones. The fragmentation behavior of flavonoid glycosides using tandem MS techniques has been previously described [19,20,226,227]. Fragmentation of flavonoids after high energy CID in MS^E mode were found to yield similar diagnostic ions as reported in these studies, which indicates that the method is indeed able to structurally characterize flavonoid glycosides.



Name	R3'	R4'	R5'	R3	R7	C2=C3
Kaempferol	H	OH	H	OH	OH	Yes
Quercetin	OH	OH	H	OH	OH	Yes
Isorhamnetin	OCH ₃	OH	H	OH	OH	Yes
Myricetin	OH	OH	OH	OH	OH	Yes
Rutin	H	OH	OH	rutinose	OH	Yes
Quercetin-3-O-glucoside	H	OH	OH	glucose	OH	Yes
Baicalin	H	H	H	H	glucuronide	Yes
Hesperidin	OH	OCH ₃	H	H	rutinose	No
Robinin	H	OH	H	robinose	rhamnose	Yes

Figure 2.1. Structures of the flavonoid standards used

2.4.2. Glycosilation of 3- and 7-mono-O-glycosides

Similar to previous studies [26,28], the deprotonated radical aglycone $[Y_0-H]^{\bullet-}$ was more abundantly present in the case of 3-O glycosides rutin and quercetin-3-O-glucoside, in contrast to 7-O glycosides hesperidin and baicalin, compared to the abundance of the deprotonated aglycone $[Y_0]^-$ after high energy CID. The formation of a radical ion $[Y_0-H]^{\bullet-}$ is due to the hemolytic cleavage of the glycosidic bond between the aglycone and glycoside conjugate at the 3-position. Therefore, the presence of a glycoside unit in the 3 position drives the formation of this radical aglycone in negative CID [26,228]. The radical aglycone was also formed in case of 7-O-glycosides but in much lower quantities. The relative abundance of $[Y_0-H]^{\bullet-}$ to the $[Y_0]^-$ in high energy CID is therefore a good indicator of glycosylation position. A detailed mechanism on the formation of this ion has been previously described in [28]. As can be seen in Figure 2.2 (C.1 and D.1), the relative abundance of the quercetin radical ($m/z=300$) is higher than the deprotonated quercetin ion ($m/z=301$) indicating that the glycosylation is indeed at the 3-O position. Fragmentation of baicalin and hesperidin, on the contrary, did hardly produce radical aglycones in high energy CID.

2.4.3. Glycosilation of 3,7-diO-glycosides

As shown in Figure 2.2C, rutin (quercetin-3-O-rhamnosylglucoside) yielded $[M-2H-308]^{\bullet-}$ (m/z 300) and $[Y_0]^-$ (m/z 301), which corresponds to the loss of the rhamnosyl-glucoside moiety at once. This result agrees with previous reports that the loss of an inner sugar from a glycoside chain does not occur in negative ionization mode [26]. Therefore, for di-

O-glycosides, the loss of 2 independent glycoside moieties from the $[M-H]^-$ ion is considered as the presence of 2 glucose units from different glycosylation sites.

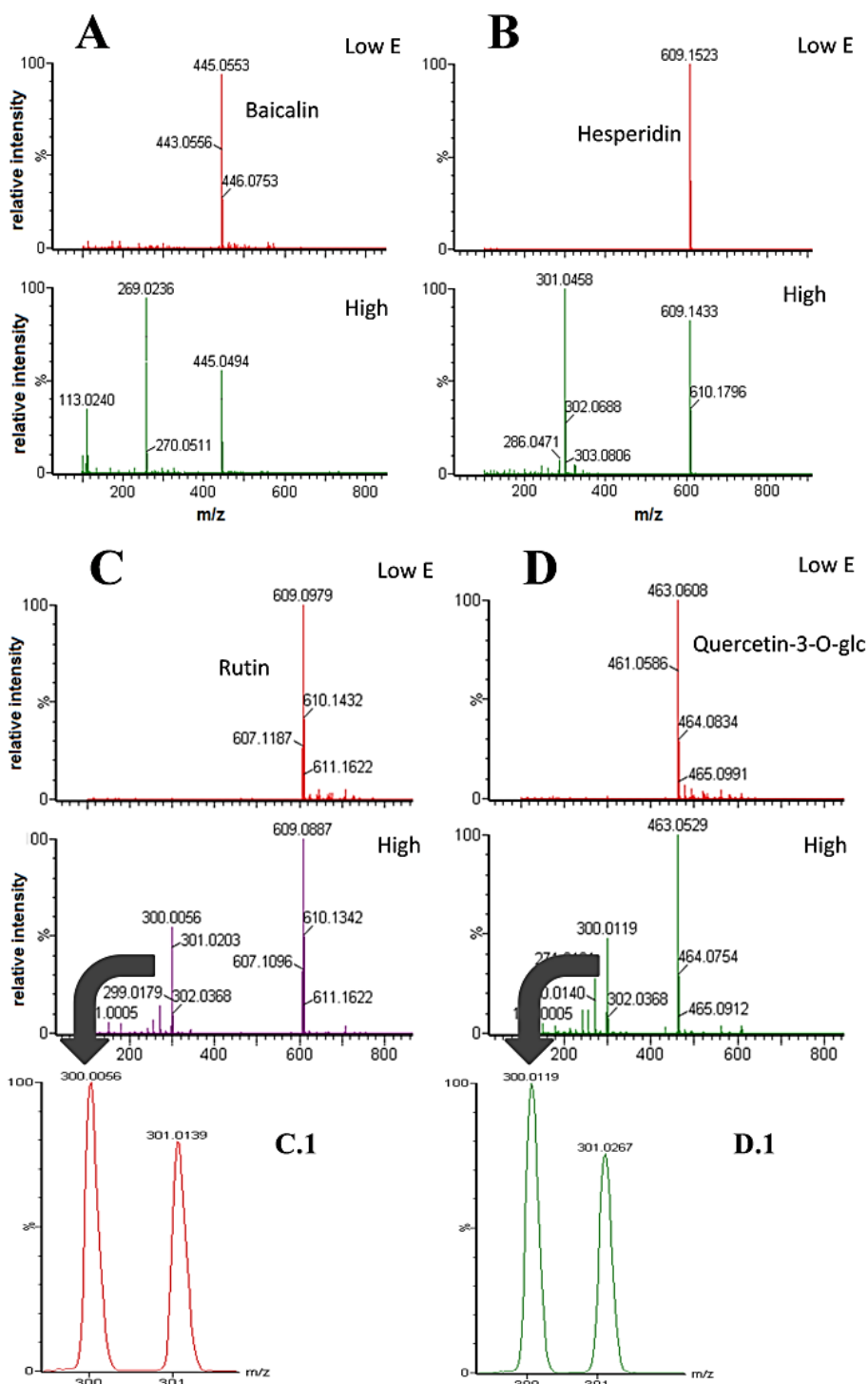


Figure 2.2. Fragmentation of flavonoid mono-*O*-glycosides in MS^E (low energy 6V; high energy 45V) in 2kV negative ionization mode. A – baicalin-7-*O*-glucuronide; B – hesperidin-7-*O*-rutinoside; C – Rutin (quercetin-3-*O*-rhamnosylglucoside); D – Quercetin-3-*O*-glucoside C.1, D.1 – relative abundance of $[Y_0-H]^+$ ($m/z=300$) to $[Y_0]^-$ ($m/z=301$)

As seen in Figure 2.3, fragmentation of robinin at 23V (Figure 2.3B) revealed a single product ion m/z 593, which corresponds to the loss of a rhamnosyl moiety located at the 7-*O* position. Increasing the voltage to 45V (Figure 2.3C) resulted into the occurrence of an additional product ion m/z 430, which corresponds to $[M-2H-(3-O\text{-galactoside-rhamnoside})]^-$, at a lower relative abundance than m/z 593. In agreement to previous reports [19,25,226-228], there is a preference in cleaving the glucose linkage at the 7-*O* position than in the 3-*O* position under negative ionization. Therefore, it is expected that the relative abundance of $[M-H-7-O\text{ glycoside}]^-$ is greater than the $[M-H-3-O\text{ glycoside}]^-$ in negative high energy CID. This implies that the rhamnose moiety must be coming from the 7 position while the diglucoside, galactose-rhamnose, comes from the 3 position. Also, the greater relative abundance of the radical ion m/z 430 compared to m/z 431, reveals that the glycosyl moiety was cleaved off from the 3-*O* position. Hence, the glycosylation position of 3,7-*O*-glycosides could be easily derived by comparing the relative abundances of the product ions. The essential fragments observed in this method were similar to those that were described for robinin using traditional tandem MS [229], which implies that this strategy indeed serves as a faster alternative for the conventional method.

Alkaline and acid hydrolysis of phenolic extracts have been routinely done to characterize the acylation and content of aglycones, respectively. In this case, hydrolysis was done as additional confirmation steps for the identification of the flavonoids in the extract. Alkaline hydrolysis of the extract removed acyl moieties thus revealing the parent flavonoid glycoside of the molecule. Acid hydrolysis on the other hand removed glycoside moieties revealing the flavonoid aglycone and phenolic acids. Figure 2.4 shows the U(H)PLC chromatograms of native, acid and alkaline hydrolyzed extracts. As shown, the region from retention time (rt) 9-12 minutes was removed after alkaline hydrolysis suggesting that this region is composed of acylated glycosides. The two remaining regions therefore are non-acylated glycosides, wherein the first eluting group is composed of highly glycosylated flavonoids while the other group is composed of glycosides with fewer glycoside attachments. The liberated phenolic acids after alkaline hydrolysis are also found in this region. The increasing number of sugar units is linked to an increased polarity of the molecule as a whole. Therefore, highly glycosylated components would be eluted first than those with lesser or no glucose moieties. Increasing acylation on the other hand has the opposite effect [20].

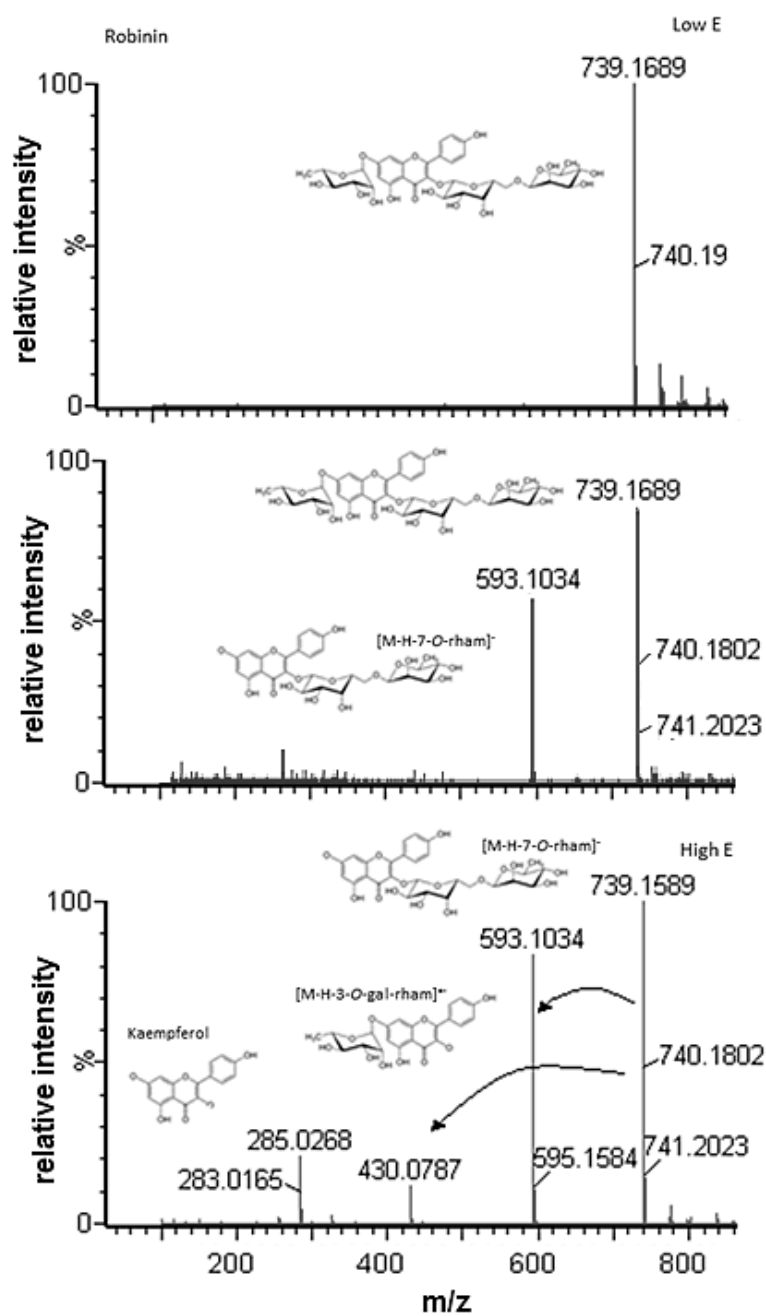


Figure 2.3. Fragmentation behavior of robinin (kaempferol-3-O-galactoside-rhamnoside-7-O-rhamnoside) MS^E (top – low energy 6V; middle – 23V; bottom – high energy 45V) in 2kV negative ionization mode

2.4.4. Analysis of phenolics from cauliflower waste methanolic extract

2.4.4.1. Chromatographic behavior and acid, alkaline hydrolysis

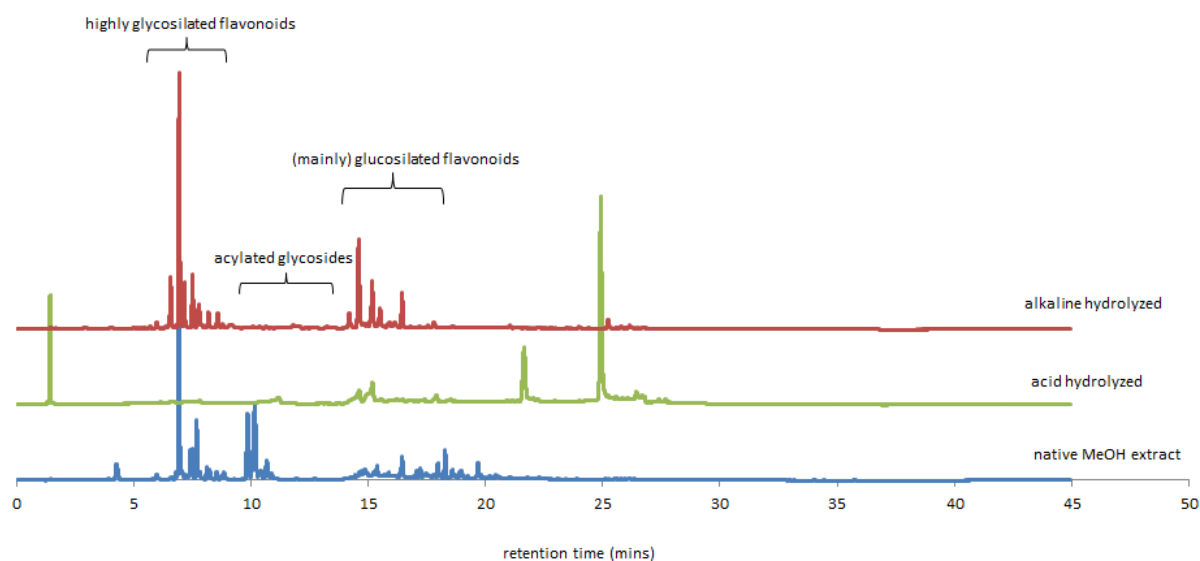


Figure 2.4. U(H)PLC-DAD (330nm) chromatogram of native, acid and alkaline hydrolysis of cauliflower waste methanolic extract.

Acid hydrolysis on the other hand revealed that the extract is mainly composed of kaempferol and quercetin with different degrees of glycosylation and acylation. Main phenolic acids present in the extract are sinapic, ferulic, hydroxyferulic and coumaric acids. Therefore, the flavonoid composition of cauliflower waste methanolic extract is a combination of these phenolic compounds with varying amounts of sugars.

2.4.4.2. Identification of flavonoid glycosides from *Brassica* waste methanolic extract

Figure 2.5 shows the U(H)PLC-DAD chromatogram of the cauliflower methanolic extract at 330nm. A 3D chromatogram from retention time 16-17 minutes is shown in Figure 2.6. Flavonoid glycosides in the methanolic extract of cauliflower waste were identified based on their retention times, UV spectra and MS^E results. Ion mobility separation (IMS) was used to further separate co-eluting compounds and to align product ions to their actual precursor ion.

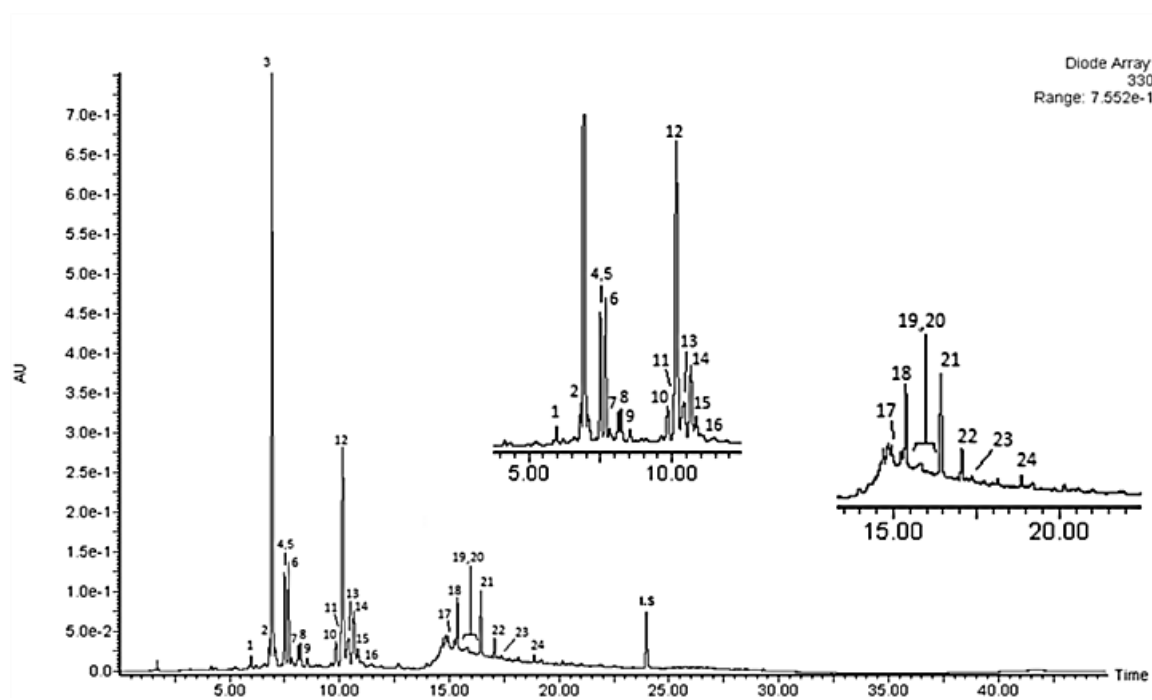


Figure 2.5. U(H)PLC-DAD (330nm) chromatogram of cauliflower waste methanol extract. I.S, hesperetin internal standard

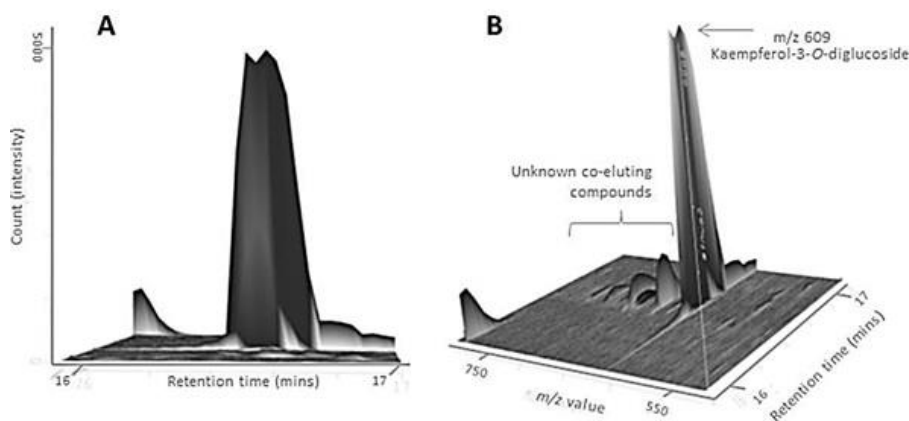


Figure 2.6. 3D chromatogram from retention time 16-17 minutes. A – a dominant peak with m/z -value of 609.1251 is detected; B – Many compounds with unknown identities elute at the same retention time as the dominant peak

2.4.4.2.1. Non-acylated flavonoid-*O*-glycosides

The determination of the non-acylated glycosides in the waste extracts was done in both the native extract and after alkaline hydrolysis to ensure that the losses corresponding to glucose (-162.053amu) and rhamnose (-146.058amu) are not confused with the losses of caffeoyl (-162.032amu) and coumaroyl (-146.037amu) moieties. Aglycone identification was carried out by comparing the exact mass and fragments with those of pure standards. As listed in Table 2.1, non-acylated flavonoid glycosides can be detected by their UV maximum absorptions (λ_{\max}). Kaempferol-3-*O*- and 3,7-di-*O*-glycoside were

found to have a λ_{\max} at 266nm and 348nm while quercetin-3-*O*- and 3,7-di-*O*-glycoside at 256nm and 354nm. Glycosides at the 7-*O*-position of kaempferol and quercetin have λ_{\max} at 266, 366 and 256, 370, respectively. These correspond to the results of Lin et al [220].

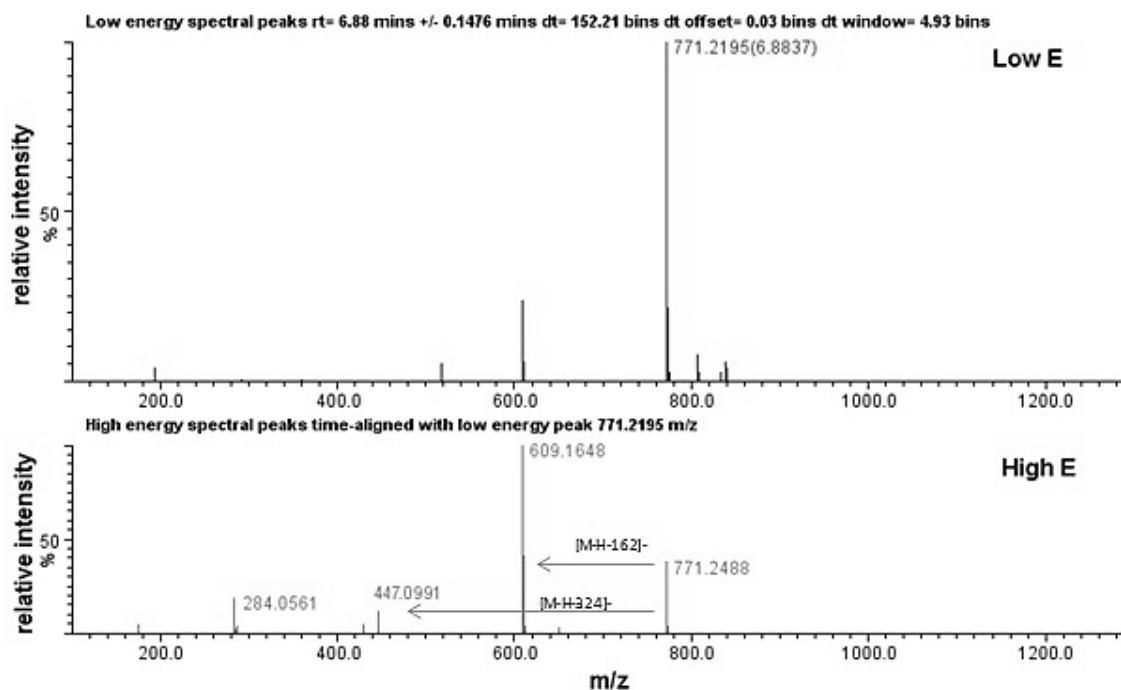


Figure 2.7. Time aligned chromatogram of peak 3 (identified as kaempferol-3-*O*-diglucoside-7-*O*-glucoside) in low (top) and high (bottom) energy CID in negative ionization mode

Table 2.1. Identification of flavonoid glycosides from *Brassica* waste methanolic extract*

Peak no.	rt (min)	Chemical formula	m/z values			λ max (nm)	Identity
			Exact mass	Fragments			
<i>non-acylated flavonoid glycosides</i>							
1	6,04	C33H40O22	787.1895	787,625,462,300		254, 348	quercetin-3-O-diglucoside-7-O-glucoside
3	6,88	C33H40O21	771.2195	771, 609, 447, 284		265, 348	kaempferol-3-O-diglucoside-7-O-glucoside
5	7,5	C39H50O26	933.2191	933,609,285		265, 345	kaempferol-3-O-diglucoside-7-O-diglucoside
7	8,13	C45H60O31	1095.343	1095, 771,609,284		268,331	kaempferol-3-O-triglucoside-7-O-diglucoside
17	15,01	C27H30O17	625.1302	625,301		nd	quercetin-7-O-diglucoside
19	15,9	C33H40O21	771.1885	771,284		267	kaempferol-3-O-triglucoside
21	16,45	C27H30O16	609.1251	609,284		265	kaempferol-3-O-diglucoside
24	19,62	C21H20O11	447.0789	447,284		nd	kaempferol-3-O-glucoside
<i>acylated flavonoid glycosides</i>							
4	7,4	C43H48O25	963.2515	963, 609, 771, 801, 284		nd	kaempferol-3-O-diglucoside-7-O-hydroxyferuloylglucoside
9	8,55	C46H48O25	963.2842	963,609,801,771,462,300		338	quercetin-3-O-coumaroylglucoside-7-O-hydroxyferuloylglucoside
10	9,78	C44H50O25	977.3577	977,815,609,284,446		268, 338	kaempferol-3-O-sinapoyldiglucoside-7-O-glucoside
12	10,17	C43H48O24	947.2400	947,785,609,284		268, 331	kaempferol-3-O-feruloyldiglucoside-7-O-glucoside
13	10,39	C52H54O27	1109.302	1109,755,947,284		329	kaempferol-3-O-coumaroyldiglucoside-7-O-hydroxyferuloylglucoside
14	10,48	C42H46O23	917.2275	917,755, 284, 609		268, 318	kaempferol-3-O-coumaroyldiglucoside-7-O-glucoside
15	10,7	C49H58O29	1109.3145	1109,785,609,284		268,331	kaempferol-3-O-feruloyldiglucoside-7-O-diglucoside
18	15,3	C43H48O24	947.2400	947,609,771,785,284		268, 327	kaempferol-3-O-diglucoside-7-O-feruloylglucoside
20	16,34	C38H40O20	815.2212	815, 609, 284		nd	kaempferol-3-O-sinapoyldiglucoside
22	17,02	C37H38O19	785.1868	785,609,284		329	kaempferol-3-O-feruloyldiglucoside
23	17,31	C36H36O18	755.1899	755,609,284		320	kaempferol-3-O-coumaroyldiglucoside
<i>other flavonoid glycosides</i>							
2	6,6	C39H50O26 ^a	950.2338	771, 609,285		nd	kaempferol-O,C-tetraglucoside
6	7,7	C45H60O31 ^a	1095.3577	933,771,609,284		nd	kaempferol-O,C-pentaglucoside
8	8,24	C51H70O36 ^a	1257.3818	1257,1095,771,609,284		330	kaempferol-O,C-hexaglucoside
11	10,1	C59H66O33 ^a	1301.3635	1139, 947, 785, 609, 591, 284		nd	kaempferol-O,C-hydroxyferuloylferuloyltetraglucoside
16	10,8	C55H68O34 ^a	1271.4026	1271,1109,947,785,284		nd	kaempferol-O,C-feruloylpentaglucoside

*m/z values for product ions arranged most abundant ion first; nd - not determined; ^aExact structure cannot be deduced

As shown in Figure 2.5, it can be seen that compound **3** was the dominant glycoside in the extract. Figure 2.7 shows the fragmentation pattern of compound **3**. A number of co-eluting components were observed in the low energy spectra, which made the identification of the target compound difficult. For this purpose, parent ions after ESI and low energy CID were further separated using ion mobility separation. Using the MS^E data viewer with HDMS function, fragment information of the target compound was obtained without interference from other co-eluting compounds. Fragmentation of the parent ion with an m/z -value of 771 [M-H]⁻ resulted in a fragment with an m/z -value of 447 ([M-H-324]⁻), and a second fragment with a higher abundance with an m/z -value of 609 [M-H-162]⁻. These two fragments corresponded to the loss of 2 glycosyl groups composed of 1 and 2 sugar units, respectively. High energy CID also revealed kaempferol (m/z 284) as the aglycone. As such, the compound was identified as kaempferol-3-*O*-diglucoside-7-*O*-glucoside. Addition of another sugar unit to the 7-position resulted in compound **5** with m/z 933, which had only m/z 609 as the fragment ion. This was named kaempferol-3-*O*-diglucoside-7-*O*-diglucoside. Compound **7** yielded fragments m/z 771, 609 and 284, which indicates loss of triglucoside and diglucoside moieties from 2 positions. Since the fragment m/z 771 is more abundant than m/z 609, this compound was named kaempferol-3-*O*-triglucoside-7-*O*-diglucoside. Fragmentation of compound **1** m/z 787 resulted in ions m/z 625, 462, 300, corresponding to 2 glycosyl losses of 1 and 2 sugar units, respectively, and the quercetin aglycone radical. This was therefore named quercetin-3-*O*-diglucoside-7-*O*-glucoside. Compounds **19**, **21** and **24** were found to be kaempferol glycosides with different number of sugar conjugates. Due to the high abundance of the kaempferol deprotonated radical ion ([Y₀-H]^{•-}) m/z 284, these three compounds were considered 3-*O*-glycosides and named as kaempferol-3-*O*-triglucoside, kaempferol-3-*O*-diglucoside, and kaempferol-3-*O*-glucoside, respectively. Elution was such that the one with the more sugar units eluted first. On the other hand, compound **17** m/z 625 was named as quercetin-7-*O*-diglucoside after fragmentation to m/z 301. While increasing number of glycoside units increase polarity, it has been reported that the position of the glucose moieties in the aglycone affects elution pattern [230]. The difference in amount of glucose units in both 7 and 3 position may have caused compound **7** (5 glucose units) to elute later than compound **5** (4 glucose units) and compound **3** (3 glucose units). Compounds **1**, **3**, **5**, **7**, **19** and **21** have previously been reported in cauliflower waste extract [224].

2.4.4.2.2. Acylated flavonoid-*O*-glycosides

A total of 11 acylated flavonoid-*O*-glycosides were detected in the cauliflower waste methanolic extract, by comparing the chromatogram of the native extract with the

chromatogram after alkaline hydrolysis. Also as reported in [220], acylated compounds were determined by observing a shift in the λ_{\max} to around 320-340nm. The acyl moieties were characterized by observing the neutral loss of -146 (coumaroyl), -206 (sinapoyl), -176 (feruloyl), and -192 (hydroxyferuloyl) amu from the glycoside molecule [20].

Compounds **20** (m/z 815), **22** (m/z 785), and **23** (m/z 755) were identified due to the observed losses of -206, -176, and -146 amu, resulting in a peak at m/z 609, which corresponds to a kaempferol diglucoside. The high relative abundance of ($[Y_0-H]^+$) m/z 284 indicates that the glycosylation site is at the 3-*O* position. Therefore, they were named as kaempferol-3-*O*-sinapoyldiglucoside, kaempferol-3-*O*-feruloyldiglucoside, and kaempferol-3-*O*-coumaroyldiglucoside, respectively.

For monoacylated di-*O*-glycosides, the position of the acyl moiety was based on the presence of both acylated and deacylated fragment ions. The number of intact glycoside groups and the number of sugars in each group was first analyzed. Then, different conformations were drawn and the possible fragments were predicted. The predicted fragments were compared to the fragments found in the MS chromatogram. As shown in Figure 2.8, compound **10** m/z 977 yielded fragment ions at m/z 815, 609, 284, which indicated the presence of a diglycosidic moiety, a single glucose moiety and a sinapoyl moiety attached to a kaempferol aglycone. Three conformations were predicted. Assigning a 3-glucose-7-sinapoyldiglucose identity should yield an abundant fragment ion m/z 447. If the sinapoyl moiety is attached to a single glucose unit, it should yield an ion fragment of m/z 653. Since both fragments were not abundant after high energy CID, the only possible identity is a kaempferol-3-*O*-sinapoyldiglucoside-7-*O*-glucoside, which would yield the observed fragments. As also seen in Figure 2.8, a number of co-eluting components were found at the low energy spectra. These compounds, when fragmented at the same time as the target compound, could yield fragments that may hinder identification of the target compound. Therefore, high definition MS along with ion mobility separation was necessary to separate these co-eluting components, thus allowing identification.

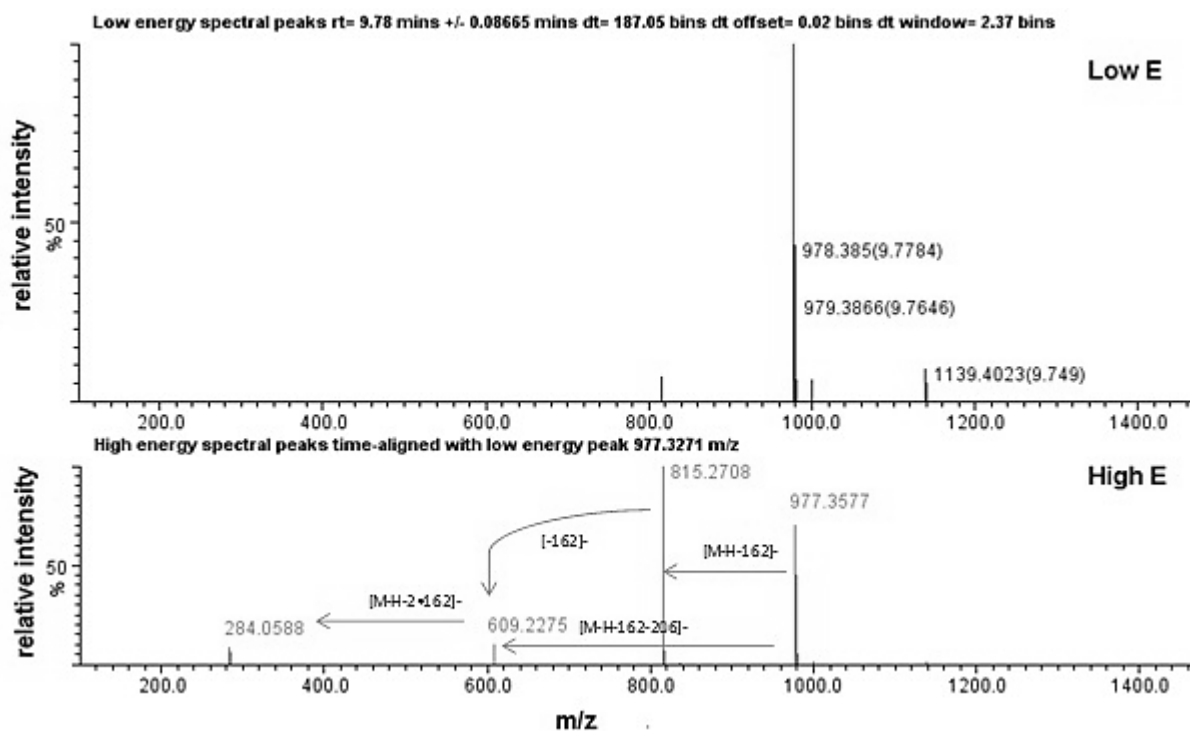


Figure 2.8. Time aligned chromatogram of peak 10 (identified as kaempferol-3-*O*-sinapoyldiglycoside-7-*O*-glucoside) in low (top) and high (bottom) energy CID in negative ionization mode

Following the same principle, compound **18** (m/z 947) with fragments m/z 609, 771, 785, 284 was named kaempferol-3-*O*-diglycoside-7-*O*-feruloylglucoside. On the other hand, compound **12** with the same m/z as compound 18, was named kaempferol-3-*O*-feruloyldiglycoside-7-*O*-glucoside, since the relative abundance of the ion m/z 785 was higher than that of m/z 609. Compound **4** m/z 963 yielded fragment ions m/z 609, 771, 801, 284 (most abundant first), which corresponded to a diglucose, glucose and a hydroxyferuloyl moiety. This was tentatively identified as kaempferol-3-*O*-diglycoside-7-*O*-hydroxyferuloylglucoside. Fragmentation of compound **14** (m/z 917) resulted into m/z 755, 284, 609 (most abundant first), which represented the presence of diglucose, glucoside and coumaroyl moieties and was then identified as kaempferol-3-*O*-coumaroyldiglycoside-7-*O*-glucoside. Compound **15** (m/z 1109), on the other hand, lost feruloyl and 2 diglucose moieties after the fragmentation, which resulted to fragments m/z 785, 609, 284. This was tentatively identified as kaempferol-3-*O*-feruloyldiglycoside-7-*O*-diglycoside.

Compound **9** (m/z 963) was fragmented into m/z 609, 801, 771, 300 which corresponded to a loss of hydroxyferuloylglucoside (-354amu), a glucose unit and a coumaroyl moiety from a quercetin aglycone. This was then named as quercetin-3-*O*-coumaroylglucoside-7-

O-hydroxyferuloylglucoside. Compound **13** (m/z 1109) on the other hand showed fragments m/z 755, 947, 284 resulting from the loss of a coumaroyl, hydroxyferuloyl, glucose and diglucose conjugates. Analyzing possible patterns, as described above, this compound was tentatively identified as kaempferol-3-*O*-coumaroyldiglucoside-7-*O*-hydroxyferuloylglucoside. Compounds **10**, **15**, **18**, **20** have been previously identified in cauliflower waste [224].

2.4.4.2.3. Other flavonoid glycosides

In principle, a glycan unit can be conjugated to any of the hydroxyl groups in the aglycone molecule. However, the 3-*O*-position is favored for flavonols, such as kaempferol and quercetin [19], which are the abundant aglycones in the extract. The 7-*O*-position is also available for glycosylation [19] while attachment of glycan constituents directly to the aglycone backbone, in the case of *C*-glycosides is not commonly reported especially for *Brassica* extracts. *C*-glycosides have only been found to be conjugated at the C-6 and/or C-8 position of the flavone aglycone [228]. When an aglycone is conjugated at both C and O positions, it is referred to as *O,C*-glycosides, and their structural characterization has been extensively discussed before [20,226].

Other flavonoid glycosides in the cauliflower extract with higher degrees of glycosylation were easily detected due their loss of 3-4 glycoside moieties. As mentioned earlier, the number of glycan neutral losses is considered as the number of glycosylation positions. Hence, the 3rd and/or 4th glycan loss must come from a C-position or the B-ring. Also, the loss of water molecules, which is typical for *C*-glycosides (more pronounced in 6-*C* glycosides) [20] was observed in some compounds. This water loss comes from the interaction of the sugar ring to the 5- or 7- hydroxyl group of the aglycone [20]. Compounds **2** (m/z 950), and **6** (m/z 1095) contained 3-4 glycoside moieties and lost water molecules, H₂O (18 Da) and 2•H₂O (36 Da), respectively, resulting in m/z 933. Compound **8** contains 5 glycan units, which is composed of 6 glucose molecules in total. Compounds **11** and **16**, on the other hand also lost hydroxyferuloyl, and feruloyl moieties. Unfortunately, the proposed method is limited to the structural characterization of *O*-glycosides and the exact structure of *O,C*-glycosides cannot be derived. However, the technique can still be useful in ascertaining the number of glycoside constituents as well as the acylation of these compounds.

The use of alternating low and high energy to provide precursor and product ions for the study of flavonol-di-*O*-glycosides has been reported earlier [227]. However, only the structural characterization of di-*O*-glycosides was reported and did not include mono-*O*-

glycosides. In addition, data-dependent acquisition was used in this study, wherein the precursor molecule was initially chosen at MS^1 and the ions were subjected to low energy and high energy CID at MS^2 . In our proposed method, a data-independent approach was used, wherein all precursor and products are simultaneously analyzed in both low and high energy CID in a single chromatographic run. This method has previously been named as an “all-in-one” analysis for metabolite identification [208]. Since all ions are collected and fragmented simultaneously, a potential problem arises when using this technique to study the phenolic content of complex matrices, such as plant extracts. Considering the vast array of metabolites and other components in plant extracts, a single peak in the U(H)PLC-DAD may not necessarily mean that it is composed of only 1 compound, as shown in Figure 2.6. This therefore brings a multitude of ions into the MS analyzer making it very challenging to elucidate the structure of the compounds of interest. For this, adequate sample clean-up using solid phase extraction and ion mobility separation (IMS) was employed. IMS has been coupled to the U(H)PLC-MS to enable an extra orthogonal dimension to sample separation and definition [215]. With this, co-eluting components are both retention and drift time-resolved, which makes structural characterization of certain components from a mixture and/or natural extract possible. Although, it must be noted that a traveling T-wave ion mobility separation (TWIMS) provides low resolving power but great sensitivity and easy integration into an MS system [214]. This drawback brings a disadvantage, wherein the mass accuracy, especially in the high energy spectra, could be lower than with conventional TOF-MS systems. The same observation was previously reported when using TWIMS in proteomics [231,232]. This was attributed to the design of the machine itself. TWIMS operate at higher pressure than TOF, therefore, an ion must traverse different pressure gradients before reaching the detector. This movement from low to high pressures lead to losses in accuracy. Also, TWIMS operate in such a way that ions are accumulated in packets before sent through the drift tube since an ion cannot enter the drift tube while another ion is being separated in the IMS. This accumulation has been thought to result in detector saturation which also reduces the sensitivity of the machine [231]. Recent advances in IMS-MS technology may solve this issue. Nonetheless, for proteomic study of *E. coli* digests, a significantly higher amount of metabolites can be detected and identified using IMS compared to not using IMS in MS^E mode, which demonstrates the advantage of using IMS especially in complex matrices [231].

Although the technology has long been available, a lot of further studies need to be done in order to improve the utility of this technology in the analysis of metabolites, especially from a complex sample. In this paper, it was demonstrated that a rapid technique such as presented could be seen as essential in routine analysis of flavonoids from natural or

complex matrices, such as agro-industrial wastes. This will pave the way to the utilization of such wastes as a source of important bioactive ingredients, such as flavonoids.

2.5. Conclusion

The proposed U(H)PLC-ESI-IMS-HDMS/MS^E method is a useful tool for the rapid detection and structural characterization of phenolics from a complex matrix, such as cauliflower waste methanolic extract. This method utilizes known principles already reported in literature, like formation of radical ions and relative abundances of product ions, but combining all these in a single chromatographic run. Because identification is done in a single injection, co-eluting compounds after U(H)PLC may prevent accurate structural elucidation in MS^E mode. With this, ion mobility separation (IMS) was used as an additional orthogonal separation tool. As a sample matrix, cauliflower waste methanolic extract was used since it contains a wide array of phenolic compounds. A total of 19 flavonoid glycosides, 8 non-acylated and 11 acylated, with kaempferol and quercetin as the aglycone were detected and structurally characterized in one chromatographic run. In addition, 6 kaempferol glycosides were suspected to be *O,C*-glycosides, although their structure could not be exactly elucidated. The technique shown therefore provides a rapid method for the determination of the flavonoid composition of plant extracts, in this case cauliflower waste, as compared to traditional LC-tandem MS experiments. This therefore could be an important tool for routine analysis of phenolics in complex matrices and to elucidate the potential of agro-industrial waste products as important source of bioactive materials.

The method developed herein was hereto used for the characterization of flavonoids in other plant matrices, as well as to investigate their bioavailability and cellular metabolism in the succeeding chapters.

Chapter 3

Combined alkaline hydrolysis and ultrasound-assisted extraction for the release of nonextractable phenolics from cauliflower (*Brassica oleracea* var *botrytis*) waste

Chapter 3: Combined alkaline hydrolysis and ultrasound-assisted extraction for the release of nonextractable phenolics from cauliflower (*Brassica oleracea* var *botrytis*) waste

3.1. Abstract

Cauliflower waste contains high amounts phenolic compounds but conventional solvent extraction miss out high amounts of nonextractable phenolics (NEP), which may contribute more to the valorization of these waste streams. In this study, the NEP content and composition of cauliflower waste was investigated. The ability of alkaline hydrolysis, sonication and their combination to release NEP was assessed. Alkaline hydrolysis with sonication was found to extract the highest NEP content (7.3 ± 0.17 mg gallic acid equivalents (GAE)/g dry waste), which was higher than the extractable fraction. The highest yield was obtained after treatment of 2M NaOH at 60 °C for 30 min of sonication. Quantification and identification was done using U(H)PLC-DAD and U(H)PLC-ESI-MS^E. Kaempferol and quercetin glucosides along with several phenolic acids were found. The results of the study show that there are higher amounts of valuable health-promoting compounds from cauliflower waste than what is currently described in literature.

Keywords: U(H)PLC-MS, ultrasound-assisted extraction, bound phenolics

Redrafted from:

Gonzales GB, Smagghe G, Raes K, Van Camp J. 2014. Combined alkaline hydrolysis and ultrasound-assisted extraction for the release of nonextractable phenolics from cauliflower (*Brassica oleracea* var. *botrytis*) waste. *Journal of agricultural and food chemistry* 62 (15), 3371-3376

3.2. Introduction

The study of nonextractable phenolics, especially in foods, is recently gaining attention since it was found that a considerable amount of phenolics are left uncharacterized due to the limitations of conventional solvent extraction methods. Apparently, high contents of phenolic compounds are ester-bound or trapped within proteins, polysaccharides or cell walls and remain in the residue after conventional solvent extraction, which are normally discarded [233]. Therefore, phenolic content of plant foods are generally underestimated in literature [233-236]. Further, it was found that the levels of nonextractable phenolics were actually higher than the extractable ones. To date, more than half of the phenolic content of the foodstuff are overlooked by current literature [237,238].

If plant foods contain these high amounts of undocumented phenolic content, it can be deduced that agricultural by-products after food processing or non-edible materials from plant foods, such as vegetables, may also contain high amounts of nonextractable phenolics. If not extracted, huge amounts of potential health-promoting substances will be discarded as waste and will remain unutilized. Efforts to release nonextractable, or so-called bound, phenolics from agricultural by-products have been made but literature reports remain scarce. The release of bound procyanidins from cranberry pomace by alkaline hydrolysis of the residue left after conventional solvent extraction was earlier reported [239]. Alkaline hydrolysis of the residue was also done with potato peels to liberate bound phenolics, which turned out to be higher than in the extractable fraction [240]. The conversion of bound procyanidins into anthocyanidins through the reaction of butanol-HCl in FeCl_3 in apple pomace and others has also been reported [234,237,241].

Vegetables belonging to the *Brassica* family are excellent sources of phenolics [219]. Considering that vegetables belonging to this group are one of the most consumed, a large amount of waste is generated each year. The phenolic content of waste from cauliflower, a widely consumed member of the *Brassica* family, has been characterized in Chapter 2 and by Llorach et al. [224] and has been proven to be a good source of antioxidants [223]. However, these reports only focused on the extractable fraction of the waste stream. Nonextractable phenolics from wastes of other members of the *Brassica* family, such as pak choi and Chinese Leaf mustard [217], and rapeseed [242], have been investigated. That study however involved pre-isolation of the plant cell walls using sodium dodecyl sulfate and thereafter alkaline hydrolysis (for 96 or 15 h), which makes the process unappealing for industrial applications. Although alkaline hydrolysis has been the most widely used and generally regarded as the most effective method for

release of bound phenolics, long incubation times are normally used, thus loss due to oxidation is a risk and industrial application is impracticable. It was previously suggested that alkaline hydrolysis at 60 °C resulted in the highest procyanidin content release from cranberry pomace in only 15 min [239]. In the case of vegetables, however, where strongly bound phenolic acids instead of procyanidins are present, these conditions might not be sufficient.

Ultrasound-assisted extraction is one of the most simple and inexpensive methods suited for industrial purposes. Several industrial scale applications have been made for extraction of different components from various sources [243-246]. Sonication involves the generation of sound waves that trigger extremely high alterations in pressure, leading to formation of cavitation bubbles, that damage the plant matrix and release extractive compounds [243,247]. The use of sonication in the release of nonextractable phenolics has not been widely investigated, more so the combination of sonication and alkaline hydrolysis.

Therefore, the aim of this study was to investigate the use of sonication and the combination of sonication and alkaline hydrolysis in the release of nonextractable phenolics from cauliflower waste. The yield of total nonextractable phenolics compared to the extractable fraction was also investigated. Different factors, such as sonication time, NaOH concentration and temperature were optimized to yield the highest total nonextractable phenolic content. Thereafter, the phenolic composition of the nonextractable fraction was characterized and quantified using advanced LC-MS techniques. Furthermore, the nonextractable phenolic compositions of the blade and petiole parts were also individually evaluated.

3.3. Materials and methods

3.3.1. Reagents

Kaempferol and quercetin, ferulic, *p*-coumaric, gallic and sinapic acids were purchased from Sigma (St. Louis, MO). U(H)PLC-MS grade methanol and formic acid were acquired from Biosolve (Valkenswaard, the Netherlands). Analytical grade methanol used for extraction, HCl and NaOH were purchased from VWR International (Leuven, Belgium).

3.3.2. Conventional extraction of EP and collection of residues containing NEP

Cauliflower (*Brassica oleracea L. var. botrytis*) wastes were obtained in a field in Ieper (Belgium) during harvest (July 2012) and stored at -20 °C and lyophilized. Dried leaves were ground and homogenized using a stirrer. Extraction was based on the method of Gonzales et al (2014). Briefly, approximately 2 g of leaves were placed in 50 mL tubes

and homogenized with 15 mL methanol at 10,000 rpm using an ultraturrax for 45 s. The tubes were then placed on ice for 15 s. The mixture was centrifuged at $13,000 \times g$ for 10 min at 4 °C. The residue was re-extracted with 80% MeOH using the same procedure. After removal of the supernatant, the residue was dried under vacuum and stored at -20 °C until further analysis. Concurrently, blade and petiole parts were also manually separated and extracted separately. Extractions and analyses were done in triplicate.

3.3.3. Measurement of total phenolic content (TPC)

TPC was analyzed using the Folin-Ciocalteu method [248] with slight modifications and expressed as mg gallic acid equivalents (GAE). Briefly, 50 μ L of sample, 100 μ L of Folin-Ciocalteu reagent and 1.2 mL of distilled water were mixed in a 2 mL cuvette. After 5 min, 150 μ L of 20% sodium carbonate was added and the mixture was incubated for 2 h in the dark. TPC was then measured at 760nm. Calibration curves were drawn using gallic acid with R^2 values >0.98 . All analyses were performed in triplicates.

3.3.4. Alkaline hydrolysis and choice of solvent on the total phenolic content (TPC) of residues

Prior to optimization of the alkaline hydrolysis conditions, the choice of a suitable solvent and the effect of sonication was investigated. For this, a method previously used for the release of bound procyanidin from cranberry pomace by alkaline hydrolysis was employed [239]. Briefly, 0.1g of residue was hydrolyzed using 2mL of 2M NaOH for 15 min at 60 °C in a screw-capped test tube previously flushed with nitrogen. The samples were then neutralized using 2M HCl and extracted twice with different solvents for 2 min under vortex. Extraction solvents used were 4mL of methanol, acetone or ethyl acetate (all containing 0.1% formic acid). The tubes were centrifuged for 10 min at $10,000 \times g$ and 4 °C. Extraction was done twice and the supernatants were pooled and standardized to 20mL using the corresponding solvents. Since methanol extracted significantly more phenolics, based on TPC, than ethyl acetate and acetone (results not shown), methanol was used as the extraction solvent for all other subsequent analyses.

3.3.5. Effect of sonication and combination with alkaline hydrolysis (sonicated alkaline hydrolysis)

The effect of sonication on the release of nonextractable phenolics was tested by mixing 0.1g of residue with 20mL of methanol in a sonicated bath for 15 min at 60 °C previously flushed with nitrogen. The ultrasonic extraction procedure was performed in an Elmasonic S60H unit with a frequency of 37kHz and nominal power of 180 W. The dimensions of the bath were 300mm (W)/150mm (D)/150mm (H) and was filled with 2L of water. The suspension was centrifuged at $10,000 \times g$ at 4 °C for 10 min. The supernatant was kept for analysis.

Subsequently, the effect of combining alkaline hydrolysis and sonication was tested by sonicating a mixture of 0.1g residue with 2mL of 2M NaOH at 60 °C for 15 min. The phenolic content was extracted with methanol, as described above. Therefore, 3 set-ups were made: 1) alkaline hydrolysis, (2) ultrasound-assisted extraction, and (3) combined alkaline hydrolysis and sonicated extraction. Considering that sonicated alkaline hydrolysis significantly increased the TPC, optimization of this treatment was performed.

3.3.6. Optimization of the sonicated alkaline treatment of the residue

The conditions for sonicated alkaline hydrolysis were optimized to increase the TPC of the extract. Hydrolysis experiments were performed using a 3³ factorial design comprising of 3 different temperatures (40 °C, 60 °C, 80 °C), NaOH concentrations (1M, 2M, 4M) and sonication time (15, 30, 45 min). Each treatment consisted of one temperature, one NaOH concentration and one sonication time, thus 27 treatments in total. The analysis was performed in triplicates. Therefore, 0.1g of residue was placed in 81 screw-capped test tubes and these were hydrolyzed under varying conditions as described in Table 3.1 and extracted as earlier described. Extracts are henceforth referred to as NEP solution.

Table 3.1. Treatment Conditions for Sonicated Alkaline Hydrolysis Treatment Optimization

Temperature (°C)	NaOH concentration (M)	Sonication time (min)
40	1	15
60	2	30
80	4	45

3.3.7. Solid phase extraction (SPE)

A 1 mL-aliquot of the NEP solution was diluted in 20 mL of 0.1% (v/v) formic acid (in ultrapure water) and loaded into a preconditioned C18 solid phase extraction (SPE) cartridge (500 mg/4 mL) (Davison Discover Science, Deerfield, IL, USA). Preconditioning was done by loading the column with 2 × 3 mL methanol and 2 × 3 mL water, which was allowed to stand for at least 2 min for every solvent, prior to use. After loading the sample, the cartridge was washed with 5 mL of 0.1% (v/v) formic acid and the phenolic compounds were recovered using 3 mL of methanol containing 0.1% (v/v) formic acid. The samples were then dried using nitrogen and re-dissolved in 1 mL of 10% methanol (0.1% v/v formic acid) prior to LC-MS analysis.

3.3.8. Identification of compounds using U(H)PLC-ESI-MS and quantification by U(H)PLC-DAD

Structural identification of the flavonoids was performed using the method developed in Chapter 2. Quantification was done using a Thermo Dionex Ultimate 3000 U(H)PLC (ThermoScientific, Landsmeer, the Netherlands) equipped with a diode-array detector at 280nm and 330nm using authentic standards. Column specifications as well as gradient elution is the same as described above. The content of flavonoid glycosides were quantified using their aglycone equivalent – kaempferol for kaempferol glycosides, and quercetin for quercetin glycosides; while phenolic acids were quantified using authentic standards. It must however be considered that quantifying flavonoid glycosides with their corresponding aglycones may lead to inaccuracies due to the bathochromic shift in the absorption maxima of the glycosides compared to aglycones. These quantifications are therefore close estimations and should not be regarded as absolute quantification of the flavonoid glycoside contents. Table 3.2 shows the R^2 values, limit of detection (LOD) and limit of quantification (LOQ) of the standards used. LOD and LOQ were calculated using the following equation:

$$\text{eq 1. } LOD = 3 \left(\frac{Sbl}{S} \right) \text{ and } LOQ = 10 \left(\frac{Sbl}{S} \right);$$

where Sbl is the standard error of the intercept and S is the slope of the respective calibration curves as calculated using the LINEST function.

Table 3.2. Standards Used for the Quantification of Phenolics

	Slope	Intercept	R^2	LOD (ppm)	LOQ (ppm)
Kaempferol	0.91	0.85	0.98	3.83	12.77
Quercetin	0.96	-0.24	0.99	1.51	5.03
caffeic acid	2.20	0.76	0.99	0.85	2.82
coumaric acid	4.50	1.12	0.99	0.57	1.91
ferulic acid	2.36	0.35	0.99	0.33	1.09
synapic acid	0.65	0.28	0.99	0.83	2.77

3.3.9. Statistical Analysis

Data were analyzed using one-way ANOVA using SPSS v.21 (IBM, Chicago, USA). Differences were considered significant when $p < 0.05$. Differences between means (post-hoc) were determined using Tukey test.

3.4. Results and Discussion

Figure 3.1 shows the TPC of the cauliflower waste after conventional extraction (EP), the residue following alkaline hydrolysis (60 °C, 2M NaOH for 30 min), sonicated extraction, and sonicated alkaline hydrolysis. The TPC of the EP fraction was 6.1 ± 0.05 mg GAE/g dry waste. However, as shown, the residue left after conventional solvent extraction of the cauliflower waste contained a considerable amount of phenolics, which current literature may have missed out, regardless of the method employed. Sonication alone of the residue yielded the lowest TPC (1.5 ± 0.12 mg GAE/g dry waste). Alkaline hydrolysis on the other hand released significantly higher amounts of phenolics from the plant matrix (6.5 ± 0.27 mg GAE/g dry waste). However, this content is ever more significantly ($p < 0.05$) increased by the combination of sonication and alkaline hydrolysis (7.3 ± 0.17 mg GAE/g dry waste). The amount of NEP therefore comprises more than half of the total phenolic content, meaning that NEP is actually more than EP in terms of content.

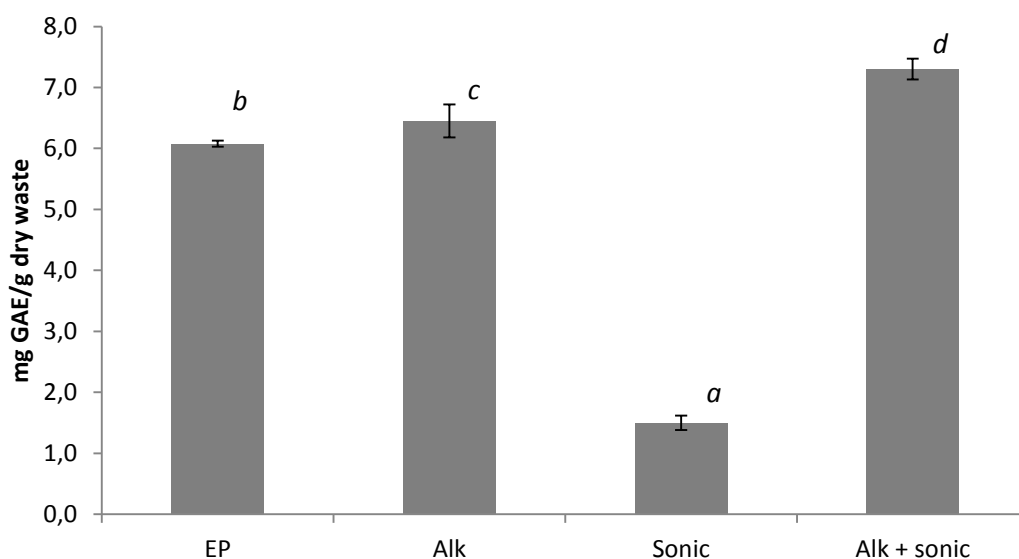


Figure 3.1. Total phenolic content of cauliflower waste (mg GAE/g dry waste) following conventional solvent extraction (EP), alkaline hydrolysis (Alk), sonicated extraction (Sonic), and sonicated alkaline hydrolysis (Alk+sonic). Different letters indicate statistical difference ($p < 0.05$).

The results reveal that alkaline hydrolysis may not necessarily liberate all bound phenolic compounds in a short time span. Increasing the incubation time however may induce oxidation and loss of target compounds. Therefore, other techniques to increase yield without increasing temperature and incubation time are necessary [239]. In this study, it was shown that using ultrasonication along with alkaline hydrolysis serves as an effective

method in increasing yield of nonextractable phenolics. Ultrasonication, as earlier mentioned, damages the plant matrix which increases the surface area of the sample. This probably allows the sodium hydroxide to react more efficiently in the matrix to break ester linkages and release the phenolic compounds. While the use of sonication has been described as an effective method of extracting cellular content to liberate phenolics from various plant matrices [244-246], its ability to break linkages that attach phenolics from other macromolecules has not been well described in literature. Therefore, combining sonication and alkaline hydrolysis seems to be a logical method. It must be considered that ultrasonication causes an increase in temperature due to the shear forces generated. Therefore, the sonication was performed in a temperature-controlled sonic bath and the temperature was manually adjusted whenever necessary. Considering that sonicated alkaline hydrolysis yielded higher TPC, the effect of temperature, NaOH concentration and sonication time was investigated.

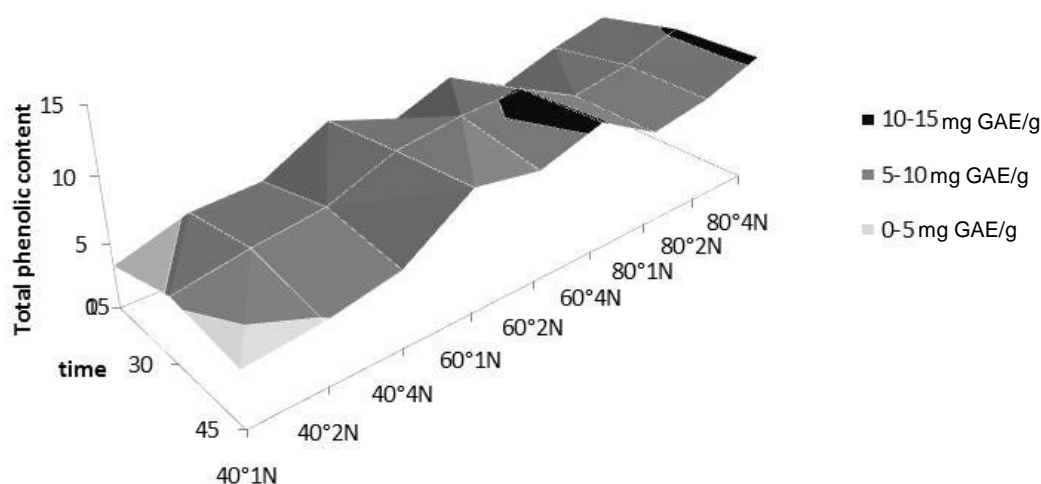


Figure 3.2. Optimization of sonicated alkaline hydrolysis treatment of residue after conventional solvent extraction

Table 3.3. Analysis of Variance for Total Phenolic Content under Sonicated Alkaline Hydrolysis Extraction

Source	df	F	Sig,
Temp	2	313.38	<0.001
M	2	60.698	<0.001
Min	2	53.908	<0.001
temp * M	4	10.443	<0.001
temp * min	4	3.966	<0.001
M * min	4	0.993	0.420
temp * M * min	8	2.391	0.028

Figure 3.2 shows the 3D plot of the TPC as affected by time, NaOH concentration and temperature. The ANOVA statistics are shown in Table 3.3. Accordingly, there are significant differences among treatments and also significant interactions among the different parameters, except for the interaction between NaOH concentration and sonication time. A significant interaction is noted when temperature is considered, which denotes the importance of this parameter. Looking at the effect of temperature alone, it was observed that TPC at 60 °C and 80 °C are not significantly different from each other, but are both significantly higher than 40 °C. Considering process efficiency, 60 °C is preferred over 80 °C. Also, it was observed that at 60 °C, TPC of 30 and 45 min of sonication were similar and are significantly higher than 15 min. Finally, TPC of 2M and 4M were similar and are both significantly higher than 1M NaOH concentration. Therefore, the optimal condition for the release of NEP from cauliflower waste was 60 °C, 2M NaOH for 30 min under sonication. In the end, the TPC of the NEP solution was found to be 9.82 ± 0.82 mg GAE/g dry residue or around 7.3 mg GAE/g dry waste sample. Adding TPC of the EP fraction, the waste material therefore contained 13.4 mg GAE/g dry waste; of which around 45% are extractable and 55% are nonextractable.

To gain better understanding on the nonextractable phenolics from cauliflower waste, the extract after sonicated alkaline hydrolysis was passed through a C18 solid-phase extraction column to remove the salts and prepare it for U(H)PLC analysis and phenolic content identification using a mass spectrometer. Figure 3.3 shows the U(H)PLC-DAD of the cauliflower waste NEP solution. Structural characterization and MS characteristics of flavonoid glycosides were described in Chapter 2. The occurrence of similar compounds in the NEP solution was detected by comparing their masses and retention times after LC-ESI and LC-DAD analysis. Table 3.4 shows the list of phenolics identified in the NEP solution as well as their content.

Table 3.4. Phenolic Profile of Nonextractable Phenolics from Cauliflower Waste

Peak no.	Identity	rt (min)	m/z values		λ max (nm)	Content ^a ($\mu\text{g/g}$ dry waste)
			MS	MS ^E		
1	quercetin-3-O-diglucoside-7-O-glucoside	6.04	787.1895	787,625,462,300	254, 348	94 \pm 0
2	kaempferol-3-O-triglucoside-7-O-glucoside	6.7	933.3650	933, 771, 446, 284	265, 348	520 \pm 28
3	kaempferol-3-O-diglucoside-7-O-glucoside	6.9	771.2859	771,609,285	265, 346	2485 \pm 66
4	kaempferol-3-O-triglucoside-7-O-diglucoside	7.08	1095.343	771,609,284, 1095,	268,331	429 \pm 16
5	kaempferol-3-O-diglucoside-7-O-diglucoside	7.45	933.3425	933,609,285	265, 345	550 \pm 21
6	caffeic acid	7.96	179.0562	179, 135	216, 323	24 \pm 4
7	coumaric acid	12.25	163.0603	163,119	218, 309	39 \pm 2
8	ferulic acid	14.97	193.0848	193, 134	223, 323	451 \pm 19
9	sinapic acid	15.52	223.0974	223,208	222,323	1071 \pm 45
10	kaempferol-3-O-triglucoside	15.90	771.1885	771,284	267, 346	134 \pm 17
11	kaempferol-3-O-diglucoside	16.60	609.1251	609,284	265, 346	479 \pm 35

^aContent of individual phenolics were based on calibration curve of their respective aglycone equivalent expressed as μg phenolic/g dry waste

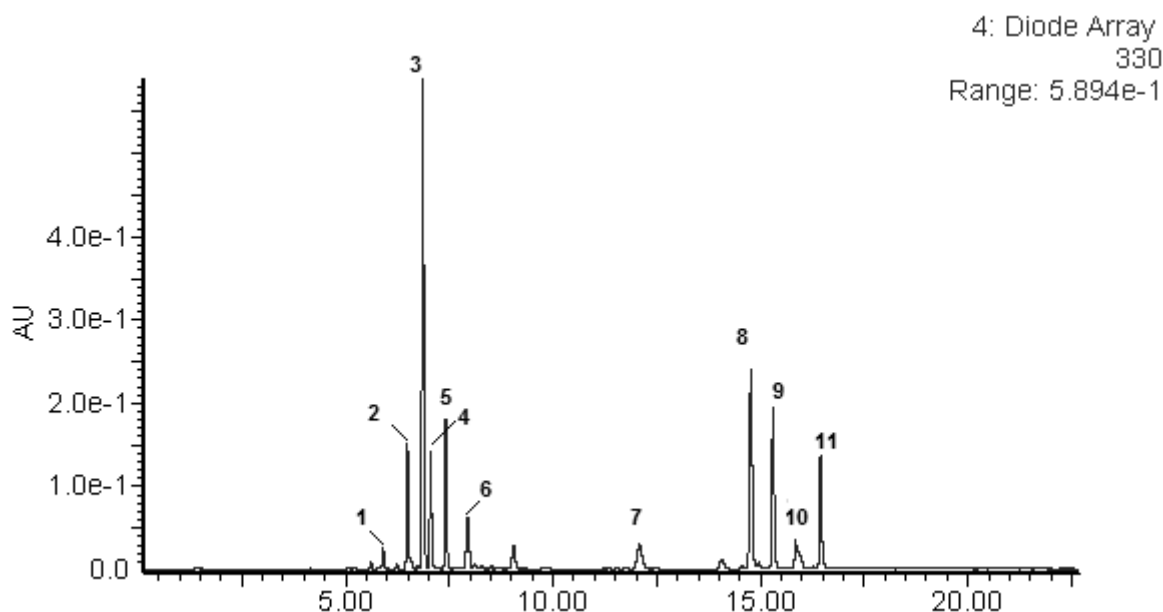


Figure 3.3. U(H)PLC-DAD chromatogram of cauliflower waste nonextractable phenolics after sonicated alkaline hydrolysis (see Table 3.4 for identities of the peaks). For comparison with the extractable fraction, please refer to Figure 2.5 in Chapter 2

As shown, NEP is comprised dominantly by flavonoid glycosides that are also found in the EP fraction. Kaempferol-3-*O*-diglucoside-7-*O*-glucoside is the most abundant flavonoid present in the NEP fraction (2.4 ± 0.1 mg/g dry waste) while sinapic acid (1.1 ± 0.0 mg/g dry waste) was the most abundant phenolic acid. It should be noted however that since the process involved alkaline hydrolysis, the analysis is limited to the fact that acylated flavonoid glycosides may also be present in the NEP fraction but cannot be determined. This is because alkaline hydrolysis also cleaves the ester linkage between the phenolic acid and the flavonoid glycoside [224]. Also, since phenolic acid-glucosides are linked via an ester linkage, which is also degraded in alkaline conditions [249], the occurrence of glucosidic forms of phenolic acids cannot be seen. Therefore, while phenolic acids and flavonoid glycosides may be isolated from the NEP fraction, the fact that they may actually come from the same parent molecule, for example kaempferol-feruloyl-glycoside, or the occurrence of phenolic acid glucosides, such as feruloyl-glucoside, cannot be determined with this current method.

The high amounts of phenolic acids found in the NEP fraction is in agreement with previously reported data on the edible parts of *Brassica* species, wherein a marked increase in yield of phenolic acids were found after alkaline hydrolysis of residue left after conventional solvent extraction [217,242,250,251]. Indeed, phenolic acids are able to

bind to macromolecules, such as fibers and other oligosaccharides, which hamper their extractability using conventional solvent extraction methods.

To investigate the distribution of these phenolic compounds within the waste stream, the waste was divided into blade, which constitutes the green leafy part; and petiole, which constitute the major vein of the leaf. As shown in Table 3.5, the blades contain significantly higher amounts of phenolics than the petioles. Furthermore, the phenolic composition of blades and petioles are found to be somewhat different. More variety and higher amount of flavonoid glucosides and phenolic acids were extracted from the blade part than from the petiole. However, there seems to be a higher ratio of nonextractable phenolic acids in the petioles (relative to phenolic content) than in the blades. The most abundant phenolic compound from the blade is kaempferol-3-O-diglucoside-7-O-glucoside (4.51 ± 0.0 mg/g dry blade powder) while sinapic acid (0.29 ± 0.0 mg/g dry petiole powder) dominated the nonextractable phenolic content of the petioles. In total, 74% of the phenolic composition of the blades is flavonoid glucosides. Conversely, most of the nonextractable phenolics in the petioles are phenolic acids, especially sinapic and ferulic acids, which comprised 57% of the phenolic content. This distribution could be due to the fact that phenolic acids are generally found to be bound to plant fibers and cell walls [217], which are higher in the petioles than in the leaves. While the linkage of phenolic acids in cell-wall components have been largely observed, especially in *Brassica* species [217,250,251], little is known about nonextractable flavonoids. Bound flavonoids have been characterized from pepper [252], Euphorbia [253] and other plants. An in-depth study on the tissue distribution of flavonoids in *Ligustrum vulgare* revealed that flavonoids, such as kaempferol and quercetin glucosides, are attached to lipid bilayers or non-covalently bound to proteins in the leaves [254]. Therefore, considering that studies of bound phenolics from *Brassica* have been done by first isolating the cell walls, information regarding flavonoids bound to membrane and membrane proteins may have been missed.

Table 3.5. Distribution Nonextractable Phenolics in the Cauliflower Waste

Compound	Content ^a	
	Blade	Petiole
Total NEP content (Folin method)	6109 ± 1045^b	940 ± 16^c
quercetin-3-O-diglucoside-7-O-glucoside	123 ± 5	54 ± 3
kaempferol-3-O-triglucoside-7-O-glucoside	1160 ± 23	nd
kaempferol-3-O-diglucoside-7-O-glucoside	4513 ± 45	98 ± 10
kaempferol-3-O-triglucoside-7-O-diglucoside	1036 ± 20	69 ± 6
kaempferol-3-O-diglucoside-7-O-diglucoside	786 ± 14	18 ± 5
caffeic acid	37 ± 2	nd
coumaric acid	6.6 ± 0	nd

ferulic acid	720±10	45±18
sinapic acid	2266±34	279±38
kaempferol-3-O-triglucoside	267±11	nd
kaempferol-3-O-diglucoside	591±25	nd
Total flavonoid glucosides	8478±79	240±23
Total phenolic acids	3030±43	324±55

^atotal phenolic content expressed as µg GAE/g dry waste; content of individual phenolics were based on calibration curve of their respective aglycone equivalent expressed as µg phenolic/g dry blade or petiole

^{b,c} different letters of the TPC indicate statistical difference ($p < 0.01$)

nd – not detected

3.5. Conclusions

In this study, we showed that there are higher amounts of valuable health-promoting compounds from cauliflower waste than what is currently described in literature. Much of the total phenolic content of this plant material rests on the NEP fraction, which eludes conventional analysis techniques. There is therefore a need to investigate further on the composition of the NEP as compared to EP. In the succeeding chapter, we investigate the use of metabolomics tools to distinguish the polyphenol composition of both EP and NEP.

Chapter 4

Liquid chromatography – mass spectrometry coupled with multivariate analysis for the characterization and discrimination of extractable and nonextractable polyphenols and glucosinolates from red cabbage and Brussels sprouts waste streams

Chapter 4: Liquid chromatography – mass spectrometry coupled with multivariate analysis for the characterization and discrimination of extractable and nonextractable polyphenols and glucosinolates from red cabbage and Brussels sprouts waste streams

4.1. Abstract

In this study, we optimized the conditions for sonicated alkaline hydrolysis to the residues left after conventional polyphenol extraction of Brussels sprouts top (80°C, 4M NaOH, 30 mins) and stalks (60°C, 4M NaOH, 30 mins), and red cabbage waste streams (80°C, 4M NaOH, 45 mins) to release and characterize the NEP fraction. The NEP fractions of Brussels sprouts top (4.8 ± 1.2 mg gallic acid equivalents [GAE]/g dry waste) and stalks (3.3 ± 0.2 mg GAE/g dry waste), and red cabbage (11.5 mg GAE/g dry waste) waste have significantly higher total polyphenol contents compared to their respective extractable polyphenol (EP) fractions (1.5 ± 0.0 , 2.0 ± 0.0 and 3.7 ± 0.0 mg GAE/g dry waste, respectively). An LC-MS method combined with principal components analysis (PCA) and orthogonal partial least squares – discriminant analysis (OPLS-DA) was used to tentatively identify and discriminate the polyphenol and glucosinolate composition of the EP and NEP fractions. Results revealed that phenolic profiles of the EP and NEP fractions are different and some compounds are only found in either fraction in all of the plant matrices. This suggests the need to account both fractions when analyzing the polyphenol and glucosinolate profiles of plant matrices to attain a global view of their composition. This is the first report on the discrimination of the phenolic and glucosinolate profiles of the EP and NEP fractions using metabolomics techniques.

Keywords: Principal components analysis (PCA), orthogonal partial least squares – discriminant analysis (OPLS-DA), polyphenols, LC-MS

Redrafted from:

Gonzales GB, Raes K, Vanhoutte H, Coelus S, Smagghe G, Van Camp J. 2015. Liquid chromatography–mass spectrometry coupled with multivariate analysis for the characterization and discrimination of extractable and nonextractable polyphenols and glucosinolates from red cabbage and Brussels sprout waste streams. *Journal of Chromatography A* 1402, 60-70

4.2. Introduction

Increasing food waste has been a growing concern in modern society. Efforts to reduce food waste have been the subject of many academic and non-academic fora. Valorization of agricultural wastes is thus a major step in alleviating this problem. We have previously shown in the previous chapters that agricultural wastes also possess high amounts of polyphenols, which could be harnessed for use in food applications, such as functional ingredients, antioxidants, etc. If these bioactive components are recovered from the waste stream, they could be used as additives to food and/or cosmetics to create high-value products. It has earlier been reported that higher amounts of phenolics are found in the NEP fraction of agricultural waste streams compared to their EP fractions [217,239,240]. Exploiting this fraction therefore results to better valorization of the waste streams. However, the differences in the phenolic profiles of the extractable and nonextractable fractions have not been deeply studied. In this paper, we investigate the EP and NEP fractions of two different waste streams belonging to the *Brassica* family, Brussels sprouts and red cabbage. Initially, the EP fraction was obtained by conventional solvent extraction and the phenolic composition was characterized. Thereafter, the residue left after solvent extraction was collected and the parameters for NEP extraction were optimized for each waste stream. This is the first report about the EP and NEP characterization of Brussels sprouts and red cabbage waste streams. More importantly, in this study, we show the use ultrahigh-pressure liquid chromatography – mass spectrometry combined with metabolomics-based analysis tools, principal components analysis (PCA) and orthogonal partial least squares – discriminant analysis (OPLS-DA), to discriminate the phenolic profile of the EP from NEP fractions and to determine which compounds cause their distinction. This provides a rapid and convenient analytical method for screening and characterizing EP and NEP without the need for quantification of the individual components or manual integration of each chromatographic peak.

4.3. Materials and Methods

4.3.1. Reagents and plant material

U(H)PLC-MS grade methanol and formic acid were acquired from Biosolve (Valkenswaard, the Netherlands) whereas analytical grade methanol, HCl and NaOH were purchased from VWR International (Leuven, Belgium).

Red cabbage (*Brassica oleracea* var. *capitata* f. *rubra*) and Brussels sprouts (*Brassica oleracea* var. *gemmifera*) waste were harvested in November 2013. For Brussels sprouts, the top leafy part was separated from the stalks and analyzed separately due to their big structural difference, while the sample material of red cabbage consisted only of the

external leaves. The plant materials were cut, blended into smaller pieces and immediately stored in a freezer at -20°C . Approximately 250 grams of each plant material were freeze-dried and ground into a fine powder with an IKA-M20 Werke Grinder and stored at -20°C until further analysis.

4.3.2. Solvent extraction of EP and collection of residues containing NEP

The solvent extraction protocol was based on the method by Olsen et al [225]. Initially, 2 grams of the freeze-dried plant powder was weighed and placed in 50 mL centrifuge tubes with 15 mL of 100% MeOH and homogenized using an IKA T25 digital Ultraturrax at 10.000 rpm for 45 seconds. The tubes were then placed on ice for 15 minutes and centrifuged at 13000 g for 10 minutes at 4°C . The supernatant (1) was collected in a 50 mL volumetric flask while the residue left in the tube was re-extracted with 10 mL 80% MeOH and re-homogenized at 10.000 rpm for 45 seconds, placed on ice for 15 minutes and then centrifuged at 13.000 g for 10 minutes at 4°C . The supernatant was added to supernatant (1) and the volume was adjusted to 50 mL using 100% MeOH. Subsequently, the residue left in the centrifuge tubes after extraction was dried under reduced pressure and was used to extract NEP.

4.3.3. Measurement of total phenolic content (TPC)

The total phenolic content (TPC) of the extracts was determined with the colorimetric Folin-Ciocalteu assay previously optimized in Chapter 3.

4.3.4. Sonicated alkaline hydrolysis of the residue left after solvent extraction

The optimization of the parameters for the sonicated alkaline hydrolysis is summarized in Table 4.1, comprising of 27 combinations, which were analyzed in triplicates.

Table 4.1. Parameters for the optimization of NEP extraction

NaOH concentration (M)	Temperature ($^{\circ}\text{C}$)	Sonication time (min)
1	40	15
2	60	30
4	80	45

Briefly, 0.1 gram of the residue was placed in a tube and mixed with 2 mL of NaOH (1M, 2M or 4M). The tubes were flushed with nitrogen for 30 seconds and sealed to prevent the oxidation of the phenolic compounds. Furthermore, the samples were incubated in a temperature-controlled ultrasonic water bath in an Elmasonic S60H unit with a frequency of 37kHz and a nominal power of 180W. The temperatures (40°C , 60°C and 80°C) and incubation times (15, 30 and 45 min) were varied depending on the set-up as earlier described in Table 4.1. Due to heating during sonication, the temperature in the water bath was checked every five minutes and adjusted if necessary.

After hydrolysis, the samples were neutralized by adding HCl. The liberated NEP was then extracted using 4 mL of MeOH (0.1% formic acid) followed by vortexing for 2 minutes. The tubes were centrifuged at 10,000 g for 10 minutes at 4°C. Extraction was performed twice and the final volume was adjusted to 20 mL using 100% methanol.

4.3.5. Solid phase extraction (SPE)

Aliquots (1 mL) of the polyphenol fractions were diluted in 20 mL of 0.1% (vol) formic acid (in ultrapure water) and loaded into a preconditioned C18 solid phase extraction (SPE) cartridge (500 mg per 4 mL) (Davison Discover Science, Deerfield, IL, USA). Columns were preconditioned by loading 2 × 3 mL methanol and 2 × 3 mL water, wherein each solvent was allowed to stand for 2 min prior to use. After loading the sample, the columns were washed with 5 mL of MilliQ water (0.1% (vol) formic acid). The polyphenols were recovered using 3 mL MeOH (0.1% (vol) formic acid). The samples were then dried using light stream of nitrogen and re-dissolved in 1 mL of 10% dimethyl sulfoxide (DMSO) in acidified water prior to LC-MS analysis.

4.3.6. Identification of compounds using U(H)PLC-ESI-MS

LC-MS analysis and structural characterization was performed following the method described in Chapter 2 while other components were tentatively identified by their exact mass and fragmentation patterns which was viewed using the MS^E data viewer software.

4.3.7. Data analysis

Data for the optimization of NEP yield (based on TPC) were analyzed by ANOVA using SPSS v.21 (IBM, Chicago, USA) while comparison between means (post-hoc) was achieved using Tukey test. Differences were considered significant when $p < 0.05$.

Principal component analysis (PCA) and orthogonal partial least squares – discriminant analysis (OPLS-DA) were used to differentiate EP versus NEP for each plant matrix. These analyses were performed using the Markerlynx™ software embedded within Masslynx (Waters Corp., Milford, MA, USA).

4.4. Results and Discussion

4.4.1. Optimization of the release of NEP from the residue of solvent extraction

Figure 4.1 shows the 3D plot of TPC as affected by temperature, NaOH concentration and time of incubation. The optimal conditions were obtained using 3-way ANOVA, wherein when 2 parameters are not significantly different, the lower value was chosen. For instance, subjecting the samples to hydrolysis for either 30 or 45 minutes does not

correspond to a significantly higher ($p < 0.05$) TPC for the Brussels sprout samples and thus, 30 minutes was chosen as the optimum condition. A list of optimal parameters is given in Table 4.2.

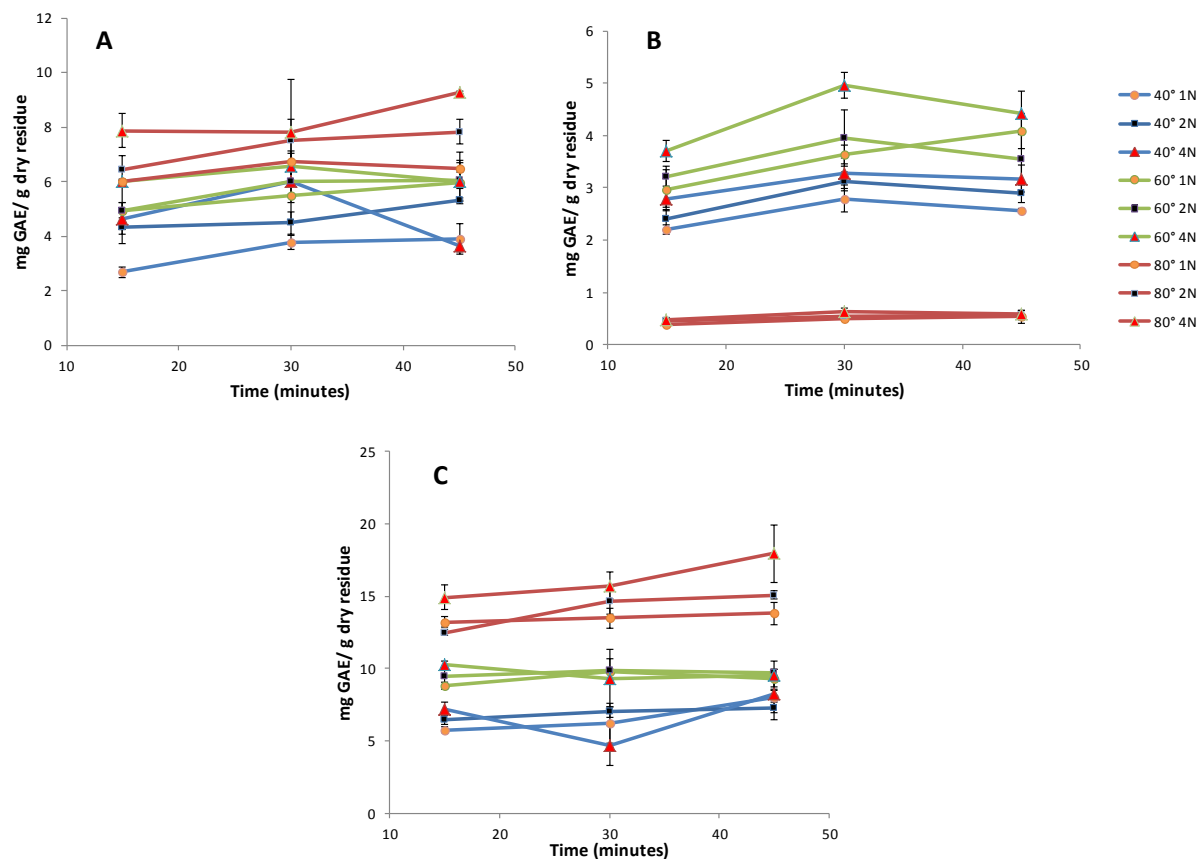


Figure 4.1. Optimization of the conditions for sonicated alkaline hydrolysis of residues after solvent extraction. A – Brussels sprouts top; B – Brussels sprouts stalk; C – red cabbage. Optimized conditions were selected based on three-way ANOVA ($p < 0.05$)

Table 4.2. Optimized conditions for the sonicated alkaline hydrolysis for the different plant materials

Plant material	Optimized condition	NEP fraction		EP fraction	
		mg GAE*/ g dry residue	g dry waste/ g dry residue	mg GAE*/ g dry waste	mg GAE*/ g dry waste
Brussels sprouts, top	80°C; 4M NaOH; 30min	7.8 ± 2.0	1.6	4.8 ± 1.2 ^a	1.5±0.0 ^b
Brussels sprouts, stalks	60°C; 4M NaOH; 30min	5.0 ± 0.3	1.5	3.3 ± 0.2 ^a	2.0±0.0 ^b
Red cabbage waste	80°C; 4M NaOH; 45min	17.9 ± 2.0	1.6	11.5 ± 1.3 ^a	3.7±0.0 ^b

*GAE = gallic acid equivalents, values are expressed as means ± SD of measurements in triplicate

^{a,b} = Different letters in the same row represent significant differences ($p < 0.05$)

The results suggest that temperature is a very important factor in the release of NEP from the plant matrix. For both Brussels sprout tops and red cabbage, an increase in temperature steadily yielded higher TPC. On the other hand, a significant increase ($p < 0.05$) was observed in the TPC of Brussels sprout stalk when the temperature was increased from 40° to 60°C but drastically dropped when the temperature reached 80°C. This suggests that the NEP profile of Brussels sprout stalk may be more thermally labile than those of the other plant matrices. In the case of red cabbage, it is however surprising that the TPC was highest at 80°C and 45 minutes considering that anthocyanins have been reported to degrade at high temperatures and pH [255,256]. Although, as will be discussed later in this chapter, other phenolic compounds compromised for the loss of anthocyanins during the hydrolysis process, which yielded a higher net TPC.

The concentration of NaOH also played a crucial role in the process as all plant matrices released more TPC when subjected to higher NaOH concentrations. NEP from plant matrices have previously been reported to be linked via ester-linkages or physically trapped within proteins, polysaccharides, or cell walls [233]. NaOH, which is known to break ester-bonds [224], to hydrolyze cell walls [239] and to solubilize proteins, is therefore needed to liberate this polyphenolic fraction. While it is true that NaOH may also accelerate the hydrolysis of polyphenols, it is apparent that the increased yield of polyphenols compensates a lot for any losses incurred due to degradation.

In the end, results revealed that TPC of the NEP fraction is consistently higher than that of the EP (Table 4.2). With the NEP taken into account, the global TPC of Brussels sprout stalk is 2.6 times more than the EP fraction alone, and 4 times more for Brussels sprout top and red cabbage.

4.4.2. Characterization of phenolic compounds

A total of 51 chromatographic peaks were identified in the plant materials, consisting of different classes of polyphenols and glucosinolates (Table 4.3). Proposed identities of these metabolites were based on their retention times, exact mass, and fragmentation patterns in both negative and positive modes. For glucosinolates, their masses were compared to those glucosinolates earlier reported in literature for *Brassica* species. The identified metabolites belonged to various classes, such as phenolic acid derivatives, flavonoid glycosides, acylated flavonoid glycosides, glucosinolates and anthocyanins. Most of metabolites identified were flavonoid glycosides. Figure 4.2 shows the DAD chromatograms of the different plant matrices at 280nm. It can already be seen that

phenolic compounds are indeed left in the plant matrix after conventional solvent extraction. However, some peaks appeared to have high absorbance at 280nm but did not have a corresponding mass spectra (due to poor ionization), which made identification impossible. For instance, the peak at 3.38 mins of the NEP of the top leaves has absorbance maxima of 282 and 227nm. No relevant ion peak could be seen at this retention time in both positive and negative mode and so this peak was considered non-phenolic.

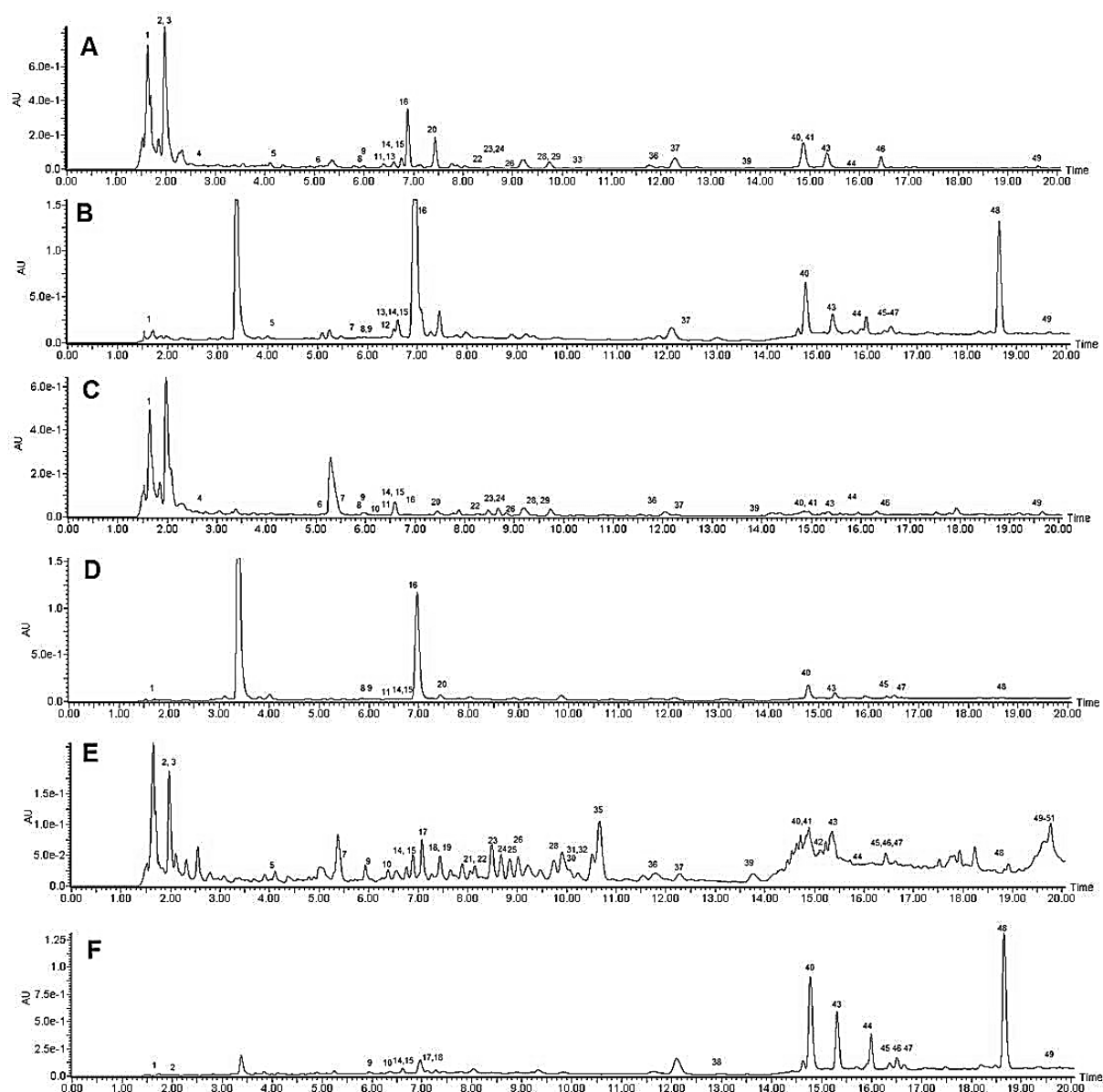


Figure 4.2. UV chromatogram (280 nm) of (A) Brussels sprouts top EP fraction, (B) Brussels sprouts top NEP fraction, (C) Brussels sprouts stalk EP fraction, (D) Brussels sprouts stalk NEP fraction, (E) Red cabbage EP fraction, (F) Red cabbage NEP fraction

Table 4.3. Identification of phenolic compounds found in the plant matrices

Peak #	Tr (mins)	MS(1)	MS ^E	Tentative identification*	Brussels sprouts				Red cabbage	
					Top EP	Top NEP	Stalk EP	Stalk NEP	EP	NEP
1	1.7	191.043		quinic acid	+	+	+	+		+
2	1.9	388.0316		progoitrin	+		+			+
3	2.0	358.0263	358, 116	sinigrin	+		+			+
4	2.7	372.043		gluconapin	+		+			+
5	4.2	463.0509		hydroxyglucobrassicin	+	+				+
6	5.1	447.0519		glucobrassicin	+		+			
7	5.7	949.2839	949, 787, 462, 300	quercetin-3-triglc-7-glc		+	+			+
8	5.9	353.1		chlorogenic acid	+	+	+	+		
9	6.0	787.1973	787, 625, 462, 299	quercetin-3-diglc-7-glc	+	+	+	+		+
10	6.3	1111.313	1111, 787, 624, 301	quercetin-3-diglc-7-triglc			+	+		+
11	6.5	787.2181	787, 463, 625, 301	quercetin-3-glc-7-diglc	+		+			
12	6.6	933.2577	933, 771, 446, 429, 609	kaempferol-3-diglc-7-glc-5-glc		+				
13	6.6	933.2463	933, 771, 446, 284	kaempferol-3-triglc-7-glc	+					
14	6.7	949.2273	949, 625, 300	quercetin-3,7-di-O-diglc	+	+	+	+		+
15	6.7	355.0998	355, 193	ferulic acid glc	+	+	+	+		+
16	7.0	771.1981	771, 609, 446, 284	kaempferol-3-diglc-7-glc	+	+	+	+		
17	7.1	1095.3069	1095, 771, 609,	kaempferol-3-triglc-7-diglc						+

				285						
18	7.2	547.1658	547, 385, 223	sinapic acid diglc					+	+
19	7.3	1273.3679	1273, 1111, 949, 787, 300	quercetin-3-triglc-7-glc-5-diglc						+
20	7.5	933.2689	933, 609, 284	kaempferol-3,7-di-O-diglc	+		+		+	
21	8.2	1257.3396	1257, 933, 771, 609, 1095, 284, 255	kaempferol-3-triglc-7-diglc-5-glc						+
22	8.2	477.0703		methoxy/neo glucobrassicin	+		+			+
23	8.6	993.2795	993, 787, 625, 462, 301	quercetin-3-diglc-7-sin-glc	+		+			+
24	8.6	1155.3181	1155, 993, 787, 769, 625, 462, 607, 300	quercetin sin-3,7-di-O-glc-5-diglc	+		+			+
25	8.8	1317.3809	1317, 787, 993, 1111, 625, 462, 300	quercetin-3,5,8-tri-O-glc-7-sin-diglc						+
26	8.9	1125.3225	1125, 949, 625, 801, 300	quercetin-3-diglc-7-fer-diglc	+		+			+
27	9.0	1287.3833	1287, 963, 1111, 787, 625, 462, 300	quercetin-3-fer-diglc-7-diglc-5-glc						
28	9.8	977.25527	977, 815, 609, 446, 284	kaempferol-3-sin-diglc-7-glc	+		+			+
29	9.9	1301.3691	1301, 977, 815, 1139, 771, 284, 255	kaempferol-3-sin-diglc-7-diglc-5-glc	+		+			
30	10.1	1139.3079	1139, 815, 609, 977, 446, 285	kaempferol-3-sin-glc-7-diglc-5-glc						+
31	10.1	815.2161	815, 785, 609, 591, 446, 284	kaempferol-3-sin-glc-7-glc						+
32	10.3	1109.2278	1109, 947, 771, 285	kaempferol-3-fer-triglc-7-glc						+

33	10.4	755.201	755, 609, 284	kaempferol-3-diglc-7-deoxyhexoside	+					
34	10.6	1109.3257	1109, 785, 609, 284	kaempferol-3-fer-diglc-7-diglc						
35	10.7	1271.3457	1271, 947, 785, 771, 1109, 609, 284	kaempferol-3-fer-diglc-7-diglc-5-glc						+
36	11.8	824.2804	771, 609, 447, 285	kaempferol-3-glc-7-diglc derivative	+		+			+
37	12.4	385.1074	385, 223	sinapic acid glc	+	+	+			+
38	13.0	771.1981	771, 447, 609, 284	kaempferol-3-glc-7-diglc						+
39	13.8	933.2463	933, 609, 285	luteolin-(4'/3'),7-di-O-glc	+		+			+
40	14.8	193.045		ferulic acid	+	+	+	+		+
41	14.9	681.2427	681, 519, 433, 301	quercetin-glc derivative	+		+			+
42	15.0	625.1343	625, 300	quercetin-3-diglc						+
43	15.4	223.058		sinapic acid	+	+	+	+		+
44	15.9	771.1981	771, 284	kaempferol-3-triglc	+	+	+			+
45	16.4	463.0792	463, 301	quercetin-7-glc			+		+	+
46	16.5	609.1489	609, 284	kaempferol-3-diglc	+	+	+			+
47	16.6	625.1434	625, 301	quercetin-7-diglc			+			+
48	18.7	609.1398	609, 447, 285	kaempferol-3,7-di-O-glc			+		+	+
49	19.6	447.0948	447, 284	kaempferol-3-glc	+	+	+			+
50	19.7	(+) 1185.2961	(+) 1185, 1023, 449, 287	cyanidin-3-disin-diglc-5glc						+
51	19.8	(+) 1155.4265	(+) 1155, 993, 449, 287	cyanidin-3-sin-fer-diglc-5glc						+

*glc – glucoside/hexoside; sin – sinapoyl; fer - feruloyl

4.4.2.1. Flavonoid glycosides

Identification of the flavonoid glycosides was based on their fragmentation pattern under MS^E mode as earlier described in Chapter 2. To recall, internal cleavage of sugar units does not occur in negative mode in high energy collision-induced dissociation (CID). Therefore, a loss of a diglucoside moiety would entail a neutral loss of 324 Da (162 Da x 2) all together. Further, the abundance of the [M-H-(7-O-glycoside)]⁻ is higher than the abundance of [M-H-(3-O-glycoside)]⁻ peak in high energy CID for flavonol-di-O-glycosides. Also, the appearance of radical aglycone pseudomolecular ion species indicates that the glycoside was attached to the C-3 position rather than to the C-7 in the case of flavonol-mono-O-glycosides. It can be seen in Table 4.3 that the majority of the compounds are flavonoid glycosides, mainly composed of kaempferol and quercetin.

Peaks **7, 9, 10, 11, 14, 42, 45** and **47** were identified as quercetin-O-glycosides due to the appearance of a quercetin pseudomolecular ion under high energy CID ($m/z = 301$, radical ion = 300) derived from the loss of glycosyl moieties mainly composed of hexose (glucose) units attached at either the C-3 of the C ring and/or C-7 of the A ring. In the same way, peaks **13, 14, 16, 17, 20, 33, 38, 44, 46, 48,** and **49** were identified as kaempferol-O-glycosides due to the appearance of a kaempferol peak under high energy CID ($m/z = 285$, radical ion = 284). Peak **39** was identified as luteolin glycoside with a diglucoside at the C7 position and a diglucoside at either the C3' or C4' position. Our current method is unfortunately unable to determine the attachment point in the B ring. Luteolin, having the same mass as kaempferol ($m/z = 285$), was identified based on retention time, UV spectra and product ions. Due to the absence of the C3-OH moiety of luteolin, radical ion formation is not likely to exist as compared to the fragmentation of kaempferol-3-O-glycoside.

Peaks **23, 24, 25,** and **26** were also found to be derivatives of quercetin. However, due to the observed neutral losses of 176 and 206 daltons, which correspond to the loss of feruloyl and sinapoyl moieties respectively, such peaks were identified as acylated quercetin glycosides. Peaks **28, 31, 32,** and **34** were identified as acylated kaempferol glycosides.

In the case of peak **19**, 3 glycoside linkages were broken at high CID, which indicated that is an acylated-O,C-glycosides, meaning that a glucose moiety is directly attached to the A ring of the flavonoid structure via a C-C bond, rather than an O-C bond. Peak **25** on the other hand possesses 4 different glycoside attachment points, making it also an O,C-glycoside with 4 glycosylation points. With the same principle, peaks **12** and **21** were

identified as kaempferol-*O,C*-glycosides due to the presence of a kaempferol ion peak at high energy CID with 3 different glycosylation positions. Peaks corresponding to losses of water from some product ions, which is typical for *C*-glycoside products ions in high CID [20], were also observed indicating that such peaks are indeed *O,C*-glycosides.

Peaks **24** and **27** were identified as acylated quercetin-*O,C*-glycosides due to the loss of a sinapoyl and feruloyl moiety respectively, and 3 different glycoside cleavages under high energy CID. However, the current method is currently unable to determine the exact location of the sinapoyl moiety in peak 24 since some peaks that would have provided clues to its position could not be seen. Meanwhile, peaks **29**, **30**, and **35** were identified as acylated kaempferol-*O,C*-glycosides with sinapoyl and feruloyl moieties.

Peak **41** has an *m/z* value of 681 and was fragmented into *m/z* 519, 433, and 301, which corresponded to a quercetin pseudomolecular ion. The 618 → 519 transition in high energy CID indicated a loss of a glucose moiety. Also peak **36** has an *m/z* value of 824 and was fragmented to 771, 609, 447, and 285, which are product ions for kaempferol triglucoside. However, a neutral loss of 53 Da indicated the presence of a 71 Da molecule attached to it. The identities of these peaks could however not be verified.

4.4.2.2. Phenolic acid glycosides

Phenolic acid glycosides were detected based on the mass of the phenolic acid aglycone and the subsequent loss of sugar moieties. Peaks **15**, **18**, and **43** were identified as ferulic and sinapic acid glucosides based on their *m/z* value of 193 and 223, respectively, after the neutral loss of a glucose unit (diglucose in the case of peak 18) under high energy CID. Peaks **8**, **40**, and **43** are chlorogenic, ferulic and sinapic acid aglycones released after alkaline hydrolysis, respectively.

4.4.2.3. Anthocyanins

Red cabbage extracts also contained anthocyanins. Identification of anthocyanins were performed under positive ionization mode due to the inherent positive charge of cyanidin. Their fragmentation behavior was compared with data available in literature. Peak **50** was identified as cyanidin-3-di-sinapoyl-diglucoside-5-glucoside due to the loss of 2 sinapoyl moieties from peak 50 with a loss of 2 glycoside moieties (diglucoside and glucoside). Peak **51** on the other hand was named cyanidin-3-sinapoyl-feruloyl-diglucoside-5-glucoside due to the loss of sinapoyl and feruloyl moieties and 2 glycoside cleavages (diglucoside and glucoside). Such peaks were earlier reported to be present in the edible part of red cabbage [257].

4.4.2.4. Glucosinolates

Several glucosinolates were also tentatively identified based on their masses as previously reported in literature. Peaks **2**, **3**, **4**, **5**, **6**, and **22** were identified as progoitrin, sinigrin, gluconapin, hydroxyglucobrassicin, glucobrassicin and methoxy/neglucobrassicin, respectively. Such glucosinolates have earlier been reported to be present in the edible parts of Brussels sprouts and red cabbage [258]. Quinic acid (peak **1**), which is a plant metabolite and a degradation product of chlorogenic acid was also detected.

4.4.3. Multivariate analysis of the polyphenolic profile of the different plant materials

4.4.3.1. Brussels sprouts

The phenolic and glucosinolate profile of the edible parts of Brussels sprouts have already been reported in literature [259,260]. However, this is the first time that the phenolic profile of their waste streams is characterized. The top leafy part was separated from the stalk due to the large variation in their morphological characteristics; the stalk is more fibrous whereas the top is leafier.

Flavonoid glycosides are the most abundant components of both EP and NEP in both top leaves and stalk. Kaempferol is the dominant flavonoid aglycone followed by quercetin with different degrees of glycosylation. It can be seen that more types of quercetin glycosides are found in the stalk than in the top leaves (Table 4.3). Further, considering that NEP has undergone alkaline hydrolysis, acylated flavonoid glycosides, phenolic acid glycosides and glucosinolates were only found in the EP fraction in both top leaves and stalk. However, their presence in nature cannot be discounted. Other means of extracting these compounds from the NEP without degrading them must therefore be sought.

To further characterize the differences in the phenolic profile between EP and NEP, we employed principal components analysis (PCA) and orthogonal partial least squares – discriminant analysis (OPLS-DA) to the peak intensities (areas) of each identified polyphenol or glucosinolate. PCA was used to explore the variability within the different samples, whereas OPLS-DA was employed to build a deeper classification model for distinguishing between the EP and NEP of each matrix, specifically to determine the phenolic compounds that influence the distinction of the EP fraction to the NEP fraction. Figure 4.3 represents the PCA plot for Brussels sprouts showing both EP and NEP fractions of both stalk and top parts. As shown, there is a very good separation between the different sample types (stalk EP, stalk NEP, top EP, top NEP) in terms of their detected phenolic profiles (total variance explained = 76.4%, 2 components). There is

also a good separation between EP and NEP in terms of all the ions detected by the MS, showing that other unidentified compounds (small molecular weight compounds of ca 150-400 daltons) were released during alkaline hydrolysis of the residue left after conventional solvent extraction (data not shown). Principal component (PC) 1 accounted for 44.87% of variance, which represented the separation between the EP to the NEP fractions. PC 2 on the other hand accounted for 31.53% of variance and represented the separation between the stalk and the top part. It can be seen that the separation of the stalk samples from the top samples is almost as relevant as the separation of the EP to the NEP samples of each plant matrix. This suggests that the phenolic composition of the different samples is unique to each other. However, the NEP composition of the top to the stalk is more similar to each other than their EP composition.

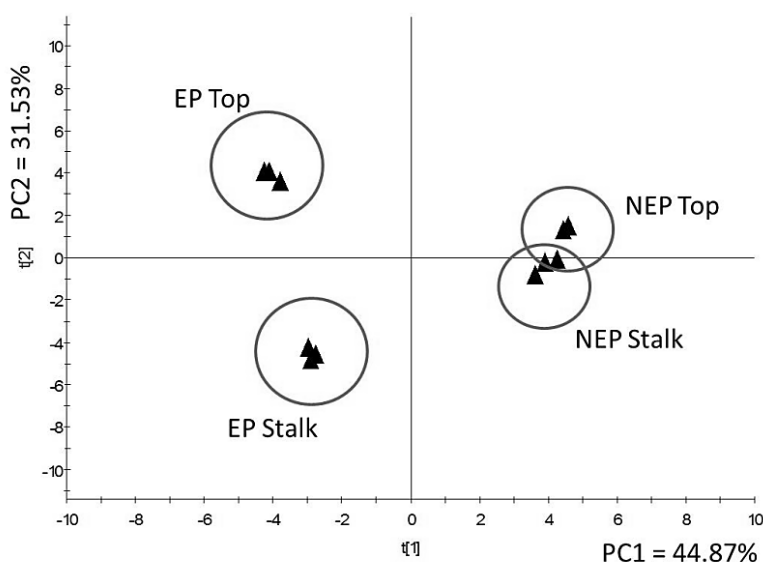


Figure 4.3. Principal component analysis of Brussels sprouts top and stalk (EP and NEP fractions). Total variance explained = 76.4% (n=3)

To establish the distinction between the EP and NEP fractions, we employed OPLS-DA on the top and stalk separately. Using the S-plot, the defining phenolic components for each plant matrix was determined. An S-plot is a plot of the covariance versus the correlation ρ (corr) of variables of the discriminating component of OPLS-DA model. In this plot, each point represents an identified polyphenol or glucosinolate (represented as retention time-m/z pair), wherein the X axis represents variable contribution, and the Y axis represents variable confidence. The farther the distance of a point to the X axis means that the polyphenol or glucosinolate contributes more to the difference between two groups. On the other hand, the farther the distance the point from the Y axis, the higher the confidence level of the polyphenol or glucosinolate to the difference between two groups. Therefore, polyphenols or glucosinolates at the two ends of "S" represent

characteristic markers with the most confidence to each group [261]. Figure 4.4 shows the OPLS-DA and S-plot of the EP versus NEP fraction of Brussels sprouts top part, while Figure 4.5 shows the same for the stalk.

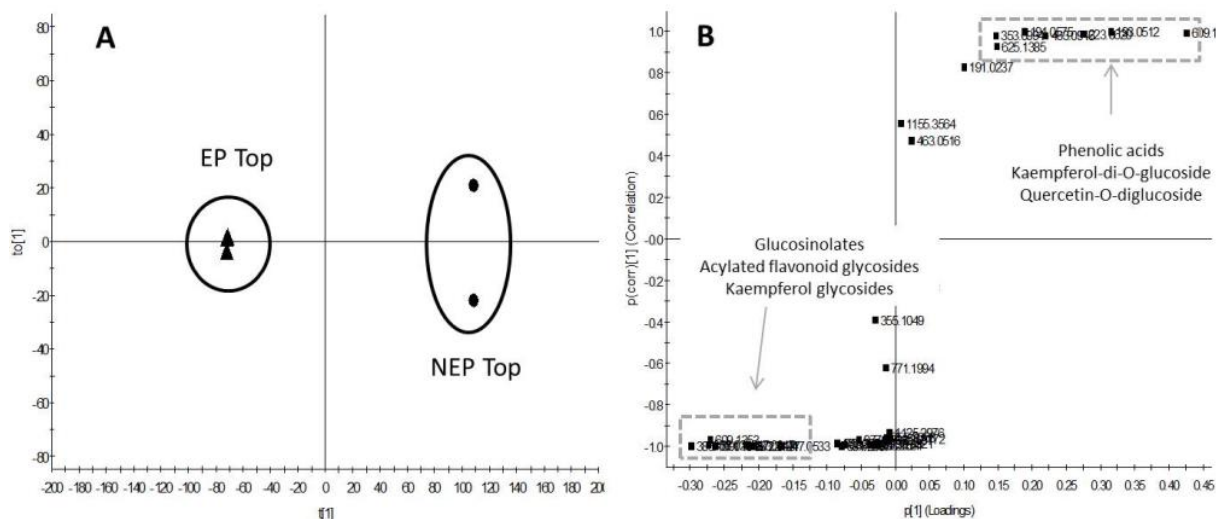


Figure 4.4. (A) OPLS-DA score plot and (B) S-plot of the Brussels sprouts top part (EP versus NEP) ($R^2X_{\text{cum}} = 0.932$). For the S-plot, upper right-hand quadrant represents NEP fraction, which consisted of phenolic acids, kaempferol-di-O-glucoside and quercetin-O-diglucoside. Lower left-hand quadrant represents EP fraction and is composed of glucosinolates, acylated flavonoid glycosides and kaempferol glycosides ($n=3$)

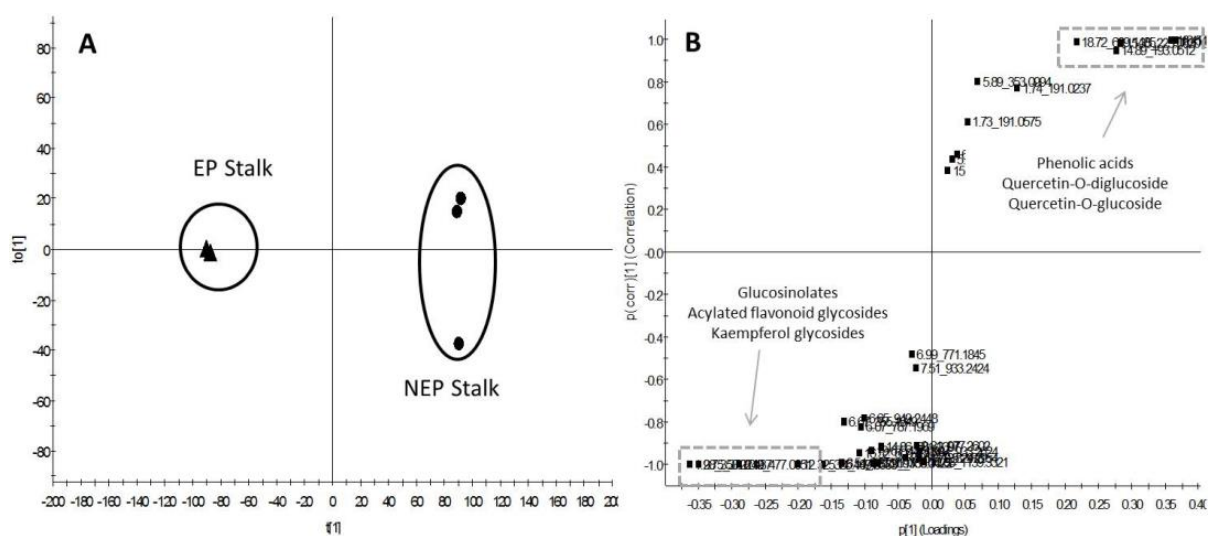


Figure 4.5. (A) OPLS-DA score plot and (B) S-plot of the Brussels sprouts stalk (EP versus NEP) ($R^2X_{\text{cum}} = 0.906$). For the S-plot, upper right-hand quadrant represents NEP fraction, which consisted of phenolic acids and quercetin glycosides. Lower left-hand quadrant represents EP fraction and is composed of glucosinolates, acylated flavonoid glycosides and kaempferol glycosides. ($n=3$)

Compared with the EP fraction, high amounts of free phenolic acids (**40**, **43**) were recovered from the NEP fraction of the Brussels sprouts top parts. Also, kaempferol-3,7-di-*O*-glucoside (**48**) is the main distinguishing compound separating EP from NEP. It is the most dominant phenolic compound and is only found in the NEP fraction. Its isomer on the other hand kaempferol-3-*O*-diglucoside (**46**) is found in both but more abundant in the EP fraction. Quercetin-7-*O*-diglucoside (**47**) was only found in the NEP fraction. The EP fraction is composed dominantly of glucosinolates (especially **3**, **4**, and **6**) and other kaempferol glycosides (especially **16**, **20**, **46**, and **49**).

Similarly, there is also a big difference in the phenolic profile of the NEP fraction of the stalk compared to its EP fraction. As mentioned, there are more types of quercetin glycosides found in the stalk than in the top parts. In addition, most of these quercetin glycosides are in the NEP fraction (**45**, and **47**), which are the distinguishing factors between EP and NEP. Like in the top parts, more phenolic acids (**40**, **43**) can be recovered from the NEP of the stalk. The EP fraction on the other hand contained glucosinolates (**2**, **3**, **4**, **6**, and **22**) and acylated flavonoids (**25**, **26**, **30**, and **31**), which were not present in the NEP fraction. Therefore, for the entire Brussels sprouts waste stream, it can be said that not only does the NEP fraction contain more total phenolics, it also contains unique compounds not found in the EP fraction, and vice versa. The analysis of both EP and NEP fraction is therefore of prime importance.

4.4.3.2. Red cabbage

The phenolic profile of the edible parts of red cabbage has already been reported elsewhere [257,262,263]. However, to the best of our knowledge, this is the first time that the phenolic composition of the waste stream of this plant is being investigated. Due to the presence of innately positively charged anthocyanins in the plant extracts, analysis of the phenolic composition required both positive and negative ionization modes in the ESI-MS.

Like in the case of Brussels sprouts, red cabbage waste stream is dominated with flavonoid glycosides composed of kaempferol and quercetin, with varying degrees of glycosylation and acylation; kaempferol species are more abundant than quercetin. Acylated cyanidin glycosides were also detected in the EP fraction. Cyanidin is highly unstable in alkaline conditions and high temperature [256]. It is therefore expected that no cyanidins are detected in the NEP fraction. Glucosinolates and phenolic acid derivatives have also been detected. Shown in Figure 4.6 is the PCA plot representing the difference between the phenolic composition of the EP and NEP fraction, which explained

a total variance of 98.61% (negative mode) and 89.96% (positive mode). For the negative mode analysis, the first principal component (PC 1) explained 84.11%, which denoted the separation between EP and NEP phenolic composition, whereas 14.5% (PC 2) accounted for the variability among the different replicates ($n=3$). For the positive mode analysis on the other hand, 71.26% (PC1) accounted for the distinction between EP and NEP, whereas 18.7% (PC2) accounted for the variability among the different replicates ($n=3$).

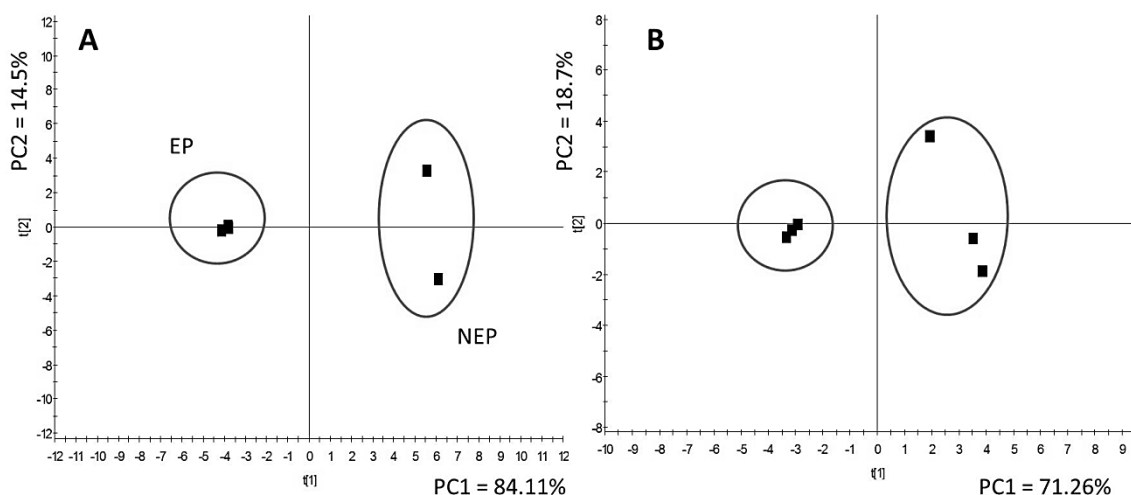


Figure 4.6. Principal component analysis of red cabbage (EP and NEP fractions) in both negative (A) and positive modes (B). Total variance explained = 98.61% and 89.96%, respectively ($n=3$)

There is also a good separation between EP and NEP in terms of all the ions detected by the MS (both negative and positive modes), showing that other unidentified compounds (small molecular weight compounds of ca 150-400 daltons) were released during alkaline hydrolysis of the residue left after conventional solvent extraction (data not shown).

Again, we employed OPLS-DA to distinguish the EP and NEP fractions from each other and to determine the compounds that influence this distinction. As shown in Figure 4.7, there is a high distinction between EP and NEP in both negative and positive modes. As shown in the S-plot, the content of phenolic acids is elevated in the NEP fraction while glucosinolates and anthocyanins are more abundant in the EP fraction.

The NEP fraction is dominated by ferulic (**40**) and sinapic (**37**) acids, which were probably linked to the plant matrix via ester-linkages [236] that were cleaved during the alkaline hydrolysis. Also, kaempferol-3,7-di-*O*-glucoside (**48**) is more abundant in the NEP fraction compared to the EP fraction. Although present in both EP and NEP fractions,

quercetin-7-*O*-glucoside (**45**) and quercetin-7-*O*-diglucoside (**47**) were also found to be more abundant in the NEP fraction. Quinic acid (**1**) was also found in the NEP fraction but not in the EP fraction. Analysis in positive mode on the other hand revealed that cyanidin glycosides (**50**, **51**) are only found in the EP fraction.

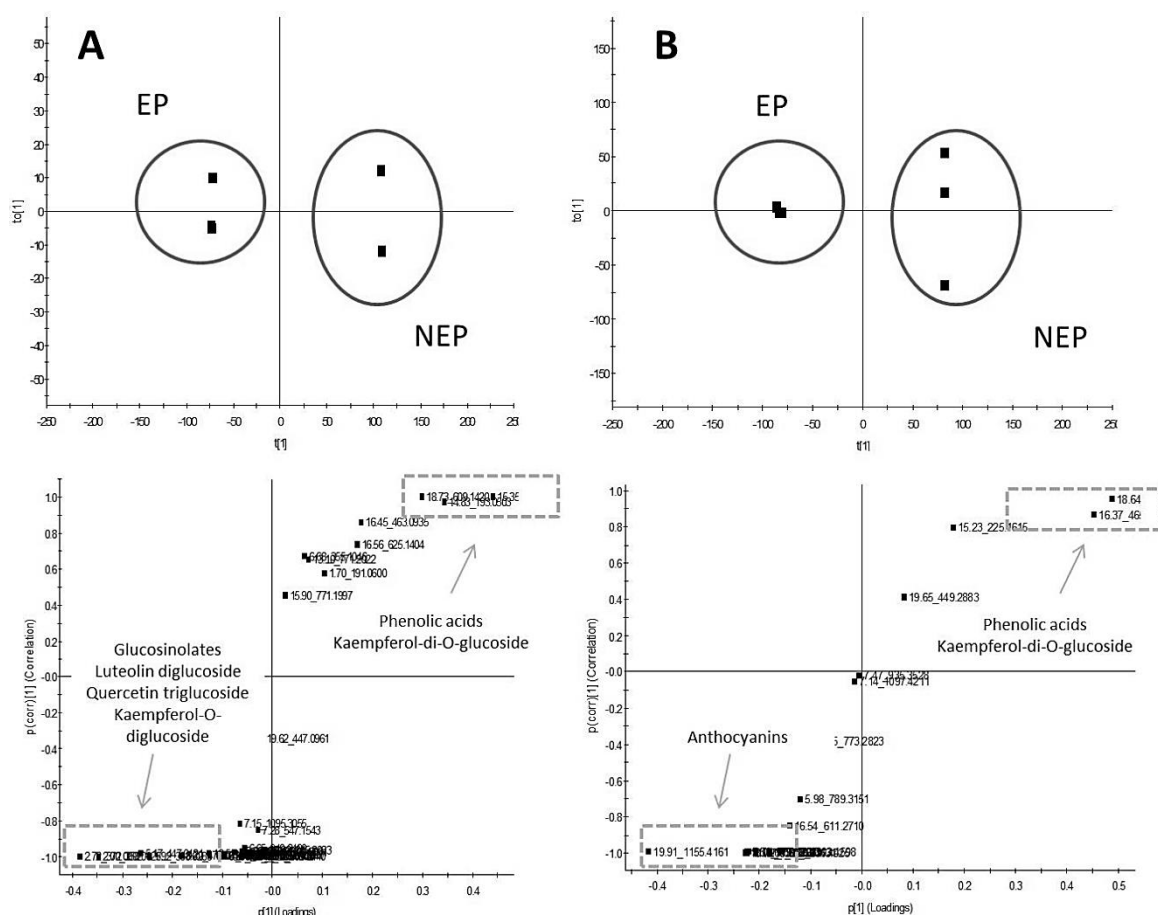


Figure 4.7. OPLS-DA score plot (above) and S-plot (below) of the red cabbage (EP versus NEP) in negative (A) and positive (B) modes. For the S-plot, upper right-hand quadrant represents NEP fraction, which consisted of phenolic acids and kaempferol glycosides.

Lower left-hand quadrant represents EP fraction and is composed of glucosinolates, acylated flavonoid glycosides and kaempferol glycosides and anthocyanins (n=3)

Multivariate techniques such as PCA and OPLS-DA have been staple techniques in metabolomics and have recently found its applications in the study of food. Metabolomics has been described as an essential tool in the analysis of food quality, compliance of new products to food regulations, food processing, food component analysis, food authenticity, and more recently, effect of food on nutrition and physiology (nutri-metabolomics) [264-266]. Recently, metabolomics approach was used to classify the metabolites (mostly phenolics) of *Brassica napus* L. from various plant organs wherein, the polyphenol distribution in different organs of the vegetable was determined [267].

Here, these techniques were used to unravel and characterize nonextractable polyphenols, an untapped resource of potential bioactive ingredients, from 2 Brassica species.

4.5. Conclusion

To the best of our knowledge, the phenolic content and profile of Brussels sprouts and red cabbage waste streams are currently not reported in literature. In this study, we have shown that Brussels sprouts and red cabbage waste streams contain high amounts of phenolics. Further, more phenolics (at least two times) could be extracted from the residues left after conventional solvent extraction, which is usually discarded in current literature. Using LC-MS^E, identities were tentatively assigned to these compounds, which comprise flavonoid glycosides, acylated flavonoid glycosides, phenolic acids, glucosinolates, quinic acid, and anthocyanidins. Using multivariate analysis usually employed in metabolomics studies, PCA and OPLS-DA, the differences in the phenolic profile among different plant matrices and between the extractable and nonextractable fractions were elucidated. It was found that the phenolic profiles of the extractable and nonextractable fractions are different and some compounds are only found in either fraction. There is therefore a need to analyze both extractable and nonextractable fractions to describe the global total phenolic content of plant materials. This is also the first time that such multivariate analysis techniques are used to distinguish different fractions of polyphenols as affected by the extraction method of the plant matrix (extractable versus nonextractable).

Chapter 5

Use of metabolomics and fluorescence recovery after photobleaching to study the *in vitro* intestinal transport and intestinal mucus diffusion of polyphenols from cauliflower waste

Chapter 5: Use of metabolomics and fluorescence recovery after photobleaching to study the *in vitro* intestinal transport and intestinal mucus diffusion of polyphenols from cauliflower waste

5.1. Abstract

The analysis of the *in vitro* bioaccessibility and intestinal transport of polyphenols from cauliflower waste was achieved using targeted metabolomics and chemometric approaches. Changes in phenolic profile throughout the *in vitro* digestion and Caco-2 transport were investigated using LC-MS combined with principal components analysis and orthogonal partial least squares – discriminant analysis, and diffusion of polyphenols through intestinal mucus was monitored using fluorescence recovery after photobleaching (FRAP). Results showed that recovery of polyphenols in the gastric phase was approximately 76-106% while losses of up to 70% were observed after the intestinal phase. Kaempferol-3-*O*-diglucoside and kaempferol-3-*O*-diglucoside-7-*O*-glucoside were found to permeate intact through the Caco-2 cells in very small amounts (0.3% recovery). Polyphenols also diffused rapidly through intestinal mucus without altering their biophysical properties. We conclude that targeted metabolomics and FRAP are rapid and convenient tools to study the recovery of polyphenols during *in vitro* digestion, mucosal diffusion and Caco-2 transport.

Keywords: Bioavailability, polyphenols, intestinal mucus, Caco-2 cells, *in vitro* digestion, fluorescence recovery after photobleaching

Redrafted from:

Gonzales GB, Smagghe G, Mackie A, Grootaert C, Bajka B, Rigby N, Raes K, Van Camp J. 2015. Use of metabolomics and fluorescence recovery after photobleaching to study the bioavailability and intestinal mucus diffusion of polyphenols from cauliflower waste. *Journal of Functional Foods* 16, 403-413

5.2. Introduction

Polyphenols have long been studied due to their health-promoting properties, such as antioxidant, antiviral, hepatoprotective, and immune-regulatory activities [8]. In fact, daily consumption of polyphenol-rich foods has been associated with improved cardiovascular health and protection against cancer and other degenerative diseases [268,269]. However, from a physiological perspective, ingested polyphenols are subjected to gastrointestinal digestion and extensive metabolism by the epithelium. Several papers have been devoted in understanding the metabolic fate of polyphenols along the digestive tract and intestinal absorption, especially in the case of polyphenol-rich foods.

Aside from food products, it has earlier been reported that agricultural waste products are an excellent source of polyphenols, which could be recovered and used as functional ingredients. As earlier discussed in the previous chapters, by-products from the harvest of *Brassica* vegetables are excellent sources of polyphenols. However, little is known about the fate of these polyphenols during digestion.

Conventionally, bioaccessibility, the fraction released from the food matrix and available for absorption, assessment was done by measuring polyphenol recovery at various stages of *in vitro* digestion using the Folin method, which provides the total phenolic content that is often expressed as gallic acid equivalents (or equivalents of other more closely related polyphenol). Although widely used, this method does not provide detailed information on the changes in the phenolic composition at every step of the digestion process. Because of this, HPLC techniques are often done to gather detailed information on the recovery of each of the polyphenols. In HPLC, polyphenols are characterized and quantified using equivalents due to the lack of standards for most phenolic compounds. While this is an accepted method when using diode array detection (DAD), quantification using mass spectrometry requires exact standards since different compounds have different abundances at certain ionization conditions. Hence, quantification using DAD is preferred for complex matrices. However, polyphenols are often difficult to separate in liquid chromatography especially when the plant matrix contains many different compounds causing co-elution, and subjecting it to *in vitro* digestion presents more peaks and noise to the chromatogram. Therefore, relying on the HPLC chromatogram to analyze the recovery of individual compounds may not be easy and accurate. Also, integrating each chromatographic peak may be cumbersome when dealing with plant extracts due to the high number of polyphenol species present. Methods to analyze the

recovery of polyphenols and the changes in its distribution in a reliable and convenient manner therefore need to be sought.

After intestinal digestion, polyphenols are faced with an immovable mucus layer that protects the epithelium from luminal contents whilst allowing the entry of nutrients [270]. Therefore, polyphenols need to diffuse through the mucus layer efficiently prior to reaching the epithelium. However, studies on the diffusive properties of polyphenols through intestinal mucus and their interactions have not been previously reported.

The use of Caco-2 cells to assess intestinal uptake of polyphenols is widely practiced [125,271]. However, no report on the Caco-2 metabolism and transport of cauliflower polyphenols could be found in the literature. This information is crucial to ascertain the final bioavailability of the polyphenols and to determine which polyphenols survive the entire gastrointestinal digestion and absorption process.

Given these open questions, this study was performed to assess the bioavailability of cauliflower waste polyphenols through digestion using an *in vitro* digestion model and Caco-2 transport experiments. More importantly, the use of multivariate analysis techniques, principal component analysis (PCA) and orthogonal partial least squares – discriminant analysis (OPLS-DA), to determine the changes in the polyphenolic profile at every stage of digestion was explored. Further, the study aimed to measure the diffusion of the polyphenols in the intestinal digesta through an *ex vivo* intestinal mucus and to investigate the interaction of the polyphenols and the intestinal mucus.

5.3. Materials and methods

5.3.1. Materials

U(H)PLC-MS grade methanol and formic acid were acquired from Biosolve (Valkenswaard, the Netherlands). Analytical grade methanol used for extraction, HCl and NaOH were purchased from VWR International (Leuven, Belgium). Kaempferol, calcium chloride, pepsin, pancreatin, 2-aminoethyl diphenylborinate and 500-nm fluorescent polystyrene beads were purchased from Sigma-Aldrich (Poole, UK; Diegem, Belgium)

For the cell culture experiments, Dulbecco's modified Eagle's medium (DMEM) supplemented with Glutamax™ was purchased from Gibco (Langley, VA, USA) while fetal bovine serum was obtained from Greiner Bio-One (Wommel, Belgium).

5.3.2. Extraction of *Brassica oleracea* polyphenols

Plant extracts were obtained following the extraction protocol discussed in Chapter 2.

5.3.3. Simulated *in vitro* digestion

An *in vitro* digestion model that mimicked the upper gastrointestinal stage of human (adult) digestion was adapted from Minekus et al. [272]. The methanolic extract was dried under reduced pressure and redissolved in distilled water to a concentration of approximately 100 µg/mL. A 1.5 mL aliquot was added with 1.2 mL of salivary fluid, 7.5 µL of 0.3M CaCl₂, 0.1 mL of amylase solution and 0.1925 mL of distilled water to attain a final volume of 3 mL. The mixture was mixed for 2 min in a temperature-controlled vessel maintained at 37°C with continuous stirring.

To simulate gastric digestion, 3 mL of gastric juice, 15 µL of 0.03M CaCl₂, 0.20 mL of pepsin solution (60,000 U/mL) were added and the pH was volumetrically adjusted to pH 3.0 using 5M HCl. The total volume of the mixture was adjusted to 6 mL with the addition of distilled water and stirred for 2 h at 37°C. Thereafter, 2 mL of sample were taken from the mixture. This was then distributed in 500 µL aliquots in ependorf tubes, dipped in liquid nitrogen and stored at -20°C until further analysis. These samples are hereto referred as gastric digesta.

The gastric digesta was subsequently subjected to simulated small intestinal digestion. The remainder of the mixture (4 mL) was mixed with 2.2 mL of duodenal juice, 0.38 mL bile (160 mM) and 8 µL 0.3M CaCl₂. The pH of the mixture was volumetrically adjusted to pH 7.0 using 5M NaOH. Then, 1 mL of pancreatin (equivalent to a trypsin activity of 800 TAME U/mL) was added to the mixture and the total volume was adjusted to 8 mL using distilled water. It was then stirred for 2 h at 37°C. After the digestion process, the digesta was distributed in 500 µL aliquots in Eppendorf tubes, dipped in liquid nitrogen and stored at -20°C until further analysis. These samples are hereto referred as intestinal digesta.

The composition of the salivary, gastric and intestinal juices are as described in Minekus et al. [272].

5.3.4. Measurement of total phenolic content (TPC)

TPC was analyzed using the Folin-Ciocalteu method with slight modifications and expressed as gallic acid equivalents (GAE). The reaction consisted of 50 µL of extract and digesta, 100 µL of Folin-Ciocalteu reagent (composed of phosphomolybdate and phosphotungstate) and 1.2 mL of distilled water, which was allowed to react for 5

minutes in a 2 mL cuvette. After, 150 μ L of 20% sodium carbonate were added and further incubated for 2 h in darkness. The absorbance associated with TPC was then read at 760nm. Quantification was made using a calibration curve of gallic acid standards and expressed as gallic acid equivalents (GAE). All analyses were performed in triplicates.

Briefly, the Folin-Ciocalteu reaction proceeds due to the reduction of molybdenum and tungsten (from 6+ to 4+ state) in the presence of a reducing agent, in this case, the polyphenols. The reaction is initiated by an increase in pH due to the addition of sodium carbonate. Since this is a reduction reaction, this assay is interfered by any reducing agents in the sample, such as reducing sugars and vitamins. Therefore, Folin-Ciocalteu assay must be regarded as an estimation, rather than an absolute method for polyphenol quantification.

5.3.5. Cell culture

Caco-2 cells were obtained from the American Type Culture Collection (Manassas, VA, USA) and grown in DMEM supplemented with Glutamax (4.5 g/L glucose), 10% heat-inactivated foetal bovine serum (FBS) and 1% non-essential amino acids in 25cm² canted neck tissue culture flasks. The cultures were maintained in a humidified atmosphere with 10% carbon dioxide in air at 37°C. Cells were used up to 40 passages. After around 80-90% confluency, cells were collected and seeded in 12 mm internal diameter Transwell polyethylene inserts (Corning Life Sciences, Amsterdam, the Netherlands) in 6-well plates. The cells were maintained and allowed to differentiate for 21 days before use in transepithelial permeation experiments.

5.3.6. Transepithelial transport experiment

Intestinal digesta from the *in vitro* digestion was diluted into various concentrations using serum free and phenol red-free medium (transport medium). The effect of the different concentrations of intestinal digesta on cell viability was analyzed via MTT and SRB assays as previously described [273,274]. The highest concentration of intestinal digesta that did not cause a significant decrease in cell viability was used for the transport experiments. In the end, intestinal digesta was diluted ten times in transport medium.

Culture media was aspirated from the Transwell plates and cells were washed with pre-warmed PBS and transport medium. Thereafter, 2 mL of intestinal digesta samples were loaded on the apical side of the Transwell plate. The basal compartment was replaced with transport medium. The Transwell plates were then incubated for 2 hours in humidified atmosphere with 10% carbon dioxide in air at 37°C. Samples were then taken from both apical and basal compartment.

5.3.7. UPLC-MS analysis

LC-MS analysis and structural characterization of the polyphenols was based on the method developed in Chapter 2. Analysis of the recovery of individual polyphenols throughout the entire *in vitro* digestion and intestinal transport was done by comparing the peak abundances of the compounds at the initial stage (undigested; 100%) to the peak abundances of the same compounds at different stages of digestion and transport.

5.3.8. Porcine small intestinal mucus collection and preparation

Collection of small intestinal mucus was performed using the method of Macierzanka et al. [275]. Briefly, fresh porcine small intestines from 3 different pigs (n=3) were obtained from the local abattoir and immediately rinsed with 67 mM phosphate buffer (pH 6.7) containing 0.02% w/v sodium azide and a mix of protease inhibitors (Roche Diagnostics GmbH, Mannheim, Germany; 1 tablet per 50 mL buffer) to remove intestinal debris. The first 2 meters from the duodenum was cut into short segments and cut open to expose the mucus layer. The mucus was then removed by gently scraping the epithelial surface by hand to avoid shear stress. The collected samples were immediately frozen in aliquots using liquid nitrogen. This *ex vivo* mucus preparation was stored at -80 °C until use.

5.3.9. Polyphenol diffusion and recovery through intestinal mucus using fluorescence recovery after photobleaching (FRAP)

Aliquots of 900 μ L of the gastric and intestinal digesta from the *in vitro* digestion were mixed with 100 μ L of 2% 2-aminoethyl diphenylborinate in dimethyl sulfoxide (DMSO) and allowed to stand for approximately 10 minutes at room temperature. Ten microlitres of this mixture were added with 40 μ L of *ex vivo* mucus and gently agitated to avoid shearing of the mucus. Thereafter, 9 μ L of this sample was loaded on a 9mm (diameter) x 0.12 mm (depth) Grace Bio-labs Secure Seal™ imaging spacer mounted on a glass slide (microscopy chamber) and covered with a coverslip. The final concentration of DMSO in the sample was 2%.

FRAP was performed using a Leica SP5 II with an 8000 Hz resonance scanner fitted with a 40x oil immersion objective (Leica, Milton Keynes, UK). A region of interest (RoI) was drawn with a diameter of 100 μ m. RoI's were scanned under fly-mode at 500 ms/frame. The fluorescence of the polyphenols was monitored through excitation at 488nm. Pre-bleach intensity was recorded for 50 frames and thereafter, the RoI was bleached at maximum laser power for 25 frames. The recovery of the fluorescence was monitored for a total of 200 frames. The total time of analysis was 62 seconds. Analysis was performed with 4 technical replicates (different chambers) x 3 biological replicates (different pigs).

For the analysis of polyphenol diffusion after photobleaching, image processing and fluorescence analysis was performed using LCS2.0 software (Leica). Generally, the fluorescence sharply decreased after photobleaching and recovered relatively fast thereafter. Individual curves were generated and the diffusion rates and recovery were calculated and averaged. FRAP data were analyzed using nonlinear least-square fitting as described by Ladha et al. [276], as follows:

$$F(t) = \frac{F(0) + F(\infty) \left(\frac{t}{\beta \tau D} \right)}{1 + \left(\frac{t}{\beta \tau D} \right)},$$

where $F(t)$ is the observed fluorescence in time, $F(0)$ is the fluorescence right after bleaching, $F(\infty)$ is the fluorescence at infinite time after bleaching, β is the depth of bleach parameter, and τD is the diffusion time. The lateral diffusion coefficient, D , is then given by $D = \omega^2 / 4\tau D$, where ω is the ROI radius.

The percent recovery (%R) is given by:

$$\%R = \frac{F(\infty) - F(0)}{F(t < 0) - F(0)},$$

where $F(t < 0)$ is the fluorescence prior to bleaching [276].

5.3.10. Effect of cauliflower waste polyphenols on the biophysical properties of intestinal mucus

5.3.10.1. Particle tracking microrheology

Particle tracking microrheology (PTM) was performed using red fluorescent 500nm polystyrene latex beads dispersed in 10mM bile solution, which acted as probe particles. A mixture composed of 39 μ L of *ex vivo* mucus mixed with 1 μ L probe particles and 10 μ L of either cauliflower waste extract (in PBS) or PBS (control) were loaded onto the microscopy chamber and covered with a coverslip. Motion of the beads was monitored with a confocal microscope equipped with a 20x objective and at a resolution of 0.5s for 25 seconds. Trajectories were analyzed using Image-Pro analyzer 7.0 software (Media Cybernetics Inc., Silver Spring, MD, USA) as 2D representation of a 3D movement.

Movement of the individual probe particles was transformed into time-dependent mean square displacement (MSD), as follows [277]:

$MSD \langle \Delta r^2(\Delta t) \rangle = \langle \Delta x^2 + \Delta y^2 \rangle$; where Δx and Δy are particle displacements in the x and y directions, respectively, and Δt is the time scale over which the displacement was observed.

By averaging the probe particles of the same Δt , ensemble mean square displacement $\langle MSD \rangle$ was calculated. The effective diffusivities (diffusion coefficient, D_{eff}) were calculate as:

$D_{eff} = MSD/4\Delta t$, and the average of the D_{eff} values of for individual particles equate to the ensemble effective diffusivity $\langle D_{eff} \rangle$. The apparent microviscosity (η) was calculated using the Stokes-Einstein equation, $D = k_B T / 6\pi\eta r$, where D is the diffusion coefficient independent of time, k_B is the Boltzmann's constant, T is the absolute temperature in Kelvin and r is the radius of diffusing particle [277].

The basis of PTM rests on the assumption that particle transport in complex environments are controlled by the local properties of the material. The movement of the beads within the local environment provides the local properties, in this case, microviscosity of the material, such as mucus.

5.3.10.1. Bulk rheology

The viscoelastic properties of the *ex vivo* mucus samples, and mucus mixed with cauliflower waste extract (80/20; vol/vol; mucus/extract) were analyzed under dynamic oscillatory and rotational tests using a controlled strain AR200 rheometer (TA Instruments, Crawley, West Sussex, UK). A thin layer of low-viscosity silicone oil was gently spread over the edge of the sample to avoid drying of the mucus. Both strain sweep tests and viscosity ramp tests were performed at $37 \pm 0.1^\circ\text{C}$. For the strain sweep test, the strain amplitude was increased stepwise from 0.01% to 100% over approximately 4 minutes. For the viscosity ramp test, the shear rate was increased stepwise from 0.1 to 500/s over a period of 15 minutes [277].

5.3.11. Data analysis

Data are shown as mean \pm standard error of mean (SEM). Differences among groups were assessed by analysis of variance (ANOVA) while post-hoc analysis was done with Tukey's test. Differences were considered significant when $p < 0.05$.

To analyze polyphenol recovery at various stages of digestion, metabolomics tools such as principal components analysis (PCA) and orthogonal partial least squares – discriminant analysis were performed using Markerlynx™, which is embedded within the Masslynx software (Waters Corp.).

5.4. Results and discussion

5.4.1. Total phenolic content during *in vitro* digestion

The total phenolic content (TPC) of cauliflower waste amounted to 3.2 mg GAE/g of dry waste material. For the *in vitro* digestion, the total polyphenol was adjusted to around 100 µg/mL (polyphenol fed in the *in vitro* digestion process) to simulate the possible polyphenol intake in a normal diet. As shown in Figure 5.1, the TPC remained relatively unchanged after gastric digestion, which indicated that the polyphenols were stable after 2 h of gastric conditions. However, during the intestinal digestion, approximately 20% of the TPC is lost. Previous reports attributed this observation to the possible binding of flavonoids to digestive enzymes and other proteins in the pancreatin mixture, which remains to be proven experimentally. This suggests that the polyphenols are stable under acidic and pepsin-containing environments while a loss in phenolic content starts during the intestinal phase. This result is in agreement with previous studies on *in vitro* digestion of polyphenols from broccoli inflorescence [278], blended fruit juice [279], apple [280], grapes [281], cinnamon beverages [282], pomegranate products [283] and orange [284].

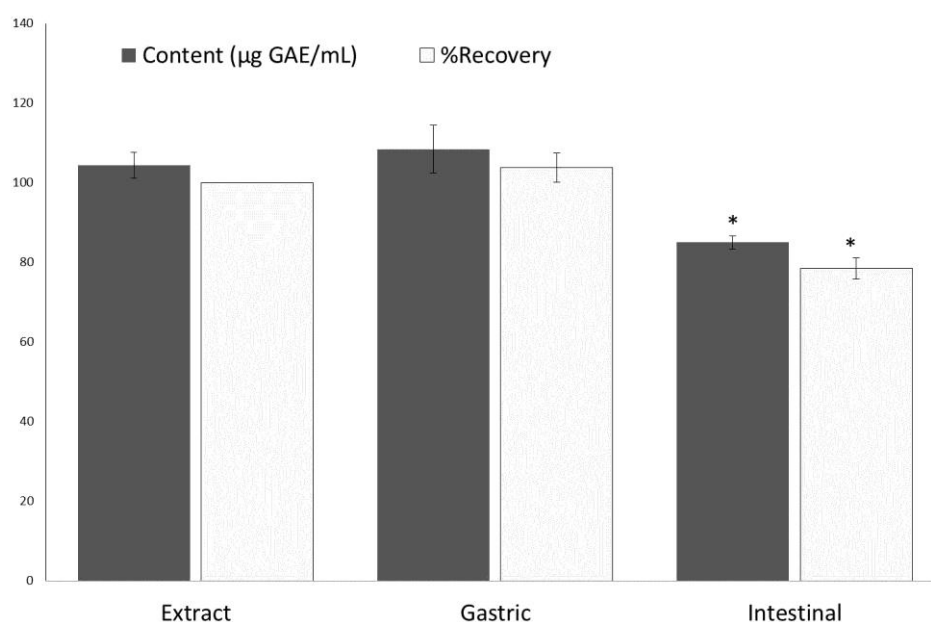


Figure 5.1. Total phenolic content and %recovery during *in vitro* gastro-intestinal digestion. n=3

5.4.2. Changes in the phenolic profile during *in vitro* digestion

The phenolic profile of cauliflower waste has earlier been reported in Chapters 2 and 3. In this paper, the survival of such compounds through the *in vitro* digestion process was analyzed using a targeted metabolomics approach. Initially, polyphenols from each stage of the digestion process were identified, especially taking note of possible new compounds that may arise due to the digestion process. Figure 5.2 shows a schematic diagram of the different compartments and stages of digestion analyzed. Shown in Figure 5.3 is the DAD chromatogram of the different digesta at 280 nm. After thorough investigation, no new compounds emerged from the *in vitro* digestion. Identities and recoveries of the polyphenols are summarized in Table 5.1.

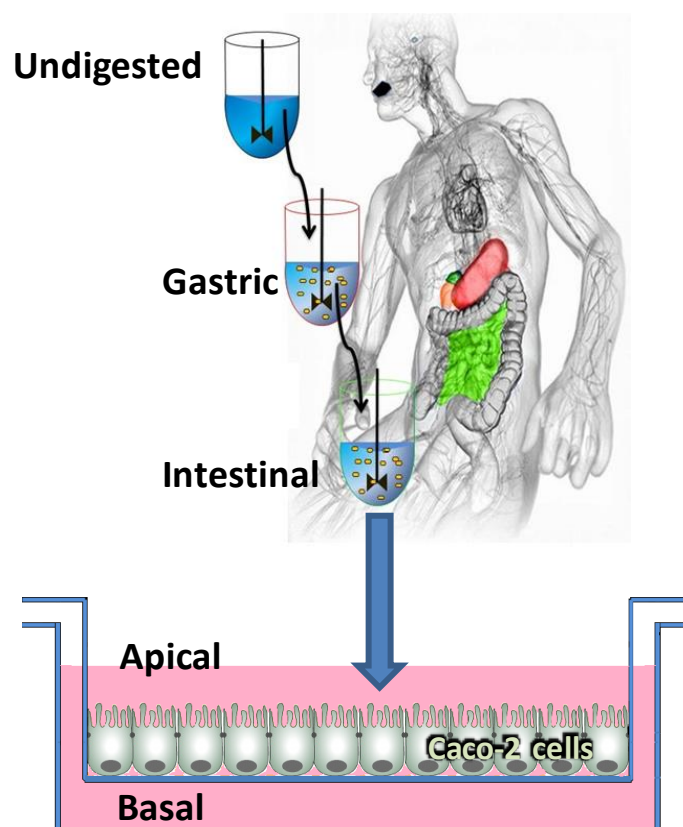


Figure 5.2. Schematic diagram explaining the different sampling points in the *in vitro* digestion and Caco-2 intestinal transport experiment

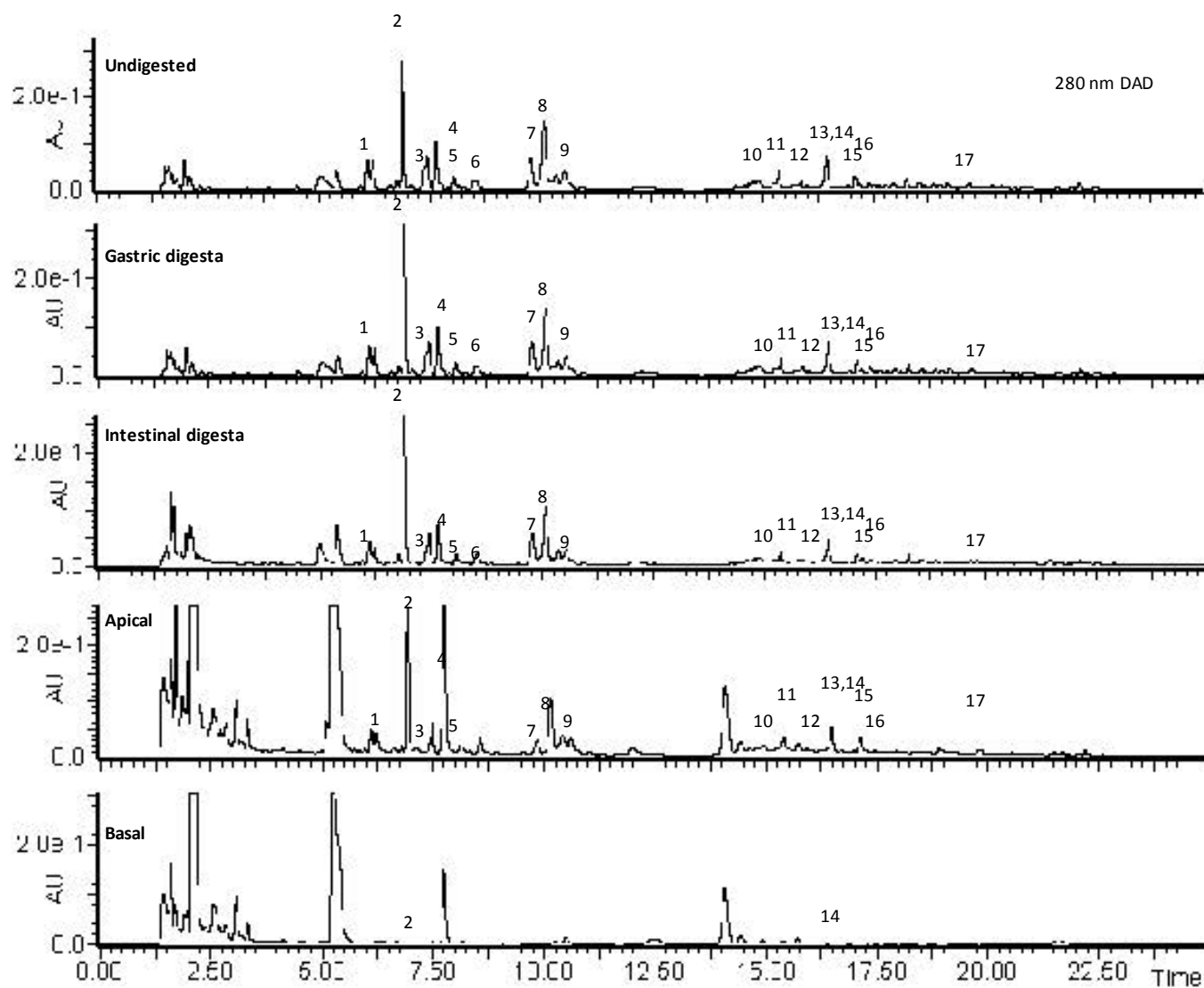


Figure 5.3. DAD chromatogram of the cauliflower extract following different stages of digestion and Caco-2 digestion and transport. For the identities of the polyphenolic peaks, refer to Table 5.1.

Table 5.1. Recoveries of the individual identified polyphenols from cauliflower waste stream methanolic extract

Ret. Time (mins)	Polyphenol*	m/z	% Recovery compared to undigested					
			Undigested	Gastric	Intestinal	Apical	Basal	
1	6.00	Quercetin-3-O-diglc-7-O-glc	787	100	91±5	109±7	38±11	0
2	7.00	Kaempferol-3-O-diglc-7-O-glc	771	100	91±3	90±4	74±2	0.3±0.1
3	7.70	Kaempferol-3-O-diglc-7-O-diglc	933	100	80±41	29±5	8±7	0
4	8.10	Kaempferol-3-O-triglc-7-O-diglc	1095	100	86±10	65±12	27±10	0
5	8.20	Kaempferol -hexaglc	1257	100	84±7	67±6	28±23	0
6	8.50	Quercetin-3-O-coumaroylglc-7-O-hydroxyferuloylgc	963	100	76±5	79±10	0	0
7	10.00	Kaempferol -hydroxyferuloylferuloyltetraglc	1301	100	106±33	97±22	52±21	0
8	10.40	Kaempferol-3-O-coumaroyldiglc-7-O-glc	917	100	92±5	66±8	77±2	0
9	10.60	Kaempferol-3-O-feruloyldiglc-7-O-diglc	1109	100	101±15	73±0	82±12	0
10	15.00	Quercetin-7-O-diglc	625	100	100±7	61±21	74±16	0
11	15.40	Kaempferol-3-O-feruloyldiglc-7-O-glc	947	100	92±10	85±8	81±10	0
12	15.90	Kaempferol-3-O-triglc	771	100	81±16	53±1	17±6	0
13	16.40	Kaempferol-3-O-sinapoyldiglc	815	100	96±1	60±3	48±21	0
14	16.50	Kaempferol-3-O-diglc	609	100	97±1	72±7	110±12	0.3±0.2
15	17.20	Kaempferol-3-O-feruloyldiglc	785	100	94±7	63±1	56±3	0
16	17.50	Kaempferol-3-O-coumaroyldiglc	755	100	98±8	60±6	70±5	0
17	19.70	Kaempferol-3-O-glc	447	100	82±9	44±2	28±0	0

*glc-glucoside/hexoside

After running the samples in the LC-MS, a post-run analysis was performed to trace the survival of each of the identified polyphenol. First, a list of the m/z values of all the identified compounds at each digestion step was made and served as a basis for creating a model mass list. Using the data-mining software MarkerLynx™, a method was created to search for the model mass list within each MS chromatogram with a window of 0.05 Da and retention time window of 0.1 min. After running the method to the undigested, gastric and intestinal digesta samples, the software automatically integrated each mass spectral peak and reported a list of each m/z value with their corresponding peak intensities and retention times. Isobaric compounds were manually removed based on their retention times. As a result, a list of markers, which corresponded to the identified polyphenols, was reported and automatically integrated. The peak intensities (area) were then used to measure the stability of each polyphenol during the *in vitro* digestion process. This method has been successfully and routinely used in metabolomics [285,286], metabonomics [287], and in data-preprocessing (alignment, peak picking, etc) [288]. In this paper, the technique is used as a new way of analyzing the bioavailability of polyphenols through an *in vitro* digestion model.

Principal components analysis (PCA) and orthogonal partial least squares – discriminant analysis (OPLS-DA) were employed to explore the data. Specifically, the changes in the phenolic profile at each step of digestion were determined. Figure 5.4 shows the PCA and OPLS-DA/S-plot results showing the differences among undigested, gastric and intestinal digesta samples.

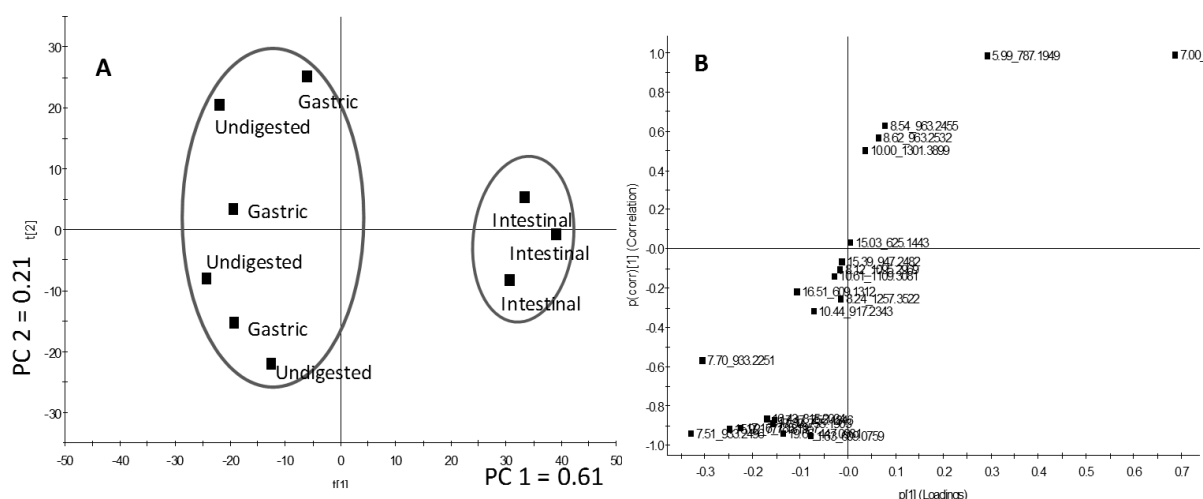


Figure 5.4. PCA (A) and OPLS-DA/S-plot (B) results for undigested, gastric and intestinal digesta. A) The PCA plot explained 82% of the total variance. B) Each dot represents an identified polyphenol. The upper right quadrant are polyphenols that are elevated in the intestinal digesta, while the lower left quadrant are those elevated in the undigested and gastric digesta. $R^2X = 0.75$, $R^2Y = 0.97$, $Q^2 = 0.90$; $n=3$

The PCA model (with 2 components) accounted for 82% of the variation in the data. The first principal component (PC) captured 61% and was attributed to the changes in the profile throughout the *in vitro* digestion. On the other hand, the second PC explained 21%, which corresponded to the variation within the replicates. As shown in Figure 5.4A, there is no distinct difference between the phenolic profile of the undigested extract and the gastric digesta. This supports the previously described data that 100% of the TPC was recovered after gastric digestion. Indeed, the individual polyphenols present in the extract remained intact after 2 hours of gastric digestion. However, losses of certain phenolic compounds were detected after intestinal digestion, which agreed with the reduction of the TPC recovery as earlier mentioned. Compared to merely relying on the results from TPC, analyzing the data using OPLS-DA revealed exactly which phenolic compounds remained stable after intestinal digestion and those that did not.

Results from the OPLS-DA revealed that levels of acylated and non-acylated kaempferol glycosides were reduced in the intestinal digesta compared to the gastric digesta. Most pronounced and consistent loss was observed from kaempferol-3-*O*-diglucoside-7-*O*-diglucoside, kaempferol-3-*O*-glucoside, kaempferol-3-*O*-triglucoside and kaempferol-3-*O*-diglucoside with sinapoyl, coumaroyl and feruloyl moieties. The loss of these polyphenols after the intestinal digestion stage could be attributed to their affinity with the digestive enzymes or other proteins in pancreatin and other digestion constituents. Considering that the level of kaempferol-3-*O*-glucoside was not elevated after intestinal digestion means that the loss of the mentioned acylated kaempferol glycosides is not due to deacylation.

Considering that flavonoid aglycones and their glycosidic moieties are bound via a β -glycosidic linkage [289], they remain stable against the amylases present in pancreatin, which normally cleave α -linkages. Therefore, flavonoid glycosides are not substrates of digestive enzymes and thus are stable during digestion. Although inter-sugar linkages within flavonoid oligoglycosides are α -linkages, cleavage of terminal sugars from the flavonoid glycosides was not observed. In fact, flavonoids have been earlier reported to inhibit, and thus bind, to α -amylase and other digestive enzymes [290-292]. This therefore may also contribute to the loss of certain types of flavonoid glycosides during intestinal digestion, especially those with fewer sugar units. The interaction of such polyphenols with digestive enzymes and other constituents may eventually lead to the low bioavailability of such polyphenols.

5.4.3. Mucosal diffusion of polyphenols using FRAP

The gastrointestinal (GI) tract is protected by a stationary water layer of mucus consisting of 90-98% water. This mucus layer protects the gut by excluding bacteria and other toxic compounds while allowing nutrients to penetrate [270,275]. In order to facilitate polyphenol absorption, they must be able to travel through the mucus layer of the GI tract [293]. The analysis of polyphenol diffusion through gastrointestinal mucus has not been reported in literature, although studies on polyphenol interaction with isolated mucins, the main component of mucus, have been undertaken [294]. Tracking the diffusion of particles through the mucus layer has been earlier performed in a 100 μm -thick optical cell, where it is filled with 80% mucus and 20% particle to be traced, without mixing. The penetration of the particle would then be traced via confocal microscopy. Using this method for polyphenol-rich plant extract was found unsuitable because the polyphenol diffused through the mucus too quickly. Therefore, a FRAP method was employed. This is the first time that FRAP has been used to analyze polyphenol diffusion through intestinal mucus. Fluorescence recovery after photobleaching (FRAP) is a microscopic technique that relies on the translational diffusion coefficient of a fluorescent molecule. Initially, an area with fluorescent molecules is bleached using a high intensity laser. Immediately after bleaching, the recovery of the fluorescence of the bleached area due to the diffusion of fluorescent molecules from the surrounding unbleached areas is measured. The diffusion coefficient is then calculated using the method described in section 5.3.9. Figure 5.5 shows the fluorescence recovery and the diffusion rate of polyphenols through the *ex vivo* porcine GI mucus.

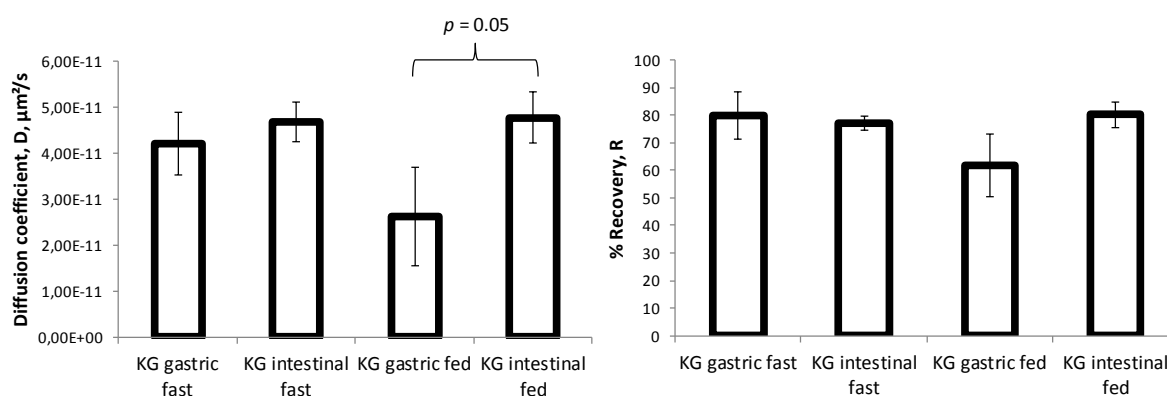


Figure 5.5. Diffusion coefficient (left) and % recovery (right) of polyphenol through *ex vivo* porcine GI mucus. Fast – no food component; fed – polyphenol embedded in food matrix (bread). $n=3$

As shown, the digested polyphenols from cauliflower waste extract rapidly diffused through the mucus layer after gastric and intestinal digestion with diffusion coefficients of $4.22 \times 10^{-11} \pm 6.7 \times 10^{-12}$ and $4.69 \times 10^{-11} \pm 4.26 \times 10^{-12}$ $\mu\text{m}^2/\text{s}$, respectively. Using the

Stokes-Einstein equation, a particle with a radius of 1 nm would have a diffusion coefficient of around 2.19×10^{-10} . Therefore, the diffusion of polyphenols through mucus would be around 5 times slower than that of a 1-nm particle in water. This high diffusion could be attributed to the fact that most of the polyphenols present in cauliflower waste are highly glycosylated flavonoids, which are relatively water soluble. The % recovery, which is often referred as the % mobile particles, suggests that more than 80% of the tracked polyphenols moved through the mucus (considering the small residual background fluorescence). This high recovery may indicate that polyphenols from cauliflower waste do not interact with the mucus layer, for instance no hydrophobic and/or hydrogen bonding interactions exist, thus allowing them to penetrate.

To test the effect of food interactions to the diffusion of polyphenols through mucus, bread was added to the *in vitro* digestion model and the effect on polyphenol diffusion was examined. As also shown in Figure 5.4, the diffusion and recovery after gastric digestion is significantly reduced, which indicate either polyphenol interaction with the food matrix or food matrix interaction with the mucus. After intestinal digestion however, where the food matrix has been broken down, the diffusion and recovery was the same as when there is no food component. The diffusion of polyphenols through mucus is therefore affected by the food matrix and that polyphenols may not interact with the mucus itself.

5.4.4. Effect of polyphenols on the biophysical properties of *ex vivo* porcine mucus

Where polyphenol interaction with mucosal components exists, the biophysical properties of the mucus would be altered. For this reason, the changes in the micro- and macroviscosity of the *ex vivo* porcine mucus as affected by polyphenols from cauliflower waste extract was monitored. Both the micro- and macro-viscosity of *ex vivo* porcine intestinal mucus were not altered by the addition of cauliflower waste polyphenols in various concentrations (Figure 5.6). Although polyphenols have earlier been reported to interact with mucins [293], such interactions may not be representative of the interaction between polyphenols and whole mucus. This may explain the rapid diffusion of the polyphenols through the mucus layer.

The limitation of this approach is the fact that the diffusive polyphenols are not identified. However, considering that no interaction between the polyphenols and the mucus were observed, it is assumed that the polyphenols recovered from the intestinal digesta are able to reach the epithelia.

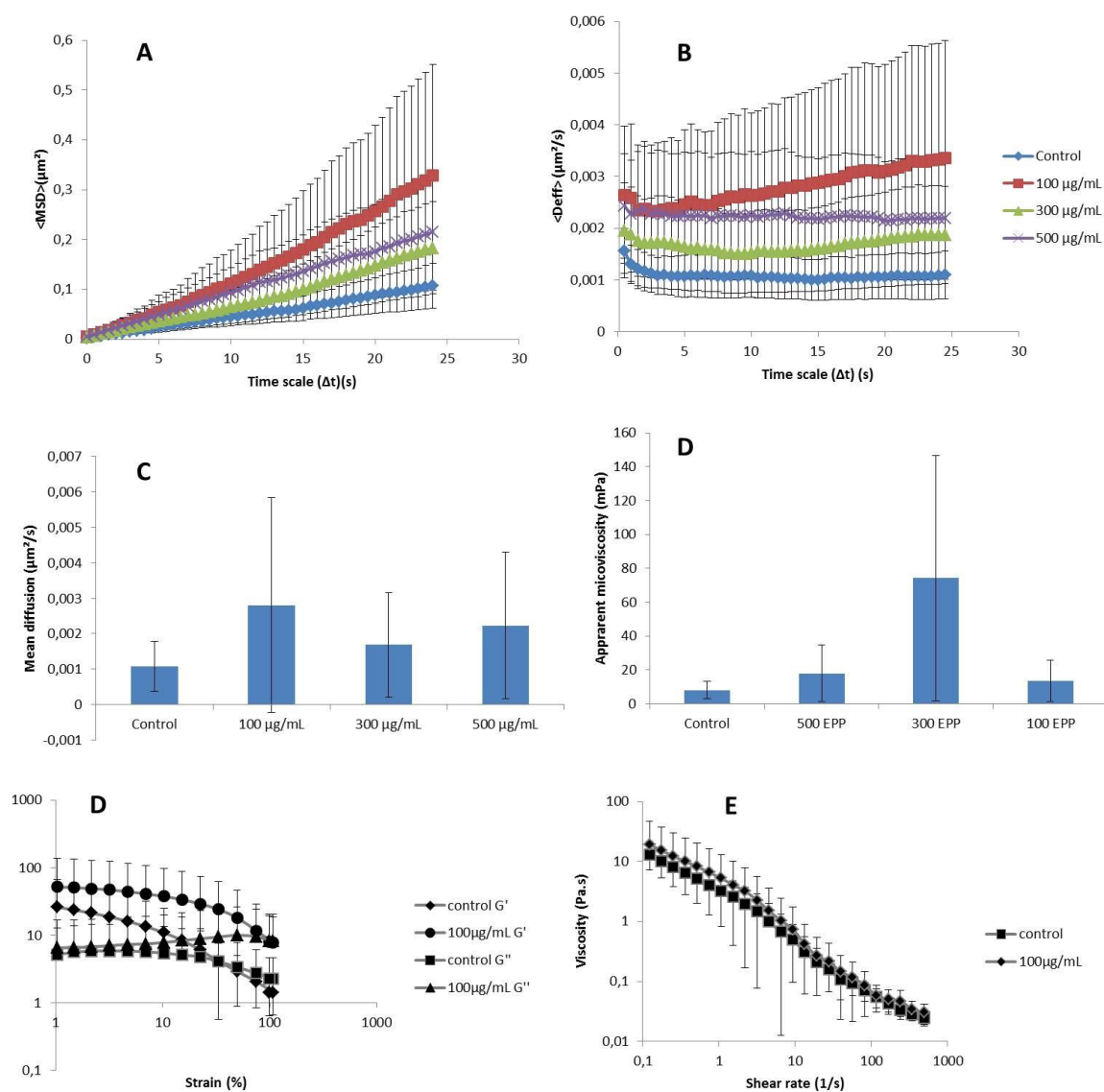


Figure 5.6. Particle tracking microviscosity results (A- mean square diffusion; B- ensemble diffusion coefficient; C- particle mean diffusion; D- apparent microviscosity) and bulk rheology results (D- G' and G'' ; E- bulk viscosity)

5.4.5. Caco-2 transport experiments

To assess the survival and metabolism of polyphenols from cauliflower waste, the intestinal digesta was subjected to Caco-2 cells metabolism and transport. Dilution of the intestinal digesta with transport medium by up to 10 times did not render any significant effect on cell viability as measured using MTT and SRB assays (data not shown). Caco-2 transport experiments were performed for 2 hours and samples from both apical and basal sides were analyzed by LC-MS. Polyphenols were detected in both apical and basal compartments. However, after thorough analysis, no new compounds, specifically phase II metabolites such as glucuronide and sulfate conjugates, were found in either the apical or basal compartments. The same result was observed even when the incubation was

extended up to 7 h. On the contrary, kaempferol glucuronides and sulfate were detected when the kaempferol aglycone was loaded onto the apical compartment.

The majority of the polyphenols from cauliflower wastes are highly glycosylated flavonoids (especially kaempferol), which are both acylated and non-acylated. It is thus unsurprising that metabolites are not found in the transport medium since glycosylation may have hampered cellular uptake and metabolism [295]. It has been well proven that deglycosylation is indeed a critical step in the absorption and metabolism of flavonoids [125,296], which explains the metabolism of kaempferol aglycone into phase II metabolites contrary to the flavonoid glycosides in the plant extract. Although β -glucosidase and lactase-phloridzin hydrolase (LPH) activities have been observed in Caco-2 cells [297-299], the results suggest that its deglycosylation activity is not as efficient as β -glucosidases isolated from human small intestines and liver [125,296,300], or *in vivo* as measured using ileostomy patients [301,302], wherein flavonoid glycosides were in both cases actively hydrolyzed into their corresponding aglycones. Moreover, limited hydrolysis of glycosides was also observed after Caco-2 cell incubations compared to perfused rat intestines [299]. The failure of the Caco-2 cells to deglycosylate the flavonoids in the plant extract resulted in the absence of aglycones and subsequently, phase II metabolites. The same was observed in Caco-2 studies involving quercetin glucoside from shallot [300], flavonoids from Chinese herbal remedy Xi-aochaihu-tang [303], St. John's wort products [304], and polyphenols from various fruit beverages [295].

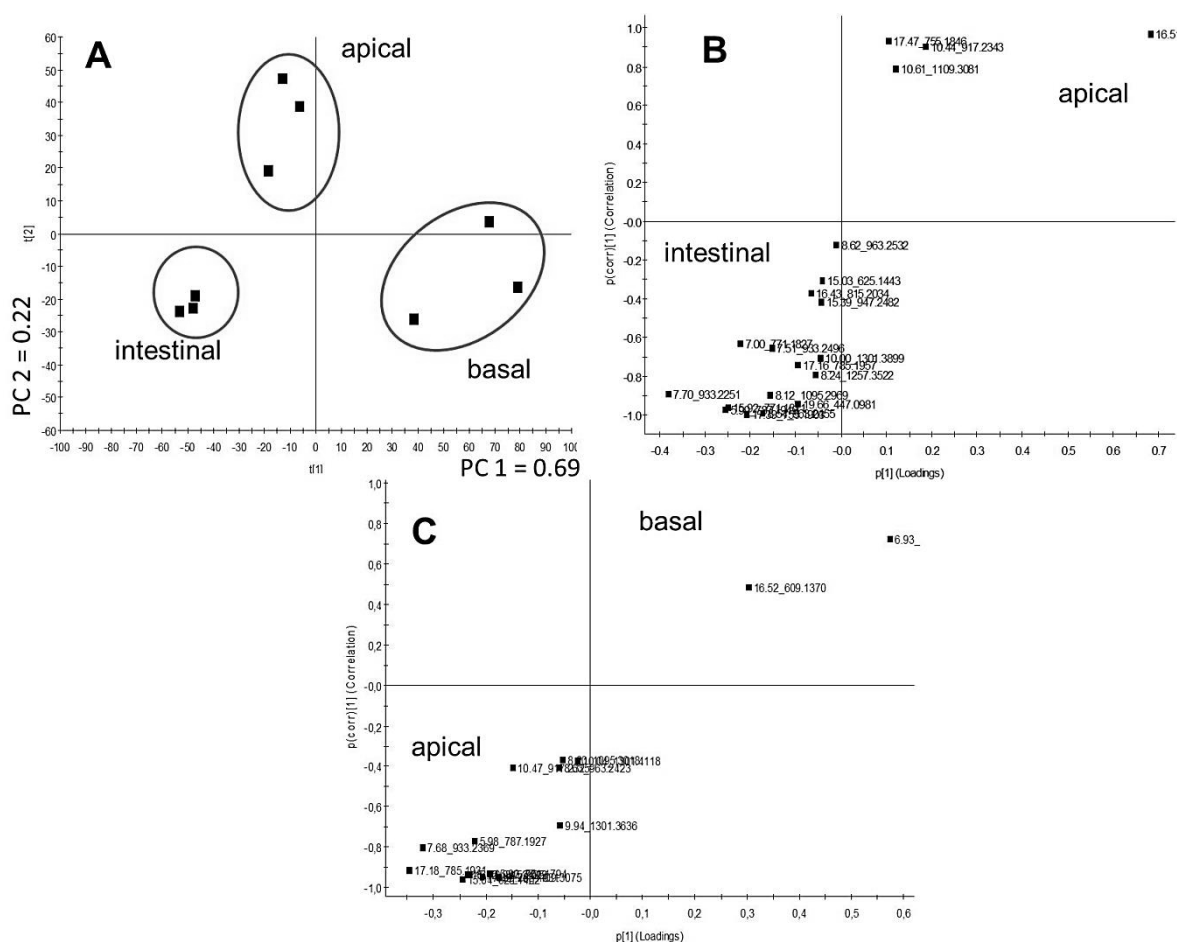


Figure 5.7. A) PCA plot representing the differences among intestinal digesta, and the apical and basal compartment of Caco-2 transport experiment. Model explains 90% of the total variance. B) OPLS-DA/S-plot of intestinal vs apical. Each dot represents a polyphenol wherein the upper right quadrant are those elevated in the apical while the lower left quadrant are those elevated in the intestinal digesta. $R^2X_{cum}=0.94$, $R^2Y_{cum}=0.99$, $Q^2_{cum}=0.98$. C) OPLS-DA/S-plot of apical vs basal. Each dot represents a polyphenol wherein the upper right quadrant are those elevated in the basal while the lower left quadrant are those elevated in the apical compartment. $R^2X_{cum}=0.87$, $R^2Y_{cum}=0.99$, $Q^2_{cum}=0.97$

As in the *in vitro* digestion, PCA and OPLS-DA were used to assess the differences in the phenolic profile among intestinal digesta, apical and the basal compartments (Figure 5.7). As shown in Figure 5.7A, there are distinct differences among intestinal and apical and basal compartments in terms of their polyphenolic composition. PC 1 of the PCA plot explained 69% of the variance and could be attributed to the change in the polyphenol composition through the absorption process. OPLS-DA results showed (Figure 5.7B) that levels of kaempferol-3-*O*-diglucoside (K3diglc), quercetin-7-*O*-diglucoside and acylated kaempferol glycosides were elevated at the apical compartment after 2 h of transport experiment. The reduction of most polyphenols in the apical compartment from the

intestinal digesta could be attributed to the ability of the Caco-2 cells to cut-off terminal glucose units from the highly glycosylated flavonoid glycosides. As observed, the levels of the most highly glycosylated flavonoids also decreased at the apical compartment compared to their respective levels in the intestinal digesta, while flavonoids with fewer sugar units were elevated. Some acylated flavonoid glycosides were also more abundant after 2 h of Caco-2 cell incubation in the apical compartment, which may imply that acylation of the flavonoid glycosides could render the flavonoid more resistant to hydrolysis by the Caco-2 cells. This could also be the reason why phenolic acid aglycones were not detected in either apical or basal compartments after 2 hours of incubation. Results revealed that K3diglc and K3diglc7glc are therefore able to permeate through the Caco-2 cells intact unlike the more glycosylated and acylated flavonoids in the plant extract (Figure 5.7C) but with a very low recovery of 0.3% each (Table 5.1). Small amounts of quercetin glucosides have earlier been reported in literature to permeate through Caco-2 cells intact [297,300,305] and even found in plasma in *in vivo* experiments [63]. Although, quercetin glycosides in the cauliflower waste extract were not found in basal compartment in this experiment.

5.5. Conclusions

In this paper, a rapid and convenient way of analyzing the phenolic profile and recoveries of individual phenolics was proposed using LC-MS coupled with multivariate analysis. By using PCA and OPLS-DA, the changes in the phenolic profile and the losses of particular polyphenols along the *in vitro* digestion were conveniently and reliably monitored. Polyphenol diffusion through the intestinal mucus was also monitored for the first time using FRAP. Polyphenols were found to diffuse rapidly through intestinal mucus without altering its biophysical properties. All in all, a complete characterization of the phenolic profile throughout the entire *in vitro* digestion process, mucosal diffusion, and metabolism and transport through Caco-2 cells was accomplished. Very small amounts of K3diglc and K3diglc7glc (0.3% recovery from original amount in the plant extract) were found to resist degradation along the digestion and intestinal absorption process. In the end, we conclude that targeted metabolomics and FRAP are rapid and convenient tools to study the recovery of polyphenols during *in vitro* digestion, mucosal diffusion and Caco-2 transport.

Chapter 6

2D and 3D quantitative structure-permeability relationship of flavonoids in Caco-2 cells using SMLR, PLS and pharmacophore (GALAHAD)-based COMSIA

Chapter 6: 2 and 3D quantitative structure-permeability relationship of flavonoids in Caco-2 cells using stepwise multiple linear regression (SMLR), partial least squares regression (PLSR), and pharmacophore (GALAHAD)-based comparative molecular similarity index analysis (COMSIA)

6.1. Abstract

Several studies have been performed to evaluate the transport characteristics of flavonoids in the intestines using cell models, such as Caco-2 cells, but information regarding the key structural features of flavonoids that influence intestinal uptake is still limited to date. In this study, quantitative structure-permeability relationship (QSPR) models were developed to study the permeability of 36 flavonoids through Caco-2 cells using both 2D and 3D approaches. For the 2D model, stepwise multiple linear regression (SMLR) and partial least squares regression (PLSR) resulted in good internal ($R^2_{\text{SMLR}} = 0.8$, $R^2_{\text{PLSR}} = 0.93$) and external ($R^2_{\text{SMLR}} = 0.93$, $R^2_{\text{PLSR}} = 0.90$) predictability using a set of 409 molecular descriptors. The high cross validated (leave-one-out) R^2 values (Q^2) for both 2D models ($Q^2_{\text{SMLR}}=0.77$, $Q^2_{\text{PLSR}}=0.67$) suggest that the models are robust and predictive. A pharmacophore (GALAHAD)-based COMSIA analysis was used to generate the 3D QSPR model, which yielded a predictive and robust model ($R^2_{\text{training}}=0.96$, $R^2_{\text{test}}=0.95$, $Q^2=0.625$) composed of hydrogen bond acceptor and donor fields. According to the contour plots, the locations of hydrogen bond acceptors and donors play a crucial role in determining Caco-2 permeability of flavonoids. The models provide deeper insight into the QSPR of flavonoids on intestinal absorption using Caco-2 cell models and could be useful for the high-throughput screening of flavonoids and/or flavonoid-like drugs with health-promoting activities.

Keywords: flavonoids, Caco-2 cells, QSPR, stepwise MLR, PLS, pharmacophore, COMSIA

Redrafted from:

Gonzales GB, Van Camp J, Zotti M, Kobayashi V, Grootaert C, Raes K, Smagghe G. 2014. Two-and three-dimensional quantitative structure–permeability relationship of flavonoids in Caco-2 cells using stepwise multiple linear regression (SMLR), partial least squares regression (PLSR), and pharmacophore (GALAHAD)-based comparative molecular similarity index analysis (COMSIA). *Medicinal Chemistry Research* 24 (4), 1696-1706

6.2. Introduction

It can be recalled from Chapter 5 that the *in vitro* intestinal transport of flavonoid glycosides are very low. In fact, only 0.3% of 2 flavonoid glycosides, K3diglc and K3diglc7glc, were recovered at the basal compartment of the Caco-2 transport system compared to the original undigested extract. One way of ascertaining why flavonoid glycosides are not permeable through Caco-2 cells is to analyze the structural characteristics necessary for a molecule to be transported by Caco-2 cells. By analyzing which structural features are shared amongst those permeable molecules in contrast to those of non-permeable molecules, an understanding of the poor *in vitro* intestinal transport of flavonoid glycosides will be attained. Although human studies have identified general structure characteristics of certain specific flavonoids that are linked with their absorptive capacity, it remains difficult to extrapolate these findings to other flavonoids due to their wide chemical diversity [63,64].

Caco-2 cells are interconnected by tight junctions, thereby creating a physical barrier between gut luminal and blood stream side and characterized by transepithelial resistance. Active transport of nutrients and drugs mainly occurs from the apical to the basal side, although exceptions exist. Paracellular transport of small molecules also occurs as passive diffusion [306,307]. Transport characteristics are often expressed as apparent permeability which is defined as the ratio of the compound concentrations in basal and apical compartment. The Caco-2 cell line is generally considered as a representative model for oral bioavailability of ingested compounds, and for flavonoids in particular as illustrated by many publications [76,125,271,308]. However, when analyzing new sources of flavonoids, such as plant extracts with different flavonoid contents, or pharmaceutical applications of flavonoid-like drugs, wherein synthesis is required, permeability studies using cells would create both financial and technical hurdles [271]. In fact, the highest number of flavonoids analyzed in one single study using CaCO-2 cells so far reported is 36 [76]. Therefore, a method that may predict bioavailability and provide deeper knowledge on the structure-permeability relationship of flavonoids would improve and hasten the search for new flavonoid-like compounds with potent biological activities. However, theoretical *in silico* models which can be used for high-throughput screening of bioavailable compounds have never been widely developed for polyphenols. In addition, the quantitative structure-permeability relationship focusing on flavonoids to Caco-2 cell transepithelial permeability has never been reported, although it exists for phenolic acids [271]. Because it was demonstrated that small differences in Caco-2 cell cultivation methods within labs may have a profound effect on gene expression in the cells [309], we will use the dataset generated by a

single lab [76,310] to develop a quantitative structure-permeability relationship (QSPR) model. In this research, both 2D- and 3D-QSPR models have been developed using molecular descriptors, together with a pharmacophore-based comparative analysis of molecular similarity (COMSIA) approach. Furthermore, a commercial prediction software for intestinal absorption was used and the results were compared to the generated model.

6.3. Materials and Methods

6.3.1. Data collection

The data set was composed of 36 compounds which were obtained from literature data [76,310]. The papers from which the data were sourced came from the same group, which is assumed to have a standardized method for analysis. Flavonoids reported to be untransported through the Caco-2 cells ($P_{app} = 0$) were removed from the data for modeling purposes. The data set was randomly divided into training set (26 molecules) and test set (10 molecules). The model was generated using the training set and was externally validated using the test set. For the QSPR analysis, the data consisted of the log of the apparent permeability coefficient ($\log P_{app}$), which was based on the amount of the original molecule that was retrieved at the basal compartment of the Caco-2 transwell experiment from the amount that was fed on the apical side, and were expressed in cm/s. The original P_{app} values were transformed to $P_{app} \times 10^{-7}$ to avoid negative log values. A complete list of $\log P_{app}$ values is presented in Table 6.1 while their structures are presented in Figure 6.1. The structures of the molecules were obtained from PubChem and their geometries were optimized using Discovery Studio 2.5 (Accelrys, San Diego, USA).

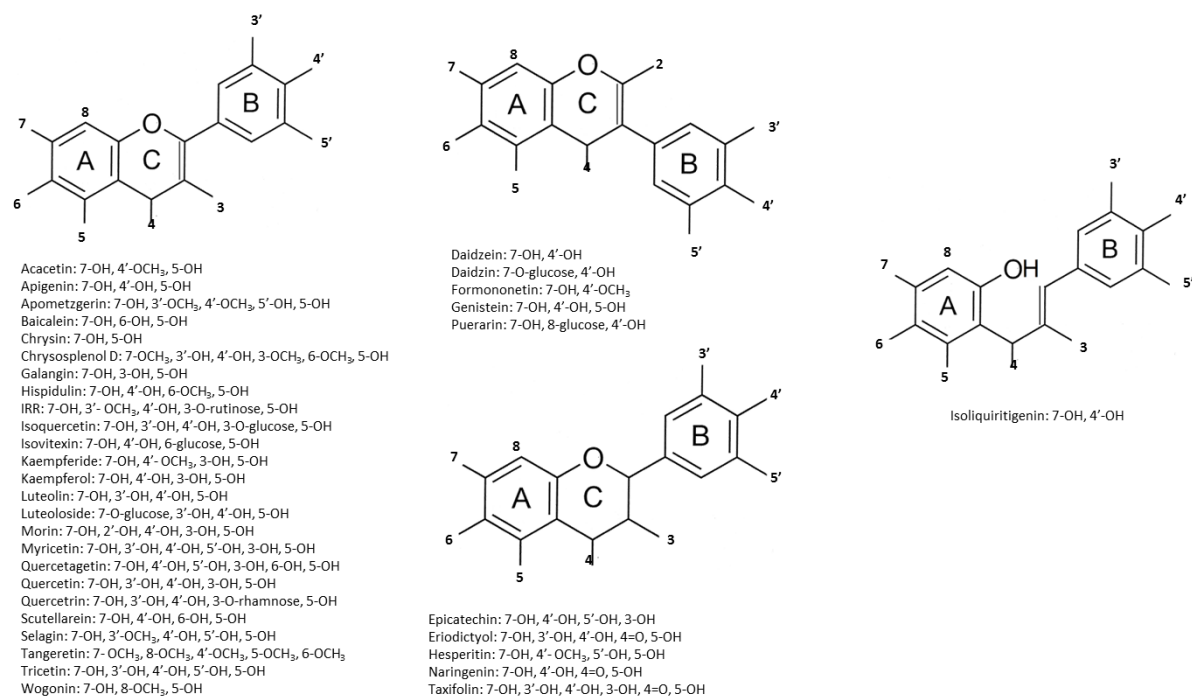


Figure 6.1. Flavonoid structures in the dataset

Table 6.1. logP_{app} values of the flavonoids

Compound name	P _{app} (×10 ⁻⁷ cm/s)	logP _{app}	set
acacetin	173	2.21	training
apigenin	109	2.04	training
apometzgerin	111	2.05	training
baicalein	72.9	1.86	test
chrysin	210	2.20	training
chryso splenol D	81	1.91	training
daidzein	210	2.32	training
daidzin	4.4	0.64	training
(-)epicatechin	6	0.78	training
eriodictyol	52.9	1.72	test
formononetin	296	2.47	training
galangin	77.2	1.89	training
genistein	225	2.35	training
hesperitin	183	2.26	training
hispidulin	66	1.82	test
IRR	2.9	0.46	test
isoliquiritigenin	176	2.21	training
isoquercetin	6.7	0.83	training
isovitexin	6.3	0.80	training
kaempferide	64.4	1.81	test
kaempferol	102	2.01	training
luteolin	88.7	1.95	test
luteoloside	4.3	0.63	training
morin	6.2	0.79	test
myricetin	17	1.23	training
naringenin	126	2.10	training
puerarin	4	0.60	test
quercetagenin	2	0.30	training

quercetin	39.1	1.59	training
quercetrin	7.9	0.90	training
scutellarein	62.4	1.80	test
selagin	10	1.00	training
tangeretin	293	2.47	training
taxifolin	3.1	0.49	training
tricetin	80	1.90	training
wogonin	232	2.37	test

6.3.2. 2D Quantitative-structure activity relationship (QSPR)

A set of 883 molecular descriptors were obtained from PaDEL-Descriptor [311], which included 1, 2 and 3D molecular descriptors. After removing descriptors with zero values and constants, the final number of descriptors was 409. Two commonly used QSAR techniques were employed: stepwise multiple linear regression (SMLR) and partial least squares regression (PLSR). Stepwise multiple regression analysis was used as a feature selection technique, which allows the exclusion of non-correlating descriptors, using the molecular descriptors as independent variables and $\log P_{app}$ as the dependent variable. SMLR was performed using SPSS v21 (IBM, Chicago, USA). Leave-one-out (LOO) cross validation of the generated model after exclusion of collinear variables and insignificant variables was performed using the “MLRMPA” package [312] of R. PLSR was performed using the “pls” package [313] using leave-one-out cross validation. To further test the predictive power and robustness of the models generated, the P_{app} of an external test set (10 molecules) was predicted and were correlated with the actual P_{app} value.

6.3.3. 3D Quantitative-structure activity relationship

All analyses for 3D QSPR (pharmacophore alignment, COMSIA) were done using Sybyl 1.2 software of Tripos (Tripos Inc, St. Louis, MO, USA).

6.3.3.1. Pharmacophore alignment

Due to the wide array of different molecular structures of the flavonoids in the dataset (flavones, flavonones, anthocyanins, etc), rigid alignment using the common substructure/core generated by distill (a phenol ring) resulted in ambiguous alignments and thus cannot be used for subsequent analysis. For this reason, molecular alignment, which is essential for COMSIA analysis, was achieved using a pharmacophore-based approach, GALAHAD. Since GALAHAD was used solely for alignment purposes, a set of 6 molecules representing the different flavonoid groups and the most active molecules was used for pharmacophore building. Default values were used for the other settings. The best generated model (based on Pareto ranking) was used for the alignment of the training and test sets. Pareto ranking is defined as the number of alternatives that are better than the model being assessed by all criteria [314].

6.3.3.2. COMSIA studies

The steric and electrostatic field energies were calculated using the Lennard-Jones and the Coulomb potentials while the electrostatic fields were computed using the Gasteiger-Huckel charge calculation methods. The interaction energies between the molecules and an sp^3 hybridized carbon atom with a +1 charge and a radius of 1.52 Å were calculated using the Tripos force field. The other standard parameters by Sybyl were used for the PLSR analysis. The COMSIA descriptors (steric, electrostatic, hydrophobic, H-bond donor and acceptor fields) served as the independent variables while the $\log P_{app}$ values were the dependent variable for the PLSR analysis. LOO cross validation was performed using the SAMPLS method [315] to optimize the number of components to be included in the PLSR model, which was based on the Q^2 value or the cross validated R^2 (>0.5). The effect of different descriptors on the Q^2 value was also investigated and the combination of COMSIA descriptors that yielded the highest Q^2 (>0.5), R^2 (>0.8) and lowest standard error of estimate (SEE) was chosen as the final PLSR model. An external set of molecules (test set) was used to validate the model as in the 2D model.

6.3.3.3. ADMET prediction using commercial application

ADMET prediction was performed using the ADMET protocol in Discovery Studio 2.5 (Accelrys, San Diego, USA) using the prediction model by Egan et al. [75,316]. Ligands were prepared as described above. ADME prediction was done by computing AlogP₉₈ and polar surface area and plotting it in a 2D plane, wherein, by virtue of pattern recognition based on absorbability data of drug and drug-like compounds [75], molecules that have more than 90% absorbability and those that are not absorbed are distinguished.

6.4. Results and Discussion

6.4.1. 2D QSPR using stepwise multiple linear regression

SMLR revealed 3 molecular descriptors that significantly affect the $\log P_{app}$ values, thus transport of flavonoids in Caco-2 cells. The SMLR equation is shown in eq 1 (standardized coefficients \pm standard error) and statistics are shown in Table 6.2.

$$\text{Eq 1. } \log P_{app} = (1.59 \pm 0.06) + (0.54 \pm 0.08) * gmin + (0.19 \pm 0.06) * maxHBa + (0.17 \pm 0.08) * maxdssC$$

($n=26$, $R^2=0.83$, $adjusted\ R^2=0.80$, $(LOO)Q^2=0.77$, $SEE = 0.31$, $F=35.36$, $Sig. < 0.001$)

Table 6.2. 2D QSPR models using stepwise multiple linear regression

Model	Adjusted R ²	SEE	F	Sig.	Q ²	R ² _{training}	R ² _{test}
SMLR	0.80	0.32	35.36	<0.01	0.77	0.83	0.93

Components	Standardized Coefficients	Std. Error	t	Sig.
(intercept)	1.59	0.06	25.59	<0.01
gmin	0.54	0.08	6.63	<0.01
maxHBa	0.19	0.06	2.93	<0.01
maxdssC	0.17	0.08	2.18	0.04

The model showed very good predictability within the training set ($R^2=0.82$) and a good Q^2 value (0.77), which suggests a good predictive capacity of the model. To further validate the model, the permeability values for the test set were predicted and compared to the reported $\log P_{app}$ values. As shown in Figure 6.2, the model showed good predictability ($R^2=0.93$) and can therefore be considered as a good QSPR model for the transepithelial permeability of flavonoids through Caco-2 cells. For all generated models, $R^2 > 0.8$ and $Q^2 > 0.5$ is regarded as a good model, as previously reported [317].

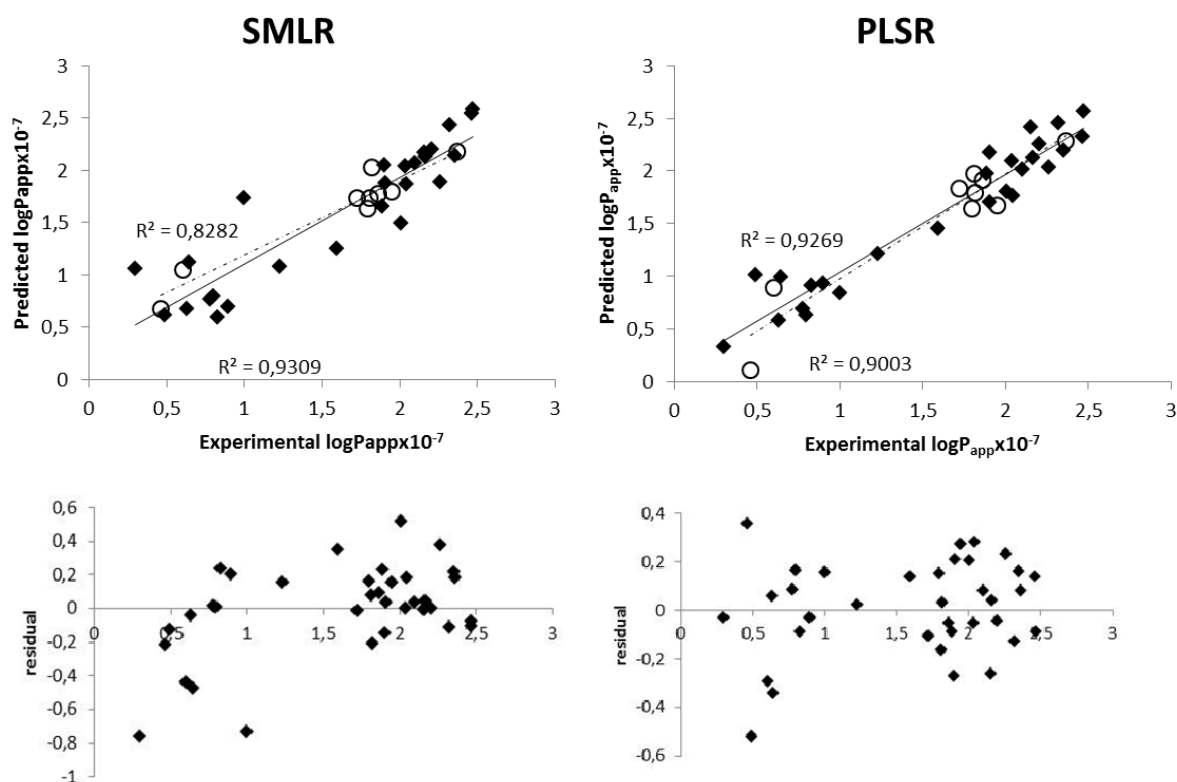


Figure 6.2. Predictability of 2D QSPR models versus observed transepithelial permeability in Caco-2 cells. (◆) training set; (○) test set (above); residuals plot (below)

Gmin, maxHBa and maxdssC belong to the group of Atom Type Electrotological State (E-state) descriptors. E-states were developed by Kier and Hall [318,319], who have

generated indices that combine both the electronic and topological characteristics of atoms in a certain molecule [320,321]. Therefore, since these E-states depend on the detailed structure of the molecule, such indices vary from molecule to molecule and thus can be used for building predictive QSAR models [322]. Such descriptors have been successfully used in generating quantitative activity/property relationships such as prediction of aqueous solubility of organic compounds [322], blood-brain barrier (BBB) partitioning of certain drugs [323], among others. Special interest was placed in these two experiments since permeability of flavonoids through intestinal cells may well be linked to their aqueous solubility and ability to penetrate through membrane, such as the BBB.

6.4.2. 2D QSPR using partial least squares regression

PLSR is a developed generalization of multiple linear regression (MLR). However, unlike MLR, PLSR can analyze data with highly correlated (multi-collinearity) and numerous independent variables [35]. Unlike in the previous SMLR model, interactions of the different variables are much more represented since variables were not removed based only on correlation, typically of SMLR. The PLSR showed good internal predictability ($R^2 = 0.93$) and robustness ($Q^2=0.67$) with minimal root mean squared error of prediction (RMSEP=0.402). The model also showed good predictability over an external test set ($R^2 = 0.90$) (Figure 6.2), which indeed proves that the model is valid. Based on the contributions of each descriptor to the model, it was found that Weighted Holistic Invariant Molecular (WHIM) descriptors contributed the most to the model. WHIM descriptors are 3D descriptors which provide information about certain molecular features such as shape, symmetry, size and atom distribution. It therefore tries to capture a global 3D chemical information of a molecule [324,325]. Since the PLSR model captured the importance of WHIM descriptors, it can be said that the physical 3D structure of flavonoids is indeed a determining factor for intestinal absorption.

Although predictive and robust, 2D molecular models can sometimes be cumbersome to interpret, especially when using indices as molecular descriptors, such as E-states and WHIM. The significance of these models therefore lies on their utility in high-throughput screening of emerging or newly discovered/synthesized flavonoids or flavonoid-like structures. Most importantly, it has been previously reported that different isomeric configurations of flavonoids affect their bioavailability and bioefficacy [326]. It has been shown, for instance, that *S*-hesperitin is more bioavailable than *R*-hesperitin [327,328]. Further, a study on flavonol bioavailability reported that stereochemical configuration influences the bioavailability of flavonols, such that (–)epicatechin is more absorbed than (+)epicatechin while (+)catechin has higher bioavailability than (–)catechin [329]. The

models were also able to distinguish kaempferol from luteolin, which have the same mass but with a different location of one hydroxyl group (isomers). Luteolin however is 8-fold more bioavailable than kaempferol [76]. Using the models, it may be possible to predict which flavonoid conformations are more bioavailable, which may be useful in designing functional foods or pharmaceutical compounds.

6.4.3. Pharmacophore (GALAHAD)-based 3D QSPR (COMSIA)

6.4.3.1. Pharmacophore alignment

The success of a COMSIA analysis relies on the molecular conformations and the quality of the alignment thereof. Thus, an essential step is the generation of a good alignment for the molecules in question [330]. As earlier mentioned, rigid alignment using a common substructure based on atom RMS fitting did not result in a good alignment of the molecules; hence, a pharmacophore-based approach was used. Pharmacophore approach has been previously shown to be superior in aligning flexible and diverse molecules [330]. As an initial step, 6 molecules were chosen for pharmacophore development based on their activity and molecular structure. Considering that isoflavones and flavonones, for instance, differ in the position of their B ring, it is important to ensure that molecular diversity is represented in the alignment protocol. The top 10 pharmacophore models were evaluated based on Pareto ranking and their ability to align all the molecules, judged visually. The best model was therefore chosen and was formed by nine features: 2 hydrogen donors (DA feature), 4 hydrogen acceptors (AA feature) and 3 hydrophobic (HY feature), as shown in Figure 6.3A. The superimposed structures of the training set are also shown in Figure 6.3B.

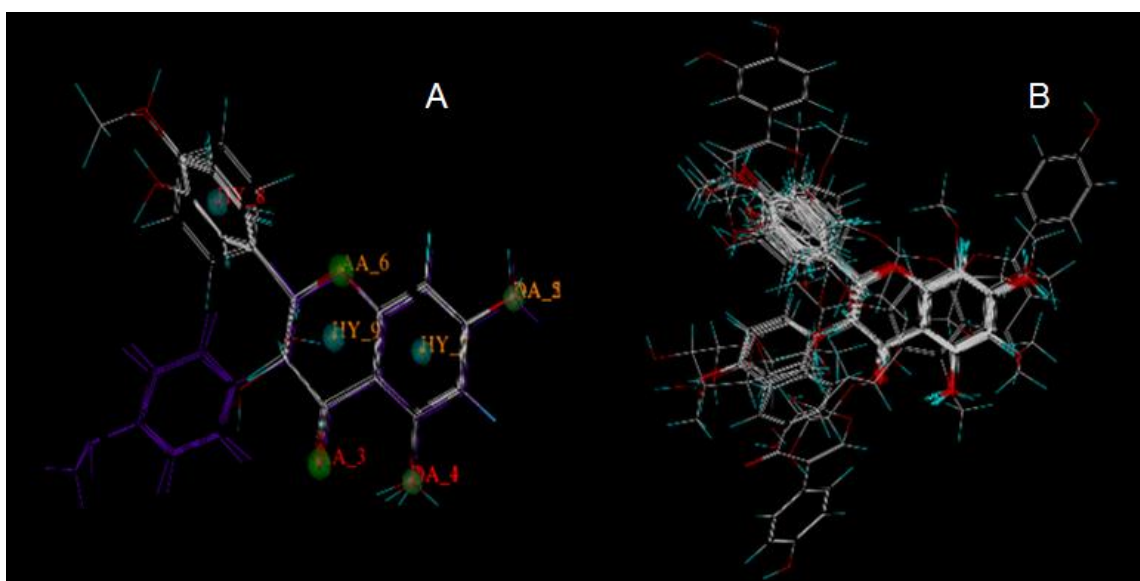


Figure 6.3. Pharmacophore alignment of the training set. A) pharmacophore generated using GALAHAD; B) alignment of training set using the pharmacophore model

6.4.3.2. COMSIA analysis

COMSIA analysis involves hydrophobic, hydrogen donor (HD) and hydrogen acceptor (HA) fields, in addition to steric and electrostatic fields that are computed in COMFA. This therefore makes COMSIA more advantageous over COMFA. Various models were developed using a combination of these fields as shown in Table 6.3. The best model was selected based on the Q^2 (LOO) value, R^2 value, and their ability to predict the $\log P_{app}$ values in both training and test sets, as previously reported [317,331]. As shown, although taking all fields into account meets the criteria for a good QSPR model, all test statistics are improved if steric and electrostatic fields are not considered. This probably explains the inability of COMFA measurements to generate a good model for flavonoid transepithelial permeability (data not shown). This concurs with most of the previously published intestinal models (to be discussed later in this paper), which found that only hydrogen bonding and hydrophobicity played significant roles. The effect of the bulky regions (steric fields) can be explained in the sense of blocking hydrogen bonding and increasing hydrophobicity, such as in the case of methylated hydroxyl moieties. In the case of flavonoid glycosides, glycosylation introduces a huge bulk to the molecular structure but it also greatly reduces their hydrophobicity. Therefore, the steric effects have been explained by the effect of hydrogen bonding and hydrophobicity. The electrostatic field did not contribute to intestinal permeation as well, indicating that electrostatic interactions do not strongly occur during the transport phenomenon of flavonoids through Caco-2 cells. This however needs to be investigated further.

Table 6.3. COMSIA models based on different parameters

	all	HDA	HSE	DA	SE	Validation criteria
Q^2	0.594	0.626	0.394	0.626	0.386	>0.5
R^2	0.968	0.954		0.956		>0.8
Std. Error of estimation	0.171	0.219		0.215		
Amount of components	4	4		4		
Training set R^2	0.968	0.954		0.956		>0.6
Test set R^2	0.88	0.909		0.946		>0.6
Passed validation? (Y/N)	Y	Y	N	Y	N	

H – hydrophobicity; D – hydrogen donor; A – hydrogen acceptor; S – steric; E – electrostatic

Using hydrophobicity, HD and HA fields, a Q^2 value of 0.63 is achieved with good internal ($R^2=0.95$) and external ($R^2=0.91$) predictability. On the other hand, using only hydrogen donor and acceptor fields as independent variables seems to perform similar results

($Q^2=0.63$, $R^2_{\text{training}}=0.96$), $R^2_{\text{test}}=0.95$) sets (Figure 6.4), which indicates that the contribution of hydrophobicity is not as significant as the HD and HA. For this reason, a model composed of hydrogen donor and acceptors fields was considered optimal due to fewer independent variables required.

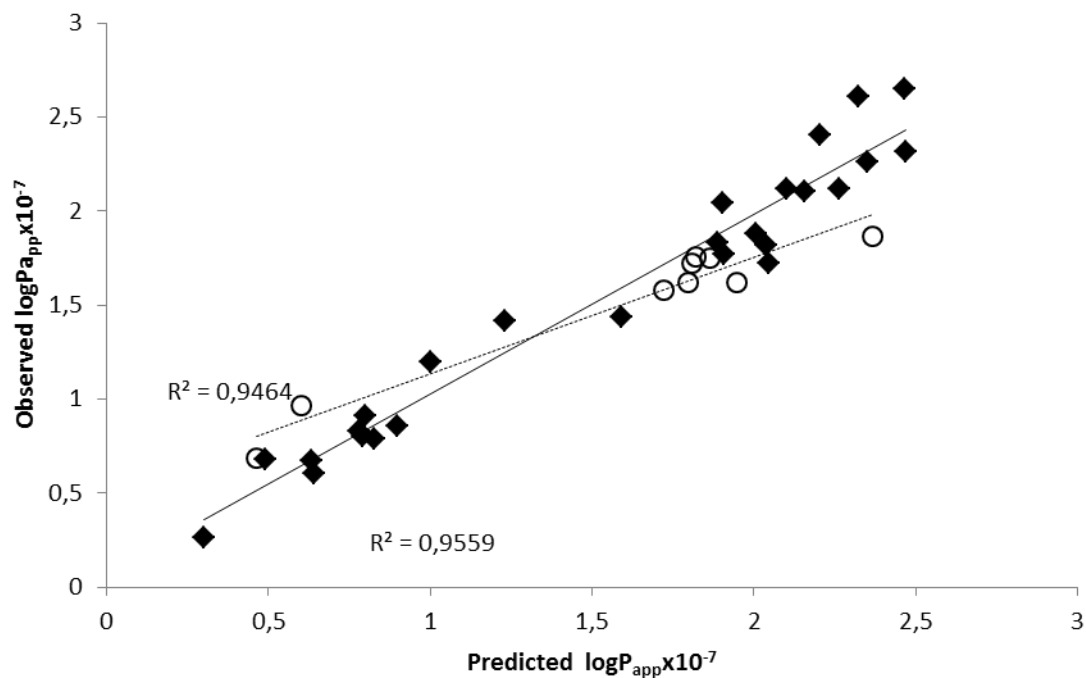


Figure 6.4. Predictability of COMSIA model versus observed transepithelial permeability in Caco-2 cells. (◆) training set; (○) test set

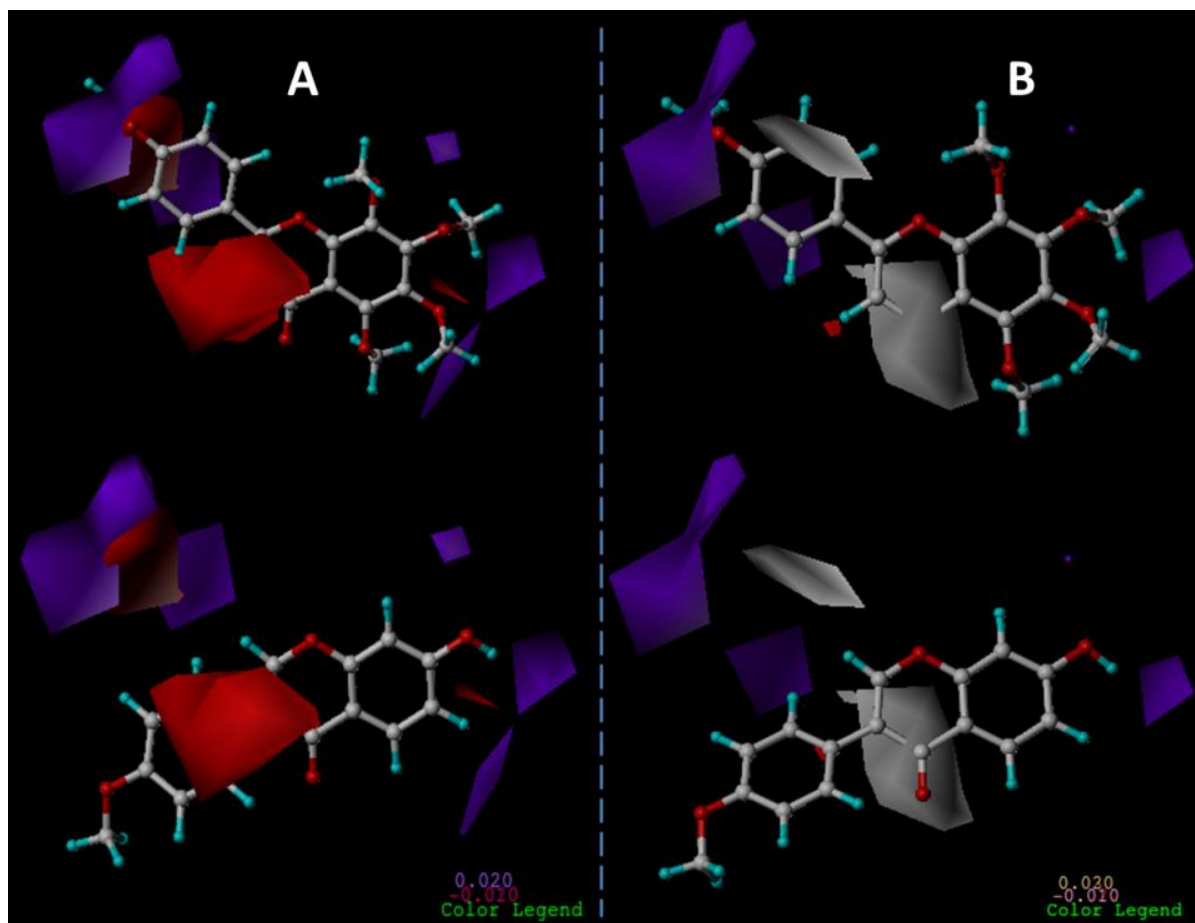


Figure 6.5. COMSIA contour plot with tangeretin (top) and formononetin (bottom) projected into the field. A) hydrogen donor and acceptor fields only (DA); B) hydrophobicity, hydrogen bond donor and acceptor fields (HDA): Purple – hydrogen acceptor group unfavored region (-0.02); red – hydrogen donor group unfavored region (-0.02). White – hydrophobic unfavored region (-0.01).

The COMSIA contour plot is shown in Figure 6.5. Shown in the figure are the 2 most permeable molecules (tangeretin and formononetin) in the dataset. As shown, both HD and HA moieties are disfavored around the A and B rings, which indicates that hydroxylation on these rings reduces transepithelial permeability of flavonoids through Caco-2 cells. Methylation of these hydroxyl groups has been found to increase permeability, like in the case of tangeretin. A focused study on methylated flavonoids revealed previously that such compounds indeed are better transported through Caco-2 cells than their non-methylated counterparts [68]. Indeed, it was found that methylated compounds are 5 to 8-fold higher in apparent permeability than unmethylated flavonoids, which was attributed to the higher susceptibility of the latter to glucuronidation and sulfation at the free hydroxyl moiety. Methylation also protects flavonoids from hepatic glucuronidation, which improves their stability in the bloodstream [68]. Therefore, and as

the current model supports, blocking the free hydroxyl groups through methylation increases permeability.

In addition, it was observed that there was a disfavored hydrogen acceptor region in the C-3 atom of the A ring. This may explain the high permeability of isoflavones such as formononetin (Figure 6.5), wherein the C ring is attached to the C-3 atom, instead of C-2 in the case of other flavonoid classes. A study on isoflavones from soybeans reveals that genistein and daidzein were absorbed intact, compared to flavonoids quercetin, luteolin, kaempferol and apigenin [308]. Two pathways were reported to be responsible for the efficient transepithelial permeation of isoflavones, 1) that such compounds resist glucuronidation and sulfation, and 2) permeate through the paracellular route because of their lipophilicity [308]. Although hydrophobicity was not included as a parameter in the COMSIA model, it seems that hydroxylation in the C-3 atom when replaced with a hydrophobic ring, in the case of isoflavones, increases permeability. However, glycosidation of this ring will therefore reduce its permeability due to the addition of hydrogen acceptors in this moiety as reflected in the model. This result was supported by a study that compared isoflavone aglycones and their glycosides, wherein isoflavone aglycones are absorbed faster and in higher amounts than their glycosidic forms [332].

Considering that hydrogen bond acceptor and donor groups influence permeability of flavonoids, it is therefore evident that flavonoid glycosides are poorly transported through Caco-2 cells. This is because addition of sugar moieties, especially in the C-O-3 region, increases the number of hydrogen bond donors and acceptors. It must be considered however, that most common glycosides, i.e, rutin, were not in the dataset since they have been found not to permeate according to the results of the same publication where the data was sourced from. This therefore indicates that glycosylation does not only reduce permeability, it might actually prevent permeation of the molecule through the membrane of the intestinal cells. Deglycosylation is thus an important step to deliver aglycones through the Caco-2 cells. This claim has been earlier supported and demonstrated [121,125].

High hydrogen bonding capacity of molecules has earlier been reported as one of the most important factors affecting intestinal absorption of new chemical entities [74]. As the generally respected “rule of 5” suggests, any molecule having more than 5 hydrogen bond donors and 10 hydrogen bond acceptors, would normally face poor absorption consequences [74]. It was also observed in previous studies that flavone structures that do not contain any free hydroxyl groups do not interact with the cell membrane and thus passively diffuse across the cell monolayer [333]. Another study reported that

polyhydroxylated flavonoids showed longer retention delays through membranes made up of dipalmitoylphosphatidylcholine (DPPC), which was attributed to the stronger interaction of flavonoids with the DPPC membrane interface [334]. As previously described, in order to cross a membrane, like the cell membrane of Caco-2 cells for instance, molecules need to break hydrogen bonds with its aqueous environment (cell medium or intestinal lumen). The higher the amount of hydrogen bond donors and/or acceptors present in the molecule, the higher the energy required to break such bonds, thus high hydrogen-bonding potential is unfavorable for membrane permeability [72]. The results of this study suggest that not only the number, but also the position of the hydrogen bond donors and acceptors affects intestinal absorption.

Although not as significant as HD and HA fields, hydrophobicity of the compounds seems to play a role in permeability. The unfavored hydrophobic region around C2 to C4 of the C ring indicates the importance of the unsaturated bond C2=C3 and the C4 ketone moiety. It has been previously reported that the C2=C3 unsaturated bond increases the planarity of the compound, which increases its lipophilicity [5] and thus membrane permeability. On the other hand, the ketone moiety of the C ring seems to be important in the bioavailability of flavonoids. As shown in Table 6.1, the absence of this moiety in epicatechin immensely reduced its Caco-2 permeation compared to naringenin. In general, the location of the HD and HA groups, as well as the presence of the C2=C3 double bond and the C4-ketone moiety are essential structural characteristics that dictate the Caco-2 cell permeability of flavonoids.

6.4.4. ADMET prediction

ADME prediction was done using a commercial software package from Discovery Studio 2.5 (Accelrys, San Diego, USA). Prediction is based on two 2D molecular descriptors, namely AlogP₉₈ and PSA. Based on a set of thousands of drug and drug-like compounds sourced from various databases (various literature, Comprehensive Medicinal Chemistry database, USAN/INN database, Physician's Desk Reference database, and Pharmacopeia) [75], a pattern recognition approach was made wherein, compounds with more than 90% absorbability would lie within the 99% confidence ellipse (shown as the green ellipse in Figure 6.6). Compounds falling out of the ellipse are those with less than 30% absorbability. As shown in Figure 6.6, glycosylated flavonoids fall outside the 99% confidence ellipse, along with flavonoids with more than 6 hydroxylation points within the aglycone structure. All the other compounds, such as those with <6 free hydroxides, isoflavones and methylated flavonoids are inside the ellipse, suggesting over 90% absorbability. Although straightforward and rather easy to interpret, the model does not provide a quantitative measure of the intestinal permeability of the compounds, or which

of the compounds are absorbed more unlike the generated QSPR models in this paper. However, it is clear that this model supports the results of both 2D and 3D QSPR models.

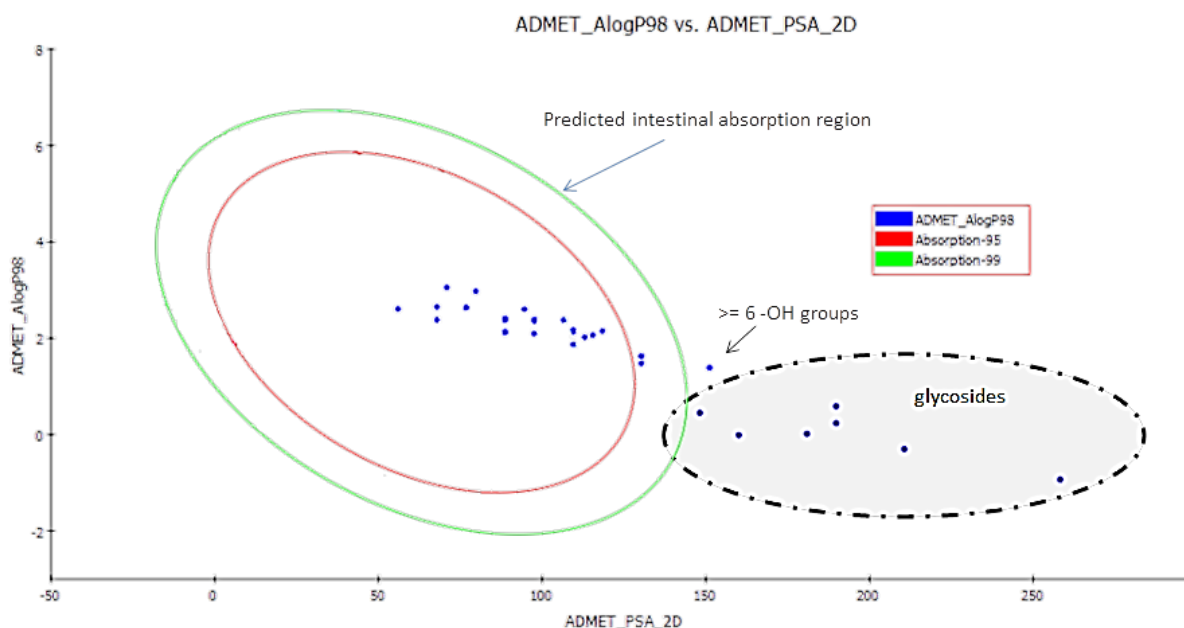


Figure 6.6. ADMET prediction of intestinal absorption using Discovery Studio 2.5 ADMET package

6.5. Conclusion

Oral bioavailability remains one of the most critical issues for flavonoids albeit their known potent bioactivities. In this present study, structural characteristics were used to develop models to predict intestinal absorption of flavonoids using Caco-2 cell transepithelial permeability as a model. Both 2D and 3D quantitative structure permeability relationship models (QSPR) were made, which yielded good correlations to actual apparent intestinal permeability with good predictive power. For 2D QSPR, SMLR and PLSR generated both good internal and external predictability and robustness. COMSIA with a pharmacophore-based alignment (GALAHAD), was used to generate the 3D model. In contrast to the commercially available ADME prediction tools, the generated model in this paper gives quantitative data on permeability instead of mere qualitative information through pattern comparison with other absorbable drugs. The results of this study are important in ascertaining the structural characteristics important to flavonoid intestinal absorption. Also since different structural characteristics affect bioavailability (for instance, isomers), using the QSPR model may provide relevant information on the type of flavonoids (or flavonoid stereoisomer) that could be developed for functional food or pharmaceutical use.

Chapter 7

Quercetin mitigates valinomycin-induced cellular stress via stress-induced metabolism and cell uptake

Chapter 7: Quercetin mitigates valinomycin-induced cellular stress via stress-induced metabolism and cell uptake

7.1. Abstract

In this study, we investigated the ability of quercetin, one of the most common flavonoids, in preventing the cytotoxicity induced by valinomycin, a dodecadesipeptide that causes membrane hyperpolarization, in undifferentiated Caco-2 cells. Further, the metabolism, accumulation and intracellular localization of quercetin and its metabolites were studied using flow cytometry, confocal microscopy and high-resolution mass spectrometry. Results showed that 0.05 μ M valinomycin induced a significant ($p < 0.05$) reduction in Caco-2 cellular mitochondrial activity, and a significant ($p < 0.05$) dose-dependent increase in the content of intracellular reactive oxygen species (ROS). However, co-administration of quercetin and valinomycin at a concentration of 50/0.05 (μ M quercetin/ μ M valinomycin) increased the mitochondrial activity and significantly reduced the ROS content to normal levels. Undifferentiated Caco-2 cells effectively metabolized quercetin into methyl, glucuronide, and sulfate conjugates, which were mostly effluxed to the culture medium. Three different methyl-quercetin isomers were detected, wherein 2 were effluxed and one remained intracellularly. This regioselectivity has not been previously reported. Further, valinomycin caused a significant increase ($p < 0.05$) in the intracellular accumulation of methyl-quercetin. In untreated cells, quercetin aglycone and its methyl derivative were localized in the cell membrane, whereas valinomycin treatment caused for these flavonoids to penetrate inside the cell to render radical scavenging activity. This is first report on the effect of valinomycin on the metabolism, localization and accumulation of methyl-quercetin in undifferentiated cells, and its ability to prevent valinomycin-induced cytotoxicity. These results indicate a potential cellular stress response mechanism in undifferentiated Caco-2 cells.

Keywords: valinomycin, quercetin, mass spectrometry, flow cytometry, confocal microscopy, metabolism

Redrafted from:

Gonzales GB, Smagghe G, Vissenaekens H, Grootaert C, Rajkovic A, Van de Wiele T, Raes K, Van Camp J. 2015. Quercetin mitigates valinomycin-induced cellular stress via stress-induced metabolism and cell uptake. *Molecular Nutrition and Food Research*. *In press*.

7.2. Introduction

Flavonoids are natural metabolites found in plants and are generally consumed through the human diet. They are widely known for their beneficial effects on human health, including anti-oxidative and anti-hypertensive effects [335]. However, their actual functionality is limited by their poor bioavailability, such that they must survive and pass through several barriers along the gastrointestinal tract before they can confer any beneficial effect [290]. They are usually ingested as glycosides (mostly composed of 1 to several glucose, galactose or rhamnose units) and their degree of glycosylation strongly influences their ability to withstand protein/enzyme interaction and acidity in the stomach, and penetrate intact through the mucus layer [290]. Upon reaching the epithelium, β -glucosidases such as lactase-phloridzin hydrolase (LPH) cleave off the sugar moieties (except for rhamnosides) to release the aglycone, which could then be absorbed and metabolized by the epithelium [301]. Circulating flavonoids are usually in the form of glucuronides, sulfate, methylates, and/or their combinations. Since their concentration in plasma is very low ($<1\mu\text{M}$) [63], the bioactivity of flavonoids has been controversial. However, the bioactivity of flavonoids on intestinal cells does not face this problem since the flavonoid concentrations to which the intestine is exposed depends on the amount of flavonoid in the diet and their survival along the digestive tract.

The intestine is constantly exposed to toxins, such as food toxins, bacterial metabolites, and other stressors from the lumen. Food components, such as flavonoids, have been reported to improve intestinal integrity via a myriad of mechanisms, including the increase in tight junction expression [336] and protection against inflammation and oxidative stress [337]. Yet, due to the fact that different toxins have different modes of action, it is likely the flavonoids also operate through different mechanisms depending on the type of insult. It is also currently unclear in the literature whether toxins influence the absorption and metabolism of flavonoids in cells. Since flavonoids are actively metabolized by cells, it is also necessary to determine the form (whether conjugated metabolite or the aglycone) of the flavonoid that confers the bioactivity.

In this study, the changes in quercetin metabolism and intracellular accumulation as affected by valinomycin treatment were monitored. Caco-2 cells, a widely used and generally accepted *in vitro* model for intestinal cells, were exposed to quercetin and/or valinomycin, a toxic cyclic dodecadepsipeptide, which is structurally similar to cereulide, an emetic toxin produced by *Bacillus cereus* that is a common cause of food poisoning [338-340]. Both valinomycin and cereulide have a central hydrophilic cavity which accommodated potassium ions, while the external surface possesses hydrophobic chains

that allow for its diffusion through the hydrophobic cell membrane. This enables valinomycin to drive K^+ ions extracellularly, thus causing hyperpolarization of the cell membrane, leading to apoptosis [338]. Valinomycin is typically used as a model since cereulide is currently not commercially available/affordable. The effect of submicromolar concentrations of valinomycin on proliferation and viability of cells over phases of the cell cycle in several cell lines have been established to be due to the disruption of the membrane potential [341].

7.3. Materials and methods

7.3.1. Materials

Quercetin, valinomycin, diphenyl boric acid 2-aminoethylester (DPBA), phosphate buffer saline (PBS), and other reagents were purchased from Sigma-Aldrich (Diegem, Belgium), unless otherwise stated. UPLC-grade methanol, formic acid were acquired from Biosolve (Valkenswaard, The Netherlands). Dulbecco's Modified Eagle's Medium (DMEM) was purchased from Life Technologies (Merelbeke, Belgium) while fetal bovine serum (FBS) was obtained from Greiner Bio-One (Wommel, Belgium).

7.3.2. Cell culture

Caco-2 cells were obtained from the American Type Culture Collection and grown in DMEM containing 4.5 g/L glucose, 10% heat-inactivated FBS, 1% non-essential amino acids supplement, and 1% penicillin-streptomycin. Cultures were maintained in humidified atmosphere at 37°C with 10% carbon dioxide. Cells were splitted at around 80-90% confluency by trypsinization for up to 40 passages. Cells were then seeded onto various plates depending on the type of analysis and were maintained for 5 days post-confluence before the analysis. All analyses were done with at least 3 biological replicates.

7.3.3. Effect of quercetin and valinomycin treatments on cellular stress

The effect of quercetin (25, 50, 100 μ M), valinomycin (0.02, 0.05, 0.1 μ M), and the combination of the two (25:0.02, 50:0.05, 100:0.1; μ M) towards cellular stress after a 24-hour exposure was assessed using standard MTT and SRB assays, as well as measurement of their intracellular reactive oxygen species (ROS).

Cells were seeded onto 96-well plates with a seeding density of 2×10^4 cells per well. Standard MTT and SRB test were performed following the methods of [273] and [274], respectively. The MTT assay is a colorimetric assay used for assessing mitochondrial activity by which NAD(P)H-dependent oxidoreductase enzymes found in active

mitochondria reduce the tetrazolium dye MTT 3-(4,5-dimethylthiazol-2-yl)-2,5-diphenyltetrazolium bromide to its insoluble formazan, which has a purple color [342]. The sulforhodamine B (SRB) assay on the other hand is used for cell density determination, based on the measurement of cellular protein content in 50% trichloroacetic acid-fixed cells [343]. The ROS assay was based on the fluorescence of dichlorofluorescein. Briefly, cells were seeded on a black 96-well plate and exposed for 24 hours. After two washing steps with PBS, 10 μ M of dichloro-dihydro-fluorescein diacetate (DCFH-DA) previously prepared in 0.1% DMSO was incubated with the cells for 30 minutes at 37°C. During this time, the non-fluorescent probe penetrates through the cell membrane where intracellular esterases convert it into dichloro-dihydro-fluorescein (DCFH), which reacts with intracellular ROS to produce the fluorescent dichlorofluorescein (DCF). The medium was then aspirated and fresh PBS was added onto the cells. The fluorescence was then measured at 485nm (ex), 535nm (em) using a plate fluorometer.

The results for MTT, SRB and ROS assays were expressed as percentages compared to the control treatment with serum-free medium.

7.3.4. Flow cytometric analysis

Cells were seeded in a 6-well plate with a density of 3x10⁵ cells/well and exposed with the treatments in serum-free medium. After 24 hours of exposure, the cells were washed with PBS. The cells were then harvested via trypsinization, collected in a 1.5mL Eppendorf tube, and centrifuged for 5 minutes at 5000 rpm. The supernatant was removed and the cells were washed with PBS and re-centrifuged. After removing the supernatant, 1mL of 3.7% paraformaldehyde was added onto the cells with repeated pipetting. Fixation was done at 5°C overnight. Thereafter, the cells were washed with 10mM ethanolamine and PBS, with centrifugation after every washing step. Triton X-100 (0.5% in PBS) was then added as a permeation agent for 5 minutes and washed with PBS, prior to incubation with 0.2% diphenylboric acid 2-aminoethyl ester (DPBA) prepared in 0.3% DMSO in PBS. After 30 minutes of staining, the cells were centrifuged and re-dissolved in water. Intracellular accumulation was measured via the fluorescence of flavonoids with DPBA using a BD Acurri™ C6 flow cytometer at 485nm excitation and 535nm emission.

Results from the flow cytometry analysis of flavonoid accumulation were expressed as uptake factors, shown below:

$$\text{Eq 1.} \quad \text{Uptake factor} = \frac{(FT - Ft) - (FU - Fu)}{(FU - Fu)};$$

Where FT is the mean fluorescence of the treated cells stained with DPBA; Ft is the mean background fluorescence (without DPBA stain) of the treated cells; FU is the mean fluorescence of the blank treatments (with DPBA stain); and Fu is the mean background fluorescence of the blank samples (without DPBA stain). In this way, the results reflect the background fluorescence and the variability incurred during staining step.

7.3.5. LC-MS analysis

Cells were grown in 25 cm² canted neck tissue culture flasks for 5 days prior to treatment with 2mL of exposure medium containing 50 μ M quercetin, 50 ng/mL valinomycin and their combination (50 μ M quercetin + 50 ng/mL valinomycin). After 24 hours of incubation, 1 mL of medium was filtered through 0.45 μ m filter and kept in a -20 $^{\circ}$ C freezer for metabolite analysis using LC-MS. The remaining medium was aspirated and the cells were scraped and transferred into pre-weighed 1.5mL Eppendorf tubes and frozen at -80 $^{\circ}$ C. Thereafter, the cells were lyophilized and weighed to obtain the cellular dry weight. Intracellular flavonoid was extracted using 50% acetonitrile and cold sonication for 5 minutes using an Elmasonic S60H unit with a frequency of 37kHz and a nominal power of 180W. Cellular debris was removed by filtration through a 0.45 μ m filter and the filtrate was injected onto the LC-MS.

LC-MS analysis was performed with a Waters Acquity UPLC system connected to a Synapt HDMS TOF mass spectrometer (Waters Corp., Milford, MA, USA). LC separation was done on a Waters Acquity BEHC18 column (2.1 mm \times 150 mm, 1.7 μ m particle size) using gradient elution of (A) water containing 0.1% (v/v) formic acid and (B) methanol containing 0.1% (v/v) formic acid, with the column temperature maintained at 40 $^{\circ}$ C. The flow rate was set at 250 μ L/min during the gradient elution, as earlier described (Chapter 2). The eluent was then directed to an electrospray ionization (ESI) source. Data were acquired in continuum negative ionization in V-mode. MS^E analysis was performed with collision energies of 6 V for the low energy and 45 V for high energy. Leucine-enkephalin (250 pg/ μ L) dissolved in 50:50:0.1 (water:acetonitrile:formic acid), [M-H]⁻ = 554.2615, was used as a lock mass. Mass range was set at 100–1500 Da with a scan speed of 0.2 s per scan using the MassLynx software 4.1 (Waters Corp.). Automated peak detection with mass defect filtering for phase I and II metabolites was done using the MetabolynxTM software embedded within the MassLynx package.

7.3.6. Cellular flavonoid localization

Cells were seeded onto a 24-well plate containing a 12mm-diameter glass cover slip. After treatment, cells were washed with pre-warmed PBS (pH 7.5) and stained with 10 μ M DiI stain. Then, the cells were fixed with 3.7% para-formaldehyde in PBS overnight at

5°C. The cover slip was then removed and placed in a washing recipient containing 10mM ethanolamine for 5 minutes and washed twice with PBS. Thereafter, PBS buffer containing 0.5% Triton X-100 was added and let standing for 5 minutes prior to washing with PBS. A staining solution containing 0.2% DPBA prepared in 0.3% DMSO in PBS, and DAPI was added onto the slides and incubated for 30 minutes. The samples were then washed with PBS and mounted onto a glass slide using 50% glycerol as a mounting agent. Cells were imaged using a Nikon A1 confocal microscope, with a Plan Apo 60x oil immersion objective with a numerical aperture of 1.27, a 488nm argon laser, a pixel size of 0.2 μ M and NIS-Elements AR v4.1004 (Build 854) software. Image processing was performed in ImageJ freeware (W.S. Rasband, U.S.A. National Institutes of Health, Bethesda, Maryland, USA, <http://rsb.info.nih.gov/ij/>, 1997–2012).

7.4. Results and Discussion

7.4.1. Effect of quercetin and valinomycin treatments on cellular viability

The intestine consists of a heterogeneous mix of mature differentiated villus enterocytes that are exposed to the luminal gut content, and poorly differentiated proliferative enterocytes that reside in the intestinal crypts. This dynamic system involves the generation of new cells from the proliferative undifferentiated cell population and their migration to the tip of the epithelium to replenish the senescent cells (differentiated) [344,345]. *In vitro* models of the gut epithelium involve the use of Caco-2 cells, which were originally obtained from a human colon adenocarcinoma that spontaneously differentiate into a monolayer of cells expressing several morphological and functional characteristics of the mature enterocyte. This process of differentiation follows a process composed of initially homogeneously undifferentiated cells (at sub-confluence), to heterogeneously polarized and differentiated (from day 1 to day 20 post-confluence), to finally homogeneously polarized and differentiated cells [82]. In this study, we chose to use cells after 5 days of confluency mainly because it better represents the heterogeneity of the intestines than when they are fully differentiated. Undifferentiated Caco-2 cells have been previously used in toxicity assays since it contains a wider plasticity in the cellular physiology, sensing and adaptation/response to stress compared to the fully differentiated Caco-2 cells [346].

Figure 7.1A and B illustrates the effect of various concentrations of quercetin, valinomycin and their combination on the viability of undifferentiated Caco-2 cells. As shown, cellular protein content was not significantly altered by the different treatments. In addition, quercetin at a concentration of 25-100 μ M did not significantly change the mitochondrial activity of the Caco-2 cells. Valinomycin, on the other hand, caused a dose

dependent decrease in mitochondrial activity, especially at concentrations of 0.02 and 0.05 μ M. Treatment with 0.005 and 0.1 μ M valinomycin caused the MTT response to drop to 78% and 73%, compared to the untreated sample.

On the contrary, the co-administration of the valinomycin and quercetin resulted in an increase in mitochondrial activity compared to the valinomycin treatments. Quercetin:valinomycin ratios of 50 μ M:0.05 μ M and 100 μ M:0.1 μ M, respectively, raised the MTT response to 89% and 83%, which are not significantly different from the untreated sample. This rise in mitochondrial activity indicates that quercetin administration protected the Caco-2 cells against valinomycin-induced mitochondrial dysfunction.

Excess production of reactive oxygen species (ROS), especially by the mitochondria, is the earliest sign of cellular dysfunction. As shown in Fig 1C, addition of up to 100 μ M quercetin to the cells did not induce the production of intracellular ROS, whereas treatment with valinomycin induced a significant dose-dependent increase in ROS production. Co-administration of valinomycin and quercetin resulted in a significant decrease in intracellular ROS level compared to treatment with valinomycin alone. The 50 μ M:0.05 μ M (quercetin:valinomycin) treatment reduced the level of intracellular ROS back to the level of an untreated cell (control).

Quercetin and its cellular metabolites have long been reported to exert strong antioxidative properties, especially via the scavenging of ROS produced due to cellular stress. Structure-antioxidant relationships suggest that the catechol moiety of the B-ring in quercetin is very important for its ability to chelate oxidizing metals and stabilize radicals, and thus scavenge ROS. Also, the presence of both C2,3-double bond and 3-OH further contributes to its anti-oxidative effect, especially when the antioxidant activity of the B-ring is small [347,348]. Therefore, cellular metabolism of quercetin also yields antioxidative metabolites, which could be responsible for the recovery of MTT and reduction of ROS levels in the valinomycin-treated cells.

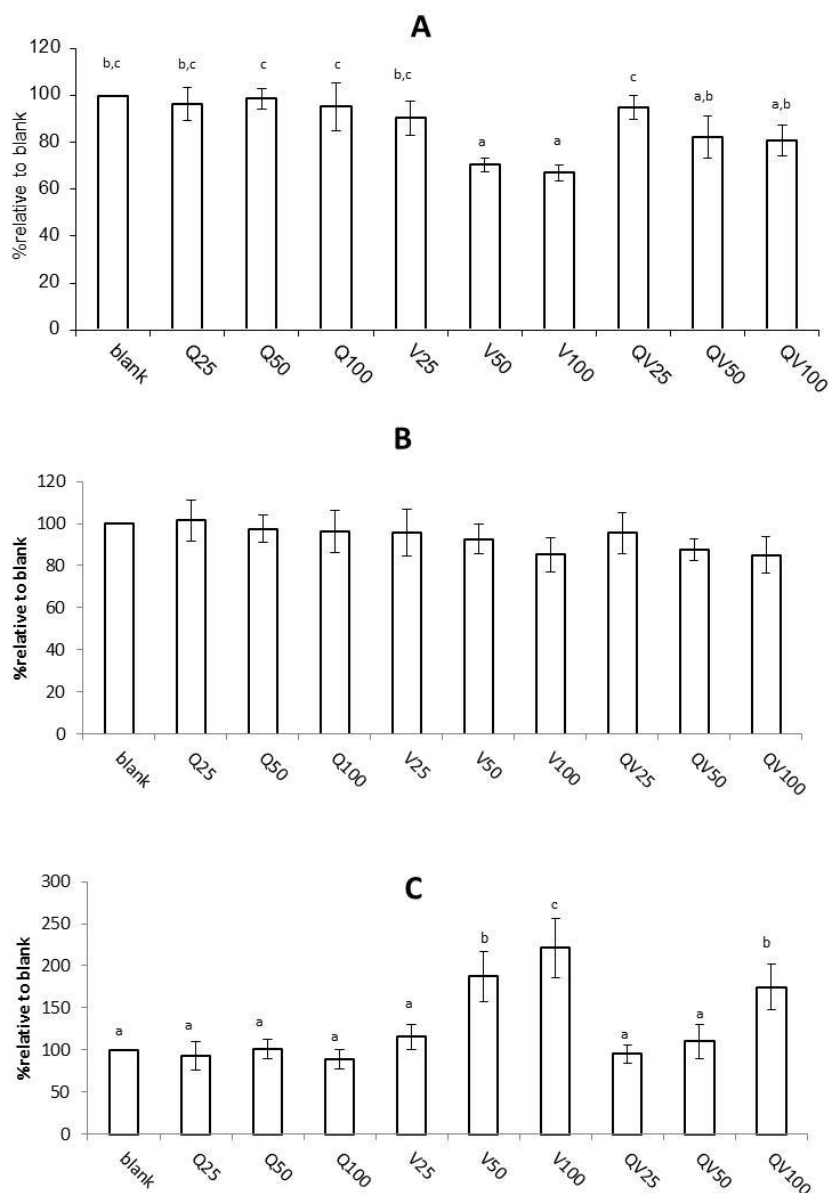


Figure 7.1. MTT (A), SRB (B), and ROS (C) response of undifferentiated Caco-2 cells exposed to 25, 50, and 100 μM quercetin (Q25, Q50, Q100); 0.02, 0.05, and 0.1 μM valinomycin (V25, V50, V100); and combination of quercetin and valinomycin – 25 μM quercetin+0.02 μM valinomycin (QV25), 50 μM quercetin+0.05 μM valinomycin (QV50), 100 μM quercetin+0.1 μM valinomycin (QV100). Results are expressed as relative percentage compared to the blank sample (treated with culture medium contain equal amount of DMSO). Different letters indicate significant difference at $\alpha=0.05$.

7.4.2. Quercetin metabolism and intracellular accumulation

After 24 hours of quercetin treatment, cellular metabolism has resulted in its conversion to several conjugates. It was observed that almost all of the original quercetin in the culture medium was effectively converted by the undifferentiated Caco-2 cells. While

most of the metabolites were effluxed back to the culture medium, a small amount of quercetin aglycone and its methyl conjugate were retained in the cells (Table 7.1). Figure 7.2 depicts the formation of quercetin metabolites post 24-hour incubation with undifferentiated Caco-2 cells for quercetin-only (50 μ M) and quercetin+valinomycin (50 μ M:0.05 μ M) treatments. The majority of the metabolites were methylated derivatives along with glucuronides and sulfates. The catechol structure in quercetin makes it very prone to *O*-methylation, which is catalyzed by the catechol-*O*-methyltransferase (COMT) and was found to reduce the cytotoxicity of quercetin *in vivo* [127,349]. Three different quercetin-*O*-methyl isomers were found – 2 that were effluxed to the cell medium and 1 that remained intracellularly, which were well separated in the LC chromatogram (rt = 22.48, 23.43, and 25.53 mins, respectively). This selectivity in undifferentiated Caco-2 cells has not been previously reported in the literature. Structure-ABC transporter affinity relationship of flavonoids reveals that *O*-methylation of the C4'-position of the B-ring increases the flavonoid's affinity to ATP-binding cassette (ABC) transporters P-glycoprotein (PgP) and breast cancer resistance proteins (BCRP) [290]. It is thus highly likely that some isomers are more favored for efflux while others are retained intracellularly. The exact masses of the observed methylates had very small mass errors of 0.9 ppm that when fragmented yielded the product ion $m/z = 301$, which correspond to the m/z value of the quercetin aglycone. The mass defect was calculated to be 16 mDa, which is only 0.3 mDa off from the typical mass defect observed for metabolism via methylation (15.7 mDa) [29]. These provide strong evidence that the observed metabolites are indeed methyl conjugates of quercetin. Our current method was however unable to unravel the exact location of the methyl conjugation site.

As shown, the relative amounts of extracellular metabolites of both treatments are not significantly different from each other. On the contrary, the level of intracellular methyl-quercetin was significantly higher ($p < 0.05$) in the quercetin+valinomycin (50 μ M:0.05 μ M) treatment compared to the cells that were treated with 50 μ M of quercetin alone, whereas the levels of intracellular quercetin aglycone in both treatments were not significantly different. Considering that the intracellular content is much lower than the effluxed metabolites, it is not peculiar that intracellular accumulation would be observed without imposing a significant change in the extracellular content. Also, intracellular content is normalized per mg of cell dry weight whereas the extracellular content was measured by direct injection to the LC-MS system.

Table 7.1. Cellular metabolism of quercetin by undifferentiated Caco-2 cells

Metabolic transformation	Molecular Formula	Mass shift (Da)	Precursor ion	Error (ppm)*	rt (mins)	Product ions
<i>Extracellular</i>						
Glucuronidation	C ₂₁ H ₁₈ O ₁₃	176	477.0685	3.3	17.33	301
Methylation + glucuronidation	C ₂₂ H ₂₀ O ₁₃	190	491.0831	1	19.82	301, 315
Quercetin aglycone	C ₁₅ H ₁₀ O ₇	0	301.0348	-0.2	22.12	
Methylation (1)	C ₁₆ H ₁₂ O ₇	14	315.0508	0.9	22.48	301
Methylation + sulfation	C ₁₆ H ₁₂ O ₁₀ S	94	395.0063	-2.6	23.14	301, 381
Methylation (2)	C ₁₆ H ₁₂ O ₇	14	315.0508	0.9	23.43	301
<i>Intracellular</i>						
Quercetin aglycone	C ₁₅ H ₁₀ O ₇	0	301.0348	-0.2	22.15	
Methylation (3)	C ₁₆ H ₁₂ O ₇	14	315.0508	0.9	25.53	301

*after mass adjustment with the Leu-Enk lock mass

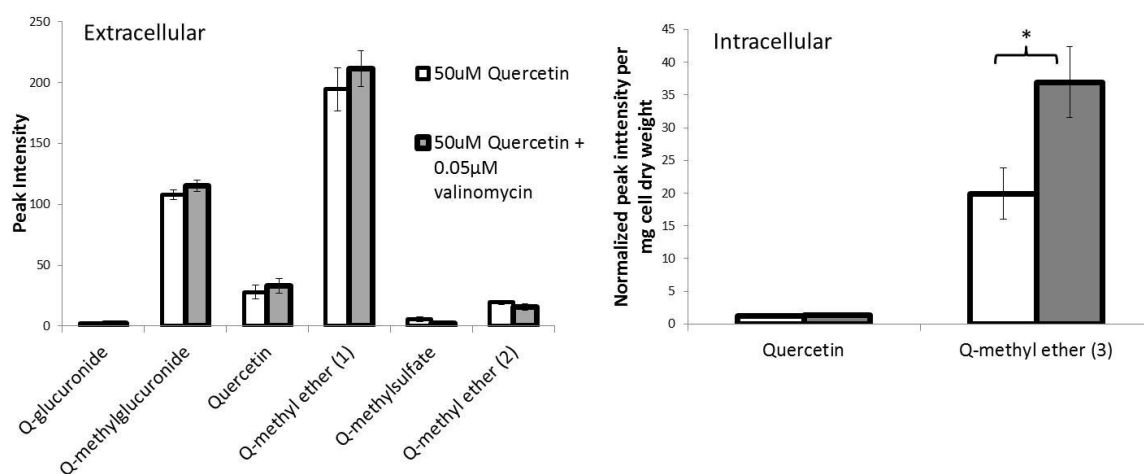


Figure 7.2. Undifferentiated Caco-2 cell metabolites of quercetin after 24 hours of incubation with 50 μ M quercetin or co-administration of 50 μ M:0.05 μ M quercetin:valinomycin. (Top) Effluxed metabolites measured by directly injecting culture medium to LC-MS, (Bottom) Intracellular metabolites normalized per dry cell weight. Results are shown as mean \pm SEM. '*' denotes significant difference (Student's T-test; $p < 0.05$)

To further validate the observed intracellular accumulation of flavonoids, a flow cytometric approach was performed by monitoring the fluorescence of flavonoids stained with DPBA. Cellular content is difficult to quantify since a large volume of cells is often required to ensure a quantifiable peak is consistently observed when using LC-MS analysis. Also, the long and numerous extraction steps required for LC-MS analysis often leads to losses of the target analyte. Flow cytometry has the advantage of being able to see changes in intracellular flavonoid accumulation without the need for extensive sample

preparation steps. Figure 7.3 shows the flavonoid uptake factor (indicating the intracellular uptake of quercetin) and side scatter (SSC) (indicating internal cellular complexity), in function of the forward scatter (FSC) (indicating cellular size). As shown in Figure 7.3, a significant increase in the fluorescence was observed for the quercetin+valinomycin (50 μ M:0.05 μ M) treatment compared to quercetin (50 μ M)-only treatment. This further validates our results suggesting that valinomycin treatment induced higher intracellular flavonoid concentrations. No significant difference in cell size or complexity was observed among the cell populations of the different treatments. This indicates that the apparent increase in intracellular flavonoid concentration is probably not caused by swelling of the cells, which could increase the surface area of the membrane that quercetin could be bound to.

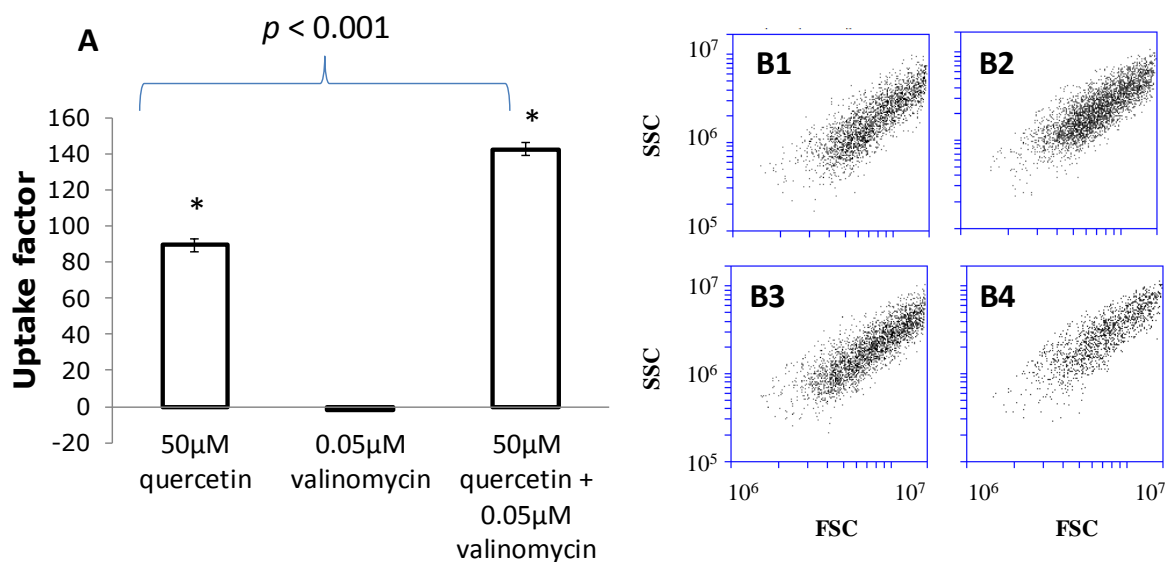


Figure 7.3. (A) Fluorescence of the quercetin-DPBA complex in cells measured by flow cytometry; (B) Forward scatter (x -axis) and side scatter (y -axis) plots of the different treatments: blank (B1), 50 μ M quercetin (B2), 0.05 μ M valinomycin (B3), combination 50 μ M quercetin:0.05 μ M valinomycin (B4). Results for (A) are shown as mean \pm SEM.

Although this technique is unable to distinguish the different metabolic transformations of the parent compound, these results also show that flow cytometry could be used to complement LC-MS analysis to study intracellular flavonoid concentrations. From the LC-MS results, we conclude that this increase in flavonoid concentration is due to the accumulation of *O*-methyl-quercetin.

7.4.3. Flavonoid intracellular location

Confocal microscopy was used to determine the site of localization of the flavonoids within the undifferentiated Caco-2 cells. Here, we imaged the midsection of the cells

using DAPI (nucleus, blue), DPBA (flavonoid, green) and DiI (cell membrane, red) fluorescent stains. As shown in Figure 7.4 (top row), our results suggests that quercetin accumulates at the cell membrane of Caco-2 cells, which corroborates earlier reports [333]. Unconjugated quercetin and (especially) its methylated derivative may remain in/on the cell owing to their relatively high octanol/water partitioning coefficient ($\log P = 1.59$ for quercetin [76]), which allows them to partition to the hydrophobic cellular membrane (for comparison, $\log P$ value of glucose is -2.82 [350]). The ability of flavonoids to accumulate in membranes has also been widely investigated using liposomes and phospholipid vesicle models, where it was found that flavonoids are incorporated with the polar head group of the phospholipid [351-353]. In Chapter 6, we have demonstrated that hydrogen bonding capacity of flavonoids limit their passive diffusion through Caco-2 cells. As the number of free hydroxyl (-OH) moieties increase, the ability of flavonoids to diffuse through the membrane is reduced due to their hydrogen bonding interaction with the hydrophilic choline head group. In contrast, when “capping” the free hydroxyl groups via methylation, their rate of membrane diffusion increases due to the decrease in hydrogen bonding potential.

Interestingly, upon co-administration of quercetin and valinomycin to the cells, the flavonoids were not solely localized in the membranes, and they had penetrated inside the cytoplasm as shown in Figure 7.4. This is probably due to the higher concentration of methyl quercetin, as methylated compounds exhibit less hydrophilic interactions with the polar head group of the cell membrane, and hence may penetrate more easily through the cell membrane. This may explain why in this case, the flavonoid is not only associated with the cell membrane. However, it must be noted that methyl-quercetin is also dominantly present in the quercetin-only treatments and yet only localized in the membrane. Therefore, another mechanism must exist for this accumulation and change in localization site.

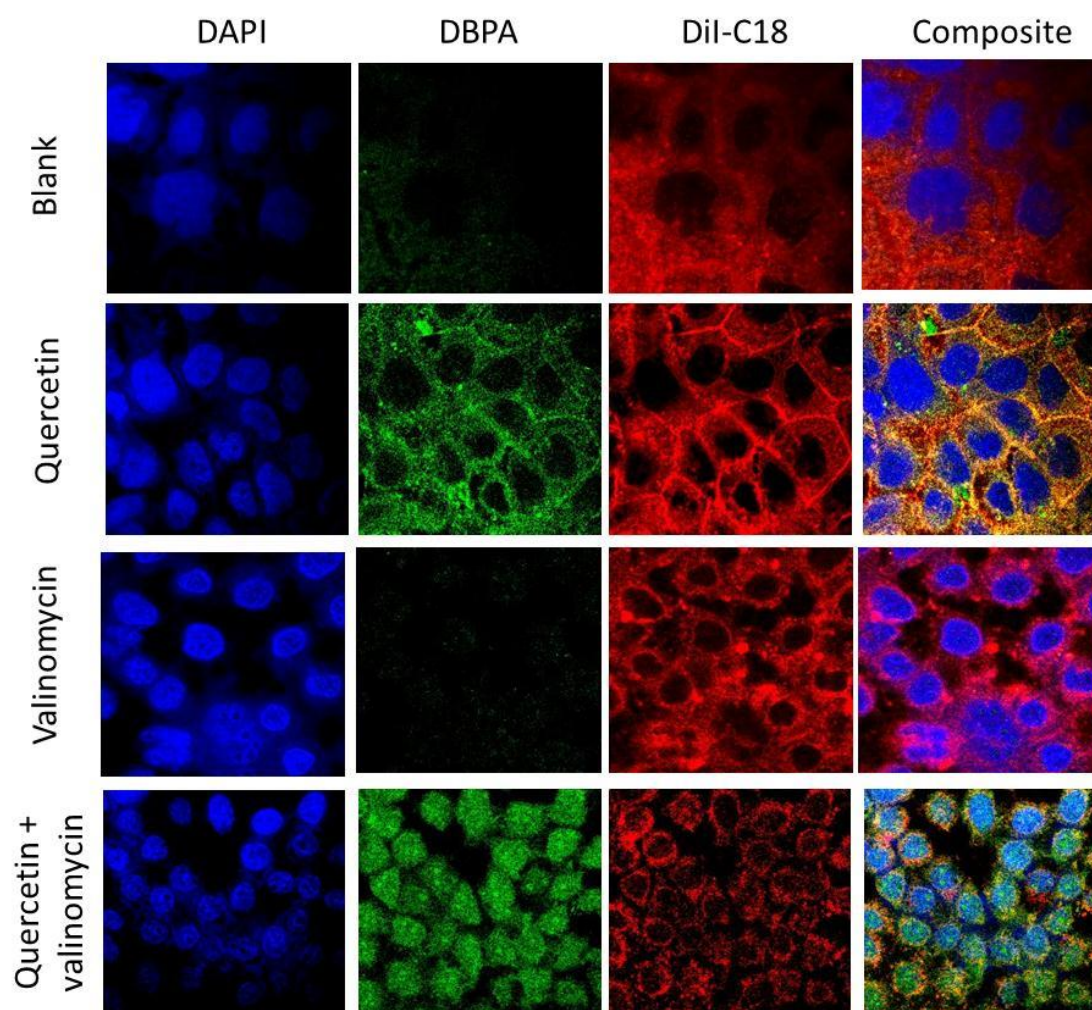


Figure 7.4. Intracellular localization of retained flavonoids (quercetin and quercetin-methyl ether)

The mechanism behind this selective accumulation of *O*-methyl-quercetin as caused by toxic components has not been previously described in literature. COMT is a phase II enzyme that is found in the intestine, liver, kidney and brain [354]. Most of the studies on flavonoids involve the use of differentiated cells and have reported the formation of mainly glucuro- and sulfo- conjugates. Yet, only a few reports are available on the COMT activity, especially in undifferentiated Caco-2 cells. For instance, a product of COMT, 3-hydroxy-4-methoxyphenylethanol was detected after exposure of differentiated Caco-2 cells with 3,4-dihydroxyphenylethanol [355]. The methylation of hydroxycinnamic acids has also been earlier reported, suggesting the activity of COMT in differentiated Caco-2 cells [356]. It is however unclear whether COMT activity towards phenolics is different in undifferentiated versus differentiated Caco-2 cells. This therefore merits further investigation.

Another hypothesis for the flavonoid accumulation is the inhibition of the ABC transporter P-glycoprotein (PgP). Valinomycin is a known inhibitor of PgP [357], which is responsible for the efflux of flavonoid conjugates and other anti-cancer drugs from cancerous cell lines. Further, a structure-activity relationship analysis of PgP with their substrates suggest that methylation of flavonoids increase their affinity towards PgP [290]. Thus, inhibition of PgP effectively prevents the efflux of methyl-quercetin. However, this mechanism does not explain the change in the location of methyl-quercetin from the cell membrane to intracellular. Therefore, an additional mechanism must be present. Also, a study on Caco-2 cells indicated that MRP2, another member of the ABC transporter family, is more important in the efflux of quercetin than PgP [97] and is not inhibited by valinomycin.

It has been earlier reported that valinomycin-induced changes in membrane potential affect the transport of certain compounds. The intracellular transport of 3-O-methylglucose was increased 10-fold upon treatment with valinomycin [358] while cellular accumulation of ^{18}F -FDG was enhanced in valinomycin treated MCF-7 cells due to the changes in membrane potential [359]. The effect of membrane potential on the transport of flavonoids has not yet been reported in literature. Although, it has been reported that membrane transporters such as the organic anion-transporting polypeptide (OATP) is highly affected by both pH and membrane potential [360]. OATPs are expressed on Caco-2 cells and have been implicated in the transport of quercetin under a pH gradient [97]. Thus, it is highly possible that the change in membrane potential caused by valinomycin positively influenced the transport of quercetin and methyl-quercetin intracellularly. The MTT and ROS results indicated that co-administration of valinomycin and quercetin improved mitochondrial function via the reduction of reactive oxygen species that are normally produced in the mitochondria. This ability to penetrate intracellularly under stressful conditions therefore has major implications to flavonoid bioactivity and indicates a potential cellular stress response mechanism in undifferentiated Caco-2 cells.

7.5. Conclusions

In this study, the effect of cellular stress caused by valinomycin, a model for the toxin cereulide, on quercetin metabolism and cellular localization was investigated. Quercetin was metabolized into methyl, glucuronide and sulfate conjugates, and their combination. Most of the metabolites were effluxed out of the cell while quercetin aglycone and a methyl-quercetin derivative were accumulated intracellularly. Further, 3 methylated derivative isomers were detected, wherein 2 of the isomers were effluxed out of the cells

and only 1 isomer was accumulated. This is the first report showing such regio-specificity in undifferentiated cells. Valinomycin induced a significantly higher accumulation of methyl-quercetin while the content of quercetin aglycone was not significantly changed. In untreated cells, quercetin and methyl-quercetin were localized at the cell membrane. The addition of valinomycin caused the increased accumulation of methyl-quercetin and its penetration inside the cell. This penetration occurred in conjunction with a reduction of valinomycin-induced ROS production and a recovery of MTT response, compared to cells treated only with valinomycin. This is the first report on the change in localization and cellular uptake and metabolism of quercetin in undifferentiated cells caused by valinomycin, which indicates a potential cellular stress response mechanism in undifferentiated Caco-2 cells.

Chapter 8

Collision cross section prediction of deprotonated phenolics
in a travelling-wave ion mobility spectrometer using
molecular descriptors and chemometrics

Chapter 8. Collision cross section prediction of deprotonated phenolics in a travelling-wave ion mobility spectrometer using molecular descriptors and chemometrics

8.1. Abstract

The combination of ion mobility and mass spectrometry (MS) affords significant improvements over conventional MS/MS, especially in the characterization of isomeric metabolites due to the differences in their collision cross sections (CCS). Experimentally obtained CCS values are typically matched with theoretical CCS values from Trajectory Method (TM) and/or Projection Approximation (PA) calculations. In this paper, predictive models for CCS of deprotonated phenolics were developed using molecular descriptors and chemometric tools, stepwise multiple linear regression (SMLR), principal components regression (PCR), and partial least squares regression (PLS). A total of 102 molecular descriptors were generated and reduced to 28 after employing a feature selection tool, composed of mass, topological descriptors, Jurs descriptors and shadow indices. Therefore, the generated models considered the effects of mass, 3D conformation and partial charge distribution on CCS, which are the main parameters for TM and PA calculations. All three techniques yielded highly predictive models for both the training ($R^2_{\text{SMLR}}=0.9911$; $R^2_{\text{PCR}}=0.9917$; $R^2_{\text{PLS}}=0.9918$) and validation datasets ($R^2_{\text{SMLR}}=0.9489$; $R^2_{\text{PCR}}=0.9761$; $R^2_{\text{PLS}}=0.9760$). Also, the high cross validated R^2 values indicate that the generated models are robust and highly predictive ($Q^2_{\text{SMLR}}=0.9859$; $Q^2_{\text{PCR}}=0.9748$; $Q^2_{\text{PLS}}=0.9760$). The predictions were also very comparable to the results from TM calculations using modified mobcal (N_2). Most importantly, this method offered a rapid (<10 minutes) alternative to TM calculations without compromising predictive ability. These methods could therefore be used in routine analysis and could be easily integrated to metabolite identification platforms.

Keywords: ion mobility, mass spectrometry, phenolics, collision cross section prediction, chemometrics, flavonoids

Redrafted from:

Gonzales GB, Smagghe G, Coelus S, Adriaenssens D, De Winter K, Desmet T, Raes K, Van Camp J. 2016. Collision cross section prediction of deprotonated phenolics in a travelling-wave ion mobility spectrometer using molecular descriptors and chemometrics. *Analytica Chimica Acta*. *In press*.

8.2. Introduction

The increased use of high resolution mass spectrometry (HRMS) in bioanalysis has prompted the need for better metabolite identification tools. For instance, the success of metabolomics, an increasingly popular and useful analytical technique to understand biological systems, relies on the confident identification of metabolites in a high-throughput scale [361]. However, although HRMS can provide elemental composition and many structural clues, it is generally not definitive, and rarely distinguishes isomeric compounds that produce identical MS/MS spectra, such as substituted metabolites [362]. Recently, the integration of ion mobility spectrometry (IMS) to mass spectrometry offered an increased capability to characterize biological mixtures both in terms of metabolite identification [361,363] and increase in peak capacity [364]. In Chapter 2, we showed the ability of IMS to resolve metabolites that co-elute during liquid chromatographic separation, thus offering a rapid characterization tool for complex matrices.

IMS has the ability to rapidly separate (microseconds to milliseconds) ions based on their mobilities in a gas-filled chamber under the influence of a weak electric field [365]. This separation is based on their size and shape (collision cross section, CCS, Ω), as well as their ionic interaction with the buffer gas, typically nitrogen or helium caused by their charge state (z) [363,365]. This technique therefore provides crucial structural and ionic information, which is essential especially in characterizing isomeric compounds [363]. For this purpose, IMS has been used in various bioanalytical research domains such as lipidomics [366,367], proteomics [368], metabolomics [361,369], analysis of large protein complexes [370] and metabolic transformations of drugs [362,371]. However, the main challenge lies on the interpretation of the data and deciphering structural information from the obtained CCS values.

In order to infer structural and conformational information from the obtained CCS values, the gold standard for IMS data interpretation is the satisfactory correlation between the measured and the theoretical CCS values calculated using computational chemistry techniques that model the interaction of the ion with the buffer gas [363,372]. The most widely used CCS prediction methods include trajectory method (TM) [373,374], the exact hard sphere scattering (EHSS) [375] and the projection approximation (PA)[373,374] calculated using the mobcal software developed by the Jarrold Group of the University of Indiana. For a comprehensive discussion of these techniques, readers are directed to the publication of [372]. TM is generally accepted as the most reliable prediction method [376]. However, the original mobcal was parametrized to predict CCS values obtained

using helium as buffer gas. A modification was later introduced to parametrize CCS calculations using nitrogen as buffer gas, which is more commonly used in commercial instrumentations [363,377].

Although a widely used and reliable method, TM calculations are highly computationally expensive [376] and hence not applicable to larger molecules, bigger sets of molecules and routine laboratory analysis. This also prevents the easy integration of CCS calculation in metabolite identification platforms especially in the absence of high-powered computational facilities. To circumvent this problem, researchers turned to chemometrics to develop accurate yet computationally efficient methods to predict CCS values. Compared to atomistic models derived from mobcal, chemometric analysis requires a database of experimentally-derived CCS values from where a predictive model is developed using molecular descriptors (such as in quantitative-structure property relationship studies). This approach has been successfully employed for the prediction of the CCS of peptides in positive mode ionization commonly using amino acid parameters and sequence information [378-381]. The success of using these descriptors owes to the fact that peptides are composed of a limited number of known and repeating units of amino acids.

However, small molecules such as non-peptide metabolites do not have a certain predictable sequence. Also, most of the chemometric predictive models in literature use positive ionization and relatively few CCS measurements have been done for negatively charged ions [382]. This is unfortunate especially because many small metabolites such as phenolics ionize better in negative ionization mode. Chemometrics-based prediction models for small molecules are thus lacking in the current literature. Therefore, identification of these metabolites remains an analytical challenge due to their wide chemical and structural diversity. Developing a CCS prediction method for negatively charged small molecules could therefore increase the capacity of IMS for confident metabolite identification.

Thus, in this study, we explored the use of chemometrics tools, stepwise multiple linear regression (SMLR), principal components analysis regression (PCR), and partial least squares regression (PLS) in predicting the CCS of 56 deprotonated phenolics using molecular descriptors. Initially, the CCS values of these compounds were measured in a travelling-wave ion mobility instrument, and the measured CCS values were correlated with their predicted CCS values. Also, the predictive performance of these models was compared to the conventional TM prediction using the modified mobcal (N_2).

8.3. Materials and Methods

8.3.1. Chemical reagents

Poly DL-alanine (P9003) and most of the small molecule standards used in this paper were purchased from Sigma-Aldrich. Many of the glycosylated derivatives were synthesized at the Center for Industrial Biotechnology and Biocatalysis of the Ghent University (Ghent, Belgium) according to the method described in [383]. The poly DL-alanine (10 μ M) and all the standards were prepared in acetonitrile/water/formic acid (50/50/0.1) and filtered through a 0.4 μ m syringe filter prior to analysis.

8.3.2. Collision cross section (CCS) measurement in TWIMS

All analytical analyses were performed using a Waters Synapt HDMS instrument (Waters Corp., Milford, MA, USA). Mass calibration of the mass spectrometer was achieved using sodium formate adducts and was assessed by analyzing the mass of leucine-enkephalin ($m/z=554.2615$). All working standards and the polyalanine calibrant were infused directly to electrospray ionization at a flow rate of 5 μ L/min using a 250 μ L glass syringe. Data were acquired in negative mode since the test compounds have been found to ionize better than in positive mode. For the source parameters, the following settings were applied: capillary voltage, -2.5kV; sampling cone, 40V; extraction cone, 4V; source temperature, 150 $^{\circ}$ C; desolvation temperature, 350 $^{\circ}$ C; cone gas flow, 50 L/h; desolvation gas flow, 550 L/h. Trap and transfer collision energies were set at 6V and 3V, respectively. Generic travelling-wave ion mobility spectrometry (TWIMS) conditions were applied to all the compounds analyzed. Optimal separation of the polyalanine ions was achieved using 20V wave height travelling at 850 m/s. IMS gas flow was at 30 mL/min at pressure $p=0.535$ mbar of nitrogen. Data acquisition and processing were carried out using MassLynx 4.1 and Driftscope 2.1 software (Waters).

Unlike in drift-tube ion mobility instruments, the IM separation in a TWIMS instrument varies with instrumental conditions (i.e., wave height and velocity) and the measured drift time values (dt) are no longer linearly related to CCS. Thus, for CCS measurements using TWIMS, a calibration approach is used [215]. The extracted dt was corrected (dt') and correlated with the corrected CCS (Ω_c) values of deprotonated polyalanine standards [365], using the data treatment explained in Ruotolo et al. [370] and Michaelevski et al. [215]. The calibration was deemed successful when the correlation coefficient is above $R^2=0.98$.

8.3.3. Collision cross section prediction

Discovery Studio (DS) version 2.5 (Accelrys, San Diego, CA, USA) was used to generate the 3D structures of the molecules obtained from Pubchem (<http://pubchem.ncbi.nlm.nih.gov/>). Structures were optimized/minimized using the *Smart Minimizer* algorithm in DS using 2000 minimizing steps with a 0.1 minimizing RMS gradient using the CHARMM forcefield. Owing to the low number of rotatable bonds and the relatively rigid structure of the test molecules, they are expected to have a relatively small distribution of conformational complexity and thus the global minimum is most likely achievable [384]. A negative charge (-1) was placed by removing a hydrogen from the all titratable regions of the structure followed by structure re-minimization. All possible deprotonation sites were considered and the most energetically stable deprotonated structure was then used for CCS prediction. Partial charges for all atoms were calculated using the Gasteiger-Marsilli method in DS. Predicted CCS values were obtained using modified mobcal algorithm in trajectory mode (TM) which simulates the conditions when using nitrogen as buffer gas [363]. Modified mobcal (N₂) calculations were implemented using a 2x8-core Intel E5-2670 (Sandy Bridge @ 2.6 GHz) processor. Processing was accomplished using a single core of this processor.

For the chemometric approach, molecular descriptors were calculated using the "Calculate Molecular Properties" function in DS from the minimized structures. A total of 102 molecular descriptors composed of 2D and 3D descriptors was generated for each compound. A set of 56 standard molecules was split into training (n=40) and validation (n=16) sets. Model generation was based on the training set data, which was then used to predict the validation set data for increased model confidence. Three different kinds of linear modeling approached were explored and compared in terms of their ability to predict CCS, namely: stepwise multiple linear regression (SMLR), principal components regression (PCR), and partial least squares regression (PLS). The open-source statistical software R was used to generate the models using the packages *MLRMPA*, *MASS*, and *pls*, respectively [312,313,385]. Cross-validation was achieved using leave-one-out (LOO) approach. Natural logarithm transformation was applied to the CCS values (dependent variable). For the SMLR model, normalization was applied to the features (independent variables) using the equation below:

$$\text{Eq1: } z(i) = \frac{x(i) - \bar{x}(x)}{s(x)};$$

where $z(i)$ is the normalized data for a particular parameter x of a particular molecule (i), $\bar{x}(x)$ and $s(x)$ are the means and standard deviation of parameter x of the training set.

The $x(x)$ and $s(x)$ of the training set were therefore used to normalize the test set. Feature selection was performed using the automated feature selection software *fscaret* in R [386]. The models were judged based on their root mean squared error of prediction (RMSEP), observed versus predicted R^2 and Q^2 , as well as their residuals (preference given to model that predicts most CCS values with <5% error) for training and validation sets. The chemometric models were developed and analyzed using an Intel® Core™ i5-3320M CPU @ 2.60 GHz processor.

8.4. Results and Discussion

8.4.1. Measurement of the CCS in negative mode

The CCS values for 56 small molecules (mostly phenolics) were measured for the first time using travelling-wave ion mobility spectrometry within a Synapt HDMS system. To validate the reliability of this method, calibration of the CCS values was derived using polyalanine standards. As shown in Figure 8.1, the correlation coefficient (R^2) between the corrected drift time ($\ln(dt')$) and the corrected CCS ($\ln(\Omega_c)$) was 0.9996, which indicates that the method employed is able to measure the CCS values of other molecules with sufficient reliability. The fit yielded a linear function corresponding to: $\ln(\Omega_c) = X \ln(dt') + A$, where X is the exponential factor and A is the fit-determined constant used to calculate the CCS of the test compounds.

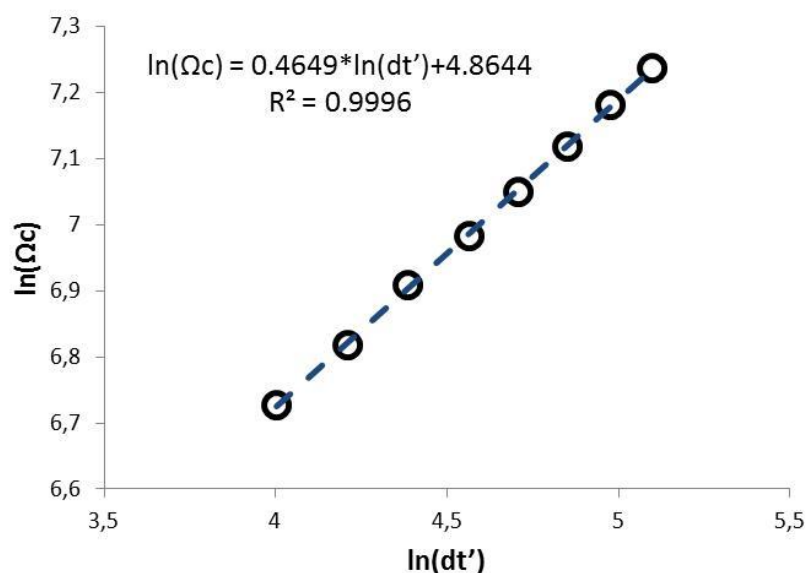


Figure 8.1. Calibration of the TWIMS using poly-DL-alanine standards. Corrected CCS (Ω_c) and drift time values (dt') were calculated using the method described by Michaelevski et al. [215]. Drift time was expressed as bins.

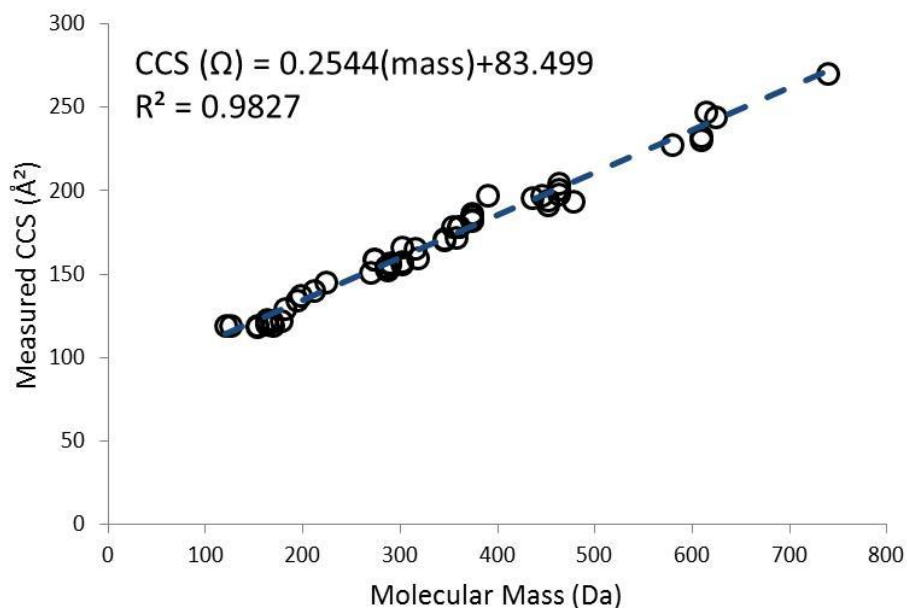


Figure 8.2. Correlation between molecular mass and CCS values (n=56)

This calibration function was then used to successfully measure the CCS values of 56 small phenolics in negative mode. The CCS values of the molecules were found to strongly correlate with their respective molecular masses ($R^2 = 0.9827$, Figure 8.2). As earlier explained, the ion mobility of molecules strongly depends on their collision with the drift gas. Naturally, bigger molecules would experience greater collision and thus would arrive at the detector slower than smaller molecules. This explains the high correlation between the mass and the CCS of the molecules. The same observation was found in an earlier study wherein the mass and number of atoms of 113 peptides correlated very well with their CCS values ($R^2=0.965$ and $R^2=0.987$, respectively) [378]. However, although this correlation is very high, relying on mass alone to predict CCS is insufficient as many molecules have the same mass but a different 3D structure, thus having different CCS values as shown in Figure 8.3.

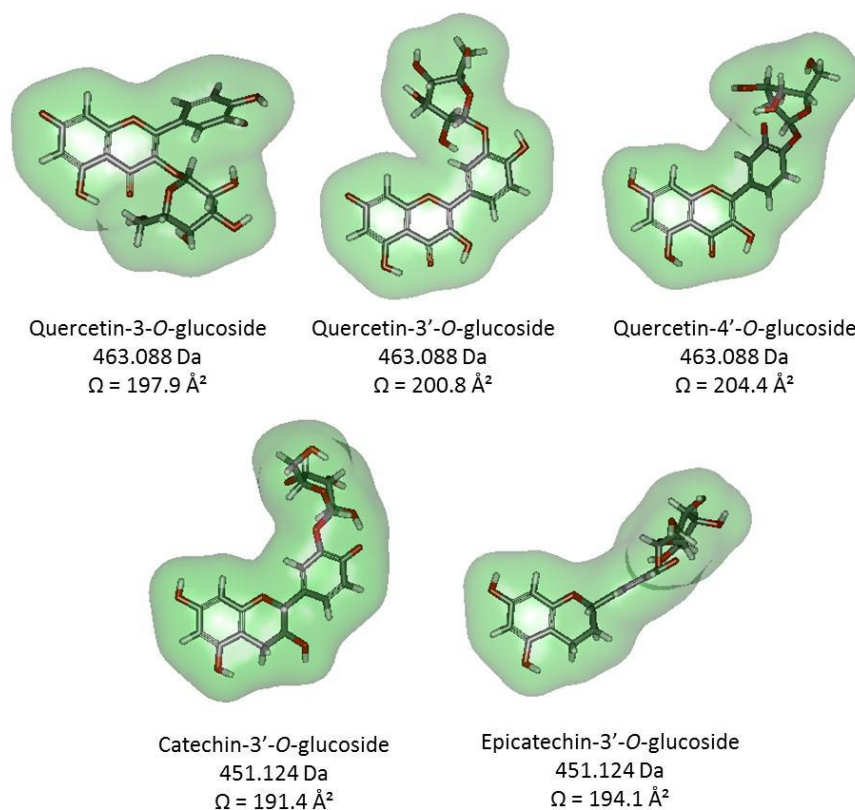


Figure 8.3. Structures and CCS values of some flavonoid isomers. Soft surface is added (green) to emphasize the overall shape of the molecule. Structure optimization and energy minimization was performed using Discovery Studio v2.5 using the *Smart Minimizer* algorithm using CHARMM forcefield.

Shown on the top row of Figure 8.3 top row are 3 different quercetin glucoside regioisomers which differ in their glucosylation sites. Since only the attachment differs, these 3 molecules have exactly the same mass and MS/MS fragmentation patterns and are therefore difficult to distinguish without comparing their LC retention times to isolated standards. As clearly shown using a soft surface, quercetin-3-*O*-glucoside has a more compact structure compared to the other two molecules. On the other hand, quercetin-4'-*O*-glucoside seems to have a more elongated structure. As molecules continually rotate in the drift tube during TWIMS separation, this elongation creates a bigger surface area available for interaction with the drift gas, hence having a longer drift time. Catechin and epicatechin, on the other hand, are stereoisomers and only differ in their 3D conformation even though the attachments of the glucosyl moiety are exactly at the same position. However, the CCS of epicatechin-3'-*O*-glucoside was found to be bigger than that of catechin-3'-*O*-glucoside by 3 \AA^2 . These results indeed show the power of ion mobility in separating and distinguishing regio- and stereo-isomers, which could therefore provide an additional tool for identification of small molecules, such as phenolics.

8.4.2. Molecular descriptors and *fscaret* feature selection

A total of 102 molecular descriptors were generated, which comprised of 2D and 3D descriptor sets. The feature selection procedure resulted in a significant reduction in the number of input variables to 28, as defined in Table 8.1. All of these selected descriptors were then used for the generation of predictive models. Variable contribution was assessed in each of the individual models, as later described

Table 8.1. Selected features used for model generation

Descriptor	Descriptor Category	Description	Reference	
Mol_Fractional PolarSurfArea	Surface Area and Volume Descriptor	The ratio of the polar surface area divided by the total surface area	[387]	
BIC	Topological Descriptor	Bonding Information Content	[388]	
CIC		Complementary Information Content		
IAC_Mean		Mean Information of Atomic Composition		
IC	Dipole Descriptor	Information Content		
JY		Balaban Index	[389]	
Kappa_3		Shape index of order three	[390]	
Dipole_mag		Strength and orientation	[391]	
Dipole_X		behavior of a molecule in an electrostatic field; and estimated using the partial atomic charges and atomic coordinates.		
Dipole_Y				
Dipole_Z				
Jurs_FNSA_3			Fractional charged partial surface area	[392]
Jurs_FPSA_1		Jurs Descriptor	Atomic charge weighted negative surface area	
Jurs_FPSA_3				
Jurs_PNSA_3				
Jurs_RASA	Relative hydrophobic surface area			
Jurs_RNCG	Relative negative charge; Charge of most negative atom divided by the total negative charge			
Jurs_RNCS	Relative negative charge surface area; Solvent-accessible surface area of most negative atom divided by Jurs_RNCG			
Jurs_RPCG	Relative positive charge; Charge of most positive atom divided by the total positive charge			
Jurs_RPCS	Relative positive charge surface area; Solvent-accessible surface area of the most positive atom divided by Jurs_RPCG			
Jurs_TASA	Total hydrophobic surface area. Sum of solvent-accessible surface areas of atoms with absolute value of partial charges			

Shadow_nu	Shadow Indices	less than 0.2 Ratio of largest to smallest shadow dimension	[393]
Shadow_Xlength		Length of molecule in the X dimension	
Shadow_Xyfrac		Area of the molecular shadow in the x	
Shadow_Xzfrac		Area of the molecular shadow in the xz plane	
Shadow_Ylength		Length of molecule in the y dimension	
Shadow_Yzfrac		Area of the molecular shadow in the yz plane	
Shadow_Zlength		Length of molecule in the z dimension	

8.4.3. Collision cross section prediction using chemometric tools

As shown previously, a high correlation exists between CCS and its corresponding deprotonated exact mass. Therefore, the exact mass of the molecule was added to the molecule along with the selected features shown above. Four different models were generated to predict CCS, namely: stepwise multiple linear regression (SMLR), principal components regression (PCR), and partial least squares regression (PLS). Table 8.2 shows the measured CCS values of both training and validation sets as well as the predictions obtained from the 3 chemometric models.

Table 8.2. CCS of 56 deprotonated phenolics used in this study

Test compounds*	Measured CCS (\AA^2)	SMLR Pred	%error	PCR pred	%error	PLS Pred	%error
Training set							
Apigenin	151.0	145.9	3.4	150.1	0.5	150.1	0.6
Benzoic acid	119.4	118.6	0.6	115.7	3.1	115.5	3.3
Catechin-3'-O-glucoside*	191.5	190.6	0.5	191.8	-0.2	191.7	-0.1
Catechin	156.5	156.7	-0.1	155.6	0.6	155.6	0.6
chlorogenic acid	178.9	179.4	-0.3	174.4	2.5	174.5	2.5
Ethylgallate-3-O-glucoside*	178.8	176.1	1.5	177.6	0.7	177.7	0.6
Epicatechin-3'-O-cellubioside*	247.1	246.1	0.4	240.5	2.7	240.3	2.8
Epicatechin-3'-O-glucoside*	194.2	206.6	-6.4	195.8	-0.8	195.8	-0.8
Epicatechin	156.8	156.2	0.4	156.5	0.2	156.5	0.2
Esculetin	122.5	124.6	-1.7	123.9	-1.2	123.9	-1.1
Eugenol	123.1	123.2	-0.1	120.7	1.9	120.9	1.8
Ferulic acid	134.7	134.2	0.3	137.9	-2.4	137.8	-2.3
Ferulic acid-4-O-sulfate	158.8	157.7	0.7	161.5	-1.7	161.3	-1.6
Fisetin	154.7	155.2	-0.4	154.1	0.3	154.3	0.3
Hesperetin	166.1	163.1	1.8	163.7	1.5	163.7	1.4
Homovanillic acid	129.8	132.2	-1.8	131.0	-0.9	130.9	-0.9
Laurylgallate-3-O-glucoside*	182.8	181.3	0.8	183.8	-0.6	184.0	-0.7
Laurylgallate-4-O-glucoside *	186.6	183.0	1.9	182.7	2.1	182.6	2.1

Luteolin	154.0	150.3	2.4	153.7	0.2	153.7	0.2
Methylgallate-3- <i>O</i> -glucoside*	171.6	174.3	-1.6	171.5	0.1	171.5	0.1
Methylgallate-4- <i>O</i> -glucoside *	170.8	171.2	-0.2	171.1	-0.1	171.2	-0.2
Naringin	228.0	234.8	-3.0	231.6	-1.6	231.5	-1.5
o-coumaric acid	120.9	124.7	-3.2	125.0	-3.4	125.1	-3.5
Propylgallate-3- <i>O</i> -glucoside *	182.5	181.2	0.7	183.8	-0.7	184.0	-0.8
Phloretin	159.0	160.6	-1.0	153.2	3.6	153.2	3.6
Phloridzin	195.8	196.5	-0.3	199.1	-1.7	199.0	-1.6
Pinoresinol	172.0	173.2	-0.7	180.1	-4.7	179.8	-4.5
Propylgallate	140.5	139.1	1.0	139.3	0.8	139.3	0.9
Protocatechuic acid	118.6	118.7	-0.1	121.9	-2.8	121.8	-2.7
Pyrogallol-2- <i>O</i> -glucoside*	152.7	155.7	-1.9	153.2	-0.4	153.2	-0.3
Pyrogallol	119.1	116.6	2.1	114.3	4.1	114.3	4.1
Quercetin-3'- <i>O</i> -glucoside*	200.9	199.8	0.5	199.3	0.8	199.5	0.7
Quercetin-4'- <i>O</i> -glucoside*	204.4	199.3	2.5	201.2	1.6	201.2	1.6
Quercetin	156.0	161.2	-3.3	158.4	-1.5	158.5	-1.6
Resveratrol-3- <i>O</i> -glucoside*	197.7	189.8	4.0	192.5	2.6	192.6	2.6
Robinin	270.1	271.8	-0.6	275.0	-1.8	275.1	-1.8
Rutin	230.6	227.7	1.3	231.9	-0.5	231.6	-0.4
Sinapic acid	145.7	142.2	2.4	140.7	3.4	140.9	3.3
Vanillic acid	121.9	124.1	-1.8	126.8	-4.0	126.7	-3.9
3,4-dihydroxyphenyl acetic acid	122.6	124.6	-1.7	126.5	-3.2	126.6	-3.3
Validation set							
Baicalin	197.6	185.4	6.1	193.5	2.1	193.4	2.1
Cyanidin	153.1	154.3	-0.8	155.7	-1.7	155.4	-1.5
Ethylgallate-4- <i>O</i> -glucoside*	178.5	178.8	-0.2	178.0	0.3	177.8	0.4
Ellagic acid	157.9	161.0	-2.0	149.5	5.3	149.5	5.3
Gallic acid	119.4	126.9	-6.3	125.2	-4.9	125.1	-4.8
Gentisic acid	119.0	112.6	5.4	118.3	0.6	118.3	0.6
Hesperidin	233.1	246.1	-5.6	247.8	-6.3	248.2	-6.5
Hesperidin methyl chalcone	244.3	220.9	9.6	239.9	1.8	240.5	1.6
Isorhamnetin	166.0	159.8	3.7	162.4	2.1	162.4	2.2
Kaempferol	153.4	155.7	-1.5	154.3	-0.6	154.5	-0.7
Myricetin	159.8	167.5	-4.8	162.9	-2.0	163.0	-2.0
p-coumaric acid	119.8	123.1	-2.8	126.3	-5.4	126.4	-5.5
Propylgallate-4- <i>O</i> -glucoside *	184.9	182.9	1.1	182.7	1.2	182.6	1.2
Quercetin-3- <i>O</i> - glucuronide	193.7	188.1	2.9	194.1	-0.2	194.1	-0.2
Quercetin-3- <i>O</i> -glucoside	197.9	196.6	0.7	192.4	2.8	192.3	2.9
Syringic acid	137.3	132.5	3.5	129.6	5.6	129.8	5.5

*compounds synthesized by the Center for Industrial Biotechnology and Biocatalysis of the Ghent University (Ghent, Belgium) [383]. All others were purchased from Sigma-Aldrich

8.4.3.1. SMLR

A problem when using linear regression generally arises when the number of features greatly exceeds the number of observations. This results in over-fitting of the model, which yields a model with very high predictive power within the dataset but generally poor for external datasets [35]. Hence, in this study, feature selection was of prime importance since it allowed the selection of significant features and reduced its number to less than the number of observations (compounds) in the entire dataset. Data normalization was performed due to the large differences in the ranges of the values of the different features. In this way, the model is not biased towards the big numerical values of some of the features. A stepwise multiple linear regression (SMLR) technique was applied to the selected features to further remove non-contributing features from the linear model, which further reduced the number to 23. Lastly, the descriptors included in the final model were required to have a $|t|$ -value of >2 to ensure that all the descriptors significantly contributed relevant information at the 95% confidence level [378]. In the end, a linear model was generated to predict CCS composed of 8 descriptors (Eq. 2).

Eq. 2.

$$\begin{aligned} \ln(\text{CCS}) = & 5.10 \pm 0.003 - 0.015 \pm 0.005 (\text{BIC}) - 0.029 \pm 0.007 (\text{IAC}_{\text{Mean}}) + 0.028 \pm 0.006 (\text{Jur}_{\text{FPSA}_1}) \\ & - 0.103 \pm 0.013 (\text{Jur}_{\text{SPNSA}_3}) - 0.073 \pm 0.010 (\text{Jur}_{\text{RNCS}}) - 0.027 \\ & \pm 0.005 (\text{Shadow}_{\text{Xyfrac}}) - 0.060 \pm 0.009 (\text{Shadow}_{\text{Ylength}}) + 0.113 \pm 0.017 (\text{mass}) \\ (\rho < 2.26 \times 10^{-16}; & \text{F-statistic} = 451.8; \text{adjusted } R^2 = 0.9942; R^2_{\text{training}} = 0.9911; \\ & R^2_{\text{validation}} = 0.9489; Q^2 = 0.9859; \text{RMSEP} = 5.39; <5\% \text{error} = 90\%) \end{aligned}$$

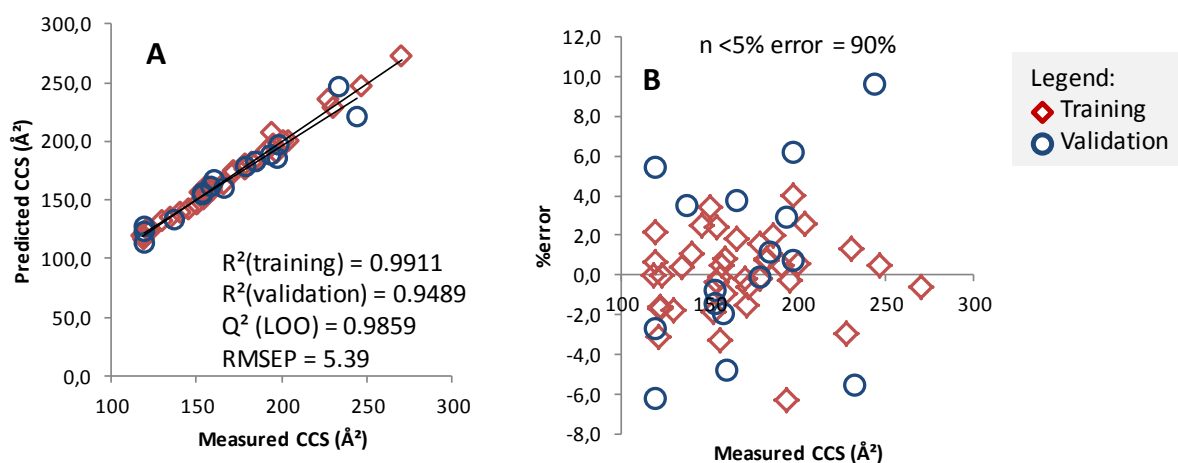


Figure 8.4. CCS prediction using stepwise multiple linear regression (SMLR)–(A) correlation between measured vs predicted CCS values; (B) residual plot expressed as %error from the measured CCS values

In the end, the SMLR model yielded high internal and external predictive ability ($R^2_{\text{training}}=0.9911$; $R^2_{\text{validation}}=0.9489$) (Figure 8.4). The high leave-one-out cross validation R^2 ($Q^2=0.9859$) further proved the robustness of the model. In total, 90% of all compounds (51/56) were predicted with <5% error. According to Equation 2, the highest contributing features were mass ($p=4.32\times 10^{-7}$) and $\text{Jurs}_{\text{PNSA3}}$ ($p=1.31\times 10^{-8}$). CCS and mass have already been shown to have a very good correlation, as earlier discussed. Thus, it not surprising that mass in this case contributed the most to the predictive ability of the SMLR model because linear regression favors features with the best linear fit (R^2 is already 0.9827 for CCS and mass alone, as earlier shown). $\text{Jurs}_{\text{PNSA3}}$ on the other hand is a 3D descriptor defined as the sum of the molecules' solvent accessible surface area multiplied by the partial charge of all negatively charged atoms [392]. Therefore, this descriptor is indicative of the total surface area and partial negative charge of the molecule. As explained, the drift time of a molecule is affected both by its collision and charge interactions with the buffer gas. Naturally, molecules having a bigger surface area have higher chances of colliding with the buffer gas, hence having a longer drift time. Therefore, the charged surface area of the molecule is directly proportional to its CCS. The negative sign ($-\text{Jurs}_{\text{PNSA3}}$) in equation 2 may appear as if the surface area is inversely proportional to CCS. However, since $\text{Jurs}_{\text{PNSA3}}$ is a product of the surface area and the charge, which is negative, the net result is a positive correlation between surface area and CCS as expected. Hence, this model reflects the positive correlation of both mass and charged collision surface area of the molecule to its CCS.

Also included in the model are topological descriptors, IAC_{Mean} and BIC, although contributed to a lesser extent. The use of topological descriptors together with amino acid parameters has previously been reported for the accurate prediction of peptide CCS in positive mode. In this study, the CCSs of 113 peptides were predicted using multiple linear regression and computational neural networks after an objective feature selection from a total of 199 descriptors [378].

8.4.3.2. PCR and PLS

PCR and (especially) PLS are commonly used in chemometrics since these techniques are insensitive to multi-collinearity issues that arise from using simple linear regression models [35]. As show in Figure 8.5, both the PCR and PLS models were equally able to predict the CCS values of the test compounds with high accuracy and robustness. During model generation, natural logarithm transformation was applied to the CCS values and the resulting RMSEP was 0.03 ($n_{\text{comp}} = 9$) for both models. Calculating the RMSEP based on the actual CCS values, a value of 4.16 was reached for both PCR and PLS within the CCS range of 118 – 270 Å². Both models have very high predictive power in the

training ($R^2_{\text{PCR}}=0.9917$; $R^2_{\text{PLS}}=0.9918$) and validation tests ($R^2_{\text{PCR}}=0.9761$; $R^2_{\text{PLS}}=0.9760$). The robustness of the models was proven by its high Q^2 values ($Q^2_{\text{PCR}}=0.9748$; $Q^2_{\text{PLS}}=0.9760$). Both models were also able to predict the CCS values of 93% (52/56) of the test compounds with <5% error. Based on the model regression coefficients (Figure 8.6), it was found that, unlike in the SMLR model, mass did not substantially contribute to the model and the most important variables are Shadow Indices ($\text{Shadow}_{\text{Xlength}}$, $\text{Shadow}_{\text{Ylength}}$, and $\text{Shadow}_{\text{Zlength}}$) and Jurs descriptors ($\text{Jurs}_{\text{RNCS}}$, $\text{Jurs}_{\text{RPCS}}$, $\text{Jurs}_{\text{PNSA3}}$), which are both 3D descriptors. This confirms that the 3D conformation of the molecule plays a pertinent role in their separation through the IMS.

Shadow indices are a set of descriptors that project the 3D structure of a molecule to a model surface with x , y , z planes. The descriptors are then derived from the "shadows" cast on the planes, such as the area of the shadow on each plane as well as the lengths of the shadows. These descriptors represent a good amount of molecular shape information, which can be used for quantitative structure-property relationships [393]. A rough visual representation of how shadow indices are derived is shown in Figure 8.7 for quercetin-4'-O-glucoside. Jurs descriptors, on the other hand, combine shape and electronic information by mapping atomic partial charges on solvent-accessible surface areas of individual atoms. $\text{Jurs}_{\text{RNCS}}$ is calculated by dividing the surface area of the most negative atom by its relative partial charge (partial charge divided by the total partial charge of all atoms). $\text{Jurs}_{\text{RPCS}}$ is the same but for the most positively charged atom [392].

Therefore like in the SMLR model, the generated PCR and PLS models reflected the actual 3D conformation as well as the charge distribution of the molecule as the main determinants of their collision cross section. Thus, these models operate in the same principle as the conventional prediction techniques, the trajectory mode (charge interactions) and projection approximation (shadow) calculation in mobcal [363,372].

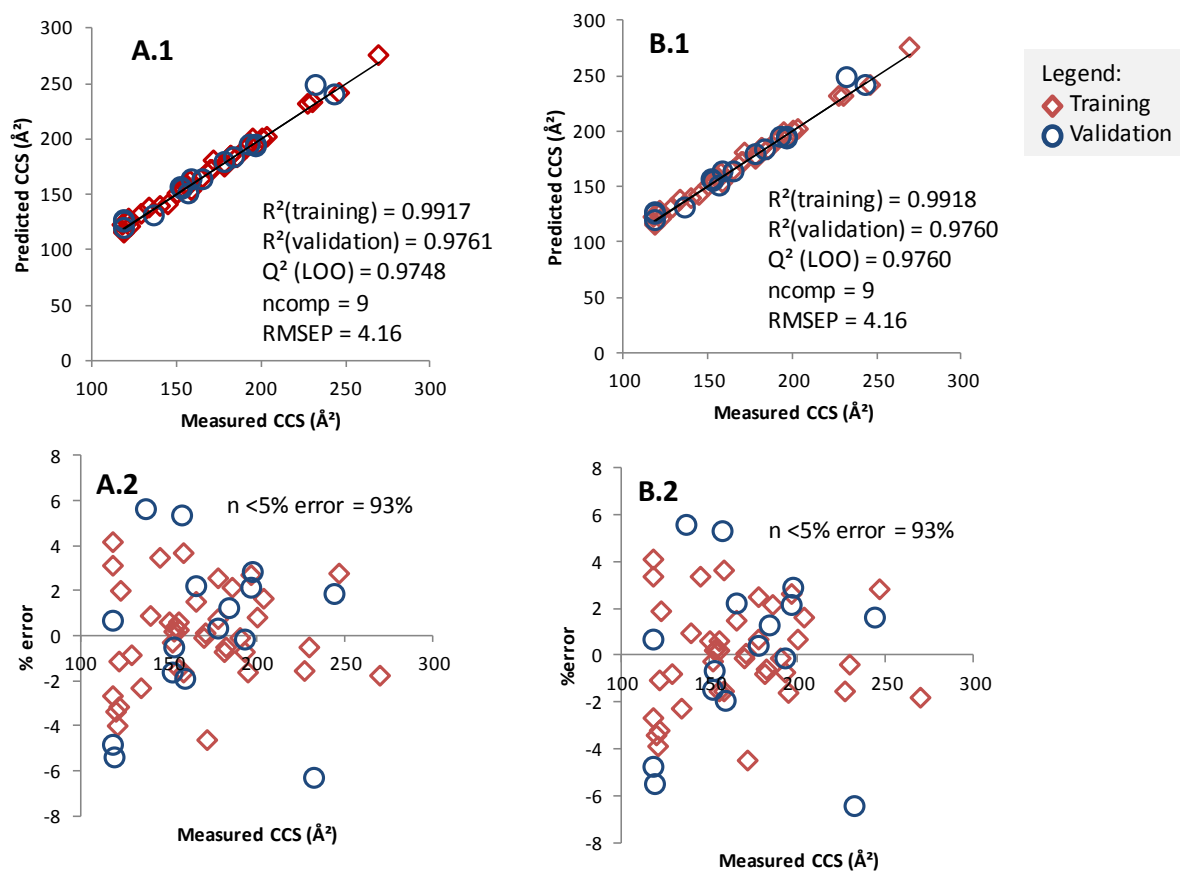


Figure 8.5. PCR (A) and PLS (B) models for CCS prediction – A.1 and B.1 represent the correlation between measured vs predicted CCS values; A.2 and B.2 show the residual plot expressed as %error from the measured CCS values

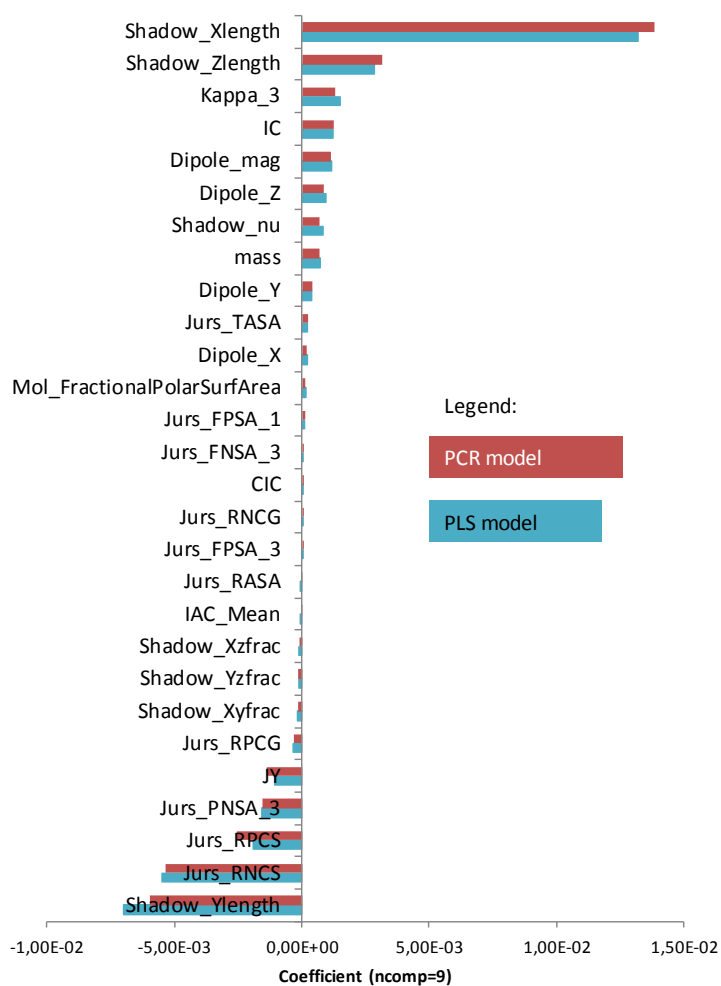


Figure 8.6. PCR and PLS regression coefficients using 9 principal components

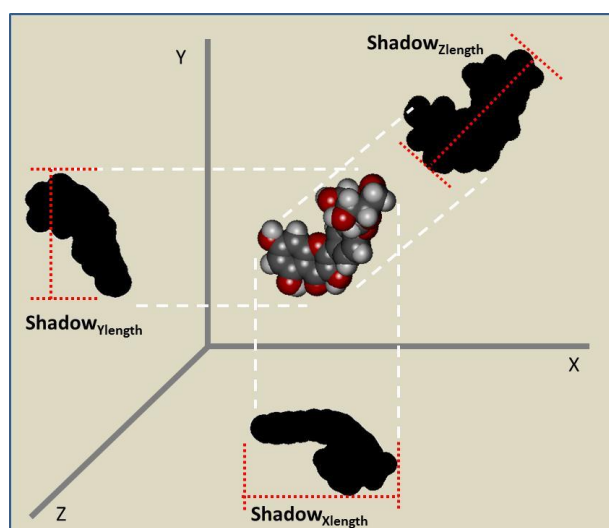


Figure 8.7. Visual representation of the Shadow index calculations for quercetin-4'-O-glucoside; for more detailed information, readers are referred to Rohrbaugh and Jurs [393].

8.4.4. Comparison of the different models with mobcal (N₂)

The most popular method to predict CCS is the method developed by the Martin Jarrold's group of Indiana University. Recently, a modification of their algorithm was proposed to simulate CCS calculations when using nitrogen as buffer gas [363]. However, although these methods have been widely implemented and proven to be highly predictive, the high computational cost of these techniques limit their applicability for routine analysis as well their easy integration into metabolite identification platforms/software. This is also in part because molecular dynamics simulation is used to prepare the molecules, which introduces many molecular conformations that need to be averaged. Therefore, the need for a more efficient technique is warranted.

In this study, we used the modified mobcal (N₂) to predict the CCS values of the molecules in the validation set in comparison with the models generated in this paper. The measured CCS values were highly correlated to the predicted CCS with a coefficient of $R^2=0.9179$ (Figure 8.8). The slope of the fit was ~ 1.12 , which is close to the reported expected slope (~ 1.15) obtained for molecules having a small number of rotatable bonds [384]. The average number of rotatable bonds for the entire dataset is 3.5 (median = 4). It has been previously hypothesized that mobcal (N₂) is sub-optimal and overestimates the calculated CCS for compounds with limited conformational flexibility [384], such as phenolics. To account for this bias, the predicted CCS values were corrected using the linear regression slope, referred as corrected modified mobcal (N₂).

As shown in Figure 8.8B, the predicted CCS values of all models correlated very well with the experimentally-derived CCS values. Also, the ability of the generated models to predict CCS yielded similar predictive ability as that of the modified mobcal (N₂) (Figure 8.8C). The average prediction %errors were 4.6%, 3.4%, 2.7% and 2.7% for modified mobcal (N₂), SMLR, PCR and PLS, respectively.

The main advantage of using the generated models is the fact that CCS prediction was completed in <10 minutes (using an office laptop) for all compounds, whereas CCS prediction using mobcal (N₂) took up to 15 hours (using a high performance computing facility) for some of the molecules. This efficiency makes the proposed method easier to integrate in metabolite identification platforms, without compromising predictive power. However, to use CCS as an additional identification tool following the techniques proposed in this paper, databases where chemometrics could be applied to needs to be built. Since these models learn from the data, it is imperative that the number of observations is large enough to ensure the validity and robustness of the generated model. This also means that the larger the database becomes the more reliable and

robust the generated model will be. Finally, larger databases permit the use of more advanced machine learning tools, which may provide even better predictive ability.

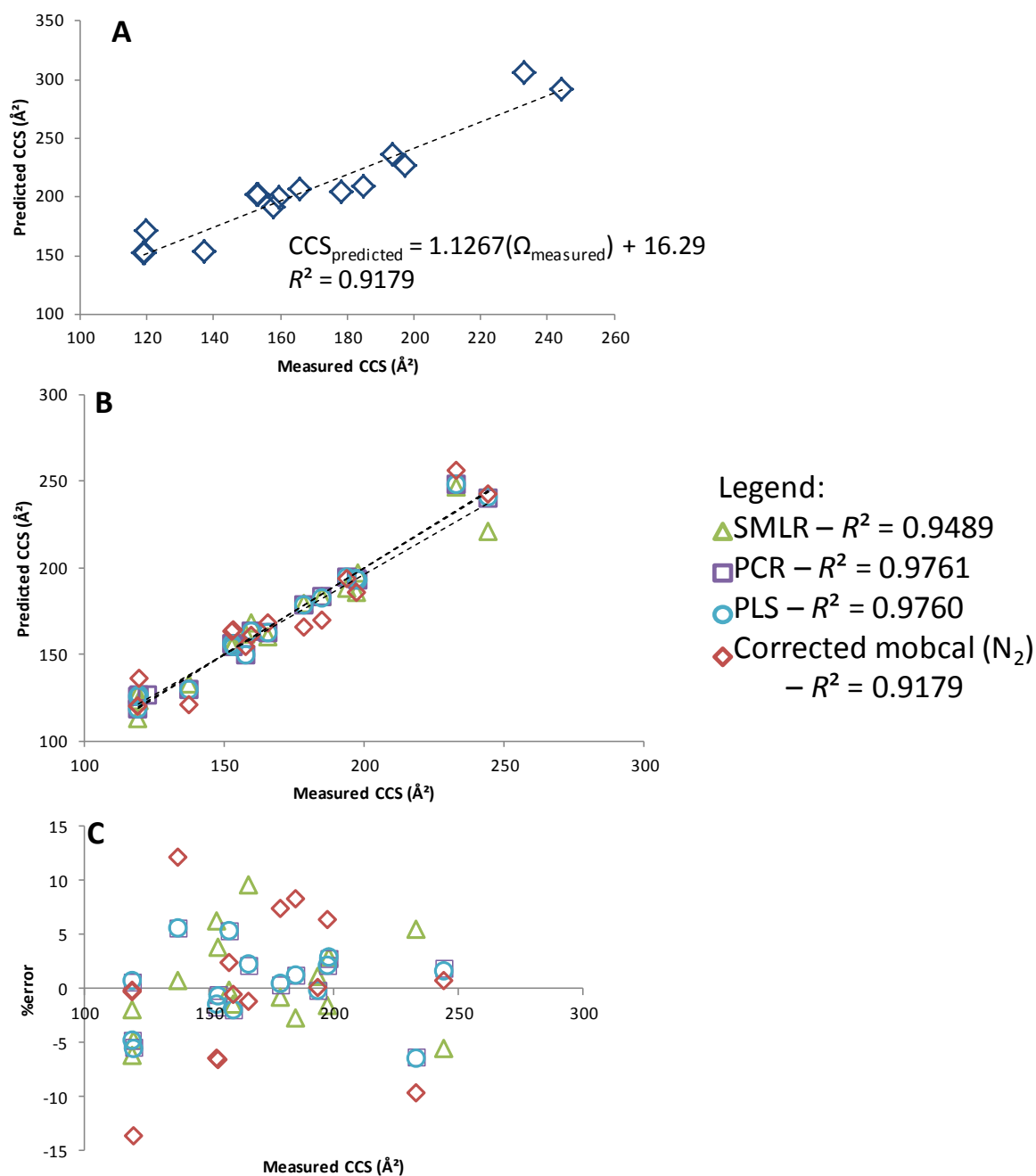


Figure 8.8. (A) correlation between prediction by modified mobcal (N_2) and measured CCS values; (B) CCS predictions using the corrected modified mobcal (N_2) and the generated models (SMLR, PCR and PLS); (C) prediction residual (%error)

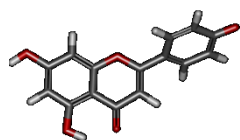
8.5. Conclusions

SMLR, PCR and PLS techniques were used to develop a prediction model for the collision cross sections of small deprotonated phenolics. All the 3 techniques yielded highly predictive models for both the training ($R^2_{\text{SMLR}}=0.9911$; $R^2_{\text{PCR}}=0.9917$; $R^2_{\text{PLS}}=0.9918$) and validation datasets ($R^2_{\text{SMLR}}=0.9489$; $R^2_{\text{PCR}}=0.9761$; $R^2_{\text{PLS}}=0.9760$). Also, the high cross validated R^2 values indicate that the generated models are robust and highly predictive ($Q^2_{\text{SMLR}}=0.9859$; $Q^2_{\text{PCR}}=0.9748$; $Q^2_{\text{PLS}}=0.9760$). Mass, Jurs descriptors and Shadow Indices were found to be the most important predictors for CCS. Most importantly, the computational cost for predicting CCS was much lower using these chemometric tools compared to using mobcal (N_2) without compromising predictive ability. Therefore, these methods could be used in routine analysis and could be easily integrated in metabolite identification platforms.

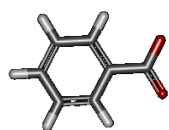
Chapter 8 Appendix

Final geometries of the studied compounds ($[M-H]^-$) after structure optimization

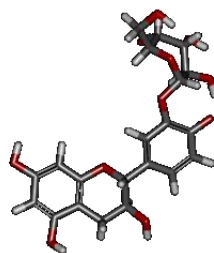
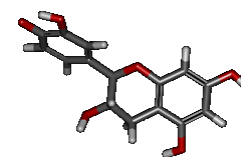
Training



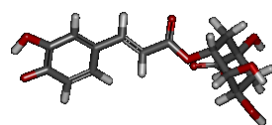
Apigenin



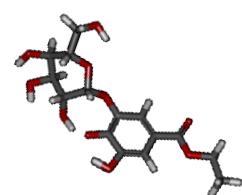
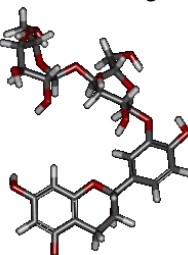
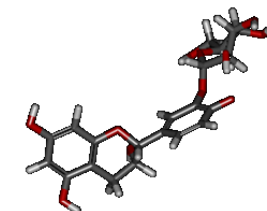
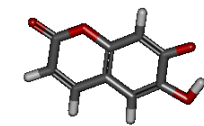
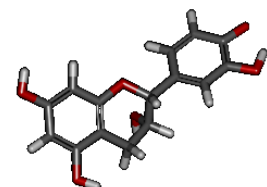
Benzoic acid

Catechin-3'-*O*-glucoside

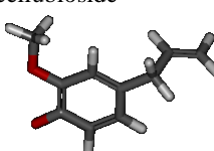
Catechin



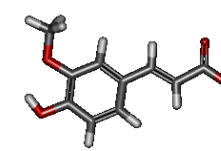
Chlorogenic acid

Ethylgallate-3-*O*-glucosideEpicatechin-3'-*O*-cellubiosideEpicatechin-3'-*O*-glucoside

Esculetin

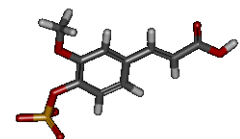
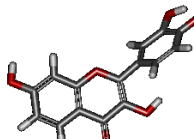


Eugenol

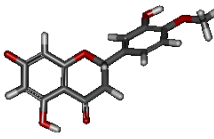


Ferulic acid

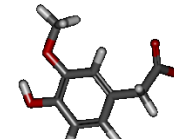
Epicatechin

Ferulic acid-4-*O*-sulfate

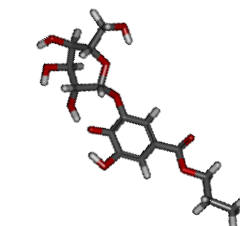
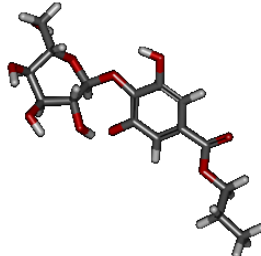
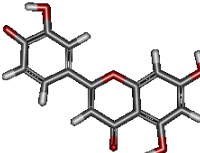
Fisetin



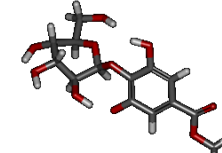
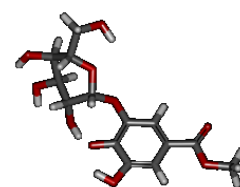
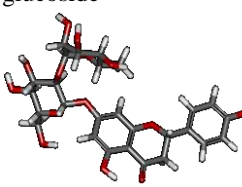
Hesperetin



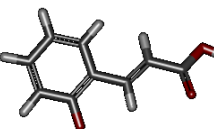
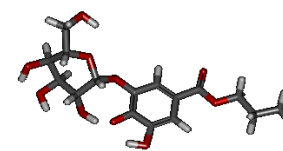
Homovanillic acid

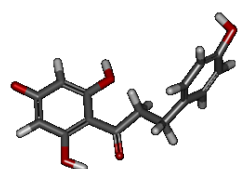
Laurylgallate-3-*O*-glucosideLaurylgallate-4-*O*-glucoside

Luteolin

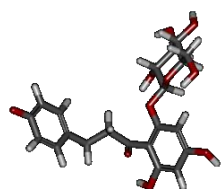
Methylgallate-3-*O*-glucosideMethylgallate-4-*O*-glucoside

Naringin

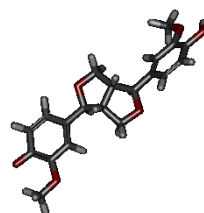
*o*-coumaric acidPropylgallate-3-*O*-glucoside



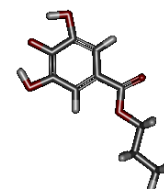
Phloretin



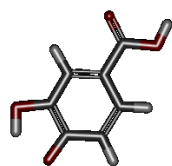
Phloridzin



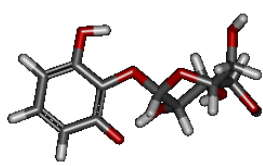
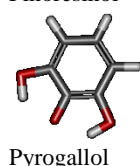
Pinoresinol



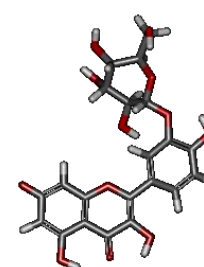
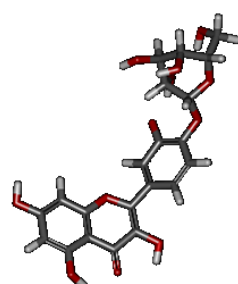
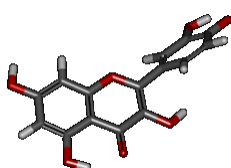
Propylgallate



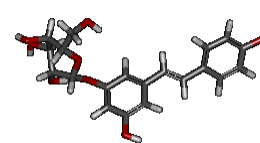
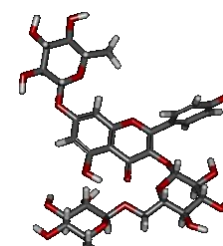
Protocatechuic acid

Pyrogallol-2-*O*-glucoside

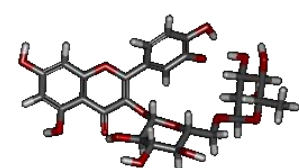
Pyrogallol

Quercetin-3'-*O*-glucosideQuercetin-4'-*O*-glucoside

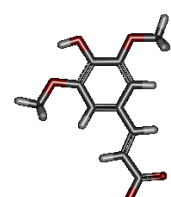
Quercetin

Resveratrol-3-*O*-glucoside

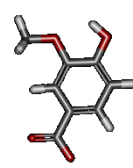
Robinin



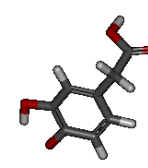
Rutin



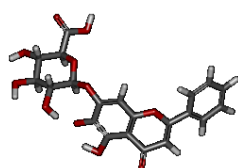
Sinapic acid



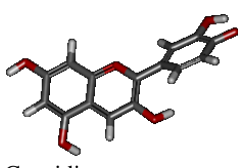
Vanillic acid



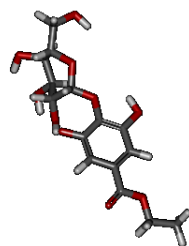
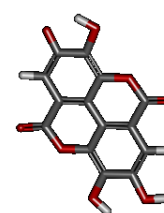
3,4-dihydroxyphenyl acetic acid

Validation

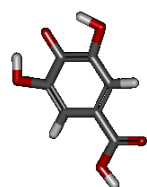
Baicalin



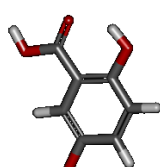
Cyanidin

Ethylgallate-4-*O*-glucoside

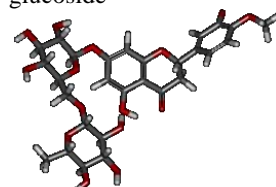
Ellagic acid



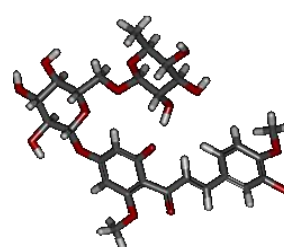
Gallic acid



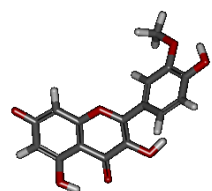
Gentisic acid



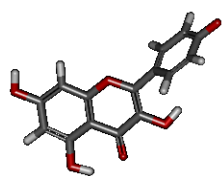
Hesperidin



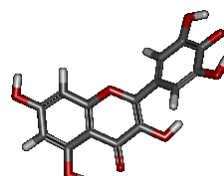
Hesperidin methylchalcone



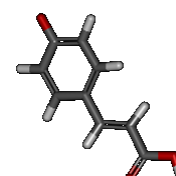
Isorhamnetin



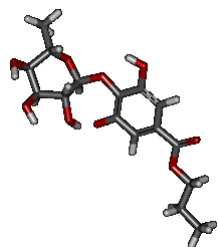
Kaempferol



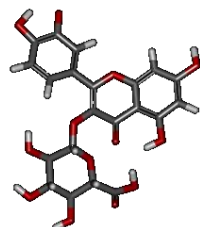
Myricetin



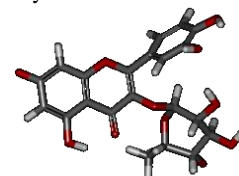
p-coumaric acid



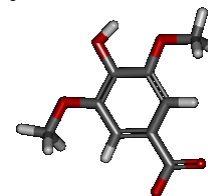
Propylgallate-4-*O*-glucoside



Quercetin-3-*O*-glucuronide



Quercetin-3-*O*-glucoside



Syringic acid

Chapter 9

General discussion, conclusions and future perspectives

Chapter 9: General discussion, conclusions and future perspectives

There has been a surge in the amount of publications on the bioactivity of plant metabolites in recent years. Due to our increased knowledge on the digestion and absorption processes and the increased efficiency and accuracy of available analytical techniques, we have come to better understand the fate of flavonoids and their potential modes of action. In fact, many of the previous publications reporting flavonoid bioactivity are now being considered invalid. Earlier, Williamson [394] questioned the use of aglycones in investigating the bioactivity of flavonoids in *in vitro* studies. For many years, and still persistent until now, many publications that reported bioactivity used aglycones in non-physiological concentrations. Williamson argued that since aglycones are actively metabolized into phase I and II metabolites and are transiently present at very low concentrations in the blood, careful consideration of the bioavailability and metabolic fate of flavonoids must be made before interpreting *in vitro* results. This commentary provided a strong argument on the necessity to carefully analyze the different stages of flavonoid absorption and metabolism prior to performing bioactivity studies.

Recently, the Journal of Agricultural and Food Chemistry released a set of guidelines on publishing papers concerning bioactivity of food components, including flavonoids [395]. In this set of guidelines, 5 focus points were listed as important features that need to be present in bioactivity studies:

- 1) Identification of bioactive molecules from agricultural and food products
- 2) Quantitation of the bioactive target
- 3) Demonstration of bioavailability
- 4) Identification and quantitation of metabolites generated upon ingestion
- 5) Mechanistic studies of the bioactivity

Indeed, these are extremely important to ensure the validity and usability of the results that arise from experiments using flavonoids. Hence in this PhD, careful consideration of the abovementioned points was made to ensure the validity, technical soundness and high quality of the work. Initially, the flavonoid composition of the plant material was characterized using high-resolution mass spectrometry techniques (points 1-2). Then, the bioavailability of the flavonoids was evaluated using a simulated gastro-intestinal digestion set-up combined with *in vitro* Caco-2 transport experiments (point 3-4). Lastly, the metabolism and bioactivity of the flavonoid and its metabolites were analyzed using mass spectrometry, flow cytometry and microscopy (point 4-5). It should however be

noted that this PhD focused on the use of mainly *in vitro* techniques, which may not fully represent the *in vivo* situation.

In this chapter, the general conclusions drawn from the different experimental chapters, as well as the current gaps in our knowledge will be presented. Further, possible routes for further studies will be recommended.

9.1. Structural characterization of flavonoids

Cauliflower waste has earlier been reported as a good source of bioactive flavonoids, especially kaempferol and quercetin, which are usually neglected. By initiating valorization activities for these waste materials, not only a new source of valuable bioactive molecules is found but also the generation of agro-industrial waste is diminished.

As mentioned above, the initial step in establishing the bioactive potential of molecules from agricultural sources is the characterization of the bioactive target. Thus, this PhD started by developing a mass spectrometric technique for the structural characterization of flavonoids from vegetable waste with cauliflower waste as a model matrix (Chapter 2). Conventionally, structural characterization is achieved by multi-stage mass spectrometry (MS^n), wherein time-consuming operator intervention is usually required. In this newly developed technique, 19 flavonoid glycosides were structurally characterized in a single chromatographic run without the need for manual identification of precursor molecules. This was achieved with the use of MS^E , a data-independent strategy that uses parallel alternating scans of low and high energy that simultaneously provides both precursor and product ion information. Our results showed that by using MS^E approach, pertinent precursor and product ions detected in conventional MS/MS experiments could be detected in a single chromatographic run. This method can therefore be used for routine assays of flavonoids from plant extracts and other matrices, especially when the demand for the equipment is high.

However, the use of MS^E technology as an alternative to MS/MS is still at its early phase and so far only 12 publications are recorded in the Web of Science database (using flavonoid and MS^E as keywords) from 2011. This could perhaps be due to the fact that MS^E technology is not available to all mass spectrometers, and that the amount of data collected is increased exponentially per chromatographic run. Also, since convolution is often inevitable in UPLC separations, especially from complex matrices such as plant extracts, correct annotation of the precursor to product ion information is difficult. To

address this, ion mobility separation (IMS) was employed to ensure that the product ions are correctly aligned with its corresponding precursor ions during fragmentation. Therefore, by combining MS^E and IMS technologies, a rapid and reliable flavonoid characterization tool was developed.

However, like conventional MS/MS approaches, the proposed method is also limited to characterizing 3-*O*, 7-*O* and 3,7-di-*O* glycosides. Glycosylation of the B ring also occurs, i.e. quercetin glycosides from onion [396], albeit not as common as in the A and C rings. Also, as mentioned in Chapter 2, other flavonoid glycosides with higher degrees of glycosylation could be detected. However, the exact structure could not be elucidated. The correct structural annotation of B ring-glycosylated and C-glycosylated flavonoids is a challenge that requires further investigation. Some alternative methods were described in Chapter 1, wherein post-column derivatization and MS^{n>3} are required. As explained, these methods require significant intervention, which limits its application in routine and rapid analyses. Also, post-column derivatization introduces salts into the source which requires frequent cleaning. Recently, IMS technique has proven to be an excellent technique to distinguish molecules based on their shape and size. The use of IMS could therefore provide additional information on the 3D structure, including the points of glycosylation of flavonoids.

9.2. Getting more out of agro-industrial by-products: there's more in waste than initially thought

According to the United Nations Food and Agriculture database (https://www.quandl.com/data/UFAO/CR_CAUL_BEL), Belgium produced a total of 94,000 tons of broccoli and cauliflower in 2007. Although no absolute data on the amount of by-products are produced by this industry, the sheer volume of their yield suggests that thousands of tons of agricultural products are left in the fields after harvest each year. If left in the field, the potential of these materials as a source of high valued materials will be underutilized. Extracting the high amounts of polyphenol in these materials could render such wastes as high value-added products.

Valorization of the flavonoids from the waste stream requires an efficient and high-yield extraction protocol. Conventionally, flavonoids from plant matrices are extracted using various solvents, most commonly water and methanol. In this thesis, we have shown that conventional extraction methods usually miss out large quantities of nonextractable polyphenols. Chapters 3 and 4 proved that the total phenolic content of *Brassica* waste streams are more than double compared to what was initially reported in literature. Further, by using chemometric analysis, it was found that some polyphenols are found

exclusively on either the extractable or nonextractable fractions. These findings suggest that valorization efforts for agro-industrial products have not really utilized the full potential of these materials to provide bioactive molecules. In fact, most of the polyphenolic content of these materials is still wasted if nonextractable phenolics are not recovered. In this thesis, we showed the potential of alkaline hydrolysis in combination with ultrasound-assisted extraction in releasing the nonextractable phenolic content of *Brassica* waste streams. However, a more environment-friendly approach must be sought to enable a large-scale application of this method. The use of large amounts of sodium hydroxide could pose harm to the analyst and to the environment. Also, the use of methanol in large-scale applications should be avoided since methanol is highly toxic to humans. Any amount of methanol in the extracts would render it unfit for human application. Thus, other methods such as fermentation using bacterial or fungal cultures, or enzymatic treatment of these waste materials could provide safe and efficient means of valorization.

9.3. Intestinal transport of flavonoid glycosides

The poor oral bioavailability of flavonoids is the major drawback for its full recognition as a potent group of bioactive compounds. Indeed, bioactivity should always be accompanied by bioavailability or bioaccessibility (if the target tissue is the intestine). Compounds that do not reach the target tissue in high enough concentrations are simply not able to render bioactivity. Chapter 1 discussed the various barriers that flavonoids need to overcome before reaching its target tissue. These barriers include food matrix interactions, intestinal metabolism and efflux mechanisms by various ATP-binding cassette (ABC) transporters. More importantly, we have shown that these interactions are highly dependent on the structure of the flavonoid in question. Table 9.1 summarizes the effect of flavonoid structure on its exhibited interactions during digestion, absorption and distribution. As shown, glycosylation generally prevents the flavonoid from interacting with the food matrix and enhances the ability of the flavonoid to penetrate through the mucus layer. This explains the relatively high recovery of flavonoid glycosides during *in vitro* gastrointestinal digestion and their ability to easily diffuse intact through the mucus layer, as shown in Chapter 5.

The use of *in vitro* gastrointestinal digestion models has become an important alternative to human feeding trials in analyzing the bioaccessibility of food components, including flavonoids. In addition, subjecting the *in vitro* digesta to Caco-2 cells transport studies has been the most common model for simulating human intestinal absorption. As discussed in Chapter 1, these cells are of intestinal origin and confer characteristics

similar to mature enterocytes of the intestines. Therefore, it provides a picture of the potential bioavailability of flavonoids.

As shown in Table 9.1, glycosylation however decreases flavonoid intestinal absorption. As presented in Chapter 5, flavonoid glycosides are not bioavailable, except for 2 flavonoid glycosides that were absorbed intact but with extremely low recovery (0.3% of the original concentration). Chapter 6 provided the structural requirements necessary for Caco-2 transport. According to the results, hydrophobicity is a key factor that affects the ability of flavonoids to be transported intact through Caco-2 cells. Since glycosylation highly decreases the hydrophobicity of flavonoids, flavonoid glycosides need to be metabolized by β -glycosidases of the intestines or intestinal bacteria to release the transportable flavonoid aglycone, unless they are directly transported via active transport. The involvement of active transporters for flavonoid glycosides still remains a topic of debate in the literature and therefore merits further investigation.

The transport of flavonoids through Caco-2 cells has been shown to be pH-sensitive and several studies have used a pH gradient (pH 6.5 apical and pH 7.5 basal) in their transport analysis. As mentioned in Chapter 1, a low pH activates OATP's which then increase flavonoid transport, whereas flavonoids rely on passive diffusion at higher pH values. In our preliminary investigations, we found that the choice of medium used in the transport study also highly affects Caco-2 transport. By using DMEM (pH 7.5) in both apical and basal compartments, neither the kaempferol aglycone nor its metabolites were detected by our LC-MS method after 2 hours of transport experiment. However, using unbuffered Hank's Balanced Salt Solution (HBSS) resulted in a 6% recovery of kaempferol aglycone at the basal compartment after 2 hours of transport experimentation (data not shown). Due to active metabolism, the pH of unbuffered HBSS is very unstable and slightly decreases. This striking result therefore highlights the need for a standardized method for Caco-2 transport analysis when reporting the *in vitro* bioavailability of flavonoids. Currently, both DMEM and HBSS are used by different reports in the literature. This therefore means that a consolidated effort by various laboratories is needed to improve our current *in vitro* bioavailability models. This effort has previously been done in the design of a valid static *in vitro* gastrointestinal digestion protocol [272].

Table 9.1. Summary of the effect of certain flavonoid structural features in various stages of digestion, absorption and distribution

Site	Interaction/occurrence	-OH	-OCH ₃	C2=C3	-glycosyl	Position of B ring	Others	
Upper gastro-intestinal tract	Interaction with α -amylase and α -glucosidase	↑	↓	↑	↓	C2		
	Interaction with food carbohydrates	<i>No studies on SAR* with flavonoids but found to generally increase flavonoid bioavailability</i>						
	Interaction with lipase	↑ _{C3}		↓		C2		
	Interaction with food fats	<i>No studies on SAR with flavonoids but found to generally increase flavonoid bioavailability</i>						↑ hydrophobicity
	Interaction with food proteins	↑	↓	↑	↓			
Brush border	Mucus penetration	<i>No studies on SAR with flavonoids</i>						↓ hydrophobicity
	Overall intestinal permeability	↓	↑	↑	↓	C3		
	Glucuronidation	↑	↓	↑	↓	C2		
	Sulfation	↑ _{C7}				C2	↓ _{C3-OH}	
	Interaction with ABC transporters	↑	↓	↑	↓	C2		
Systemic circulation and target tissues	Plasma protein binding	↑	↑	↑	↓	C2		
	Deglucuronidation	<i>No studies on SAR with flavonoids</i>						

↑ denotes an increase in the interaction or occurrence; ↓ denotes a decrease in the interaction or occurrence; *SAR – structure-activity relationship

9.4. Disadvantages of current *in vitro* models for intestinal absorption

Although a generally accepted model to simulate intestinal digestion, the use of Caco-2 cells suffers 2 major disadvantages: (1) the lack of β -glucosidases, such as the lactase-phloridzin hydrolase, and (2) the lack of intestinal mucus layer. Given these, interpretation of *in vitro* results needs to be carefully done and should be compared or (better) translated to *in vivo* findings. Certainly, *in vivo* experiments provide a more accurate picture of flavonoid bioavailability but *in vitro* experiments also offer substantial amount of information, especially in terms of its mechanism. Thus, results from *in vitro* experiments, although having major drawbacks, cannot be discounted.

9.4.1. Lack of β -glucosidases in current *in vitro* intestinal models

As explained in Chapter 1, deglycosylation is an important prerequisite for flavonoid intestinal absorption. However, this mechanism cannot be studied using Caco-2 cells because its expression of lactase-phloridzin hydrolase is very low compared to the *in vivo* situation. Hence, as shown in Chapter 5, kaempferol phase I and II metabolites such as kaempferol glucuronides and sulfates, which are expected in plasma after ingestion of kaempferol glycosides [397], or when kaempferol aglycone is applied to a Caco-2/TC7 model [90], were not found after 2 hours of incubation in a Caco-2 transport experiment. This proves that Caco-2 cells, at least the cultures we used in the experiment, are incapable of deglycosylation. Therefore the use of Caco-2 cells to study the metabolic fate of flavonoid glycosides should be revalidated. Considering that active deglycosylation occurs in the small intestines, applying glycosides on Caco-2 cells may not be very relevant for studying the bioavailability and metabolic fate of the flavonoid in question. Of course, several exemptions could be drawn, for instance, intact anthocyanidin glucosides have been detected in plasma after oral administration of anthocyanin-rich foods. The involvement of active transporters in the transport of flavonoid glycosides remains a subject for further investigation.

9.4.2. Intestinal mucus layer: a missing link in the study of flavonoid bioavailability

There are currently conflicting results derived from both *in vitro* and *in vivo* reports on the fate and efficiency of intestinal absorption of different flavonoid forms. For instance, while *in vitro* results point to the higher bioavailability of flavonoid aglycones, some *in vivo* experiments reported higher levels of flavonoid metabolites upon ingestion of flavonoid glucosides. Certain gaps in our knowledge on the bioavailability of flavonoids and other phytochemicals have been reviewed [398]. For instance, the involvement of

the mucus layer in most flavonoid digestion and bioavailability studies remains largely unexplained in current literature.

Mucus is a highly complex viscoelastic secretion that covers epithelial surfaces, such as respiratory, ocular, reproductive and gastrointestinal (GI) tissues. It is composed of ~95% water with salts (up to 1%), lipids (1-2%), proteins (growth factors, lysozymes, immunoglobulins, etc), cellular debris, DNA (around 0.02%) and mucin, which is primarily responsible for its viscoelastic properties [399,400]. In the GI tract, the mucus layer is the first line of protection against infection and intoxication, but also serves as a selective barrier to allow nutrients to diffuse to the epithelial layer. This selectivity is most important in the small intestine, where most of the nutrient absorption takes place. The mucus layer is thinnest and loose in the small intestines; whereas the large intestines are covered by two layers of mucus, a loose layer exposed to the lumen and a densely packed immovable layer at the epithelium. The rules governing the selective barrier function of mucus however remain unclear [277,399].

As explained in Chapter 6, flavonoid membrane permeability is influenced by its hydrophobicity and is important for efficient passive transport through Caco-2 cells. Therefore, flavonoid glycosides are generally poorly absorbed through the intestinal cells/walls due to their hydrophilicity. Interestingly, animal and human studies suggest that certain flavonoid glucosides are absorbed more efficiently than their aglycone forms. In a feeding study in humans, it was found that quercetin glucoside is absorbed more than quercetin aglycone [69,401,402]. The same observation was obtained from feeding studies using pigs [71], rats [403], and dogs [404]. While several hypotheses have been formulated, such as effective deglycosylation by bacteria or brush border enzymes of the epithelial cells, current literature has failed to provide a concrete explanation of this inconsistency. Cermak et al. [71] hypothesized that the hydrophilic quercetin glucoside may have concentrated at the brush border, where deglycosylation occurs. This implies that the glucoside may have been able to penetrate through the mucus layer intact.

Strategies to enhance the absorption of flavonoids include increasing their aqueous solubility [405]. Several techniques to increase bioavailability include incorporation of flavonoids to borneol/methanol eutectic mixtures, micro-emulsions, polyvinylpyrrolidone dispersion, lecithin complexation, cyclodextrin complexation, etc [66]. The formulation of flavonoid aglycones into nanocrystals has also been previously described as an effective way of improving bioavailability [406]. All of these methods increase aqueous solubility of the flavonoid aglycone. However, the mechanisms of absorption enhancement remain unclear [407].

Given these findings, it is apparent that while hydrophobic flavonoid aglycones are favorably absorbed by intestinal cells, glycosylation and increasing aqueous solubility increase overall intestinal absorption. A logical mechanism therefore is the possible involvement of the mucus layer, which only allows the penetration of hydrophilic compounds (flavonoid glycosides or hydrophilic flavonoid complexes) and that deglycosylation occurs after the compound has penetrated through the mucus releasing the aglycone, which could then passively diffuse through the cell membrane. This hypothesis is summarized in Figure 9.1.

Hydrophobic flavonoid aglycones that reach the small intestines are unable to penetrate through the mucus layer and are thus pushed to the large intestines via peristalsis and are then metabolized (i.e. into smaller phenolic acid derivatives) by intestinal bacteria. However, in the presence of dietary fat and bile, micelles form and serve as carriers of aglycones through the mucus layer. They are then released upon contact with the brush border where passive diffusion is likely to occur through the cells. Soluble flavonoid glycosides on the other hand, are able to penetrate through the mucus layer to reach the epithelium. Upon contact with the brush border, β -glucosidases, such as LPH, cleave-off the glucose moiety to release the aglycone, which could then passively diffuse through the cells. Since intestinal cells are unable to produce rhamnosidases, flavonoids containing rhamnose moieties, such as rutin (quercetin-3-rutinoside) and hesperidin (hesperitin-7-rutinoside), remain intact in the small intestines and are thus pushed to the large intestines, where fermentation by intestinal bacteria occur or where secreted bacterial rhamnosidases act to release the aglycone. In the end, the aglycones that were released on the brush borders, or smaller phenolic acid derivatives that were produced after bacterial metabolism both in the small and the large intestines, reach the epithelia, where phase I and II metabolism takes place. It must be noted however that while bacteria also exist in the small intestines, the rate of diffusion (Chapter 5) and intestinal uptake at this stage occurs rapidly and thus the effect of duodenal bacteria is not as pronounced as in the colon, where the absorption is slower and longer. This proposed hypothesis may explain the delayed occurrence of rutin and hesperidin metabolites in plasma and the higher bioavailability of glucosides compared with aglycones under low a fat diet, and the increase in flavonoid bioavailability in high fat diets.

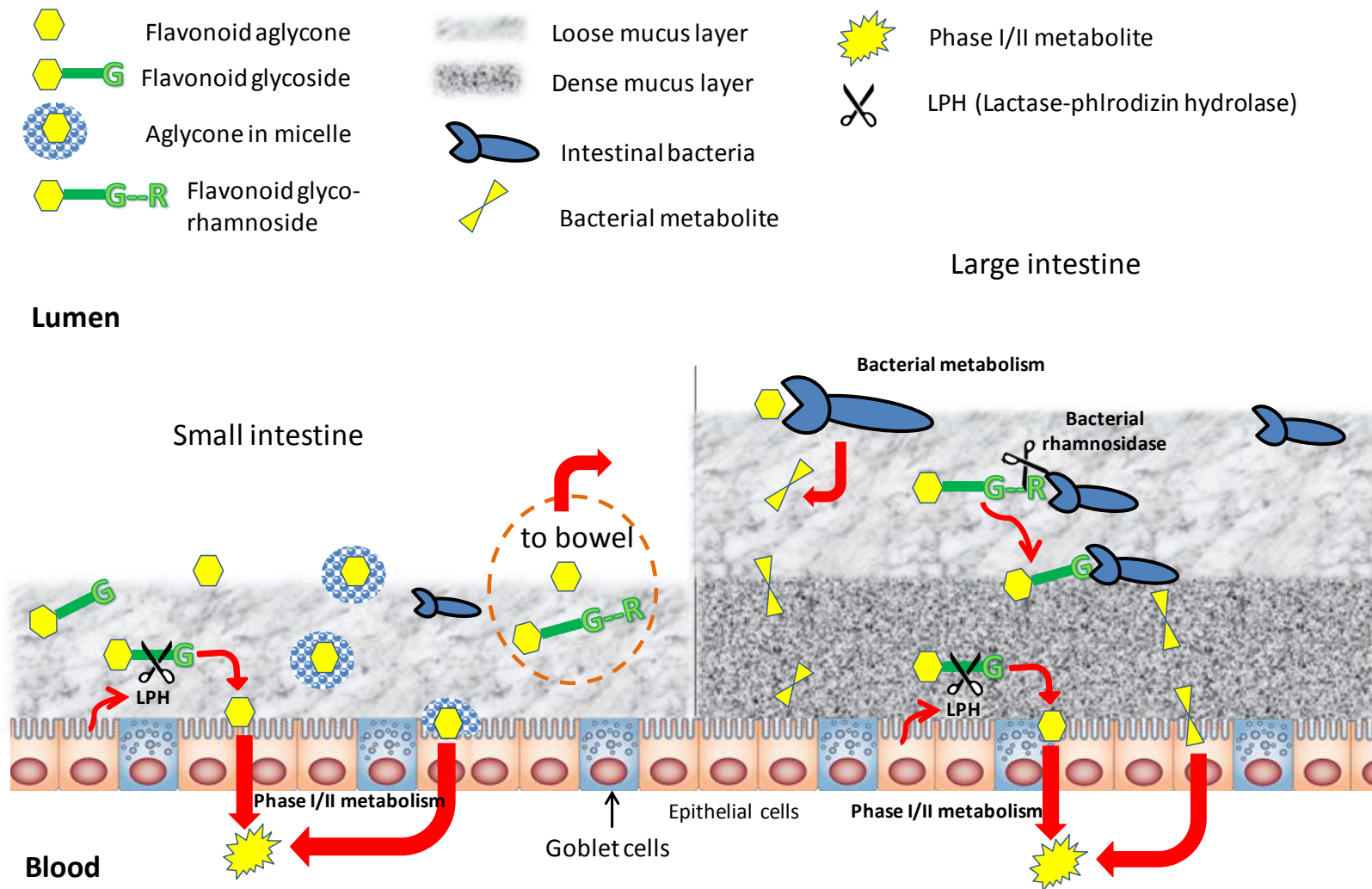


Figure 9.1. Proposed mechanism in the small and large intestines on the role of the mucus layer on the bioavailability of flavonoid aglycone, flavonoid glycoside, flavonoid in micelles (or other complexes such as nanoparticles), flavonoid glycorhamnosides

To compensate for the lack of mucus layer in Caco-2 cells, Chapter 1 described the use of co-culture systems comprising of Caco-2 cells combined with a mucin-secreting cell line, most popularly, HT29-MTX. However, as explained, HT29-MTX produces a gastric-type mucin, MUC5, instead of the intestinal types, MUC2 and MUC3. Therefore, better cell line models need to be sought. Hence, in this thesis, the ability of flavonoid glycosides to diffuse through the mucus layer was analyzed using an *ex vivo* porcine intestinal mucus sample. It was found that flavonoid glycosides diffuse rapidly through the mucus layer, which was analyzed using fluorescence recovery after photobleaching (FRAP) microscopy as shown in Chapter 5. However, since this confocal microscopy technique relies on the fluorescence of flavonoids, the identities of the diffusive and non-diffusive flavonoids could not be known. Thus, this technique could not determine which flavonoid could actually reach the epithelial surface. Nonetheless, this is the first time that the intestinal mucus diffusion of flavonoids has been taken into consideration in the study of flavonoid bioavailability and thus provides a new line of future research.

9.5. Cellular bioactivity and the role of local concentration

As mentioned earlier, the ultimate prerequisite for bioactivity is to ensure that the bioactive compound reaches its target. Since the epithelium is constantly exposed to toxins, we investigated whether flavonoids are able to protect intestinal cells from the cytotoxic effect of certain toxins. In Chapter 7, we tested the ability of quercetin, one of the most common flavonoids found in the diet, to protect undifferentiated cells from the cytotoxic effects of valinomycin. In this study, we found several striking results especially on the cellular metabolism of quercetin and the actual causative agent responsible for its bioactivity.

The radical scavenging activity of quercetin and other flavonoids have long been established. As explained in Chapter 1, this is due to their ability to sequester oxidizing agents, stabilize radical ions, and its influence on the integrity of the cell membrane. However, most studies do not consider the metabolic fate of quercetin, and thus any bioactivity observed is attributed to the bioactivity of quercetin. In this study, we proved that quercetin is metabolized into methyl-conjugates, which reduced the intracellular reactive oxygen species (ROS) and revived the mitochondrial activity of undifferentiated Caco-2 cells. In cells treated with quercetin alone, quercetin and methyl-quercetin was found to accumulate locally at the cell membrane. Upon co-administration with valinomycin, flow cytometry, mass spectrometry and confocal microscopy results showed that the intracellular methyl-quercetin content significantly increased, which was also accompanied by a shift in the intracellular localization; the flavonoid could now be found

within the cytosol and even in the nucleus. This mechanism has never been reported in the literature.

This observation indicates a potential cellular stress response mechanism, since the metabolism and flavonoid localization was altered during stress, which ultimately prevented further stress-induced damage. Also, since the level of quercetin aglycone did not change, it can be deduced that quercetin per se was not responsible for the bioactivity observed. Phase II metabolism has long been regarded as a mechanism to reduce the reactivity of xenobiotics, such as flavonoids. This reduction in reactivity has also been associated to a reduction in bioactivity. The catechol moiety of the quercetin molecule is responsible for the majority of the antioxidative property of quercetin, and as such, methylation of this moiety should reduce the antioxidative capacity of quercetin. However, as earlier explained in Chapter 7, 3 mono-methyl-*O*-quercetin isomers have been detected, wherein 2 were effluxed and one remained intracellularly. It could be that the intracellularly localized isomer retained its catechol moiety and the methylated may have occurred in another site, either at the C7 or C3 position. However, determination of the exact methylation site requires higher order fragmentation ($>MS^3$) or more complex techniques.

These results suggest that careful consideration of the cellular metabolic fate of flavonoids must be taken in associating bioactivity to the actual causative agent. Numerous studies have used flavonoid aglycones or phase II conjugates without monitoring in which form these flavonoids accumulate in the cells. This is currently a major issue, especially when determining the mechanisms of bioactivity of flavonoid metabolites that circulate in the blood. The bioactivity of flavonoids has constantly been questioned since the plasma concentration is low and they exist as glucuronides, sulfates and methyl-conjugates, which have been regarded as inactive and non-bioactive. Figure 9.2 shows that flavonoids undergo a cycle of conjugation and deconjugation before intestinal absorption until they reach their target organs.

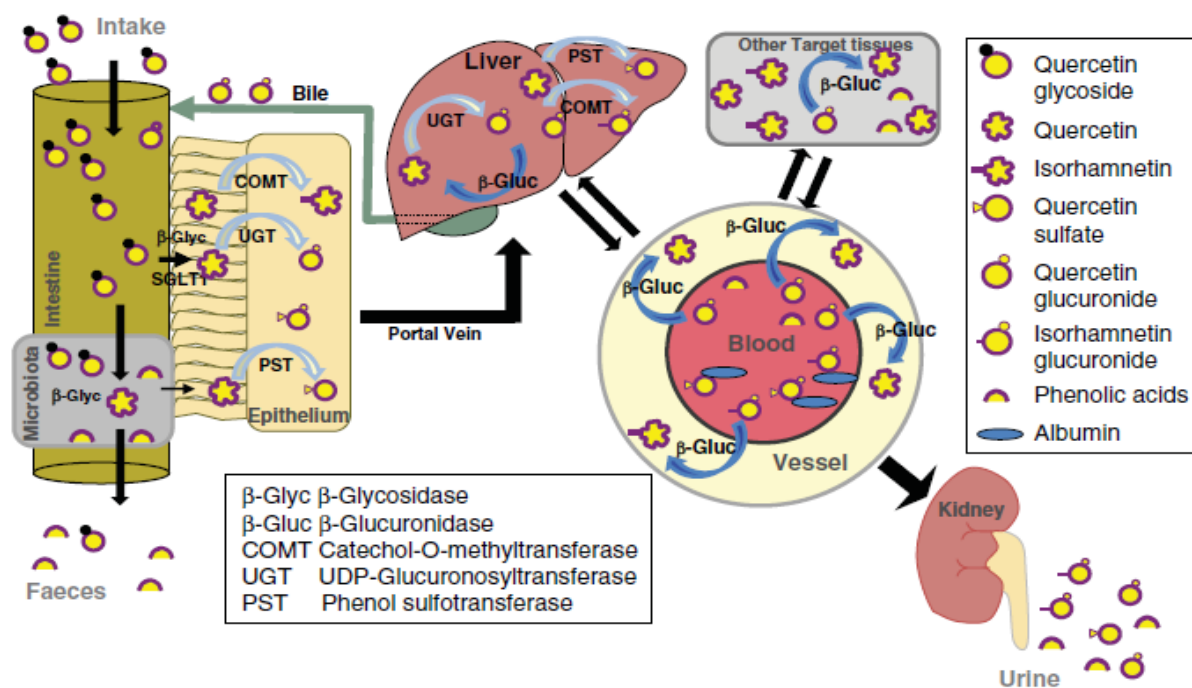


Figure 9.2. Schematic representation of the conjugation-deconjugation cycle of quercetin *in vivo*. Taken from Perez-Vizcaino et al. [167]

This schematic overview perfectly explains that flavonoids undergo several metabolic processes and that the actual compound that renders the bioactivity may not be what was initially ingested. Like in Chapter 7, we saw that the methylated form was the bioactive molecule and not quercetin per se, and that the methyl-quercetin only entered the cell upon stress induction. This presents not only a bioanalytical challenge but also an ethical issue when we translate it to human nutrition. To be able to really determine the bioactive form of the flavonoid, tissue samples must be taken from people with dysfunctional cells or tissues during a feeding intervention study. Although, animal studies may be performed to possibly explain this mechanism.

9.6. Towards better metabolite identification using ion mobility spectrometry

Nuclear magnetic resonance (NMR) spectrometry has been the most widely accepted method to elucidate the molecular structure of compounds. However, the use of NMR requires the isolation of the metabolite in large (mg) quantities, which is cumbersome when studying biological materials. Mass spectrometry has been the method of choice of most studies due to its sensitivity even at sub-ppm concentrations. However, the main challenge to use mass spectrometry in studying the metabolism of xenobiotics is the correct identification of its metabolites. Several techniques have been developed to aid metabolite identification, especially because of high mass accuracy. One such example is mass defect filtering, as explained in Chapter 1. However, these techniques are not able

to distinguish isomers, especially when the only difference among the molecules is the attachment point of functional groups.

In Chapter 2, we have shown the potential of ion mobility spectrometry (IMS) in separating the precursor ions based on their size and ability to interact with a drift gas (nitrogen). Recently, the use of IMS has made its way into various bioanalytical domains, such as lipidomics, metabolomics, proteomics, analysis of large protein complexes, and the analysis of drug metabolism. It is increasingly being used as a tool in aid of confident metabolite identification due to its ability to distinguish isomers with different 3D conformations. In Chapter 8, we explored the use of this emerging technology to separate and identify phenolics in conjunction with chemometric techniques.

By utilizing 3 common chemometric tools, such as SMLR, PCR and PLS, highly predictive models were developed that are able to predict the collision cross sections (CCS) of different phenolics. This CCS information can then be used to verify the identity of target metabolites together with product ion information obtained in MS^E analysis. Therefore, the combination of ion mobility separation, CCS information, and MS^E fragmentation could offer an invaluable technique to bioanalysis. For instance, the major difficulty faced in Chapter 7 was the structural characterization of the 3 methyl-quercetin isomers found. The finding that 2 of the isomers were effluxed while the 1 remained in the cells, suggest a regio-specificity in the cells that requires further investigation. A bioanalytical platform composed of LC-ESI-IMS- MS^E could potentially determine the exact methylation points of these metabolites in the quercetin aglycone structure.

However, since this technology is still emerging, several restraints exist in our current instrumentation that prevents us from analyzing these isomers. Most importantly, since cellular concentrations are very low, this analysis requires a highly sensitive MS. Due to the fact that ions in the MS travel from atmospheric pressure to a vacuum, then being pushed back by the buffer gas in the TWIMS, and then back to vacuum, ions do not arrive at the detector in the same abundance as was injected. Therefore, when the IMS mode is activated, only highly abundant ions arrive at the detector, which are usually not the metabolites of interest. The problem of sensitivity in first generation TWIMS-MS instrumentation has been the focus of MS manufacturers in the past years and has now been accordingly dealt with. Higher generation TWIMS-MS promise increased sensitivity even under IMS conditions, which could therefore provide CCS information for cellular metabolites that occur in very small concentrations in the sample. Nonetheless, the strategy presented in Chapter 8 could be employed in any newer TWIMS instrumentation and thus offers opportunities for further investigation. An integrated platform of liquid

chromatography, ion mobility separation, MS^E fragmentation and CCS determination and prediction is foreseen to be an important strategy in the future of bioanalysis.

9.7. Generalization

In this PhD, a highly multi-disciplinary approach, involving *in vitro*, *in silico*, *ex vivo*, analytical and computational analytical techniques, was employed to deepen our understanding and contribute to the current knowledge in flavonoid research. Furthermore, the gaps in our current knowledge were exposed and recommendations on how to circumvent existing issues are presented. Lastly, the future of bioanalysis is forecasted and a first step on this emerging technology has been taken.

References

References

- [1] S. Kumar, A.K. Pandey, Chemistry and Biological Activities of Flavonoids: An Overview, *The Scientific World Journal* 2013 (2013) 16.
- [2] J. Dai, R.J. Mumper, Plant phenolics: extraction, analysis and their antioxidant and anticancer properties, *Molecules* 15 (2010) 7313-7352.
- [3] P.-G. Pietta, Flavonoids as Antioxidants, *J Nat Prod* 63 (2000) 1035-1042.
- [4] M. Fiol, S. Adermann, S. Neugart, S. Rohn, C. Mügge, M. Schreiner, A. Krumbein, L.W. Kroh, Highly glycosylated and acylated flavonols isolated from kale (*Brassica oleracea* var. *sabellica*) — Structure–antioxidant activity relationship, *Food Res Int* 47 (2012) 80-89.
- [5] N. Al Shukor, J. Van Camp, G.B. Gonzales, D. Staljanssens, K. Struijs, M.J. Zotti, K. Raes, G. Smagghe, Angiotensin-Converting Enzyme Inhibitory Effects by Plant Phenolic Compounds: A Study of Structure Activity Relationships, *J Agric Food Chem* 61 (2013) 11832-11839.
- [6] N. Balasuriya, H.P.V. Rupasinghe, Antihypertensive properties of flavonoid-rich apple peel extract, *Food Chem* 135 (2012) 2320-2325.
- [7] C.L. Hsu, G.C. Yen, Phenolic compounds: evidence for inhibitory effects against obesity and their underlying molecular signaling mechanisms, *Mol Nutr Food Res* 52 (2008) 53-61.
- [8] E. Middleton, C. Kandaswami, T.C. Theoharides, The Effects of Plant Flavonoids on Mammalian Cells: Implications for Inflammation, Heart Disease, and Cancer, *Pharmacol Rev* 52 (2000) 673-751.
- [9] C. Manach, A. Scalbert, C. Morand, C. Rémésy, L. Jiménez, Polyphenols: food sources and bioavailability, *The American Journal of Clinical Nutrition* 79 (2004) 727-747.
- [10] M. D'Archivio, C. Filesi, R. Vari, B. Scaccocchio, R. Masella, Bioavailability of the polyphenols: status and controversies, *Int J Mol Sci* 11 (2010) 1321-1342.
- [11] A. de Villiers, P. Venter, H. Pasch, Recent advances and trends in the liquid-chromatography-mass spectrometry analysis of flavonoids, *J Chromatogr A* (*In press*).
- [12] M.-I. Aguilar, in *HPLC of Peptides and Proteins: Methods and Protocols*, 2003, p. 9-22.
- [13] K. Vande Castele, H. Geiger, C.F. Van Sumere, Separation of flavonoids by reversed-phase high-performance liquid chromatography, *J Chromatogr A* 240 (1982) 81-94.
- [14] Z. Lei, L. Jing, F. Qiu, H. Zhang, D. Huhman, Z. Zhou, L.W. Sumner, Construction of an Ultrahigh Pressure Liquid Chromatography-Tandem Mass Spectral Library of Plant Natural Products and Comparative Spectral Analyses, *Anal Chem* 87 (2015) 7373-7381.
- [15] J. Akbar, S. Iqbal, F. Batool, A. Karim, K. Chan, Predicting Retention Times of Naturally Occurring Phenolic Compounds in Reversed-Phase Liquid Chromatography: A Quantitative Structure-Retention Relationship (QSRR) Approach, *Int J Mol Sci* 13 (2012) 15387.
- [16] M. Gumustas, S. Kurbanoglu, B. Uslu, S.A. Ozkan, UPLC versus HPLC on Drug Analysis: Advantageous, Applications and Their Validation Parameters, *Chromatographia* 76 (2013) 1365-1427.
- [17] Waters Corporation Ultra Performance LC™ by design, USA, 720000880EN LL&LW-UL. 2004.
- [18] M.-J. Motilva, A. Serra, A. Macià, Analysis of food polyphenols by ultra high-performance liquid chromatography coupled to mass spectrometry: An overview, *J Chromatogr A* 1292 (2013) 66-82.
- [19] V. Vukics, A. Guttman, Structural characterization of flavonoid glycosides by multi-stage mass spectrometry, *Mass Spectrom Rev* 29 (2010) 1-16.
- [20] F. Cuyckens, M. Claeys, Mass spectrometry in the structural analysis of flavonoids, *J Mass Spectrom* 39 (2004) 1-15.
- [21] E. de Hoffmann, V. Stroobant, *Mass Spectrometry: Principles and Applications*, Wiley, 2007.
- [22] M. Stobiecki, Application of mass spectrometry for identification and structural studies of flavonoid glycosides, *Phytochemistry* 54 (2000) 237-256.

- [23] C.S. Ho, C.W.K. Lam, M.H.M. Chan, R.C.K. Cheung, L.K. Law, L.C.W. Lit, K.F. Ng, M.W.M. Suen, H.L. Tai, *Electrospray Ionisation Mass Spectrometry: Principles and Clinical Applications*, *The Clinical Biochemist Reviews* 24 (2003) 3-12.
- [24] T.M. Annesley, Ion suppression in mass spectrometry, *Clin Chem* 49 (2003) 1041-1044.
- [25] K. Ablajan, A. Tuoheti, Fragmentation characteristics and isomeric differentiation of flavonol O-rhamnosides using negative ion electrospray ionization tandem mass spectrometry, *Rapid Commun Mass Spectrom* 27 (2013) 451-460.
- [26] A. Petsalo, J. Jalonen, A. Tolonen, Identification of flavonoids of *Rhodiola rosea* by liquid chromatography-tandem mass spectrometry, *J Chromatogr A* 1112 (2006) 224-231.
- [27] F. Cuyckens, R. Rozenberg, E. de Hoffmann, M. Claeys, Structure characterization of flavonoid O-diglycosides by positive and negative nano-electrospray ionization ion trap mass spectrometry, *J Mass Spectrom* 36 (2001) 1203-1210.
- [28] E. Hvattum, D. Ekeberg, Study of the collision-induced radical cleavage of flavonoid glycosides using negative electrospray ionization tandem quadrupole mass spectrometry, *J Mass Spectrom* 38 (2003) 43-49.
- [29] H. Zhang, D. Zhang, K. Ray, M. Zhu, Mass defect filter technique and its applications to drug metabolite identification by high-resolution mass spectrometry, *J Mass Spectrom* 44 (2009) 999-1016.
- [30] L. Zhang, Z. Zuo, G. Lin, Intestinal and hepatic glucuronidation of flavonoids, *Mol Pharm* 4 (2007) 833-845.
- [31] B.D. Davis, P.W. Needs, P.A. Kroon, J.S. Brodbelt, Identification of isomeric flavonoid glucuronides in urine and plasma by metal complexation and LC-ESI-MS/MS, *J Mass Spectrom* 41 (2006) 911-920.
- [32] Y. Gandhi, M. Morris, Structure-Activity Relationships and Quantitative Structure-Activity Relationships for Breast Cancer Resistance Protein (ABCG2), *The AAPS Journal* 11 (2009) 541-552.
- [33] J.D. McKinney, A. Richard, C. Waller, M.C. Newman, F. Gerberick, The Practice of Structure Activity Relationships (SAR) in Toxicology, *Toxicol Sci* 56 (2000) 8-17.
- [34] A.Z. Dudek, T. Arodz, J. Galvez, Computational methods in developing quantitative structure-activity relationships (QSAR): a review, *Comb Chem High Throughput Screen* 9 (2006) 213-228.
- [35] S. Wold, M. Sjöström, L. Eriksson, PLS-regression: a basic tool of chemometrics, *Chemometrics Intellig Lab Syst* 58 (2001) 109-130.
- [36] R. Perkins, H. Fang, W. Tong, W.J. Welsh, Quantitative structure-activity relationship methods: perspectives on drug discovery and toxicology, *Environ Toxicol Chem* 22 (2003) 1666-1679.
- [37] S.S. Nilewar, M.K. Kathiravan, 3D CoMFA, CoMSIA, topomer CoMFA and HQSAR studies on aromatic acid esters for carbonic anhydrase inhibitory activity, *J Chemom* 28 (2014) 60-70.
- [38] K.-T. Kim, L.-E. Rioux, S.L. Turgeon, Alpha-amylase and alpha-glucosidase inhibition is differentially modulated by fucoidan obtained from *Fucus vesiculosus* and *Ascophyllum nodosum*, *Phytochemistry* 98 (2014) 27-33.
- [39] H. Wang, Y.-J. Du, H.-C. Song, α -Glucosidase and α -amylase inhibitory activities of guava leaves, *Food Chem* 123 (2010) 6-13.
- [40] K. Tadera, Y. Minami, K. Takamatsu, T. Matsuoka, Inhibition of alpha-glucosidase and alpha-amylase by flavonoids, *J Nutr Sci Vitaminol (Tokyo)* 52 (2006) 149-153.
- [41] E. Lo Piparo, H. Scheib, N. Frei, G. Williamson, M. Grigorov, C.J. Chou, Flavonoids for controlling starch digestion: structural requirements for inhibiting human alpha-amylase, *J Med Chem* 51 (2008) 3555-3561.
- [42] J. Xiao, X. Ni, G. Kai, X. Chen, A review on structure-activity relationship of dietary polyphenols inhibiting alpha-amylase, *Crit Rev Food Sci Nutr* 53 (2013) 497-506.

- [43] S. Fatmawati, R. Kondo, K. Shimizu, Structure–activity relationships of lanostane-type triterpenoids from *Ganoderma lingzhi* as α -glucosidase inhibitors, *Bioorg Med Chem Lett* 23 (2013) 5900-5903.
- [44] J. Xiao, G. Kai, K. Yamamoto, X. Chen, Advance in dietary polyphenols as alpha-glucosidases inhibitors: a review on structure-activity relationship aspect, *Crit Rev Food Sci Nutr* 53 (2013) 818-836.
- [45] H. Cao, X.Q. Chen, Structures Required of Flavonoids for Inhibiting Digestive Enzymes, *Anticancer Agents Med Chem* 12 (2012) 929-939.
- [46] M. Miao, H. Jiang, B. Jiang, Y. Li, S.W. Cui, T. Zhang, Structure elucidation of catechins for modulation of starch digestion, *LWT - Food Science and Technology* 57 (2014) 188-193.
- [47] V. Rastija, D. Bešlo, S. Nikolić, Two-dimensional quantitative structure–activity relationship study on polyphenols as inhibitors of α -glucosidase, *Med Chem Res* 21 (2012) 3984-3993.
- [48] D.D. Schramm, M. Karim, H.R. Schrader, R.R. Holt, N.J. Kirkpatrick, J.A. Polagruto, J.L. Ensunsa, H.H. Schmitz, C.L. Keen, Food effects on the absorption and pharmacokinetics of cocoa flavanols, *Life Sci* 73 (2003) 857-869.
- [49] A.P. Neilson, J.C. George, E.M. Janle, R.D. Mattes, R. Rudolph, N.V. Matusheski, M.G. Ferruzzi, Influence of Chocolate Matrix Composition on Cocoa Flavan-3-ol Bioaccessibility In Vitro and Bioavailability in Humans, *J Agric Food Chem* 57 (2009) 9418-9426.
- [50] H. Zhang, D. Yu, J. Sun, X. Liu, L. Jiang, H. Guo, F. Ren, Interaction of plant phenols with food macronutrients: characterisation and nutritional–physiological consequences, *Nutrition Research Reviews* 27 (2014) 1-15.
- [51] G. Kottra, H. Daniel, Flavonoid glycosides are not transported by the human Na⁺/glucose transporter when expressed in *Xenopus laevis* oocytes, but effectively inhibit electrogenic glucose uptake, *J Pharmacol Exp Ther* 322 (2007) 829-835.
- [52] R.B. Birari, K.K. Bhutani, Pancreatic lipase inhibitors from natural sources: unexplored potential, *Drug Discovery Today* 12 (2007) 879-889.
- [53] J.W. Yun, Possible anti-obesity therapeutics from nature – A review, *Phytochemistry* 71 (2010) 1625-1641.
- [54] M.D. Wilcox, I.A. Brownlee, J.C. Richardson, P.W. Dettmar, J.P. Pearson, The modulation of pancreatic lipase activity by alginates, *Food Chem* 146 (2014) 479-484.
- [55] M.T. Gatto, S. Falcocchio, E. Grippa, G. Mazzanti, L. Battinelli, G. Nicolosi, D. Lambusta, L. Saso, Antimicrobial and Anti-Lipase Activity of Quercetin and its C2-C16 3-O-Acyl-Esters, *Biorg Med Chem* 10 (2002) 269-272.
- [56] N. Bordenave, B.R. Hamaker, M.G. Ferruzzi, Nature and consequences of non-covalent interactions between flavonoids and macronutrients in foods, *Food & Function* 5 (2014) 18-34.
- [57] F. Jailani, G. Williamson, Effect of edible oils on quercetin, kaempferol and galangin transport and conjugation in the intestinal Caco-2/HT29-MTX co-culture model, *Food & Function* 5 (2014) 653-662.
- [58] S. Lesser, R. Cermak, S. Wolffram, Bioavailability of Quercetin in Pigs Is Influenced by the Dietary Fat Content, *The Journal of Nutrition* 134 (2004) 1508-1511.
- [59] J. Xiao, F. Mao, F. Yang, Y. Zhao, C. Zhang, K. Yamamoto, Interaction of dietary polyphenols with bovine milk proteins: Molecular structure–affinity relationship and influencing bioactivity aspects, *Mol Nutr Food Res* 55 (2011) 1637-1645.
- [60] C. Xu, X. Chen, Molecular property-affinity relationship of the interaction between dietary polyphenols and bovine milk proteins, *Food & Function* 2 (2011) 368-372.
- [61] M.C. Bohin, J.P. Vincken, H.T. van der Hijden, H. Gruppen, Efficacy of food proteins as carriers for flavonoids, *J Agric Food Chem* 60 (2012) 4136-4143.
- [62] P.C.H. Hollman, Absorption, Bioavailability, and Metabolism of Flavonoids, *Pharm Biol* 42 (2004) 74-83.

- [63] C. Manach, G. Williamson, C. Morand, A. Scalbert, C. Rémésy, Bioavailability and bioefficacy of polyphenols in humans. I. Review of 97 bioavailability studies, *Am J Clin Nutr* 81 (2005) 230S-242S.
- [64] A. Scalbert, G. Williamson, Dietary intake and bioavailability of polyphenols, *The Journal of Nutrition* 130 (2000) 2073S-2085S.
- [65] A. Crozier, D. Del Rio, M.N. Clifford, Bioavailability of dietary flavonoids and phenolic compounds, *Molecular Aspects of Medicine* 31 (2010) 446-467.
- [66] S. Thilakarathna, H. Rupasinghe, Flavonoid Bioavailability and Attempts for Bioavailability Enhancement, *Nutrients* 5 (2013) 3367-3387.
- [67] T. Walle, Methylation of Dietary Flavones Greatly Improves Their Hepatic Metabolic Stability and Intestinal Absorption, *Mol Pharm* 4 (2007) 826-832.
- [68] X. Wen, T. Walle, Methylated Flavonoids Have Greatly Improved Intestinal Absorption and Metabolic Stability, *Drug Metab Dispos* 34 (2006) 1786-1792.
- [69] C. Morand, C. Manach, V. Crespy, C. Remesy, Respective bioavailability of quercetin aglycone and its glycosides in a rat model, *Biofactors* 12 (2000) 169-174.
- [70] S. Karakaya, Bioavailability of phenolic compounds, *Crit Rev Food Sci Nutr* 44 (2004) 453-464.
- [71] R. Cermak, S. Landgraf, S. Wolffram, The Bioavailability of Quercetin in Pigs Depends on the Glycoside Moiety and on Dietary Factors, *The Journal of Nutrition* 133 (2003) 2802-2807.
- [72] H. van de Waterbeemd, E. Gifford, ADMET in silico modelling: towards prediction paradise?, *Nat Rev Drug Discov* 2 (2003) 192-204.
- [73] M.D. Wessel, P.C. Jurs, J.W. Tolan, S.M. Muskal, Prediction of Human Intestinal Absorption of Drug Compounds from Molecular Structure, *J Chem Inf Comput Sci* 38 (1998) 726-735.
- [74] C.A. Lipinski, F. Lombardo, B.W. Dominy, P.J. Feeney, Experimental and computational approaches to estimate solubility and permeability in drug discovery and development settings, *Adv Drug Del Rev* 46 (2001) 3-26.
- [75] W.J. Egan, K.M. Merz, J.J. Baldwin, Prediction of Drug Absorption Using Multivariate Statistics, *J Med Chem* 43 (2000) 3867-3877.
- [76] X.J. Tian, X.W. Yang, X. Yang, K. Wang, Studies of intestinal permeability of 36 flavonoids using Caco-2 cell monolayer model, *Int J Pharm* 367 (2009) 58-64.
- [77] L. Mahraoui, M. Rousset, E. Dussaulx, D. Darmoul, A. Zweibaum, E. Brotlaroche, Expression and Localization of Glut-5 in Caco-2 Cells, Human Small-Intestine, and Colon, *Am J Physiol* 263 (1992) G312-G318.
- [78] J.E. Polli, M.J. Ginski, Human drug absorption kinetics and comparison to Caco-2 monolayer permeabilities, *Pharm Res* 15 (1998) 47-52.
- [79] D.T. Lowenthal, M.B. Affrime, Pharmacology and pharmacokinetics of minoxidil, *J Cardiovasc Pharmacol* 2 Suppl 2 (1980) S93-106.
- [80] H. Lennernäs, K. Palm, U. Fagerholm, P. Artursson, Comparison between active and passive drug transport in human intestinal epithelial (caco-2) cells in vitro and human jejunum in vivo, *Int J Pharm* 127 (1996) 103-107.
- [81] M. Pinto, S. Robineleon, M.D. Appay, M. Kedinger, N. Triadou, E. Dussaulx, B. Lacroix, P. Simonassmann, K. Haffen, J. Fogh, A. Zweibaum, Enterocyte-like differentiation and polarization of the human-colon carcinoma cell-line Caco-2 in culture, *Biol Cell* 47 (1983) 323-330.
- [82] Y. Sambuy, I. Angelis, G. Ranaldi, M.L. Scarino, A. Stammati, F. Zucco, The Caco-2 cell line as a model of the intestinal barrier: influence of cell and culture-related factors on Caco-2 cell functional characteristics, *Cell Biol Toxicol* 21 (2005) 1-26.
- [83] L. Turco, T. Catone, F. Caloni, E. Di Consiglio, E. Testai, A. Stammati, Caco-2/TC7 cell line characterization for intestinal absorption: how reliable is this in vitro model for the prediction of the oral dose fraction absorbed in human?, *Toxicol In Vitro* 25 (2011) 13-20.
- [84] M. Fiorentino, K.M. Lammers, M.M. Levine, M.B. Sztejn, A. Fasano, In Vitro intestinal mucosal epithelial responses to wild-type Salmonella Typhi and attenuated typhoid vaccines, *Frontiers in Immunology* 4 (2013).

- [85] E. Cohen, I. Ophir, Y.B. Shaul, Induced differentiation in HT29, a human colon adenocarcinoma cell line, *J Cell Sci* 112 (1999) 2657-2666.
- [86] G. Huet, I. Kim, C. de Bolos, J.M. Lo-Guidice, O. Moreau, B. Hemon, C. Richet, P. Delannoy, F.X. Real, P. Degand, Characterization of mucins and proteoglycans synthesized by a mucin-secreting HT-29 cell subpopulation, *J Cell Sci* 108 (1995) 1275-1285.
- [87] A. Le Bivic, M. Hirn, H. Reggio, HT-29 cells are an in vitro model for the generation of cell polarity in epithelia during embryonic differentiation, *Proc Natl Acad Sci U S A* 85 (1988) 136-140.
- [88] S. Hennebicq-Reig, D. Tetaert, B. Soudan, I. Kim, G. Huet, G. Briand, C. Richet, D. Demeyer, P. Degand, O-Glycosylation and cellular differentiation in a subpopulation of mucin-secreting HT-29 cell line, *Exp Cell Res* 235 (1997) 100-107.
- [89] T. Lesuffleur, A. Barbat, E. Dussaulx, A. Zweibaum, Growth adaptation to methotrexate of HT-29 human colon carcinoma cells is associated with their ability to differentiate into columnar absorptive and mucus-secreting cells, *Cancer Res* 50 (1990) 6334-6343.
- [90] R. Barrington, G. Williamson, R.N. Bennett, B.D. Davis, J.S. Brodbelt, P.A. Kroon, Absorption, Conjugation and Efflux of the Flavonoids, Kaempferol and Galangin, Using the Intestinal CACO-2/TC7 Cell Model, *J Funct Foods* 1 (2009) 74-87.
- [91] G. Nollevaux, C. Deville, B. El Moualij, W. Zorzi, P. Deloyer, Y.-J. Schneider, O. Peulen, G. Dandrifosse, Development of a serum-free co-culture of human intestinal epithelium cell-lines (Caco-2/HT29-5M21), *BMC Cell Biol* 7 (2006) 20.
- [92] C. Hilgendorf, H. Spahn-Langguth, C. Regardh, E. Lipka, G. Amidon, P. Langguth, Caco-2 versus Caco-2/HT29-MTX co-cultured cell lines: permeabilities via diffusion, inside- and outside-directed carrier-mediated transport, *J Pharm Sci* 89 (2000) 63 - 75.
- [93] T. Lesuffleur, N. Porchet, J. Aubert, D. Swallow, J. Gum, Y. Kim, F. Real, A. Zweibaum, Differential expression of the human mucin genes MUC1 to MUC5 in relation to growth and differentiation of different mucus-secreting HT-29 cell subpopulations, *J Cell Sci* 106 (1993) 771 - 783.
- [94] T. Lesuffleur, A. Barbat, C. Luccioni, J. Beaumatin, M. Clair, A. Kornowski, E. Dussaulx, B. Dutrillaux, A. Zweibaum, Dihydrofolate reductase gene amplification-associated shift of differentiation in methotrexate-adapted HT-29 cells, *J Cell Biol* 115 (1991) 1409 - 1418.
- [95] D.J. McCool, J.F. Forstner, G.G. Forstner, Regulated and unregulated pathways for MUC2 mucin secretion in human colonic LS180 adenocarcinoma cells are distinct, *Biochem J* 312 (1995) 125-133.
- [96] H.J. Eppele, K.M. Kreuzel, C. Hanski, J.D. Schulzke, E.O. Riecken, M. Fromm, Differential stimulation of intestinal mucin secretion by cholera toxin and carbachol, *Pflugers Arch* 433 (1997) 638-647.
- [97] M.N. Chabane, A. Al Ahmad, J. Peluso, C.D. Muller, G. Ubeaud, Quercetin and naringenin transport across human intestinal Caco-2 cells, *J Pharm Pharmacol* 61 (2009) 1473-1483.
- [98] Y. Liu, M. Hu, Absorption and metabolism of flavonoids in the Caco-2 cell culture model and a perfused rat intestinal model, *Drug Metab Dispos* 30 (2002) 370-377.
- [99] J.B. Vaidyanathan, T. Walle, Cellular uptake and efflux of the tea flavonoid (-)-epicatechin-3-gallate in the human intestinal cell line Caco-2, *J Pharmacol Exp Ther* 307 (2003) 745-752.
- [100] C.C. Wong, Y. Akiyama, T. Abe, J.D. Lippiat, C. Orfila, G. Williamson, Carrier-mediated transport of quercetin conjugates: Involvement of organic anion transporters and organic anion transporting polypeptides, *Biochem Pharmacol* 84 (2012) 564-570.
- [101] A.I. Alvarez, R. Real, M. Perez, G. Mendoza, J.G. Prieto, G. Merino, Modulation of the Activity of ABC Transporters (P-Glycoprotein, MRP2, BCRP) by Flavonoids and Drug Response, *Journal of Pharmaceutical Sciences* 99 (2010) 598-617.
- [102] Y. Meier, J.J. Eloranta, J. Darimont, M.G. Ismail, C. Hiller, M. Fried, G.A. Kullak-Ublick, S.R. Vavricka, Regional distribution of solute carrier mRNA expression along the human intestinal tract, *Drug Metab Dispos* 35 (2007) 590-594.

- [103] S. Leuthold, B. Hagenbuch, N. Mohebbi, C.A. Wagner, P.J. Meier, B. Stieger, Mechanisms of pH-gradient driven transport mediated by organic anion polypeptide transporters, *American Journal of Physiology-Cell Physiology* 296 (2009) C570-C582.
- [104] C.L. Hammond, R. Marchan, S.M. Krance, N. Ballatori, Glutathione export during apoptosis requires functional multidrug resistance-associated proteins, *J Biol Chem* 282 (2007) 14337-14347.
- [105] W.S. Lee, Y. Kanai, R.G. Wells, M.A. Hediger, The high-affinity Na⁺/glucose cotransporter - reevaluation of function and distribution of expression, *J Biol Chem* 269 (1994) 12032-12039.
- [106] K. Amsler, J.S. Cook, Development of Na⁺-Dependent Hexose-Transport in a Cultured Line of Porcine Kidney-Cells, *Am J Physiol* 242 (1982) C94-C101.
- [107] X. Jin, L. Yi, M.-l. Chen, C.-y. Chen, H. Chang, T. Zhang, L. Wang, J.-d. Zhu, Q.-y. Zhang, M.-t. Mi, Delphinidin-3-glucoside protects against oxidized low-density lipoprotein-induced mitochondrial dysfunction in vascular endothelial cells via the sodium-dependent glucose transporter SGLT1, *PLoS ONE* 8 (2013) e68617.
- [108] R.A. Walgren, J.T. Lin, R.K. Kinne, T. Walle, Cellular uptake of dietary flavonoid quercetin 4'-beta-glucoside by sodium-dependent glucose transporter SGLT1, *J Pharmacol Exp Ther* 294 (2000) 837-843.
- [109] S. Wolffram, M. Block, P. Ader, Quercetin-3-glucoside is transported by the glucose carrier SGLT1 across the brush border membrane of rat small intestine, *J Nutr* 132 (2002) 630-635.
- [110] W. Andlauer, J. Kolb, P. Furst, Phloridzin improves absorption of genistin in isolated rat small intestine, *Clin Nutr* 23 (2004) 989-995.
- [111] S. Passamonti, M. Terdoslavich, R. Franca, A. Vanzo, F. Tramer, E. Braidot, E. Petrusa, A. Vianello, Bioavailability of flavonoids: a review of their membrane transport and the function of bilitranslocase in animal and plant organisms, *Curr Drug Metab* 10 (2009) 369-394.
- [112] A. Karawajczyk, V. Dran, N. Medic, G. Oboh, S. Passamonti, M. Novic, Properties of flavonoids influencing the binding to bilitranslocase investigated by neural network modelling, *Biochem Pharmacol* 73 (2007) 308-320.
- [113] S. Passamonti, M. Terdoslavich, A. Margon, A. Cocolo, N. Medic, F. Micali, G. Decorti, M. Franko, Uptake of bilirubin into HepG2 cells assayed by thermal lens spectroscopy - Bilitranslocase, *FEBS J* 272 (2005) 5522-5535.
- [114] S. Passamonti, A. Vanzo, U. Vrhovsek, M. Terdoslavich, A. Cocolo, G. Decorti, F. Mattivi, Hepatic uptake of grape anthocyanins and the role of bilitranslocase, *Food Res Int* 38 (2005) 953-960.
- [115] X.D. Wang, M.X. Meng, L.B. Gao, T. Liu, Q. Xu, S. Zeng, Permeation of astilbin and taxifolin in Caco-2 cell and their effects on the P-gp, *Int J Pharm* 378 (2009) 1-8.
- [116] P.A. Kroon, M.N. Clifford, A. Crozier, A.J. Day, J.L. Donovan, C. Manach, G. Williamson, How should we assess the effects of exposure to dietary polyphenols in vitro?, *The American Journal of Clinical Nutrition* 80 (2004) 15-21.
- [117] P.A. Kroon, M.N. Clifford, A. Crozier, A.J. Day, J.L. Donovan, C. Manach, G. Williamson, How should we assess the effects of exposure to dietary polyphenols in vitro?, *American Journal of Clinical Nutrition* 80 (2004) 15-21.
- [118] F. Perez-Vizcaino, J. Duarte, C. Santos-Buelga, The flavonoid paradox: conjugation and deconjugation as key steps for the biological activity of flavonoids, *Journal of the Science of Food and Agriculture* 92 (2012) 1822-1825.
- [119] R.A. Conradi, A.R. Hilgers, N.F.H. Ho, P.S. Burton, The influence of peptide structure on transport across Caco-2 cells, *Pharm Res* 8 (1991) 1453-1460.
- [120] A. Scalbert, G. Williamson, Dietary intake and bioavailability of polyphenols, *Journal of Nutrition* 130 (2000) 2073s-2085s.
- [121] A.J. Day, M.S. DuPont, S. Ridley, M. Rhodes, M.J.C. Rhodes, M.R.A. Morgan, G. Williamson, Deglycosylation of flavonoid and isoflavonoid glycosides by human small intestine and liver β -glucosidase activity, *FEBS Lett* 436 (1998) 71-75.

- [122] A.J. Day, F.J. Canada, J.C. Diaz, P.A. Kroon, R. Mclauchlan, C.B. Faulds, G.W. Plumb, M.R.A. Morgan, G. Williamson, Dietary flavonoid and isoflavone glycosides are hydrolysed by the lactase site of lactase phlorizin hydrolase, *FEBS Lett* 468 (2000) 166-170.
- [123] J.M. Gee, M.S. DuPont, A.J. Day, G.W. Plumb, G. Williamson, I.T. Johnson, Intestinal transport of quercetin glycosides in rats involves both deglycosylation and interaction with the hexose transport pathway, *J Nutr* 130 (2000) 2765-2771.
- [124] K. Nemeth, G.W. Plumb, J.G. Berrin, N. Juge, R. Jacob, H.Y. Naim, G. Williamson, D.M. Swallow, P.A. Kroon, Deglycosylation by small intestinal epithelial cell beta-glucosidases is a critical step in the absorption and metabolism of dietary flavonoid glycosides in humans, *European Journal of Nutrition* 42 (2003) 29-42.
- [125] K. Németh, G.W. Plumb, J.-G. Berrin, N. Juge, R. Jacob, H.Y. Naim, G. Williamson, D.M. Swallow, P.A. Kroon, Deglycosylation by small intestinal epithelial cell β -glucosidases is a critical step in the absorption and metabolism of dietary flavonoid glycosides in humans, *Eur J Nutr* 42 (2003) 29-42.
- [126] H.K. Chang, M.S. Shin, H.Y. Yang, J.W. Lee, Y.S. Kim, M.H. Lee, J. Kim, K.H. Kim, C.J. Kim, Amygdalin induces apoptosis through regulation of Bax and Bcl-2 expressions in human DU145 and LNCaP prostate cancer cells, *Biol Pharm Bull* 29 (2006) 1597-1602.
- [127] T. Walle, Absorption and metabolism of flavonoids, *Free Radical Biol Med* 36 (2004) 829-837.
- [128] Y. Zhang, T.T. Song, J.E. Cunnick, P.A. Murphy, S. Hendrich, Daidzein and genistein glucuronides in vitro are weakly estrogenic and activate human natural killer cells at nutritionally relevant concentrations, *J Nutr* 129 (1999) 399-405.
- [129] M. Harada, Y. Kan, H. Naoki, Y. Fukui, N. Kageyama, M. Nakai, W. Miki, Y. Kiso, Identification of the major antioxidative metabolites in biological fluids of the rat with ingested (+)-catechin and (-)-epicatechin, *Biosci, Biotechnol, Biochem* 63 (1999) 973-977.
- [130] B. Wu, K. Kulkarni, S. Basu, S. Zhang, M. Hu, First-pass metabolism via UDP-glucuronosyltransferase: a barrier to oral bioavailability of phenolics, *J Pharm Sci* 100 (2011) 3655-3681.
- [131] A.J. Day, Y. Bao, M.R.A. Morgan, G. Williamson, Conjugation position of quercetin glucuronides and effect on biological activity, *Free Radical Biol Med* 29 (2000) 1234-1243.
- [132] A.J. Day, Y.P. Bao, M.R.A. Morgan, G. Williamson, Conjugation position of quercetin glucuronides and effect on biological activity, *Free Radical Biology and Medicine* 29 (2000) 1234-1243.
- [133] B. Wu, S. Basu, S. Meng, X. Wang, M. Hu, Regioselective sulfation and glucuronidation of phenolics: insights into the structural basis, *Curr Drug Metab* 12 (2011) 900-916.
- [134] L. Tang, J. Zhou, C.-H. Yang, B.-J. Xia, M. Hu, Z.-Q. Liu, Systematic Studies of Sulfation and Glucuronidation of 12 Flavonoids in the Mouse Liver S9 Fraction Reveal both Unique and Shared Positional Preferences, *J Agric Food Chem* 60 (2012) 3223-3233.
- [135] R.H. Lewinsky, P.A. Smith, P.I. Mackenzie, Glucuronidation of bioflavonoids by human UGT1A10: structure-function relationships, *Xenobiotica* 35 (2005) 117-129.
- [136] K. Shimoi, N. Saka, R. Nozawa, M. Sato, I. Amano, T. Nakayama, N. Kinoshita, Deglucuronidation of a flavonoid, luteolin monoglucuronide, during inflammation, *Drug Metab Dispos* 29 (2001) 1521-1524.
- [137] S. Meng, B. Wu, R. Singh, T. Yin, J.K. Morrow, S. Zhang, M. Hu, SULT1A3-mediated regiospecific 7-O-sulfation of flavonoids in Caco-2 cells can be explained by the relevant molecular docking studies, *Mol Pharm* 9 (2012) 862-873.
- [138] C.H. Yang, L. Tang, C. Lv, L. Ye, B.J. Xia, M. Hu, Z.Q. Liu, Sulfation of selected monohydroxyflavones by sulfotransferases in vitro: a species and gender comparison, *J Pharm Pharmacol* 63 (2011) 967-970.
- [139] M.M. Elias, G.C. Lunazzi, S. Passamonti, B. Gazzin, M. Miccio, G. Stanta, G.L. Sottocasa, C. Tiribelli, Bilirubin translocase localization and function in basolateral plasma-membrane of renal proximal tubule in rat, *Am J Physiol* 259 (1990) F559-F564.

- [140] W. Brand, M.E. Schutte, G. Williamson, J.J. van Zanden, N.H.P. Cnubben, J.P. Groten, P.J. van Bladeren, I.M.C.M. Rietjens, Flavonoid-mediated inhibition of intestinal ABC transporters may affect the oral bioavailability of drugs, food-borne toxic compounds and bioactive ingredients, *Biomedicine & Pharmacotherapy* 60 (2006) 508-519.
- [141] X.J. Tian, X.W. Yang, X.D. Yang, K. Wang, Studies of intestinal permeability of 36 flavonoids using Caco-2 cell monolayer model, *International Journal of Pharmaceutics* 367 (2009) 58-64.
- [142] M. Takano, R. Yumoto, T. Murakami, Expression and function of efflux drug transporters in the intestine, *Pharmacol Ther* 109 (2006) 137-161.
- [143] C.G. Dietrich, A. Geier, R.P.J.O. Elferink, ABC of oral bioavailability: transporters as gatekeepers in the gut, *Gut* 52 (2003) 1788-1795.
- [144] L.M.S. Chan, S. Lowes, B.H. Hirst, The ABCs of drug transport in intestine and liver: efflux proteins limiting drug absorption and bioavailability, *Eur J Pharm Sci* 21 (2004) 25-51.
- [145] G.L. Scheffer, M. Kool, M. de Haas, J.M.L. de Vree, A.C.L.M. Pijnenborg, D.K. Bosman, R.P.J.O. Elferink, P. van der Valk, P. Borst, R.J. Scheper, Tissue distribution and induction of human multidrug resistant protein 3, *Lab Invest* 82 (2002) 193-201.
- [146] H.M. Prime-Chapman, R.A. Fearn, A.E. Cooper, V. Moore, B.H. Hirst, Differential multidrug resistance-associated protein 1 through 6 isoform expression and function in human intestinal epithelial Caco-2 cells, *J Pharmacol Exp Ther* 311 (2004) 476-484.
- [147] T. Hirohashi, H. Suzuki, X.Y. Chu, I. Tamai, A. Tsuji, Y. Sugiyama, Function and expression of multidrug resistance-associated protein family in human colon adenocarcinoma cells (Caco-2), *J Pharmacol Exp Ther* 292 (2000) 265-270.
- [148] J. Taipalensuu, H. Tornblom, G. Lindberg, C. Einarsson, F. Sjoqvist, H. Melhus, P. Garberg, B. Sjoström, B. Lundgren, P. Artursson, Correlation of gene expression of ten drug efflux proteins of the ATP-binding cassette transporter family in normal human jejunum and in human intestinal epithelial Caco-2 cell monolayers, *J Pharmacol Exp Ther* 299 (2001) 164-170.
- [149] E.C.M. de Lange, Potential role of ABC transporters as a detoxification system at the blood-CSF barrier, *Adv Drug Del Rev* 56 (2004) 1793-1809.
- [150] A.I. Alvarez, R. Real, M. Perez, G. Mendoza, J.G. Prieto, G. Merino, Modulation of the activity of ABC transporters (P-glycoprotein, MRP2, BCRP) by flavonoids and drug response, *J Pharm Sci* 99 (2010) 598-617.
- [151] A. Boumendjel, A. Di Pietro, C. Dumontet, D. Barron, Recent advances in the discovery of flavonoids and analogs with high-affinity binding to P-glycoprotein responsible for cancer cell multidrug resistance, *Med Res Rev* 22 (2002) 512-529.
- [152] G. Kothandan, C.G. Gadhe, T. Madhavan, C.H. Choi, S.J. Cho, Docking and 3D-QSAR (quantitative structure activity relationship) studies of flavones, the potent inhibitors of p-glycoprotein targeting the nucleotide binding domain, *Eur J Med Chem* 46 (2011) 4078-4088.
- [153] M.E. Morris, S. Zhang, Flavonoid-drug interactions: effects of flavonoids on ABC transporters, *Life Sci* 78 (2006) 2116-2130.
- [154] E. Nicolle, J. Boccard, D. Guilet, M.-G. Dijoux-Franca, F. Zelefac, S. Macalou, J. Grosselin, J. Schmidt, P.-A. Carrupt, A. Di Pietro, A. Boumendjel, Breast cancer resistance protein (BCRP/ABCG2): New inhibitors and QSAR studies by a 3D linear solvation energy approach, *Eur J Pharm Sci* 38 (2009) 39-46.
- [155] G. Conseil, H. Baubichon-Cortay, G. Dayan, J.M. Jault, D. Barron, A. Di Pietro, Flavonoids: a class of modulators with bifunctional interactions at vicinal ATP- and steroid-binding sites on mouse P-glycoprotein, *Proc Natl Acad Sci U S A* 95 (1998) 9831-9836.
- [156] G. Conseil, A. Decottignies, J.M. Jault, G. Comte, D. Barron, A. Goffeau, A. Di Pietro, Prenyl-flavonoids as potent inhibitors of the Pdr5p multidrug ABC transporter from *Saccharomyces cerevisiae*, *Biochemistry (Mosc)* 39 (2000) 6910-6917.
- [157] M.T. Sheu, Y.B. Liou, Y.H. Kao, Y.K. Lin, H.O. Ho, A quantitative structure-activity relationship for the modulation effects of flavonoids on p-glycoprotein-mediated transport, *Chem Pharm Bull (Tokyo)* 58 (2010) 1187-1194.

- [158] J.J. van Zanden, H.M. Wortelboer, S. Bijlsma, A. Punt, M. Usta, P.J.v. Bladeren, I.M.C.M. Rietjens, N.H.P. Cnubben, Quantitative structure activity relationship studies on the flavonoid mediated inhibition of multidrug resistance proteins 1 and 2, *Biochem Pharmacol* 69 (2005) 699-708.
- [159] S. Zhang, X. Yang, R.A. Coburn, M.E. Morris, Structure activity relationships and quantitative structure activity relationships for the flavonoid-mediated inhibition of breast cancer resistance protein, *Biochem Pharmacol* 70 (2005) 627-639.
- [160] K. Katayama, K. Masuyama, S. Yoshioka, H. Hasegawa, J. Mitsuhashi, Y. Sugimoto, Flavonoids inhibit breast cancer resistance protein-mediated drug resistance: transporter specificity and structure–activity relationship, *Cancer Chemother Pharmacol* 60 (2007) 789-797.
- [161] A. Ahmed-Belkacem, A. Pozza, F. Muñoz-Martínez, S.E. Bates, S. Castanys, F. Gamarro, A. Di Pietro, J.M. Pérez-Victoria, Flavonoid Structure-Activity Studies Identify 6-Prenylchrysin and Tectochrysin as Potent and Specific Inhibitors of Breast Cancer Resistance Protein ABCG2, *Cancer Res* 65 (2005) 4852-4860.
- [162] A. Bolli, M. Marino, G. Rimbach, G. Fanali, M. Fasano, P. Ascenzi, Flavonoid binding to human serum albumin, *Biochem Biophys Res Commun* 398 (2010) 444-449.
- [163] F. Zsila, Z. Bikadi, M. Simonyi, Probing the binding of the flavonoid, quercetin to human serum albumin by circular dichroism, electronic absorption spectroscopy and molecular modelling methods, *Biochem Pharmacol* 65 (2003) 447-456.
- [164] J. Xiao, G. Kai, A Review of Dietary Polyphenol-Plasma Protein Interactions: Characterization, Influence on the Bioactivity, and Structure-Affinity Relationship, *Crit Rev Food Sci Nutr* 52 (2011) 85-101.
- [165] D.A. Smith, L. Di, E.H. Kerns, The effect of plasma protein binding on in vivo efficacy: misconceptions in drug discovery, *Nat Rev Drug Discov* 9 (2010) 929-939.
- [166] J. Terao, K. Murota, Y. Kawai, Conjugated quercetin glucuronides as bioactive metabolites and precursors of aglycone in vivo, *Food & Function* 2 (2011) 11-17.
- [167] F. Perez-Vizcaino, J. Duarte, C. Santos-Buelga, The flavonoid paradox: conjugation and deconjugation as key steps for the biological activity of flavonoids, *J Sci Food Agric* 92 (2012) 1822-1825.
- [168] D.H. Kim, E.A. Jung, I.S. Sohng, J.A. Han, T.H. Kim, M.J. Han, Intestinal bacterial metabolism of flavonoids and its relation to some biological activities, *Arch Pharmacol Res* 21 (1998) 17-23.
- [169] K.A. O'Leary, A.J. Day, P.W. Needs, F.A. Mellon, N.M. O'Brien, G. Williamson, Metabolism of quercetin-7- and quercetin-3-glucuronides by an in vitro hepatic model: the role of human beta-glucuronidase, sulfotransferase, catechol-O-methyltransferase and multi-resistant protein 2 (MRP2) in flavonoid metabolism, *Biochem Pharmacol* 65 (2003) 479-491.
- [170] N. Oi, T. Hashimoto, K. Kanazawa, Metabolic conversion of dietary quercetin from its conjugate to active aglycone following the induction of hepatocarcinogenesis in fisher 344 rats, *J Agric Food Chem* 56 (2008) 577-583.
- [171] J. Bieger, R. Cermak, R. Blank, V.C.J. de Boer, P.C.H. Hollman, J. Kamphues, S. Wolfram, Tissue distribution of quercetin in pigs after long-term dietary supplementation, *J Nutr* 138 (2008) 1417-1420.
- [172] A. Rodriguez-Mateos, N. Toro-Funes, T. Cifuentes-Gomez, M. Cortese-Krott, C. Heiss, J.P.E. Spencer, Uptake and metabolism of (-)-epicatechin in endothelial cells, *Arch Biochem Biophys* 559 (2014) 17-23.
- [173] O. Naomi, H. Takashi, K. Kazuki, in *Functional Food and Health*, American Chemical Society, 2008, p. 102-107.
- [174] A. Ishisaka, K. Kawabata, S. Miki, Y. Shiba, S. Minekawa, T. Nishikawa, R. Mukai, J. Terao, Y. Kawai, Mitochondrial dysfunction leads to deconjugation of quercetin glucuronides in inflammatory macrophages, *PLoS ONE* 8 (2013) e80843.
- [175] C. Menendez, M. Duenas, P. Galindo, S. Gonzalez-Manzano, R. Jimenez, L. Moreno, M.J. Zarzuelo, I. Rodriguez-Gomez, J. Duarte, C. Santos-Buelga, F. Perez-Vizcaino, *Vascular*

- deconjugation of quercetin glucuronide: the flavonoid paradox revealed?, *Mol Nutr Food Res* 55 (2011) 1780-1790.
- [176] S.P. Zhang, Y.J. Zhou, Y. Liu, Y.Q. Cai, Effect of liquiritigenin, a flavanone existed from *Radix glycyrrhizae* on pro-apoptotic in SMMC-7721 cells, *Food Chem Toxicol* 47 (2009) 693-701.
- [177] Y.J. Choi, J.S. Kang, J.H.Y. Park, Y.J. Lee, J.S. Choi, Y.H. Kang, Polyphenolic flavonoids differ in their antiapoptotic efficacy in hydrogen peroxide-treated human vascular endothelial cells (vol 133, pg 985, 2003), *J Nutr* 133 (2003) 2394-2394.
- [178] P.G. Pietta, Flavonoids as antioxidants, *J Nat Prod* 63 (2000) 1035-1042.
- [179] I. Rodriguez-Ramiro, M.A. Martin, S. Ramos, L. Bravo, L. Goya, Comparative effects of dietary flavanols on antioxidant defences and their response to oxidant-induced stress on Caco2 cells, *Eur J Nutr* 50 (2011) 313-322.
- [180] C. Rice-Evans, Flavonoids and isoflavones: Absorption, metabolism, and bioactivity, *Free Radical Biol Med* 36 (2004) 827-828.
- [181] K.M. Min, S.E. Ebeler, Quercetin inhibits hydrogen peroxide-induced DNA damage and enhances DNA repair in Caco-2 cells, *Food Chem Toxicol* 47 (2009) 2716-2722.
- [182] A.I. Potapovich, V.A. Kostyuk, Comparative study of antioxidant properties and cytoprotective activity of flavonoids, *Biochemistry-Moscow* 68 (2003) 514-519.
- [183] F. Ursini, M. Maiorino, P. Morazzoni, A. Roveri, G. Pifferi, A Novel Antioxidant Flavonoid (Idb-1031) Affecting Molecular Mechanisms of Cellular Activation, *Free Radical Biol Med* 16 (1994) 547-553.
- [184] Y. Hanasaki, S. Ogawa, S. Fukui, The Correlation between Active Oxygens Scavenging and Antioxidative Effects of Flavonoids, *Free Radical Biol Med* 16 (1994) 845-850.
- [185] J.E. Brown, H. Khodr, R.C. Hider, C.A. Rice-Evans, Structural dependence of flavonoid interactions with Cu²⁺ ions: implications for their antioxidant properties, *Biochem J* 330 (1998) 1173-1178.
- [186] K. Keyer, J.A. Imlay, Superoxide accelerates DNA damage by elevating free-iron levels, *Proc Natl Acad Sci U S A* 93 (1996) 13635-13640.
- [187] T.D. Rae, P.J. Schmidt, R.A. Pufahl, V.C. Culotta, T.V. O'Halloran, Undetectable intracellular free copper: The requirement of a copper chaperone for superoxide dismutase, *Science* 284 (1999) 805-808.
- [188] S. Valcic, A. Muders, N.E. Jacobsen, D.C. Liebler, B.N. Timmermann, Antioxidant chemistry of green tea catechins. Identification of products of the reaction of (-)-epigallocatechin gallate with peroxy radicals, *Chem Res Toxicol* 12 (1999) 382-386.
- [189] T. Sawa, M. Nakao, T. Akaike, K. Ono, H. Maeda, Alkylperoxy radical-scavenging activity of various flavonoids and other phenolic compounds: Implications for the anti-tumor-promoter effect of vegetables, *J Agric Food Chem* 47 (1999) 397-402.
- [190] Z.H. Gao, K.X. Huang, X.L. Yang, H.B. Xu, Free radical scavenging and antioxidant activities of flavonoids extracted from the radix of *Scutellaria baicalensis* Georgi, *Biochimica Et Biophysica Acta-General Subjects* 1472 (1999) 643-650.
- [191] A.J. Dugas, J. Castaneda-Acosta, G.C. Bonin, K.L. Price, N.H. Fischer, G.W. Winston, Evaluation of the total peroxy radical-scavenging capacity of flavonoids: Structure-activity relationships, *J Nat Prod* 63 (2000) 327-331.
- [192] J.W. Chen, Z.Q. Zhu, T.X. Hu, D.Y. Zhu, Structure-activity relationship of natural flavonoids in hydroxyl radical-scavenging effects, *Acta Pharmacol Sin* 23 (2002) 667-672.
- [193] G.E. Arteel, P. Schroeder, H. Sies, Reactions of peroxy nitrite with cocoa procyanidin oligomers, *J Nutr* 130 (2000) 2100s-2104s.
- [194] G.R. Buettner, The Pecking Order of Free-Radicals and Antioxidants - Lipid-Peroxidation, Alpha-Tocopherol, and Ascorbate, *Arch Biochem Biophys* 300 (1993) 535-543.
- [195] R. Masella, R. Di Benedetto, R. Vari, C. Filesi, C. Giovannini, Novel mechanisms of natural antioxidant compounds in biological systems: Involvement of glutathione and glutathione-related enzymes, *Journal of Nutritional Biochemistry* 16 (2005) 577-586.

- [196] A. Argyrou, J.S. Blanchard, Flavoprotein disulfide reductases: Advances in chemistry and function, *Progress in Nucleic Acid Research and Molecular Biology*, Vol 78 78 (2004) 89-142.
- [197] J. Cadet, T. Douki, D. Gasparutto, J.L. Ravanat, Oxidative damage to DNA: formation, measurement and biochemical features, *Mutat Res-Fundam Mol Mech Mutag* 531 (2003) 5-23.
- [198] A.A. Ramos, C. Pereira-Wilson, A.R. Collins, Protective effects of Ursolic acid and Luteolin against oxidative DNA damage include enhancement of DNA repair in Caco-2 cells, *Mutat Res-Fundam Mol Mech Mutag* 692 (2010) 6-11.
- [199] G. Fritz, Human APE/Ref-1 protein, *International Journal of Biochemistry & Cell Biology* 32 (2000) 925-929.
- [200] K. Ramadan, I. Shevelev, U. Hubscher, The DNA-polymerase-X family: controllers of DNA quality?, *Nature Reviews Molecular Cell Biology* 5 (2004) 1038-1043.
- [201] C.L. Powell, J.A. Swenberg, I. Rusyn, Expression of base excision DNA repair genes as a biomarker of oxidative DNA damage, *Cancer Lett* 229 (2005) 1-11.
- [202] T.K. Hazra, A. Das, S. Das, S. Choudhury, Y.W. Kow, R. Roy, Oxidative DNA damage repair in mammalian cells: A new perspective, *DNA Repair* 6 (2007) 470-480.
- [203] V. Abalea, J. Cillard, M.P. Dubos, O. Sergent, P. Cillard, I. Morel, Repair of iron-induced DNA oxidation by the flavonoid myricetin in primary rat hepatocyte cultures, *Free Radical Biol Med* 26 (1999) 1457-1466.
- [204] K. Gao, S.M. Henning, Y.T. Niu, A.A. Youssefian, N.P. Seeram, A.L. Xu, D. Heber, The citrus flavonoid naringenin stimulates DNA repair in prostate cancer cells, *Journal of Nutritional Biochemistry* 17 (2006) 89-95.
- [205] M. Francisco, D.A. Moreno, M.E. Cartea, F. Ferreres, C. Garcia-Viguera, P. Velasco, Simultaneous identification of glucosinolates and phenolic compounds in a representative collection of vegetable Brassica rapa, *J Chromatogr A* 1216 (2009) 6611-6619.
- [206] H. Olsen, K. Aaby, G.I.A. Borge, Characterization, Quantification, and Yearly Variation of the Naturally Occurring Polyphenols in a Common Red Variety of Curly Kale (*Brassica oleracea* L. convar. acephala var. sabellica cv. 'Redbor'), *J Agric Food Chem* 58 (2010) 11346-11354.
- [207] L. Actis-Goretta, J.I. Ottaviani, C.G. Fraga, Inhibition of Angiotensin Converting Enzyme Activity by Flavanol-Rich Foods, *J Agric Food Chem* 54 (2005) 229-234.
- [208] M. Wrona, T. Mauriala, K.P. Bateman, R.J. Mortishire-Smith, D. O'Connor, 'All-in-one' analysis for metabolite identification using liquid chromatography/hybrid quadrupole time-of-flight mass spectrometry with collision energy switching, *Rapid Commun Mass Spectrom* 19 (2005) 2597-2602.
- [209] S.M. Ni, D.W. Qian, J.A. Duan, J.M. Guo, E.X. Shang, Y. Shu, C.F. Xue, UPLC-QTOF/MS-based screening and identification of the constituents and their metabolites in rat plasma and urine after oral administration of Glechoma longituba extract, *Journal of Chromatography B-Analytical Technologies in the Biomedical and Life Sciences* 878 (2010) 2741-2750.
- [210] L.P. Kang, K.T. Yu, Y. Zhao, Y.X. Liu, H.S. Yu, X. Pang, C.Q. Xiong, D.W. Tan, Y. Gao, C. Liu, B.P. Ma, Characterization of steroidal glycosides from the extract of Paris Polyphylla var. Yunnanensis by UPLC/Q-TOF MSE, *J Pharm Biomed Anal* 62 (2012) 235-249.
- [211] R.S. Plumb, K.A. Johnson, P. Rainville, B.W. Smith, I.D. Wilson, J.M. Castro-Perez, J.K. Nicholson, UPLC/MSE; a new approach for generating molecular fragment information for biomarker structure elucidation, *Rapid Commun Mass Spectrom* 20 (2006) 1989-1994.
- [212] K.P. Bateman, J. Castro-Perez, M. Wrona, J.P. Shockcor, K. Yu, R. Oballa, D.A. Nicoll-Griffith, MSE with mass defect filtering for in vitro and in vivo metabolite identification, *Rapid Commun Mass Spectrom* 21 (2007) 1485-1496.
- [213] C. Xie, K. Yu, D. Zhong, T. Yuan, F. Ye, J.A. Jarrell, A. Millar, X. Chen, Investigation of Isomeric Transformations of Chlorogenic Acid in Buffers and Biological Matrixes by Ultraperformance Liquid Chromatography Coupled with Hybrid Quadrupole/Ion Mobility/Orthogonal Acceleration Time-of-Flight Mass Spectrometry, *J Agric Food Chem* 59 (2011) 11078-11087.

- [214] S. Garmon-Lobato, B. Abad-Garcia, M.B. Sanchez-Ilarduya, M. Romera-Fernandez, L.A. Berrueta, B. Gallo, F. Vicente, Improvement using chemometrics in ion mobility coupled to mass spectrometry as a tool for mass spectrometry fragmentation studies: Flavonoid aglycone cases, *Anal Chim Acta* 771 (2013) 56-64.
- [215] I. Michaelevski, N. Kirshenbaum, M. Sharon, T-wave ion mobility-mass spectrometry: basic experimental procedures for protein complex analysis, *Journal of Visualized Experiments* 41 (2010) 1985.
- [216] A.B. Kanu, P. Dwivedi, M. Tam, L. Matz, H.H. Hill, Jr., Ion mobility-mass spectrometry, *J Mass Spectrom* 43 (2008) 1-22.
- [217] B. Harbaum, E.M. Hubbermann, Z. Zhu, K. Schwarz, Free and bound phenolic compounds in leaves of pak choi (*Brassica campestris* L. ssp. *chinensis* var. *communis*) and Chinese leaf mustard (*Brassica juncea* Coss), *Food Chem* 110 (2008) 838-846.
- [218] B. Harbaum, E.M. Hubbermann, C. Wolff, R. Herges, Z. Zhu, K. Schwarz, Identification of Flavonoids and Hydroxycinnamic Acids in Pak Choi Varieties (*Brassica campestris* L. ssp. *chinensis* var. *communis*) by HPLC-ESI-MS n and NMR and Their Quantification by HPLC-DAD, *J Agric Food Chem* 55 (2007) 8251-8260.
- [219] M.E. Cartea, M. Francisco, P. Soengas, P. Velasco, Phenolic Compounds in Brassica Vegetables, *Molecules* 16 (2010) 251-280.
- [220] L.-Z. Lin, J. Sun, P. Chen, J. Harnly, UHPLC-PDA-ESI/HRMS/MSⁿ Analysis of Anthocyanins, Flavonol Glycosides, and Hydroxycinnamic Acid Derivatives in Red Mustard Greens (*Brassica juncea* Coss Variety), *J Agric Food Chem* 59 (2011) 12059-12072.
- [221] P. Soengas, M.E. Cartea, M. Francisco, T. Sotelo, P. Velasco, New insights into antioxidant activity of Brassica crops, *Food Chem* 134 (2012) 725-733.
- [222] P. Velasco, M. Francisco, D.A. Moreno, F. Ferreres, C. García-Viguera, M.E. Cartea, Phytochemical fingerprinting of vegetable *Brassica oleracea* and *Brassica napus* by simultaneous identification of glucosinolates and phenolics, *Phytochem Anal* 22 (2011) 144-152.
- [223] R. Llorach, J.C. Espín, F.A. Tomás-Barberán, F. Ferreres, Valorization of Cauliflower (*Brassica oleracea* L. var. *botrytis*) By-Products as a Source of Antioxidant Phenolics, *J Agric Food Chem* 51 (2003) 2181-2187.
- [224] R. Llorach, A. Gil-Izquierdo, F. Ferreres, F.A. Tomás-Barberán, HPLC-DAD-MS/MS ESI Characterization of Unusual Highly Glycosylated Acylated Flavonoids from Cauliflower (*Brassica oleracea* L. var. *botrytis*) Agroindustrial Byproducts, *J Agric Food Chem* 51 (2003) 3895-3899.
- [225] H. Olsen, K. Aaby, G.I.A. Borge, Characterization and Quantification of Flavonoids and Hydroxycinnamic Acids in Curly Kale (*Brassica oleracea* L. Convar. *acephala* Var. *sabellica*) by HPLC-DAD-ESI-MSⁿ, *J Agric Food Chem* 57 (2009) 2816-2825.
- [226] F. Cuyckens, Y. Ma, L., G. Pocsfalvi, M. Claeys, Tandem mass spectral strategies for the structural characterization of flavonoid glycosides, *Analisis* 28 (2000) 888-895.
- [227] A.A. Shahat, F. Cuyckens, W. Wang, K.A. Abdel-Shafeek, H.A. Hussein, S. Apers, S. Van Miert, L. Pieters, A.J. Vlietinck, M. Claeys, Structural characterization of flavonol di-O-glycosides from *Farsetia aegyptia* by electrospray ionization and collision-induced dissociation mass spectrometry, *Rapid Commun Mass Spectrom* 19 (2005) 2172-2178.
- [228] F. Cuyckens, M. Claeys, Determination of the glycosylation site in flavonoid mono-O-glycosides by collision-induced dissociation of electrospray-generated deprotonated and sodiated molecules, *J Mass Spectrom* 40 (2005) 364-372.
- [229] R.E. March, X.-S. Miao, C.D. Metcalfe, A fragmentation study of a flavone triglycoside, kaempferol-3-O-robinoside-7-O-rhamnoside, *Rapid Commun Mass Spectrom* 18 (2004) 931-934.
- [230] B.D. Davis, J.S. Brodbelt, Regioselectivity of human UDP-glucuronosyl-transferase 1A1 in the synthesis of flavonoid glucuronides determined by metal complexation and tandem mass spectrometry, *J Am Soc Mass Spectrom* 19 (2008) 246-256.

- [231] P.V. Shliaha, N.J. Bond, L. Gatto, K.S. Lilley, Effects of traveling wave ion mobility separation on data independent acquisition in proteomics studies, *J Proteome Res* 12 (2013) 2323-2339.
- [232] J.A. McLean, B.T. Ruotolo, K.J. Gillig, D.H. Russell, Ion mobility–mass spectrometry: a new paradigm for proteomics, *Int. J. Mass. Spectrom.* 240 (2005) 301-315.
- [233] F. Saura-Calixto, Concept and Health-Related Properties of Nonextractable Polyphenols: The Missing Dietary Polyphenols, *J Agric Food Chem* 60 (2012) 11195-11200.
- [234] S. Arranz, F. Saura-Calixto, S. Shaha, P.A. Kroon, High Contents of Nonextractable Polyphenols in Fruits Suggest That Polyphenol Contents of Plant Foods Have Been Underestimated, *J Agric Food Chem* 57 (2009) 7298-7303.
- [235] J. Perez-Jimenez, F. Saura-Calixto, Literature Data May Underestimate the Actual Antioxidant Capacity of Cereals, *J Agric Food Chem* 53 (2005) 5036-5040.
- [236] J. Pérez-Jiménez, J.L. Torres, Analysis of Nonextractable Phenolic Compounds in Foods: The Current State of the Art, *J Agric Food Chem* 59 (2011) 12713-12724.
- [237] S. Arranz, J.M. Silván, F. Saura-Calixto, Nonextractable polyphenols, usually ignored, are the major part of dietary polyphenols: A study on the Spanish diet, *Mol Nutr Food Res* 54 (2010) 1646-1658.
- [238] M. Bonoli, V. Verardo, E. Marconi, M.F. Caboni, Antioxidant Phenols in Barley (*Hordeum vulgare* L.) Flour: Comparative Spectrophotometric Study among Extraction Methods of Free and Bound Phenolic Compounds, *J Agric Food Chem* 52 (2004) 5195-5200.
- [239] B.L. White, L.R. Howard, R.L. Prior, Release of bound procyanidins from cranberry pomace by alkaline hydrolysis, *J Agric Food Chem* 58 (2010) 7572-7579.
- [240] T. Albishi, J.A. John, A.S. Al-Khalifa, F. Shahidi, Phenolic content and antioxidant activities of selected potato varieties and their processing by-products, *Journal of Functional Foods* 5 (2013) 590-600.
- [241] W.W. Tow, R. Premier, H. Jing, S. Ajlouni, Antioxidant and Antiproliferation Effects of Extractable and Nonextractable Polyphenols Isolated from Apple Waste Using Different Extraction Methods, *J Food Sci* 76 (2011) T163-T172.
- [242] A. Frolov, A. Henning, C. Böttcher, A. Tissier, D. Strack, An UPLC-MS/MS Method for the Simultaneous Identification and Quantitation of Cell Wall Phenolics in Brassica napus Seeds, *J Agric Food Chem* 61 (2012) 1219-1227.
- [243] C.-H. Kuo, B.-Y. Chen, Y.-C. Liu, C.-M. Chang, T.-S. Deng, J.-H. Chen, C.-J. Shieh, Optimized Ultrasound-Assisted Extraction of Phenolic Compounds from *Polygonum cuspidatum*, *Molecules* 19 (2013) 67-77.
- [244] D.B. Muñoz-Márquez, G.C. Martínez-Ávila, J.E. Wong-Paz, R. Belmares-Cerda, R. Rodríguez-Herrera, C.N. Aguilar, Ultrasound-assisted extraction of phenolic compounds from *Laurus nobilis* L. and their antioxidant activity, *Ultrason Sonochem* 20 (2013) 1149-1154.
- [245] Z. Izadifar, Ultrasound pretreatment of wheat dried distiller's grain (DDG) for extraction of phenolic compounds, *Ultrason Sonochem* 20 (2013) 1359-1369.
- [246] A. Golmohamadi, G. Möller, J. Powers, C. Nindo, Effect of ultrasound frequency on antioxidant activity, total phenolic and anthocyanin content of red raspberry puree, *Ultrason Sonochem* 20 (2013) 1316-1323.
- [247] D. Horžić, A. Jambrak, A. Belščak-Cvitanović, D. Komes, V. Lelas, Comparison of Conventional and Ultrasound Assisted Extraction Techniques of Yellow Tea and Bioactive Composition of Obtained Extracts, *Food and Bioprocess Technology* 5 (2012) 2858-2870.
- [248] V.L. Singleton, R. Orthofer, R.M. Lamuela-Raventos, in L. Packer (Editor), *Oxidants and Antioxidants*, Pt A, Elsevier Academic Press Inc, San Diego, 1999, p. 152-178.
- [249] P. Mattila, J. Hellström, Phenolic acids in potatoes, vegetables, and some of their products, *Journal of Food Composition and Analysis* 20 (2007) 152-160.
- [250] F.A. Ayaz, S. Hayırlıoglu-Ayaz, S. Alpay-Karaoglu, J. Grúz, K. Valentová, J. Ulrichová, M. Strnad, Phenolic acid contents of kale (*Brassica oleracea* L. var. *acephala* DC.) extracts and their antioxidant and antibacterial activities, *Food Chem* 107 (2008) 19-25.

- [251] Q. Liu, L. Wu, H. Pu, C. Li, Q. Hu, Profile and distribution of soluble and insoluble phenolics in Chinese rapeseed (*Brassica napus*), *Food Chem* 135 (2012) 616-622.
- [252] Y. Lee, L.R. Howard, B. Villalón, Flavonoids and Antioxidant Activity of Fresh Pepper (*Capsicum annuum*) Cultivars, *J Food Sci* 60 (1995) 473-476.
- [253] G. Singh, P. Kumar, Phytochemical study and screening for antimicrobial activity of flavonoids of *Euphorbia hirta*, *Int J Appl Basic Med Res* 3 (2013) 111-116.
- [254] G. Agati, G. Stefano, S. Biricolti, M. Tattini, Mesophyll distribution of 'antioxidant' flavonoid glycosides in *Ligustrum vulgare* leaves under contrasting sunlight irradiance, *Ann Bot* 104 (2009) 853-861.
- [255] Z. Yang, Y. Han, Z. Gu, G. Fan, Z. Chen, Thermal degradation kinetics of aqueous anthocyanins and visual color of purple corn (*Zea mays* L.) cob, *Innovative Food Science & Emerging Technologies* 9 (2008) 341-347.
- [256] P. Arapitsas, C. Turner, Pressurized solvent extraction and monolithic column-HPLC/DAD analysis of anthocyanins in red cabbage, *Talanta* 74 (2008) 1218-1223.
- [257] G.J. McDougall, S. Fyffe, P. Dobson, D. Stewart, Anthocyanins from red cabbage – stability to simulated gastrointestinal digestion, *Phytochemistry* 68 (2007) 1285-1294.
- [258] B. Kuznierewicz, R. Iori, A. Piekarska, J. Namiesnik, A. Bartoszek, Convenient identification of desulfoglucosinolates on the basis of mass spectra obtained during liquid chromatography-diode array-electrospray ionisation mass spectrometry analysis: method verification for sprouts of different Brassicaceae species extracts, *J Chromatogr A* 1278 (2013) 108-115.
- [259] D. Heimler, P. Vignolini, M.G. Dini, F.F. Vincieri, A. Romani, Antiradical activity and polyphenol composition of local Brassicaceae edible varieties, *Food Chem* 99 (2006) 464-469.
- [260] T.K. Smith, E.K. Lund, R.G. Clarke, R.N. Bennett, I.T. Johnson, Effects of Brussels Sprout Juice on the Cell Cycle and Adhesion of Human Colorectal Carcinoma Cells (HT29) in Vitro, *J Agric Food Chem* 53 (2005) 3895-3901.
- [261] S.-L. Li, J.-Z. Song, C.-F. Qiao, Y. Zhou, K. Qian, K.-H. Lee, H.-X. Xu, A novel strategy to rapidly explore potential chemical markers for the discrimination between raw and processed *Radix Rehmanniae* by UHPLC–TOFMS with multivariate statistical analysis, *J Pharm Biomed Anal* 51 (2010) 812-823.
- [262] P. Arapitsas, P.J.R. Sjöberg, C. Turner, Characterisation of anthocyanins in red cabbage using high resolution liquid chromatography coupled with photodiode array detection and electrospray ionization-linear ion trap mass spectrometry, *Food Chem* 109 (2008) 219-226.
- [263] C.S. Charron, B.A. Clevidence, S.J. Britz, J.A. Novotny, Effect of Dose Size on Bioavailability of Acylated and Nonacylated Anthocyanins from Red Cabbage (*Brassica oleracea* L. Var. *capitata*), *J Agric Food Chem* 55 (2007) 5354-5362.
- [264] D.S. Wishart, Metabolomics: applications to food science and nutrition research, *Trends Food Sci Technol* 19 (2008) 482-493.
- [265] J.M. Cevallos-Cevallos, J.I. Reyes-De-Corcuera, E. Etxeberria, M.D. Danyluk, G.E. Rodrick, Metabolomic analysis in food science: a review, *Trends Food Sci Technol* 20 (2009) 557-566.
- [266] C. Simó, C. Ibáñez, A. Valdés, A. Cifuentes, V. García-Cañas, Metabolomics of Genetically Modified Crops, *Int J Mol Sci* 15 (2014) 18941-18966.
- [267] M.A. Farag, M.G. Sharaf Eldin, H. Kassem, M. Abou el Fetouh, Metabolome classification of *Brassica napus* L. organs via UPLC-QTOF-PDA-MS and their anti-oxidant potential, *Phytochem Anal* 24 (2013) 277-287.
- [268] J.A. Vita, Polyphenols and cardiovascular disease: effects on endothelial and platelet function, *Am J Clin Nutr* 81 (2005) 292S-297S.
- [269] R.K. Baboota, M. Bishnoi, P. Ambalam, K.K. Kondepudi, S.M. Sarma, R.K. Boparai, K. Podili, Functional food ingredients for the management of obesity and associated co-morbidities – A review, *Journal of Functional Foods* 5 (2013) 997-1012.
- [270] A.R. Mackie, A.N. Round, N.M. Rigby, A. Macierzanka, The Role of the Mucus Barrier in Digestion, *Food Digestion* 3 (2012) 8-15.

- [271] T.L. Farrell, L. Poquet, T.P. Dew, S. Barber, G. Williamson, Predicting Phenolic Acid Absorption in Caco-2 Cells: A Theoretical Permeability Model and Mechanistic Study, *Drug Metab Dispos* 40 (2012) 397-406.
- [272] M. Minekus, M. Alming, P. Alvito, S. Ballance, T. Bohn, C. Bourlieu, F. Carriere, R. Boutrou, M. Corredig, D. Dupont, C. Dufour, L. Egger, M. Golding, S. Karakaya, B. Kirkhus, S. Le Feunteun, U. Lesmes, A. Macierzanka, A. Mackie, S. Marze, D.J. McClements, O. Menard, I. Recio, C.N. Santos, R.P. Singh, G.E. Vegarud, M.S.J. Wickham, W. Weitschies, A. Brodkorb, A standardised static in vitro digestion method suitable for food - an international consensus, *Food & Function* 5 (2014) 1113-1124.
- [273] M. Notarnicola, S. Pisanti, V. Tutino, D. Bocale, M.T. Rotelli, A. Gentile, V. Memeo, M. Bifulco, E. Perri, M.G. Caruso, Effects of olive oil polyphenols on fatty acid synthase gene expression and activity in human colorectal cancer cells, *Genes & Nutrition* 6 (2011) 63-69.
- [274] F. Gosse, S. Guyot, S. Roussi, A. Lobstein, B. Fischer, N. Seiler, F. Raul, Chemopreventive properties of apple procyanidins on human colon cancer-derived metastatic SW620 cells and in a rat model of colon carcinogenesis, *Carcinogenesis* 26 (2005) 1291-1295.
- [275] A. Macierzanka, N.M. Rigby, A.P. Corfield, N. Wellner, F. Bottger, E.N.C. Mills, A.R. Mackie, Adsorption of bile salts to particles allows penetration of intestinal mucus, *Soft Matter* 7 (2011) 8077-8084.
- [276] S. Ladha, A.R. Mackie, L.J. Harvey, D.C. Clark, E.J. Lea, M. Brullemans, H. Duclouhier, Lateral diffusion in planar lipid bilayers: a fluorescence recovery after photobleaching investigation of its modulation by lipid composition, cholesterol, or alamethicin content and divalent cations, *Biophys J* 71 (1996) 1364-1373.
- [277] A. Macierzanka, A.R. Mackie, B.H. Bajka, N.M. Rigby, F. Nau, D. Dupont, Transport of Particles in Intestinal Mucus under Simulated Infant and Adult Physiological Conditions: Impact of Mucus Structure and Extracellular DNA, *PLoS ONE* 9 (2014) e95274.
- [278] F. Vallejo, A. Gil-Izquierdo, A. Perez-Vicente, C. Garcia-Viguera, In vitro gastrointestinal digestion study of broccoli inflorescence phenolic compounds, glucosinolates, and vitamin C, *J Agric Food Chem* 52 (2004) 135-138.
- [279] M.J. Rodriguez-Roque, M.A. Rojas-Grau, P. Elez-Martinez, O. Martin-Belloso, Changes in vitamin C, phenolic, and carotenoid profiles throughout in vitro gastrointestinal digestion of a blended fruit juice, *J Agric Food Chem* 61 (2013) 1859-1867.
- [280] J. Bouayed, H. Deußer, L. Hoffmann, T. Bohn, Bioaccessible and dialysable polyphenols in selected apple varieties following in vitro digestion vs. their native patterns, *Food Chem* 131 (2012) 1466-1472.
- [281] D. Tagliazucchi, E. Verzelloni, D. Bertolini, A. Conte, In vitro bio-accessibility and antioxidant activity of grape polyphenols, *Food Chem* 120 (2010) 599-606.
- [282] A. Helal, D. Tagliazucchi, E. Verzelloni, A. Conte, Bioaccessibility of polyphenols and cinnamaldehyde in cinnamon beverages subjected to in vitro gastro-pancreatic digestion, *Journal of Functional Foods* 7 (2014) 506-516.
- [283] J.I. Mosele, A. Macià, M.-P. Romero, M.-J. Motilva, L. Rubió, Application of in vitro gastrointestinal digestion and colonic fermentation models to pomegranate products (juice, pulp and peel extract) to study the stability and catabolism of phenolic compounds, *Journal of Functional Foods* 14 (2015) 529-540.
- [284] A. Gil-Izquierdo, P. Zafrilla, F. Tomás-Barberán, An in vitro method to simulate phenolic compound release from the food matrix in the gastrointestinal tract, *Eur Food Res Technol* 214 (2002) 155-159.
- [285] S. Peters, E. van Velzen, H.-G. Janssen, Parameter selection for peak alignment in chromatographic sample profiling: objective quality indicators and use of control samples, *Anal Bioanal Chem* 394 (2009) 1273-1281.
- [286] A.D. Patterson, H. Li, G.S. Eichler, K.W. Krausz, J.N. Weinstein, A.J. Fornace, F.J. Gonzalez, J.R. Idle, UPLC-ESI-TOFMS-Based Metabolomics and Gene Expression Dynamics Inspector Self-

- Organizing Metabolomic Maps as Tools for Understanding the Cellular Response to Ionizing Radiation, *Anal Chem* 80 (2008) 665-674.
- [287] L.W. Jia, J. Chen, P.Y. Yin, X. Lu, G.W. Xu, Serum metabolomics study of chronic renal failure by ultra performance liquid chromatography coupled with Q-TOF mass spectrometry, *Metabolomics* 4 (2008) 183-189.
- [288] E.D. Ciappio, K.W. Krausz, M. Rochman, T. Furusawa, J.A. Bonzo, L. Tessarollo, F.J. Gonzalez, M. Bustin, Metabolomics Reveals a Role for the Chromatin-Binding Protein HMGN5 in Glutathione Metabolism, *PLoS ONE* 9 (2014) e84583.
- [289] M.G.L. Hertog, P.C.H. Hollman, M.B. Katan, Content of potentially anticarcinogenic flavonoids of 28 vegetables and 9 fruits commonly consumed in the Netherlands, *J Agric Food Chem* 40 (1992) 2379-2383.
- [290] G.B. Gonzales, G. Smagghe, C. Grootaert, M. Zotti, K. Raes, J. Van Camp, Flavonoid interactions during digestion, absorption, distribution and metabolism: a sequential structure-activity/property relationship based approach in the study of bioavailability and bioactivity, *Drug Metab Rev* 47 (2015) 175-190.
- [291] Z. Zhang, A. Luo, K. Zhong, Y. Huang, Y. Gao, J. Zhang, H. Gao, Z. Xu, X. Gao, α -Glucosidase inhibitory activity by the flower buds of *Lonicera japonica* Thunb, *Journal of Functional Foods* 5 (2013) 1253-1259.
- [292] G. Oboh, A.O. Ademiluyi, A.J. Akinyemi, T. Henle, J.A. Saliu, U. Schwarzenbolz, Inhibitory effect of polyphenol-rich extracts of jute leaf (*Corchorus olitorius*) on key enzyme linked to type 2 diabetes (α -amylase and α -glucosidase) and hypertension (angiotensin I converting) in vitro, *Journal of Functional Foods* 4 (2012) 450-458.
- [293] P. Georgiades, P.D.A. Pudney, S. Rogers, D.J. Thornton, T.A. Waigh, Tea Derived Galloylated Polyphenols Cross-Link Purified Gastrointestinal Mucins, *PLoS ONE* 9 (2014) e105302.
- [294] E.M. D'Agostino, D. Rossetti, D. Atkins, D. Ferdinando, G.E. Yakubov, Interaction of tea polyphenols and food constituents with model gut epithelia: the protective role of the mucus gel layer, *J Agric Food Chem* 60 (2012) 3318-3328.
- [295] A. Cilla, A. González-Sarrías, F.A. Tomás-Barberán, J.C. Espín, R. Barberá, Availability of polyphenols in fruit beverages subjected to in vitro gastrointestinal digestion and their effects on proliferation, cell-cycle and apoptosis in human colon cancer Caco-2 cells, *Food Chem* 114 (2009) 813-820.
- [296] A.J. Day, M.S. DuPont, S. Ridley, M. Rhodes, M.J. Rhodes, M.R. Morgan, G. Williamson, Deglycosylation of flavonoid and isoflavonoid glycosides by human small intestine and liver beta-glucosidase activity, *FEBS Lett* 436 (1998) 71-75.
- [297] J. Boyer, D. Brown, R.H. Liu, Uptake of Quercetin and Quercetin 3-Glucoside from Whole Onion and Apple Peel Extracts by Caco-2 Cell Monolayers, *J Agric Food Chem* 52 (2004) 7172-7179.
- [298] C. Henry-Vitrac, A. Desmoulière, D. Girard, J.-M. Mérillon, S. Krisa, Transport, deglycosylation, and metabolism of trans-piceid by small intestinal epithelial cells, *Eur J Nutr* 45 (2006) 376-382.
- [299] Y. Liu, M. Hu, Absorption and Metabolism of Flavonoids in the Caco-2 Cell Culture Model and a Perused Rat Intestinal Model, *Drug Metab Dispos* 30 (2002) 370-377.
- [300] J. Boyer, D. Brown, R.H. Liu, In vitro digestion and lactase treatment influence uptake of quercetin and quercetin glucoside by the Caco-2 cell monolayer, *Nutr J* 4 (2005) 1.
- [301] T. Walle, Y. Otake, U.K. Walle, F.A. Wilson, Quercetin Glucosides Are Completely Hydrolyzed in Ileostomy Patients before Absorption, *The Journal of Nutrition* 130 (2000) 2658-2661.
- [302] K.R. Walsh, S.J. Haak, T. Bohn, Q. Tian, S.J. Schwartz, M.L. Failla, Isoflavonoid glucosides are deconjugated and absorbed in the small intestine of human subjects with ileostomies, *The American Journal of Clinical Nutrition* 85 (2007) 1050-1056.
- [303] J.Y. Dai, J.L. Yang, C. Li, Transport and metabolism of flavonoids from Chinese herbal remedy Xiaochaihu- tang across human intestinal Caco-2 cell monolayers, *Acta Pharmacol Sin* 29 (2008) 1086-1093.

- [304] S. Gao, W. Jiang, T. Yin, M. Hu, Highly variable contents of phenolics in St. John's Wort products affect their transport in the human intestinal Caco-2 cell model: pharmaceutical and biopharmaceutical rationale for product standardization, *J Agric Food Chem* 58 (2010) 6650-6659.
- [305] R.A. Walgren, U.K. Walle, T. Walle, Transport of Quercetin and Its Glucosides across Human Intestinal Epithelial Caco-2 Cells, *Biochem Pharmacol* 55 (1998) 1721-1727.
- [306] K. Hashimoto, M. Shimizu, Epithelial properties of human intestinal Caco-2 cells cultured in a serum-free medium, *Cytotechnology* 13 (1993) 175-184.
- [307] M. Shimizu, Interaction between food substances and the intestinal epithelium, *Biosci Biotechnol Biochem* 74 (2010) 232-241.
- [308] K. Murota, S. Shimizu, S. Miyamoto, T. Izumi, A. Obata, M. Kikuchi, J. Terao, Unique Uptake and Transport of Isoflavone Aglycones by Human Intestinal Caco-2 Cells: Comparison of Isoflavonoids and Flavonoids, *The Journal of Nutrition* 132 (2002) 1956-1961.
- [309] R. Hayeshi, C. Hilgendorf, P. Artursson, P. Augustijns, B. Brodin, P. Dehertogh, K. Fisher, L. Fossati, E. Hovenkamp, T. Korjamo, C. Masungi, N. Maubon, R. Mols, A. Mullertz, J. Monkkonen, C. O'Driscoll, H.M. Oppers-Tiemissen, E.G. Ragnarsson, M. Rooseboom, A.L. Ungell, Comparison of drug transporter gene expression and functionality in Caco-2 cells from 10 different laboratories, *Eur J Pharm Sci* 35 (2008) 383-396.
- [310] Y. Wang, Q. Wu, X.-W. Yang, X. Yang, K. Wang, The membrane transport of flavonoids from *Crossostephium chinense* across the Caco-2 monolayer, *Biopharm Drug Disposition* 32 (2011) 16-24.
- [311] C.W. Yap, PaDEL-descriptor: An open source software to calculate molecular descriptors and fingerprints, *J Comput Chem* 32 (2011) 1466-1474.
- [312] X.Z. Meihong Xie, in, 2013.
- [313] R.W.a.K.H.L. Bjørn-Helge Mevik, in, 2013.
- [314] R.D. Clark, E. Abrahamian, Using a staged multi-objective optimization approach to find selective pharmacophore models, *J Comput Aided Mol Des* 23 (2009) 765-771.
- [315] B. Bush, R. Nachbar, Jr., Sample-distance partial least squares: PLS optimized for many variables, with application to CoMFA, *J Comput Aided Mol Des* 7 (1993) 587-619.
- [316] W.J. Egan, G. Lauri, Prediction of intestinal permeability, *Adv Drug Del Rev* 54 (2002) 273-289.
- [317] A. Golbraikh, A. Tropsha, Beware of q^2 !, *J Mol Graphics Modell* 20 (2002) 269-276.
- [318] L. Kier, L. Hall, An Electrotopological-State Index for Atoms in Molecules, *Pharm Res* 7 (1990) 801-807.
- [319] L.H. Hall, B. Mohny, L.B. Kier, The electrotopological state: structure information at the atomic level for molecular graphs, *J Chem Inf Comput Sci* 31 (1991) 76-82.
- [320] J.J. Huuskonen, A.E. Villa, I.V. Tetko, Prediction of partition coefficient based on atom-type electrotopological state indices, *J Pharm Sci* 88 (1999) 229-233.
- [321] D. Butina, Performance of Kier-Hall E-state descriptors in quantitative structure activity relationship (QSAR) studies of multifunctional molecules, *Molecules* 9 (2004) 1004-1009.
- [322] J. Huuskonen, J. Rantanen, D. Livingstone, Prediction of aqueous solubility for a diverse set of organic compounds based on atom-type electrotopological state indices, *European Journal of Medicinal Chemistry* 35 (2000) 1081-1088.
- [323] K. Rose, L.H. Hall, L.B. Kier, Modeling blood-brain barrier partitioning using the electrotopological state, *J Chem Inf Comput Sci* 42 (2002) 651-666.
- [324] P. Gramatica, WHIM Descriptors of Shape, *QSAR & Combinatorial Science* 25 (2006) 327-332.
- [325] G. Bravi, E. Gancia, P. Mascagni, M. Pegna, R. Todeschini, A. Zaliani, MS-WHIM, new 3D theoretical descriptors derived from molecular surface properties: a comparative 3D QSAR study in a series of steroids, *J Comput Aided Mol Des* 11 (1997) 79-92.
- [326] M.J. Rein, M. Renouf, C. Cruz-Hernandez, L. Actis-Goretta, S.K. Thakkar, M. da Silva Pinto, Bioavailability of bioactive food compounds: a challenging journey to bioefficacy, *Br J Clin Pharmacol* 75 (2013) 588-602.

- [327] W. Brand, J. Shao, E.F. Hoek-van den Hil, K.N. van Elk, B. Spengelink, L.H.J. de Haan, M.J. Rein, F. Dionisi, G. Williamson, P.J. van Bladeren, I.M.C.M. Rietjens, Stereoselective Conjugation, Transport and Bioactivity of S- and R-Hesperetin Enantiomers in Vitro, *J Agric Food Chem* 58 (2010) 6119-6125.
- [328] A. Lévêques, L. Actis-Goretta, M.J. Rein, G. Williamson, F. Dionisi, F. Giuffrida, UPLC–MS/MS quantification of total hesperetin and hesperetin enantiomers in biological matrices, *J Pharm Biomed Anal* 57 (2012) 1-6.
- [329] J.I. Ottaviani, T.Y. Momma, C. Heiss, C. Kwik-Urbe, H. Schroeter, C.L. Keen, The stereochemical configuration of flavanols influences the level and metabolism of flavanols in humans and their biological activity in vivo, *Free Radical Biol Med* 50 (2011) 237-244.
- [330] Y. Chen, H. Li, W. Tang, C. Zhu, Y. Jiang, J. Zou, Q. Yu, Q. You, 3D-QSAR studies of HDACs inhibitors using pharmacophore-based alignment, *European Journal of Medicinal Chemistry* 44 (2009) 2868-2876.
- [331] P. Jing, S. Zhao, S. Ruan, Z. Sui, L. Chen, L. Jiang, B. Qian, Quantitative studies on structure–ORAC relationships of anthocyanins from eggplant and radish using 3D-QSAR, *Food Chem* 145 (2014) 365-371.
- [332] T. Izumi, M.K. Piskula, S. Osawa, A. Obata, K. Tobe, M. Saito, S. Kataoka, Y. Kubota, M. Kikuchi, Soy Isoflavone Aglycones Are Absorbed Faster and in Higher Amounts than Their Glucosides in Humans, *The Journal of Nutrition* 130 (2000) 1695-1699.
- [333] P. Tammela, L. Laitinen, A. Galkin, T. Wennberg, R. Heczko, H. Vuorela, J.P. Slotte, P. Vuorela, Permeability characteristics and membrane affinity of flavonoids and alkyl gallates in Caco-2 cells and in phospholipid vesicles, *Arch Biochem Biophys* 425 (2004) 193-199.
- [334] F. Ollila, K. Halling, P. Vuorela, H. Vuorela, J.P. Slotte, Characterization of Flavonoid–Biomembrane Interactions, *Arch Biochem Biophys* 399 (2002) 103-108.
- [335] C.G. Fraga, M. Galleano, S.V. Verstraeten, P.I. Oteiza, Basic biochemical mechanisms behind the health benefits of polyphenols, *Mol Aspects Med* 31 (2010) 435-445.
- [336] D. Ulluwishewa, R.C. Anderson, W.C. McNabb, P.J. Moughan, J.M. Wells, N.C. Roy, Regulation of Tight Junction Permeability by Intestinal Bacteria and Dietary Components, *The Journal of Nutrition* 141 (2011) 769-776.
- [337] F. Biasi, M. Astegiano, M. Maina, G. Leonarduzzi, G. Poli, Polyphenol supplementation as a complementary medicinal approach to treating inflammatory bowel disease, *Curr Med Chem* 18 (2011) 4851-4865.
- [338] M.H. Tempelaars, S. Rodrigues, T. Abee, Comparative Analysis of Antimicrobial Activities of Valinomycin and Cereulide, the *Bacillus cereus* Emetic Toxin, *Appl Environ Microbiol* 77 (2011) 2755-2762.
- [339] A. Makarasen, K. Yoza, M. Isobe, Higher Structure of Cereulide, an Emetic Toxin from *Bacillus cereus*, and Special Comparison with Valinomycin, an Antibiotic from *Streptomyces fulvissimus*, *Chemistry – An Asian Journal* 4 (2009) 688-698.
- [340] V.V. Teplova, R. Mikkola, A.A. Tonshin, N.-E.L. Saris, M.S. Salkinoja-Salonen, The higher toxicity of cereulide relative to valinomycin is due to its higher affinity for potassium at physiological plasma concentration, *Toxicol Appl Pharmacol* 210 (2006) 39-46.
- [341] B. Kleuser, H. Rieter, G. Adam, Selective Effects by Valinomycin on Cytotoxicity and Cell Cycle Arrest of Transformed versus Nontransformed Rodent Fibroblasts in Vitro, *Cancer Res* 45 (1985) 3022-3028.
- [342] J.C. Stockert, A. Blázquez-Castro, M. Cañete, R.W. Horobin, Á. Villanueva, MTT assay for cell viability: Intracellular localization of the formazan product is in lipid droplets, *Acta Histochem* 114 (2012) 785-796.
- [343] V. Vichai, K. Kirtikara, Sulforhodamine B colorimetric assay for cytotoxicity screening, *Nat. Protocols* 1 (2006) 1112-1116.
- [344] Y.D. Benoit, M.B. Lepage, T. Khalfaoui, E. Tremblay, N. Basora, J.C. Carrier, L.J. Gudas, J.F. Beaulieu, Polycomb repressive complex 2 impedes intestinal cell terminal differentiation, *J Cell Sci* 125 (2012) 3454-3463.

- [345] C.M. Thompson, Y. Fedorov, D.D. Brown, M. Suh, D.M. Proctor, L. Kuriakose, L.C. Haws, M.A. Harris, Assessment of Cr(VI)-Induced Cytotoxicity and Genotoxicity Using High Content Analysis, *PLoS ONE* 7 (2012) e42720.
- [346] E. Bajak, M. Fabbri, J. Ponti, S. Gioria, I. Ojea-Jiménez, A. Collotta, V. Mariani, D. Gilliland, F. Rossi, L. Gribaldo, Changes in Caco-2 cells transcriptome profiles upon exposure to gold nanoparticles, *Toxicol Lett* 233 (2015) 187-199.
- [347] M.M. Silva, M.R. Santos, G. Caroco, R. Rocha, G. Justino, L. Mira, Structure-antioxidant activity relationships of flavonoids: a re-examination, *Free Radic Res* 36 (2002) 1219-1227.
- [348] G.C. Justino, M.R. Santos, S. Canario, C. Borges, M.H. Florencio, L. Mira, Plasma quercetin metabolites: structure-antioxidant activity relationships, *Arch Biochem Biophys* 432 (2004) 109-121.
- [349] B.T. Zhu, E.L. Ezell, J.G. Liehr, Catechol-O-methyltransferase-catalyzed rapid O-methylation of mutagenic flavonoids. Metabolic inactivation as a possible reason for their lack of carcinogenicity in vivo, *J Biol Chem* 269 (1994) 292-299.
- [350] M.F. Mazzobre, M.V. Román, A.F. Mourelle, H.R. Corti, Octanol–water partition coefficient of glucose, sucrose, and trehalose, *Carbohydr Res* 340 (2005) 1207-1211.
- [351] V. Abram, B. Berlec, A. Ota, M. Šentjurc, P. Blatnik, N.P. Ulrih, Effect of flavonoid structure on the fluidity of model lipid membranes, *Food Chem* 139 (2013) 804-813.
- [352] B. Pawlikowska-Pawłęga, H. Dziubińska, E. Król, K. Trębacz, A. Jarosz-Wilkolazka, R. Paduch, A. Gawron, W.I. Gruszecki, Characteristics of quercetin interactions with liposomal and vacuolar membranes, *Biochim Biophys Acta* 1838 (2014) 254-265.
- [353] B. Pawlikowska-Pawłęga, W. Ignacy Gruszecki, L. Misiak, R. Paduch, T. Piersiak, B. Zarzyka, J. Pawelec, A. Gawron, Modification of membranes by quercetin, a naturally occurring flavonoid, via its incorporation in the polar head group, *Biochim Biophys Acta* 1768 (2007) 2195-2204.
- [354] P. Jancova, P. Anzenbacher, E. Anzenbacherova, Phase II drug metabolizing enzymes, *Biomed Pap Med Fac Univ Palacky Olomouc Czech Repub* 154 (2010) 103-116.
- [355] C. Manna, P. Galletti, G. Maisto, V. Cucciolla, S. D'Angelo, V. Zappia, Transport mechanism and metabolism of olive oil hydroxytyrosol in Caco-2 cells, *FEBS Lett* 470 (2000) 341-344.
- [356] S.M. Kern, R.N. Bennett, P.W. Needs, F.A. Mellon, P.A. Kroon, M.-T. Garcia-Conesa, Characterization of Metabolites of Hydroxycinnamates in the in Vitro Model of Human Small Intestinal Epithelium Caco-2 Cells, *J Agric Food Chem* 51 (2003) 7884-7891.
- [357] M.N. Borrel, E. Pereira, M. Fiallo, A. Garnier-Suillerot, Mobile ionophores are a novel class of P-glycoprotein inhibitors. The effects of ionophores on 4'-O-tetrahydropyranyl-adriamycin incorporation in K562 drug-resistant cells, *Eur J Biochem* 223 (1994) 125-133.
- [358] C. Carter-Su, G.A. Kimmich, Effect of membrane potential on Na⁺-dependent sugar transport by ATP-depleted intestinal cells, *Am J Physiol* 238 (1980) C73-80.
- [359] T.A.D. Smith, M.G. Blaylock, Treatment of Breast Tumor Cells In Vitro with the Mitochondrial Membrane Potential Dissipater Valinomycin Increases 18F-FDG Incorporation, *J Nucl Med* 48 (2007) 1308-1312.
- [360] B. Stieger, B. Hagenbuch, Organic Anion Transporting Polypeptides, *Curr Top Membr* 73 (2014) 205-232.
- [361] G. Paglia, J.P. Williams, L. Menikarachchi, J.W. Thompson, R. Tyldesley-Worster, S. Halldórsson, O. Rolfsson, A. Moseley, D. Grant, J. Langridge, B.O. Palsson, G. Astarita, Ion Mobility Derived Collision Cross Sections to Support Metabolomics Applications, *Anal Chem* 86 (2014) 3985-3993.
- [362] G.J. Dear, J. Munoz-Muriedas, C. Beaumont, A. Roberts, J. Kirk, J.P. Williams, I. Campuzano, Sites of metabolic substitution: investigating metabolite structures utilising ion mobility and molecular modelling, *Rapid Commun Mass Spectrom* 24 (2010) 3157-3162.
- [363] I. Campuzano, M.F. Bush, C.V. Robinson, C. Beaumont, K. Richardson, H. Kim, H.I. Kim, Structural Characterization of Drug-like Compounds by Ion Mobility Mass Spectrometry:

- Comparison of Theoretical and Experimentally Derived Nitrogen Collision Cross Sections, *Anal Chem* 84 (2012) 1026-1033.
- [364] B.T. Ruotolo, K.J. Gillig, E.G. Stone, D.H. Russell, Peak capacity of ion mobility mass spectrometry: separation of peptides in helium buffer gas, *J Chromatogr B Analyt Technol Biomed Life Sci* 782 (2002) 385-392.
- [365] M.F. Bush, I.D.G. Campuzano, C.V. Robinson, Ion Mobility Mass Spectrometry of Peptide Ions: Effects of Drift Gas and Calibration Strategies, *Anal Chem* 84 (2012) 7124-7130.
- [366] G. Paglia, P. Angel, J.P. Williams, K. Richardson, H.J. Olivos, J.W. Thompson, L. Menikarachchi, S. Lai, C. Walsh, A. Moseley, R.S. Plumb, D.F. Grant, B.O. Palsson, J. Langridge, S. Geromanos, G. Astarita, Ion Mobility-Derived Collision Cross Section As an Additional Measure for Lipid Fingerprinting and Identification, *Anal Chem* 87 (2015) 1137-1144.
- [367] M. Kliman, J.C. May, J.A. McLean, Lipid analysis and lipidomics by structurally selective ion mobility-mass spectrometry, *Biochim Biophys Acta* 1811 (2011) 935-945.
- [368] S.J. Valentine, M.D. Plasencia, X. Liu, M. Krishnan, S. Naylor, H.R. Udseth, R.D. Smith, D.E. Clemmer, Toward Plasma Proteome Profiling with Ion Mobility-Mass Spectrometry, *J Proteome Res* 5 (2006) 2977-2984.
- [369] P. Dwivedi, P. Wu, S. Klopsch, G. Puzon, L. Xun, H. Hill, Jr., Metabolic profiling by ion mobility mass spectrometry (IMMS), *Metabolomics* 4 (2008) 63-80.
- [370] B.T. Ruotolo, J.L.P. Benesch, A.M. Sandercock, S.-J. Hyung, C.V. Robinson, Ion mobility-mass spectrometry analysis of large protein complexes, *Nat Protoc* 3 (2008) 1139-1152.
- [371] F. Cuyckens, C. Wassvik, R.J. Mortishire-Smith, G. Tresadern, I. Campuzano, J. Claereboudt, Product ion mobility as a promising tool for assignment of positional isomers of drug metabolites, *Rapid Commun Mass Spectrom* 25 (2011) 3497-3503.
- [372] V. D'Atri, M. Porrini, F. Rosu, V. Gabelica, Linking molecular models with ion mobility experiments. Illustration with a rigid nucleic acid structure, *J Mass Spectrom* 50 (2015) 711-726.
- [373] M.F. Mesleh, J.M. Hunter, A.A. Shvartsburg, G.C. Schatz, M.F. Jarrold, Structural Information from Ion Mobility Measurements: Effects of the Long-Range Potential, *J Phys Chem* 100 (1996) 16082-16086.
- [374] A.A. Shvartsburg, G.C. Schatz, M.F. Jarrold, Mobilities of carbon cluster ions: Critical importance of the molecular attractive potential, *J Chem Phys* 108 (1998) 2416-2423.
- [375] A.A. Shvartsburg, M.F. Jarrold, An exact hard-spheres scattering model for the mobilities of polyatomic ions, *Chem Phys Lett* 261 (1996) 86-91.
- [376] T.W. Knapman, J.T. Berryman, I. Campuzano, S.A. Harris, A.E. Ashcroft, Considerations in experimental and theoretical collision cross-section measurements of small molecules using travelling wave ion mobility spectrometry-mass spectrometry, *Int J Mass spectrom* 298 (2010) 17-23.
- [377] H. Kim, H.I. Kim, P.V. Johnson, L.W. Beegle, J.L. Beauchamp, W.A. Goddard, I. Kanik, Experimental and theoretical investigation into the correlation between mass and ion mobility for choline and other ammonium cations in N₂, *Anal Chem* 80 (2008) 1928-1936.
- [378] P.D. Mosier, A.E. Counterman, P.C. Jurs, D.E. Clemmer, Prediction of peptide ion collision cross sections from topological molecular structure and amino acid parameters, *Anal Chem* 74 (2002) 1360-1370.
- [379] A.R. Shah, K. Agarwal, E.S. Baker, M. Singhal, A.M. Mayampurath, Y.M. Ibrahim, L.J. Kangas, M.E. Monroe, R. Zhao, M.E. Belov, G.A. Anderson, R.D. Smith, Machine learning based prediction for peptide drift times in ion mobility spectrometry, *Bioinformatics* 26 (2010) 1601-1607.
- [380] P. Zhou, F. Tian, Z. Li, Quantitative structure–property relationship studies for collision cross sections of 579 singly protonated peptides based on a novel descriptor as molecular graph fingerprint (MoGF), *Anal Chim Acta* 597 (2007) 214-222.

- [381] S.J. Valentine, A.E. Counterman, D.E. Clemmer, A database of 660 peptide ion cross sections: use of intrinsic size parameters for bona fide predictions of cross sections, *J Am Soc Mass Spectrom* 10 (1999) 1188-1211.
- [382] J.V. Hamilton, J.B. Renaud, P.M. Mayer, Experiment and theory combine to produce a practical negative ion calibration set for collision cross-section determinations by travelling-wave ion-mobility mass spectrometry, *Rapid Commun Mass Spectrom* 26 (2012) 1591-1595.
- [383] K. De Winter, G. Dewitte, M.E. Dirks-Hofmeister, S. De Laet, H. Pelantová, V. Křen, T. Desmet, Enzymatic Glycosylation of Phenolic Antioxidants: Phosphorylase-Mediated Synthesis and Characterization, *J Agric Food Chem* 63 (2015) 10131-10139.
- [384] C. Laphorn, F.S. Pullen, B.Z. Chowdhry, P. Wright, G.L. Perkins, Y. Heredia, How useful is molecular modelling in combination with ion mobility mass spectrometry for 'small molecule' ion mobility collision cross-sections?, *Analyst* 140 (2015) 6814-6823.
- [385] W.N. Venables, B.D. Ripley, *Modern Applied Statistics with S*, Springer New York, New York, USA, 2003.
- [386] J. Szlek, A. Paclawski, R. Lau, R. Jachowicz, A. Mendyk, Heuristic modeling of macromolecule release from PLGA microspheres, *Int J Nanomedicine* 8 (2013) 4601-4611.
- [387] P. Ertl, B. Rohde, P. Selzer, Fast Calculation of Molecular Polar Surface Area as a Sum of Fragment-Based Contributions and Its Application to the Prediction of Drug Transport Properties, *J Med Chem* 43 (2000) 3714-3717.
- [388] D. Bonchev, *Information theoretic indices for characterization of chemical structures*, Research Studies Press, Chichester West Sussex ; New York, 1983.
- [389] A.T. Balaban, Highly discriminating distance-based topological index, *Chem Phys Lett* 89 (1982) 399-404.
- [390] S.R. Hall, F.H. Allen, I.D. Brown, The crystallographic information file (CIF): a new standard archive file for crystallography, *Acta Crystallographica Section A* 47 (1991) 655-685.
- [391] A. Hopfinger, *Conformational properties of macromolecules*, Academic Press, New York, USA, 1973.
- [392] D.T. Stanton, P.C. Jurs, Development and use of charged partial surface area structural descriptors in computer-assisted quantitative structure-property relationship studies, *Anal Chem* 62 (1990) 2323-2329.
- [393] R.H. Rohrbaugh, P.C. Jurs, Descriptions of molecular shape applied in studies of structure/activity and structure/property relationships, *Anal Chim Acta* 199 (1987) 99-109.
- [394] G. Williamson, The use of flavonoid aglycones in in vitro systems to test biological activities: based on bioavailability data, is this a valid approach?, *Phytochem Rev* 1 (2002) 215-222.
- [395] V. Somoza, R.J. Molyneux, Z.-Y. Chen, F. Tomás-Barberán, T. Hofmann, Guidelines for Research on Bioactive Constituents – A Journal of Agricultural and Food Chemistry Perspective, *J Agric Food Chem* 63 (2015) 8103-8105.
- [396] J. Lee, A.E. Mitchell, Quercetin and isorhamnetin glycosides in onion (*Allium cepa* L.): varietal comparison, physical distribution, coproduct evaluation, and long-term storage stability, *J Agric Food Chem* 59 (2011) 857-863.
- [397] M.S. DuPont, A.J. Day, R.N. Bennett, F.A. Mellon, P.A. Kroon, Absorption of kaempferol from endive, a source of kaempferol-3-glucuronide, in humans, *Eur J Clin Nutr* 58 (2004) 947-954.
- [398] T. Bohn, G.J. McDougall, A. Alegría, M. Alminger, E. Arrigoni, A.-M. Aura, C. Brito, A. Cilla, S.N. El, S. Karakaya, M.C. Martínez-Cuesta, C.N. Santos, Mind the gap—deficits in our knowledge of aspects impacting the bioavailability of phytochemicals and their metabolites—a position paper focusing on carotenoids and polyphenols, *Mol Nutr Food Res* (2015) n/a-n/a.
- [399] S.K. Lai, Y.-Y. Wang, D. Wirtz, J. Hanes, Micro- and macrorheology of mucus, *Adv Drug Del Rev* 61 (2009) 86-100.
- [400] R. Bansil, B. Turner, Mucin structure, aggregation, physiological functions and biomedical applications, *Current Opinion in Colloid & Interface Science* 11 (2006) 164-170.

-
- [401] P.C. Hollman, J.H. de Vries, S.D. van Leeuwen, M.J. Mengelers, M.B. Katan, Absorption of dietary quercetin glycosides and quercetin in healthy ileostomy volunteers, *The American Journal of Clinical Nutrition* 62 (1995) 1276-1282.
- [402] P.C.H. Hollman, J.M.P. van Trijp, M.N.C.P. Buysman, M.S. v.d. Gaag, M.J.B. Mengelers, J.H.M. de Vries, M.B. Katan, Relative bioavailability of the antioxidant flavonoid quercetin from various foods in man, *FEBS Lett* 418 (1997) 152-156.
- [403] C. Morand, C. Manach, V. Crespy, C. Remesy, Quercetin 3-O-beta-glucoside is better absorbed than other quercetin forms and is not present in rat plasma, *Free Radic Res* 33 (2000) 667-676.
- [404] M. Reinboth, S. Wolffram, G. Abraham, F.R. Ungemach, R. Cermak, Oral bioavailability of quercetin from different quercetin glycosides in dogs, *Br J Nutr* 104 (2010) 198-203.
- [405] H. Kaur, G. Kaur, A Critical Appraisal of Solubility Enhancement Techniques of Polyphenols, *Journal of Pharmaceutics* 2014 (2014) 14.
- [406] Y. Li, S. Sun, Q. Chang, L. Zhang, G. Wang, W. Chen, X. Miao, Y. Zheng, A Strategy for the Improvement of the Bioavailability and Antiosteoporosis Activity of BCS IV Flavonoid Glycosides through the Formulation of Their Lipophilic Aglycone into Nanocrystals, *Mol Pharm* 10 (2013) 2534-2542.
- [407] Q. Shen, X. Li, W. Li, X. Zhao, Enhanced intestinal absorption of daidzein by borneol/menthol eutectic mixture and microemulsion, *AAPS PharmSciTech* 12 (2011) 1044-1049.

CURRICULUM VITAE

GERARD BRYAN L. GONZALES

Education

PhD Applied Biological Sciences: Chemistry and Bioprocess Technology
16/09/2012 – present
Ghent University, Belgium

ERASMUS MUNDUS FOOD OF LIFE (double-degree)
09/2010 – 07/2012
MSc Food Science and Technology – University of Copenhagen, Denmark
MSc Food Products of Animal Origin – Universitat Autònoma de Barcelona, Spain
MSc thesis – Universitat de Barcelona

BSc Food Technology – University of the Philippines Mindanao, Philippines
06/2005 – 03/2009

Relevant trainings

9th Mass Spectrometry in Biotechnology and Medicine (MSBM) Summer School
Dubrovnik, Croatia; 5-11/07/2015
Fellowship awardee by the British Mass Spectrometry Society

1st International Mass Spectrometry School
Siena, Italy; 15-20/09/2013
Fellowship awardee by the International Mass Spectrometry Foundation

1st Infogest International School on Food Digestion and Human Health
Gdansk, Poland; 22-26/04/2013
Fellowship awardee by the COST Action Infogest

Experience

Short-term Scientific Mission
1/10/2014 – 31/11/2014
Institute of Food Research (IFR), United Kingdom
Description: Experience in proposal writing and organizing research collaboration.
Obtained funding from the EU-COST action (Infogest) to perform experiments regarding mucus biophysics

Science Research Specialist I
18/05/2009 – 31/07/2010
Special Projects Division, Department of Science and Technology (Government), Republic of the Philippines, Gen. Santos Ave., Bicutan, 1631 Taguig (Philippines)

Publications

1. **Gonzales** et al. Collision cross section prediction of deprotonated phenolics in a travelling-wave ion mobility spectrometer using molecular descriptors and chemometrics. *Analytica Chimica Acta. In press*

2. **Gonzales** et al. 2015. Quercetin mitigates valinomycin-induced cellular stress via stress-induced metabolism and cell uptake. *Molecular Nutrition and Food Research*. *In press*.
3. **Gonzales** et al. 2015. Flavonoid-gastrointestinal mucus interaction and its potential role in regulating flavonoid bioavailability and mucosal biophysical properties. *Food Research International*. *In press*.
4. Huynh, Smagghe, **Gonzales** et al. 2015. Extraction and bioconversion of kaempferol metabolites from cauliflower waste outer leaves through fungal fermentation. *Biochemical Engineering Journal*. *In press*
5. Kamiloglu, Capanoglu, Bilen, **Gonzales** et al. 2015. Bioaccessibility of polyphenols from plant-processing byproducts of black carrot (*Daucus carota* L.). *Journal of Agricultural and Food Chemistry*. *In press*
6. **Gonzales** et al. 2015. Review on the use of cell culture to study metabolism, transport, and accumulation of flavonoids: from mono-cultures to co-culture systems. *Comprehensive Reviews in Food Science and Food Safety*. *In press*
7. **Gonzales** et al. 2015. Use of metabolomics and fluorescence recovery after photobleaching to study the bioavailability and intestinal mucus diffusion of polyphenols from cauliflower waste. *Journal of Functional Foods* 16, 403-413
8. **Gonzales** et al. 2015. Liquid chromatography–mass spectrometry coupled with multivariate analysis for the characterization and discrimination of extractable and nonextractable polyphenols and glucosinolates from red cabbage and Brussels sprout waste streams. *Journal of Chromatography A*. 1402:60-70
9. **Gonzales** et al. 2015. Flavonoid interactions during digestion, absorption, distribution and metabolism: a sequential structure-activity/property relationship based approach in the study of bioavailability and bioactivity, *Drug Metabolism Reviews*. 47(2):175-90
10. **Gonzales** et al. 2014. Two- and three-dimensional quantitative structure–permeability relationship of flavonoids in Caco-2 cells using stepwise multiple linear regression (SMLR), partial least squares regression (PLSR), and pharmacophore (GALAHAD)-based comparative molecular similarity index analysis (COMSIA). *Medicinal Chemistry Research*. 24:1696-1706
11. **Gonzales** et al. 2014. Combined alkaline hydrolysis and ultrasound-assisted extraction for the release of nonextractable phenolics from cauliflower (*Brassica oleracea* var. *botrytis*) waste. *Journal of Agricultural and Food Chemistry*; 62(15):3371-6.
12. **Gonzales** et al. 2014. Ultra(high)-pressure liquid chromatography-electrospray ionization-time-of-flight-ion mobility-high definition mass spectrometry for the rapid identification and structural characterization of flavonoid glycosides from cauliflower waste. *Journal of Chromatography A*; 1323:39-48
13. Huynh, Smagghe, **Gonzales** et al. 2014. Enzyme-Assisted Extraction Enhancing the Phenolic Release from Cauliflower (*Brassica oleracea* L. var. *botrytis*) Outer Leaves. *Journal of Agricultural and Food Chemistry*; 62(30):7468-76.
14. **Gonzales** et al. 2014. Quantitative structure (inhibitory) activity relationship and molecular docking studies of phenolic acids to angiotensin-converting enzyme. *Communications in Agricultural and Applied Biological Sciences*: 79(1). pp 41-44. Ghent University Press.
15. Al Shukor, Van Camp, **Gonzales**, et al. 2013. Angiotensin-converting enzyme inhibitory effects by plant phenolic compounds: a study of structure activity relationships. *Journal of Agricultural and Food Chemistry*; 61(48): 11832-9
16. **Gonzales** and Flores. 2010. Angiotensin-1-converting Enzyme Inhibitory Activity of Milk Hydrolysate by LAB Fermentation. *Proceedings of the 2010 International Conference on Biotechnology and Food Science*. pp 172-176. World Academic Press. UK

Submitted for publication

1. **Gonzales** et al. Metabolism of quercetin and naringenin by food-grade fungal inoculum, *Rhizopus azygosporus* Yuan et Jong (ATCC 48108)
2. Grootaert, **Gonzales** et al. Flow cytometric method for the detection of flavonoids in cell lines
3. Toaldo, Van Camp, **Gonzales** et al. Resveratrol improves TNF- α -induced endothelial dysfunction in a co-culture model for a Caco-2 with an endothelial cell line

Awards and Recognition

Journal of Mass Spectrometry Postgraduate Award 2016: 21st International Mass Spectrometry Conference. 20-26/08/2016. Toronto, Canada

Belgian representative to the International Nutrition Student Research Championship, 11-14/07/2016. Dublin, Ireland

Best Poster. Annual Belgian Society for Mass Spectrometry Meeting, 18/09/2015, Vrije Universiteit Brussel, Brussels, Belgium

Student Travel Fellowship – British Mass Spectrometry Society

Short-term Scientific Mission Grant – EU-COST action Infogest

Fellowship – International Mass Spectrometry Foundation

Best Oral Communication: 19th National Conference on Applied Biological Sciences. 7/02/2014. Gembloux, Belgium.

Erasmus Mundus Food of Life (EMFOL) International Scholarship 2010-2012

1st Runner Place: 48th Annual Philippine Society for Food Technologists Undergraduate Research Competition. 22/09/2011. Pasay City, Philippines

Oral presentations in conferences

Gonzales et al. IMS-MS^E and molecular modeling for structure identification of flavonoid and their O-glycoside derivatives, Annual Meeting of the Belgian Society for Mass Spectrometry, 18/9/2015, Brussels, BELGIUM

Gonzales et al. Recent updates on the flavonoid paradox: are conventional methods still valid? 5th Annual Belgian Nutrition Society Congress, 3/4/2015, Brussels, BELGIUM

Gonzales et al. Metabolomics- and chemometrics- based approaches on the study of polyphenol bioavailability and intestinal mucus diffusion, 4th International Conference on Food Digestion, 17-19/3/2015, Naples, ITALY

Gonzales et al. Combined alkaline hydrolysis and sonication of cauliflower waste releases two times more total phenolics than conventional extraction, TotalFood 2014: Science and technology for the economic and sustainable exploitation of agri-food chain wastes and co-products, 11-13/11/2014, Institute of Food Research, Norwich, UNITED KINGDOM

Gonzales et al. Quantitative structure (inhibitory) activity relationship and molecular docking studies of phenolic acids to angiotensin-converting enzyme, 19th National Symposium on Applied Biological Sciences, 7/2/2014, Gembloux, BELGIUM

Gonzales. Mass Spectrometry and Protein Modeling, 1st Brazil-Belgium conference of innovative technologies applied to pest control, 4-6/12/2013, EMBRAPA, Pelotas, BRAZIL

Gonzales et al. Chicken meat lipid characteristic from animals fed native, acid and partially re-esterified oils. COST Action Feed for Health, 1st Early-stage researcher workshop, 7-8/6/2012, Barcelona, SPAIN

Gonzales and Flores. Angiotensin-I converting enzyme inhibitory activity of milk hydrolysate by LAB fermentation, 4th International Conference on Fermented Foods, Health Status and Social Well-being, 11-12/12/2009, Anand Agricultural University, Anand, INDIA

Affiliations

Member, Belgian Society for Mass Spectrometry

Member, British Mass Spectrometry Society

Member, Belgian Nutrition Society